

PALM FIBER COMPOSITES FOR AIRCRAFT INTERIOR

BY

POORIA KHALILI

THESIS SUBMITTED TO THE UNIVERSITY OF NOTTINGHAM FOR THE DEGREE OF DOCTOR OF PHILOSOPHY

SEPTEMBER 2017

Abstract

Over the last decades, aircraft manufacturers have produced synthetic fiber thermoset composites to be used for interior components of aircraft. However, the ever increasing dependence on synthetic fibers and thermosetting resin has set the aerospace industry under considerable pressure to reduce its carbon footprint and enhance its sustainable credentials. The unrelenting passion of sustainability has led to an expanding search for eco-friendly fiber reinforced composite from renewable sources. However, there remains a significant challenge to produce palm fiber composite fit for aircraft interiors owing to its ease of combustibility.

Various flame retardants and expandable graphite (EG) at different concentrations were introduced into the epoxy composites reinforced with approximately 18 to 20% fiber (mass fraction). Amongst the flame retardant filled composites fabricated by resin infusion technique, two formulations with incorporation of (i) 10% ammonium phosphate (APP) and 5% alumina tri-hydrate (ATH) hybrid and (ii) 10% ammonium phosphate (APP) and 5% zinc borate (ZB) hybrid into EFB fiber reinforced epoxy composites demonstrated promising capability to meet the vertical Bunsen burner requirements for aircraft interiors, where zero molten drip time and zero flame time were observed, along with the lowest recorded gross heat of combustion being less than 27.4 MJ/kg from bomb calorimeter instrument. It was found that the lab-scale mechanical performances enhanced with inclusion of alkaline treated fibre compared with those of untreated fibre composites.

For expandable graphite filled composites fabricated by compression molding technique, all the composites containing EG was observed to possess the capability to meet the vertical Bunsen burner test requirements of aircraft interior parts. Palm fibre composites with inclusion of 5 %wt and 7 %wt EG fillers showed zero flame time, drip flame time and negligible burned length. From Bomb calorimetry and TGA tests, formulation with 7% EG filler (CEG7) recorded a gross heat of combustion of 27.91 MJ/kg and mass residue of 28.31 wt% at 700 °C. In a separate approach where 3 wt% and 5 wt% EG were coated onto the exterior surface of neat EFB fiber reinforced epoxy composite without any additional fillers, it was observed that composite coated with 5 wt% EG met the requirements of vertical Bunsen burner test. With regards to mechanical properties, the incorporation of EG fillers into EFB fiber composite dropped the mechanical behaviors. The

mechanical performances of EG filled composite was found to improve with the alkali treatment of EFB fibers. Lab scale measured mechanical behaviors were observed to be in the acceptable range for the required application.

Finally, an aerospace grade Nomex honeycomb was used to fabricate laminate with the natural fibre composite skins, which could be a structure of an aircraft interior component for a sidewall, ceiling or partition. Two different types of composite face sheets were used, one with the optimum formulation from flame retardant filled composite (hybrid 10 wt% APP with 5 wt% ATH) and the other with 7 wt% expandable graphite. The requirements of 12 s vertical Bunsen burner testing were fully met for the panels. Three of the optimum formulations (APP/ATH hybrid, APP/ZB hybrid and EG7) were tested against 60 s vertical Bunsen burner experiment and found capable of meeting the test specifications of flame time, drip flame time and burn length.

List of publications

1. **P. Khalili**, K.Y. Tshai, I. Kong. Development of fire resistivity of natural fibre composite encouraged by a synergy between zinc borate and ammonium polyphosphate. Composites Part B: Engineering (under review)-2017.
2. **P. Khalili**, K.Y. Tshai, I. Kong. Natural fibre reinforced expandable graphite filled composites: Evaluation of the flame retardancy, thermal and mechanical performances. Composites Part A: Applied Science and Manufacturing- 2017.
3. **P. Khalili**, K.Y. Tshai, I. Kong, David Hui. Synergistic of ammonium polyphosphate and alumina trihydrate as fire retardants for natural fiber reinforced epoxy composite. Composites Part B: Engineering- 2017.
4. **Pooria Khalili**, Kim Yeow Tshai, Ing Kong. Comparative thermal and physical investigation of chemically treated and untreated oil palm EFB fiber. Materials Today: Proceedings- 2017.
5. **Pooria Khalili**, Kim Yeow Tshai, Ing Kong, Mike Clifford. Flammability performances of honeycomb panels. The 24th Annual International Conference on Composites/Nano Engineering (ICCE-25), July 16-22, 2017, Rome, Italy.
6. **Pooria Khalili**, Kim Yeow Tshai, Ing Kong. Natural fiber composite flame retarded by zinc borate or hybrid of zinc borate and alumina tri-hydrate: Evaluation of flame retardants on the flammability, thermal and mechanical properties of composite. Emerging Polymer Technologies Summit (EPTS), Sep 14-16, 2016, Melbourne, Australia
7. **Pooria Khalili**, Kim Yeow Tshai, Ing Kong. Effects of organophosphorus and mineral based flame retardants on combustibility and mechanical performances of natural fiber reinforced composites. World Journal of Engineering- 2016.
8. **P. Khalili**, K.Y. Tshai, I. Kong c, J.H. Lee, F.A. Mostafa. The synergistic effect of flame retardants on flammability, thermal and mechanical properties of natural fiber reinforced epoxy composite. Key Engineering Materials- 2016.
9. **P. Khalili**, K.Y. Tshai b, I. Kong c, C.H. Yeoh. The effects of graphene and flame retardants on flammability and mechanical properties of natural fibre reinforced polymer composites. Key Engineering Materials- 2016.
10. Kim Yeow Tshai, **Pooria Khalili**, Ing Kong. Synthetization of graphene and its incorporation into natural fibre reinforced thermosetting nanocomposite. ARPN Journal of Engineering and Applied Science- 2016.
11. **Pooria Khalili**, Kim Yeow Tshai, Ing Kong. Oil Palm EFB Fibre Honeycomb Panels. The 24_{th} Annual International Conference on Composites/Nano Engineering (ICCE-24), July 17-23, 2016, Haikou, Hainan Island, China.
12. **P. Khalili**, K.Y. Tshai, I. Kong. Presentations of papers numbered 8 and 9. 2nd International Conference on the Science and Engineering of Materials (ICoSEM2015), Kuala Lumpur, Malaysia.
13. **P. Khalili**, K.Y. Tshai, M. Clifford, I. Kong. Mechanical properties of resin infused Palm EFB epoxy composite. The 23_{rd} Annual International Conference on Composites/Nano Engineering (ICCE-23), July 12-18, 2015, Chengdu, China.

Acknowledgements

The author is greatly beholden to his supervisors, Dr Albert Tshai, Dr Ing Kong and Dr Mike Clifford, for their support, patience and guidance throughout the PhD degree.

The author is grateful to the financial support of the Ministry of Science, Technology and Innovation (MOSTI) Malaysia under Grant 03-02-12-SF0212 as well as the Faculty of Engineering at the University of Nottingham, Malaysia Campus.

Lastly, special thanks to the author's mom for all her unfailing and inspiring encouragement through the PhD degree.

Table of contents

Abstract i

List of publications iii

Acknowledgements iv

Table of contents v

List of figures xi

List of tables xix

List of abbreviations xxiii

1. Introduction 1

1.1 Problem statement and objectives 3

1.2 Hypothesis 4

2. Literature review 7

2.1 Introduction 7

2.2 Aircraft Interiors 9

2.3 Requirements and design for interior components of aircraft 10

2.3.1 Aircraft materials and interior panel structures 11

2.3.2 Fire-resistant criteria 14

2.3.3 Lab scale mechanical standards of interior aircraft components 17

2.3.4 The most probable parts to be fabricated from natural fibre composite 18

2.4 Characteristics of oil palm and natural fibers 19

2.4.1 Physico-mechanical properties of natural fibers, their potentials and drawbacks .. 19

2.4.2 Characteristics of EFB fiber 21

2.5 The properties of EFB and natural fiber based composites 25

2.5.1 The effects of natural fiber treatment on the mechanical and thermal properties .. 25

2.5.2 The effects of fiber type on thermal stability and the effect of fiber fraction on mechanical properties of composite 29

2.6 Polymeric Materials currently used for aircraft interiors: Thermosets vs. thermoplastics 32

2.6.1 Epoxy thermoset 34

2.6.2 Phenolic resin (PF) in aircraft interiors 35

2.6.3 Recently used thermoplastics for aircraft interiors 37

2.7 Flame retardants 38

2.8 Flammability and smoke properties of natural fiber composites 41

2.8.1 Flame retardants for natural fiber reinforced polymer composite 43

2.8.2 Expandable graphite as flame retardant in composites 50

2.9 Federation Aviation Regulation testing 56

2.9.1 Vertical Bunsen burner experiment 56

2.10 Nomex honeycomb panels using composite skins 58

2.11 Summary 60

3. Methodology 64

3.1 Materials 64
3.2 Fiber mat fabrication 67
3.3 FRs- based composite fabrications 69
3.3.1 Initial set up 69
3.3.2 Resin infusion 71
3.4 Fiber treatment 72
3.5 Preparation of EG filled EFB epoxy composites and formulations with EG coating 73
3.6 Characterization 76
3.6.1 Vertical Bunsen burner test 76
3.6.2 Bomb calorimeter 78
3.6.3 Thermogravimetric analysis 78
3.6.4 Dynamic thermal mechanical analysis 79
3.6.5 Fourier Transformed Infrared spectroscopy (FTIR) analysis 80
3.6.6 Tensile testing 81
3.6.7 Flexural testing 82
3.6.8 Compression test 83
3.6.9 Plate shear test 83
3.6.10 Field emission scanning electron microscopy (FESEM) 84
3.6.11 Energy dispersive spectroscopy (EDX) 84
3.6.12 Furnace test 84

3.6.13 Coupled confocal Raman and AFM (atomic force microscopy) Microscopy 85

4. Thermal and mechanical properties of flame retardant filled EFB reinforced epoxy composite 86

4.1 Introduction 86

4.2 Flammability and thermal properties of the FR filled EFB epoxy composites 88

4.2.1 Flammability of FR filled EFB epoxy composite 88

4.2.2 Heat release properties of FR filled EFB epoxy composites 99

4.2.3 Thermal properties of FRs filled EFB epoxy composite 103

4.2.4 EDX study 109

4.2.5 Morphological features of composites 116

4.3 Comparative Thermal and Physical Investigation of Chemically Treated and Untreated Oil Palm EFB Fiber 119

4.3.1 Evaluation of fiber surface morphology 119

4.3.2 EDX study of EFB fibers 120

4.3.3 FTIR study 121

4.3.4 Thermal stability 122

4.4 Mechanical characterizations of EFB fiber composites and formulations containing optimum flame retardants 125

4.4.1 Tensile properties 125

4.4.2 Flexural properties 129

4.5 Summary 130

5. Expandable graphite filled EFB fibre reinforced epoxy composite 134

5.1 Introduction 134

5.2 Characterizations of expandable graphite 136

5.2.1 EG expansion analysis 136

5.2.2 Diameter of expandable and expanded graphite 137

5.2.3 Flammability of EFB epoxy composites containing EG as filler and coating 138

5.3 Heat release properties 142

5.4 Thermal properties of EFB fibre epoxy composites containing EG as filler and coating 143

5.5 DMA analysis 147

5.6 Combined confocal Raman-AFM analysis 149

5.7 EDX analysis 154

5.8 Morphology of composites 156

5.9 Tensile properties 158

5.10 Flexural properties 161

5.11 Summary 162

6. Nomex honeycomb panels with EFB composite skins 164

6.1 Introduction 164

6.2 Fabrication of honeycomb panels 168

6.2.1 Preparation of face sheets of honeycomb panel 168
6.2.2 Preparation of the sandwiched panels 169
6.3 Characterizations of Nomex honeycomb sandwich structure 171
6.3.1 Compressive properties 171
6.3.2 Flexural properties of honeycomb core sandwich panels 175
6.3.3 Core shear ultimate stress from bending test 179
6.3.4 Bending stiffness 179
6.3.5 Plate core shear properties 181
6.3.6 Flammability of Nomex honeycomb panels with natural fibre based composite skins 184
6.3.7 SEM study 191
6.4 Summary 193
7. Conclusions and future work 195
7.1 Principle findings 195
7.2 Limitations 198
7.3 Recommendation for future work 199
References 201

List of figures

Figure 2-1 Physical and mechanical properties of various materials including several types of composites [30]. 8

Figure 2-2 Schematic view of airplane cabin [34]. 11

Figure 2-3 Typical cabin panel installation [33]. 12

Figure 2-4 The influence of different types of treatment on the EFB fiber [77]. 24

Figure 2-5 Justification of polymer type selection for this study. 33

Figure 2-6 Detailed categories of flame retardants [102] 39

Figure 2-7 Swelling system when polymer is exposed to fire in the presence of APP (the figure was quoted from Norwegian Pollution Control Authority or SFT). 40

Figure 2-8 Self-sustaining polymer composite burning cycle [110]. 42

Figure 2-9 The impact of EG particles on oxygen index percentage of PUR-PIR foam composites with different isocyanate index (150 and 250) [165]. 51

Figure 2-10 Cone calorimeter measurements of time to ignition (TTI), peak of heat release rate (p-HRR) and total of heat release (THR) for epoxy resin flame retarded with 5-50 wt% of EG [170]. 54

Figure 2-11 Flame adjustment and the specimen positioned for vertical Bunsen burner test [10]. 57

Figure 2-12 The specimens still burning after 180 s. a) TW_2 natural fiber, b) TW_1 natural fiber, c) UNI natural fiber, d) TW glass, e) PW glass and UNI glass fibre composite specimens [10]. 58

Figure 3-1 Chemical structure of epoxy compounds and amines [195]. 66

Figure 3-2 SEM micrographs of (a) untreated EFB fiber, (b) untreated EFB fiber after drying in the oven, which were purchased from Szetech Engineering Sdn. Bhd. and (c) EFB fiber provided from PolyComposie Sdn Bhd. 66
Figure 3-3 The chemical structure of Acrodur DS 3530. 66
Figure 3-4 SEM micrograph depicts the particle size of expandable graphite. 67
Figure 3-5 Mat fabrication process. (a) preparation of the required amount of fiber, (b) fiber soaking and dispersion, (c) draining the water, (d) filtered mat was shifted to plates with blotting papers, (e) sieve removal, (f) the fiber mat was placed between the metal plates, (g) the required load was applied, (h) the mat with an applied weight on top of it was placed in a convection oven, (i) removal of fiber mat from oven and (j) an evenly distributed EFB fiber mat. 68
Figure 3-6 Fabrication process using resin infusion technique. 69
Figure 3-7 Composite fabrication process. (a) plastic mould, (b) applying the gum tape and placing the EFB fiber mat, (c) laying the infusion mesh and peel ply, (d) laying the aluminum foil, (e) sonication process, (f) resin infusion, (g) curing for 24 hours and (h) a near view of composite. 70
Figure 3-8 The process of EFB fiber chemical treatment. 73
Figure 3-9 (a) control and EG filled composites and (b) EG coating composites. 76
Figure 3-10. Bomb Calorimeter equipment. 78
Figure 3-11. TGA testing instrument. 79
Figure 3-12 DMA instrument. 80
Figure 3-13 Preparation procedure of FTIR test. 81
Figure 3-14 Fractured tensile samples right after tensile testing. 82
Figure 3-15 A composite sample fractured under a three point bending load. 83

Figure 3-16 The furnace used for the tests. 85
Figure 4-1 The results of vertical Bunsen burner testing for the control specimen and the composite specimens filled with FR. 90
Figure 4-2 The chemical structures of APP (a) and ATH (b) [219]. 91
Figure 4-3 Reactions between ATH and APP [219]. 91
Figure 4-4. Reactions between ATH and APP at elevated temperatures [219]. 92
Figure 4-5. The test samples of (a) CAPP5, (b) CAPP10, (c) CAPP15, (d) CATH5APP10 and (e) CATH10APP5 composites after vertical Bunsen burner experiment. 94
Figure 4-6 The intumescent char of CATH5APP10 after vertical Bunsen burner test. 94
Figure 4-7. Bunsen burner results of formulations containing ZB, hybrid of ZB/ATH and hybrid of APP/ZB. 96
Figure 4-8 Images of burnt FR-based composites after veritcal Bunsen burner tests. (a) CZB5, (b) CZB10, (c) CZB15, (d) CATH10ZB5 and (e) CATH5ZB10. 98
Figure 4-9 The intumescent char of CAPP10ZB5 after vertical Bunsen burner test. 99
Figure 4-10. The degradation behaviors of the selected formulations containing APP and ATH. 105
Figure 4-11 Reaction 14 illustrates the charring mechanism of natural fibre without APP and reaction 15 shows the charring process with the presence of APP (fibre phosphorylation) [233, 237]. 106
Figure 4-12. Thermogravimetric analysis (TGA) curves of the control and composites containing ZB. 109
Figure 4-13 EDX analysis of CATH5APP10 sample. (a) spectrum magnified on the fiber after TGA test, (b, c and d) the spectrum magnified on all sample surface. 111

Figure 4-14. SEM micrographs of intumescent char of CAPP10ZB5 in different areas at magnifications of 1200 ×. 112
Figure 4-15. EDX of the intumescent char of CAPP10ZB5 and presence of elements. 113
Figure 4-16. The mapping of dispersion of the elements on the intumescent char surface (CAPP10ZB5) shown in this image. 114
Figure 4-17. EDX analysis and the mapping of dispersion of different elements in CAPP10ZB5 composite prior to the combustion. 115
Figure 4-18. SEM micrographs of char residue of the control in different areas at magnifications of 10000 ×, 1200× and 300×. 115
Figure 4-19. Morphology of (a) fiber/epoxy (control), (b) CATH5, (c) CATH10, (d) CATH15, (e) CAPP10 and (f) CAPP5ATH10 at 600 X. 117
Figure 4-20 SEM micrographs of (a) CZB5, (b) CZB10, (c) CZB15 and (d) CATH5ZB10. 118
Figure 4-21 SEM micrographs of (a) untreated EFB fibre, (b) 5% alkali treated EFB fibre. 119
Figure 4-22 The EDX results of (a) alkaline treated fiber, (b) untreated fiber. 120
Figure 4-23 FTIR spectra of untreated and alkali treated EFB fiber. 122
Figure 4-24 TGA analysis of untreated and treated fibres. 123
Figure 4-25 DTG curves of untreated and treated fibers. 124
Figure 4-26 (a) The stress-strain curves and (b) tensile strength and strain of formulations. 127
Figure 4-27 The Young's modulus of formulations. 128
Figure 4-28 SEM micrographs of (a) control, (b) treated control, (c) CATH5APP10 and (d) TATH5APP10. 128
Figure 4-29 The flexural properties of formulations. 130
Figure 5-1. Protection of expandable graphite for material during fire [267]. 135

Figure 5-2 SEM images of expandable graphite at 150 °C, 200 °C (Mag 250X) and 300 °C (Mag 250X was used to illustrate a clearer image of the expansion). 137
Figure 5-3 EDX results of EG heated at 300 °C and 200 °C (Mag 250X). 137
Figure 5-4 SEM micrographs of expandable graphite, expanded graphite from vertical Bunsen burner test and expanded graphite from TGA test (Mag 100X). 138
Figure 5-5 The CEG3, CEG5 and CEG7 specimens burned by vertical Bunsen burner test are shown along the width. 141
Figure 5-6 The CEG7 specimen burned by vertical Bunsen burner test are shown at different views along the thickness. 141
Figure 5-7 The images of coating5 sample at different views after Bunsen burner tests. 142
Figure 5-8. TGA results for formulations fabricated. 145
Figure 5-9 DTG curves for E100, EFB20E80, CEG3, CEG5 and CEG7. 146
Figure 5-10 Storage modulus of formulations. 148
Figure 5-11 Loss factor of neat epoxy, control and EG filled composites. 149
Figure 5-12 Elastic modulus of formulations at 30 °C. 149
Figure 5-13 White-light images of unburned and burned composite specimens. 150
Figure 5-14 Raman spectra attained from expandable and expanded graphite particles. 151
Figure 5-15 White-light images of (a) expandable graphite and (b) expanded graphite. AFM images of (c) expandable graphite and (d) expanded graphite. 152
Figure 5-16 Topography images of expandable graphite (a) 2-D and (b) 3-D as well as expanded graphite (c) 2-D and (d) 3-D. 153
Figure 5-17. EDX analysis of char residue for CEG7 after vertical Bunsen burner test in the air atmosphere at 100X: (a) the selected spectrum, (b) elements in the char residue. 155

Figure 5-18. EDX analysis of char residue for CEG5 after TGA test in the N_2 atmosphere at (a, b) 5000 X and (c, d) 1000 X. 155
Figure 5-19 Micrographs of EFB20E80 at magnifications of 300×, 600× and 1000× after tensile test. 156
Figure 5-20. SEM micrographs of control, EG filled composites and EG5 at 300X. 158
Figure 5-21 Tensile stress-strain curve of E100, C, CEG3, CEG5, CEG7 and EG5. 160
Figure 5-22 Young's modulus of E100, C, CEG3, CEG5, CEG7 and EG5. 160
Figure 5-23 Flexural properties of formulations. 162
Figure 6-1 A few cabin parts made of honeycomb composites are exhibited (Source: Aerospace DELO). 166
Figure 6-2 The core and face sheets of composite sandwich fabricated a sandwich panel (sources: NauticEXPO and Hexaflex). 167
Figure 6-3 Principle of bending strength and second moment of inertia for honeycomb core composites (Source: STRESS EBOOK LLC.). 167
Figure 6-4 Bonding of honeycomb to one of the skins which is at the bottom of core. 170
Figure 6-5 The final product which is a honeycomb core panel with 6 mm thickness. 170
Figure 6-6 Test set-up of a honeycomb sandwich structure subjected to the stabilized compression. 172
Figure 6-7 Specimen geometry of flat-wise stabilized compressive test at different views. 172
Figure 6-8 Deformation stages: Honeycomb panels prior to compressive test on the left images (initial regime) and honeycomb panels crushed after applying the load on the right side (crushing regime and densification). 174

Figure 6-9 Flat-wise stabilized compressive stress-strain curves of 4 selected specimens of sandwich composite panels (all specimens from different panels show similar trends). 175
Figure 6-10 Bending stress-displacement curves of all panel specimens with EG filled skins.. 177
Figure 6-11 Bending stress-displacement curves of all panel specimens with FR filled skins. . 177
Figure 6-12 Failure mode of honeycomb sandwiched panel with EG filled composite skin. 178
Figure 6-13 Failure mode of honeycomb core panel with FR filled composite skin. 178
Figure 6-14 (a) Plate shear test conducted by employing force line of action and (b) shear failure of Nomex core at different areas. 183
Figure 6-15 Shear stress-strain response where core was tensioned in its longitudinal direction. 183
Figure 6-16 Shear stress-strain response where core was tensioned in its W direction. 184
Figure 6-17 Detailed set-up of vertical burner test. Specimens located in a lab cabinet which has an exhaust hood: (a) Honeycomb core and (b) panel. 185
Figure 6-18 Vertical section of the specimens: (a) Nomex honeycomb core, (b) panel with EG filled composite skins and (c) panel with FR filled composite skins. Front section of specimens: (d) Nomex honeycomb core, (e) panel with EG filled composite skins and (f) panel with FR filled composite skins. 187
Figure 6-19 Smoke produced: (a) during the burning of Nomex honeycomb in the presence of Bunsen burner; and right after withdrawing the Bunsen burner from underneath (b) the EG panel's specimen and (c) FR panel's specimen. 188
Figure 6-20 Different sections of the composite specimens including (a) ATH5APP10, (b) EG7 and (c) APP10ZB5 burned by applying 60 s Bunsen burner flame vertically..... 190

Figure 6-21 (a) ATH5APP10 and (b) APP10ZB5 specimens produced visible smoke, (c) EG7 specimens showed lesser smoke. 191
Figure 6-22 SEM images of Nomex honeycomb core. Transverse section of Nomex honeycomb cell at (a) 60 × and (b) 36 ×. 192
Figure 6-23 SEM micrographs of panel with EG filled skin from two different cells. Vertical section of panel after removal of top skin after flexural test. 193

List of tables

Table 1-1 Cone calorimetry results of some NF epoxy composites. 3

Table 2-1 Natural fiber composites in automotive applications. 9

Table 2-2 Materials applied in current aircraft interiors [32]. 13

Table 2-3 Flammability criteria for partitions, ceilings, lavatory, stowage bins, flooring, upper sidewall, and lower sidewall (cabin liners). 14

Table 2-4 Definition and measuring method of burn length, drip flame time, flame time and ignition time. 16

Table 2-5 The flammability requirements of FAR 25.853 (a) and FAR 25.853 (b) for cabin materials [34]. 16

Table 2-6 The limit values for toxic gases (Airbus specifications) as collected from pinfa association. 17

Table 2-7 Minimum requirements of lab scale mechanical properties for aircraft interior furnishings) based on ASTM standards. Compilation from major aircraft companies [37-51]. .. 18

Table 2-8 Merits and drawbacks of crop fibers over traditional inorganic fibers as reinforcement in a polymeric material [31, 59-65]. 20

Table 2-9 Comparison of the density and mechanical properties among different fibers and thermoset material [19, 66-75]. 21

Table 2-10 Oil pam fiber contents [77]. 23

Table 2-11 Physical and mechanical characteristics of oil palm fiber [77]. 23

Table 2-12 Varying mechanical and thermal properties of palm and other natural fibers composites due to different fiber treatments (comparison between treated and untreated fibers composites). 27

Table 2-13 Comparison of mechanical properties between the palm/sisal rubber composites reinforced with either optimal alkali treated (4 wt% concentration) fibers or silane treated fibers [90]. 29
Table 2-14 Thermal degradation temperatures of different natural fibers and EFB fiber composite. 30
Table 2-15 The impact of fiber mass fractions on the mechanical properties of natural fiber composites..... 31
Table 2-16 Comparision between thermoset and thermoplastic properties [96]. 33
Table 2-17 Advantages and disadvantages of thermosets [96]..... 34
Table 2-18 Merits and drawbacks of thermoplastics [96]. 34
Table 2-19 Thermosets vs. thermoplastics in aero-grade industry. 34
Table 2-20 Typical Physical, chemical and mechanical properties of phenol formaldehyde resin (resole type) [97]..... 36
Table 2-21. General properties of epoxy vs. phenol resins [96]..... 37
Table 2-22 TGA results for biocomposites [4]. 44
Table 2-23 Cone calorimetry results of composites [4]..... 44
Table 2-24 LOI and UL-94 classification results [124]..... 45
Table 2-25 The calorimetry test results of the biocomposites [124]. 45
Table 2-26 The results obtained from cone calorimetry tests [125]. 46
Table 2-27 The results of flammability test [126]. 46
Table 2-28 The results of cone calorimetry study for PP, OPP (nanoclay filled PP composite) and nanocomposites reinforced with 10 wt%, 20 wt% and 30 wt% fiber [132]. 47

Table 2-29 Suitable halogen-free flame retardants (HFFR) for various resins and polymers used for interior components of car, bus, rail vehicles, ship and aviation. (pinfa association [164])... 49

Table 2-30 Cone calorimeter test results of PUR-PIR foam composites and the effect of EG on flammability parameters [165]..... 52

Table 2-31 TGA results of foam based composites varying expandable graphite [165]..... 52

Table 2-32 UL-94 and LOI results of polystyrene flame retarded by EG [170]. 53

Table 2-33 The physical and chemical properties of different types of EGs..... 55

Table 2-34 The EVA formulations loaded with several types of EG show different flammability characteristics..... 55

Table 2-35 The effective heat of combustion (EHC) and time to ignition (IT) obtained from cone calorimeter test..... 56

Table 2-36 The results of vertical burner tests for the epoxy composites reinforced with flax and glass fibres [10]..... 57

Table 2-37 Summary of the recent researches on Nomex core panels with composite skins. 59

Table 3-1 Sample designation (The concentration of constituents is shown by wt%). 72

Table 3-2 Sample designation (values represent wt %)..... 74

Table 4-1 The gross heat of combustion of E100, control and composite samples filled with FR from bomb calorimeter experiment. 102

Table 4-2 Gross heat of formulations. 103

Table 4-3 TGA results of the control and formulations loaded with APP and ATH..... 105

Table 4-4. TGA results of the control and formulations containing ZB..... 108

Table 4-5 T_{onset} (°C) at 5 wt%, T_{20}, T_{max} and residual weight (%) at 600 °C. 123

Table 5-1 The results of vertical Bunsen burner tests..... 140

Table 5-2. Gross heat of combustion for E100, C and EG filled formulations. 143

Table 5-3 Residual weight at varying weight temperatures..... 145

Table 5-4 Surface roughness of expandable and expanded graphite particles. 154

Table 6-1 Formulations used for the fabrication of face sheets with their constituents by weight percentage (wt%). 169

Table 6-2 Out-of-plane compression performances of honeycomb panels. 175

Table 6-3 Vertical Bunsen burner results of different structures..... 186

Table 6-4 Vertical Bunsen burner results (60s test) of Nomex core and different optimum composites..... 189

List of abbreviations

ATH Alumina Tri-hydrate

APP Ammonium Phosphate

ZB Zinc Borate

EFB Empty Fruit Bunch

OPF Oil Palm Fiber

FR Flame Retardant

IFR Intumescent Flame Retardant

EG Expandable Graphite

FAA Federal Aviation Administration

FAR Federal Aviation Regulations

GH Gross Heat of combustion

TGA Thermogravimetric Analysis

DMA Dynamic Mechanical Analysis

NF Natural Fibre

NBS National Bureau of Standards

OSU Ohio State University

SEM Scanning Electron Microscopy

EDX Energy Dispersive Spectroscopy

AFM Atomic Force Microscopy

NaOH Sodium Hydroxide

FTIR Fourier Transformed Infrared Spectroscopy

ASTM American Society for Testing and Materials

T_g Glass Transition Temperature

wt Weight

T_{onset} Onset Temperature

pHRR Peak of Heat Release Rate

TTI Time to Ignition

EHC Effective Heat Combustion

T_d Thermal Degradation Temperature

HRR Heat Release Rate

tHR Total Heat Release

TSR Total Smoke Release

PF Phenol Resin

SEA Specific Extinction Area

LOI Limit Oxygen Index

Chapter 1

1. Introduction

The market of components for aircraft interior is doubled in terms of its manufacturing services and consumption of composite materials compared to the usage of composites in aircraft structural parts. In the commercial industry, the weight of aircraft composites used for interior parts surpasses the weight of those employed in composite airframe, and it is no less crucial to the revenue generation and operating cost relative to primary structures. The projected plan expects a dramatic increase in production of interior components beyond 14.5 million kg by 2022, which demonstrates 50 percent higher demand than composite airframe parts ordered in 2012 [1]. Aircraft interior parts such as overhead storage bin, partition panel, sidewalls, lavatory compartment, door and window liners, flooring and seat backing must meet the stringent aviation requirements generally governed by the Federal Aviation Administration (FAA) agency and aircraft manufacturers.

To enhance sustainable credential of carbon footprint, the dependence on thermoset matrix and synthetic fibers are needed to be reduced. The unrelenting passion of sustainability has led to an expanding search for eco-friendly fiber reinforcement composites from renewable sources. Demand for replacement of synthetic fibers materials with natural fiber composites is growing. Production of carbon or glass fiber composites consumes a large quantity of energy cost and also these materials experience difficulty in their disposal at the end of life cycle due to their poor recyclability [2]. Industry has been compelled by consumer awareness and stringent environmental registration to develop usage of natural resources. Lignocellulosic fibers are capable of contributing to the stiffness and strength of composites [3]. The usage of natural fiber (NF) composites have been gaining momentum in several applications such as non-structural parts of

automotive, furniture and food packaging industries due to their renewability, availability, low density, low cost, suitable mechanical performances, good acoustic insulation properties, non-abrasiveness and green working environment [4-8]. However, there are several drawbacks in the use of natural fiber reinforcement in composite, e.g. price and quality variation, low durability and low moisture resistance, limited application temperature and poor fire resistance. The hydrophilicity of natural fibers causes moisture absorption and increases the potential of delimitation and swelling within the composite. Flammability of natural fiber polymeric composite is required to be extensively investigated as fire risk and hazard to both aircraft and human is of critical concern.

Several reports have been published on the flammability properties of NF reinforced epoxy composites, as shown in Table 1-1. It can be observed that natural fibre composites not containing phosphorous content or FR additives [9-11] presented higher values of PHRR, tHR, HRR, TSR, mean CO_2, CO_2/CO ratio and mass loss. With the incorporation of a curing agent possessing 1.75 wt% P content, as recorded in [11], the values of PHRR, tHR, mean CO_2, CO_2/CO ratio and mass loss reduced relative to those of without phosphorus filled composites whereas the mean CO increased. Increasing content of APP (P content) in the natural fibre composites, as reported in [9], further decreased the PHRR, tHR, HRR, TSR, mean CO_2, CO_2/CO ratio and mass loss while mean CO increased.

The effects of other FR agents such as ATH and ZB on the flame resistivity of NF epoxy composites are required to be investigated. Combinations of different FRs have not been investigated for this kind of composites. The addition of EG particles has not been studied for NF epoxy based composites. Most importantly, NF epoxy composites have not been used as skin sheets for Nomex honeycomb panels.

Table 1-1 Cone calorimetry results of some NF epoxy composites.

NF (wt%)	Epoxy	FR (wt%) and P content	PHRR (kW/m^2)	tHR (MJ/m^2)	Mean HRR (kW/m^2)	TSR (m^2/m^2)	Mean CO_2 (kg/kg)	Mean CO (kg/kg)	CO_2/ CO ratio	Residue (wt%)	Ref.
40	infusion grade (epoxy) A 10% fast /90% slow (curing agent)	–	426-563	143-157	–	3788-4332	–	–	–	–	[10]
30	tetraglycidyl ether of pentaerythritol (epoxy) 3,30´-dimethyl-4,40´-diamino-dicyclohexyl-methane (curing agent)	–	~1320	84.91	–	–	1.3534	0.0352	38.4	1.8	[11]
30	tetraglycidyl ether of pentaerythritol (epoxy) phosphorus-containing amine (TEDAP) (curing agent)	1.75 % P content in hardener	~780	45.89	–	–	0.8948	0.0723	12.3	20.1	[11]
35	Bisphenol A epoxy resin modified (epoxy) Modified cycloaliphatic polyamine (curing agent)	–	720.5	68	121.6	1612.2	1.7953	0.0655	27.4	11.8	[9]
30	Bisphenol A epoxy resin modified (epoxy) Modified cycloaliphatic polyamine (curing agent)	APP (3 wt%) and 0.94%	375.3	42	69.2	1233.3	1.4838	0.1313	11.3	22.3	[9]
30	Bisphenol A epoxy resin modified (epoxy) Modified cycloaliphatic polyamine (curing agent)	APP (8.8 wt%) and 2.77%	293.8	33	59.5	1104.5	1.3275	0.1532	8.6	24.3	[9]
30	Bisphenol A epoxy resin modified (epoxy) Modified cycloaliphatic polyamine (curing agent)	APP (16 wt%) and 5%	186.7	27	48.6	1006.7	1.2884	0.1641	7.8	31.1	[9]

In this research, the application of palm EFB fiber epoxy composites for aerospace industry was investigated. Interior parts were targeted to be fabricated by palm fiber polymeric composite for the evaluation against the requirements of aerospace components.

1.1 Problem statement and objectives

The main purpose of this study is to overcome the poor nature of natural fibers in terms of moisture, thermal and mechanical properties to be potentially capable of meeting the aircraft interior requirements of FAA, other aircraft agencies and aircraft manufacturers. Fire safety is the main specification of these requirements. Overall, in order to employ any components in aircraft interior, the flammability, smoke, toxicity and thermal as well as mechanical requirements are required to meet. To date [9, 10], very few researches have been carried out on the usage of natural fiber polymeric composites for aircraft industry. The question is that whether NF based composites can

be used to replace glass/carbon fibre reinforced polymeric composites employed in aircraft interiors? In fact, are they capable of passing the FAA and aircraft manufacturer requirements after enhancing their flame resistivity, reduced heat release and mechanical performances?

The core objectives of this study were:

(a) To characterize, optimize and gain an enhanced understanding of, the fire, heat release, thermal resistive and mechanical performances of EFB fibre reinforced composites following the inclusion of flame retardant agents (APP, ATH and ZB) and their hybrids.

(b) To characterize, optimize and gain an improved understanding of, the ignitibility, heat release and thermal degradation behaviors as well as the lab-scale mechanical properties of EFB fibre composite filled/coated with EG particles.

(c) To determine the improvement of mechanical performances of EFB fibre composites following the alkaline treatment.

(d) To investigate the structural and flammability responses of honeycomb sandwiched panels with EFB fiber reinforced composite skins.

1.2 Hypothesis

Bio-fiber polymeric composites have engaging properties e.g. their cheap price, renewability and high strength to weight ratio. One of the potentials of empty fruit bunch, except for its availability, is possessing lower density in comparison with that of other natural and synthetic fibers. Its low density is one of the main drivers which demonstrates potential in the field of aerospace industry. However, the fallbacks such as flammability behavior of EFB (similar to other NFs), poor compatibility of EFB with polymeric matrices of hydrophobic nature, and the high processing temperature of thermoplastic polymers (which adversely affects physio-mechanical performances

of NFs) [4] broadly limits their wider application, in particular towards aviation industry which governs by an exhaustive set of stringent regulatory requirements. Natural fiber reinforcement polymeric composites have been widely used in the automotive, furniture and packaging industry where the requirement of fire safety is not as stringent as federal aviation administration (FAA) [12, 13]. The appealing properties of NF outweigh their unfavorable characteristics and some remedies can be applied for the latter.

Remedial measures such as physical and chemical modification, in particular inclusion of fire retardant additives, enhanced the flame resistivity of composites [14, 15]. The main role of a flame retardant is to discontinue or suppress the burning of materials [16-18]. FRs are capable of acting either physically or chemically in the form of condensed, gas or solid states. Physical mode occurs by fuel dilution and creation of a defensive layer upon combustion, whereas chemical mode takes place by condensed phases and gaseous reactions [15].

Cellulose, hemicellulos and lignin are the main elements of natural fibers. Cellulose parts affect directly the flammability; more cellulose content causes greater flammability. Additionally, higher lignin content makes higher charring properties and reduces the degradation temperature [19-21]. Once natural fiber is exposed to high thermal condition, it leads to swelling, contradiction or expansion in natural fiber composite. One of the methods to partially alleviate the moisture absorption is heating the natural fibers at about 80 ºC for 24 h prior to composite fabrication. Chemical fibre treatment can significantly alleviate all the above-mentioned issues relevant to NFs.

Thermosets create a greater cross-linked 3-D network with natural fibers upon curing than that of thermoplastics [22]. Thermosetting resins possess low viscosity prior to crosslinking which eases fabrication process through liquid composite molding techniques and demonstrate low processing temperature. In addition, processing of thermosetting composites can be performed with much

lower processing pressure than that of the thermoplastic polymers [23]. Resin infusion technique and compression molding process can be of the best methods for fabrication of the composite. Fabrication of complex and relatively large shapes is of the merits of these techniques. On the other hand thermoplastics can be reprocessed a few times, however their thermal and mechanical properties decreased after each repeated thermal recycling [24]. Moreover, reusability of thermoplastics dramatically decreased with the addition of natural fibers [24, 25].

The key elements in the design of interior components, according to FAA and aircraft manufacturers, are the investigation and analysis of flammability, smoke, heat release as well as mechanical behaviors of materials. The fabrication, characterizations, formulations and optimizations of EFB fiber reinforced composite were carried out using

- different flame retardant fillers including Alumina trihydrate (ATH), Ammonium polyphosphate (APP) and Zinc borate (ZB), which have been shown to be suitable fire retardants to be mixed with epoxy resin in interior parts of transportation industry (as recommended by pinfa association of flame retardants in transportation; pinfa is a sector group of Cefic, the European Chemical Industry Council),
- expandable graphite (EG) particles as an effective sort of flame retardant,
- varying flame retardant loadings,
- fiber chemical treatment and
- composites with honeycomb structure.

2. Literature review

2.1 Introduction

The superiorities of composites over metals in aircraft industry emerge as feasibility to be tailored into more complex form, greater physical characteristics, corrosion resistance, stiffness to density ratio and unique strength. The application of composites structures has been rising in primary structures such as fuselages and wings. As knowledge in this technology flourished, the fuselage weight of A380 consists of approximately 20-22 % carbon fiber reinforced polymer (CFRP) and glass-fibre reinforced aluminum alloy composites, and 40 % weight of modern Eurolighter is made of CFRP [26].

Why composites are preferred over other materials in aircraft industry? The composites show greater stiffness and strength over weight. Figure 2-1 provides some comparative information on the mechanical and physical properties of wood, plastics, fibre reinforced composites and several metal materials. Wood, plastics and composites show lower density than that of concretes, aluminum, titanium and steel. It also displays that the tensile strength and modulus of composites are comparable with those of metals.

However, the purpose of today's world in aerospace sector is to improve material's sustainable credentials and lower carbon footprints. The ambition of science would be reaching lower cost and renewable reinforcement materials with great performance. A lot of progress has been achieved on the replacement of carbon and glass fibers with natural fibers from sources such as agro waste, animals, crops and plants sources i.e. oil palm, sisal, flax, hemp, kenaf, cotton, bamboo, coconut, coir and so on [27-29], which mostly non-structural automotive parts and common household utilities have been targeted for this replacement.

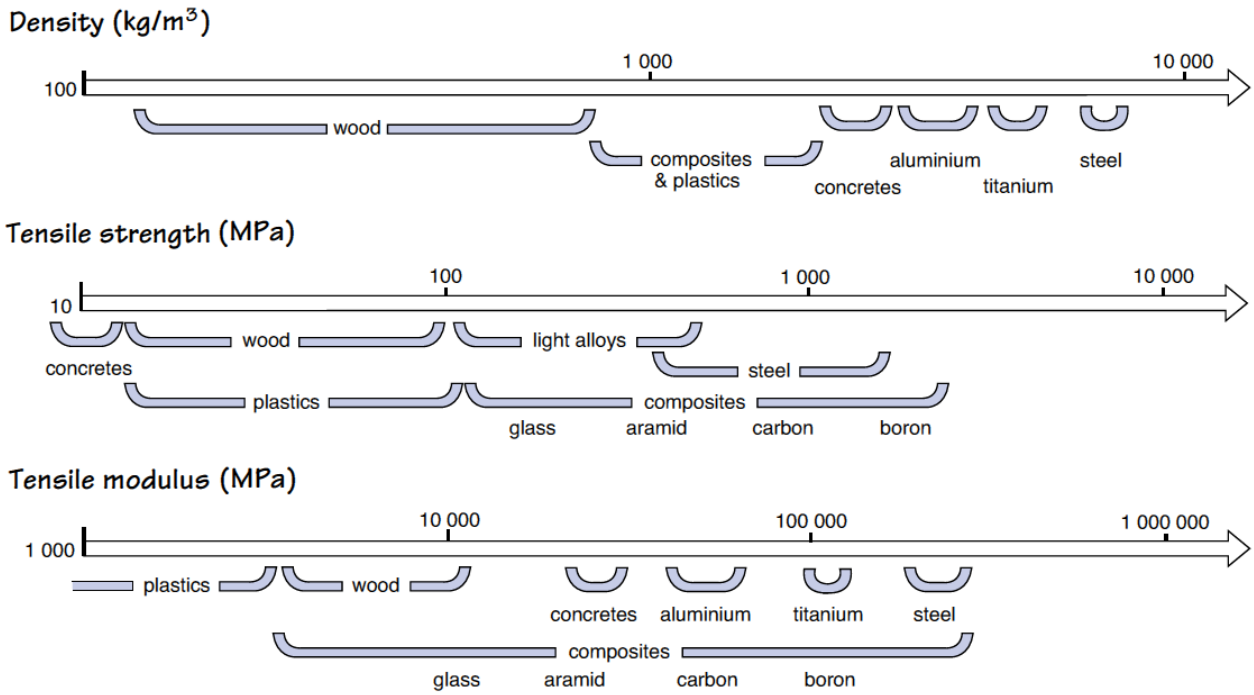


Figure 2-1 Physical and mechanical properties of various materials including several types of composites [30].

Currently natural fiber composites have been used in different application of automotive industry, as shown in Table 2-1, but very few studies have been carried out for their usage in aerospace applications. Considering the applications of natural fiber composite in automotive parts, employing composites in aerospace interior parts is a practical possibility but with impending issue requiring further improvement which formed part of the major aim of the current research work.

In essence, the main objective of this study is to overcome the drawbacks of natural fibers reinforced composite through methodologies such as incorporation of varying formulations of flame retardants, fiber treatments, suitable thermosetting choice, expandable graphite and honeycomb structure to enhance its mechanical, thermal and flame retardation properties.

Table 2-1 Natural fiber composites in automotive applications.

Material	Application	Vehicle's part	Ref.
Sisal-flax fiber mat epoxy composite	Mercedes benz (E-class)	Door panels	[14]
Lingnocellulosic fiber	Construction industry	Partition board, ceiling and panel	[31]
Flax fiber-reinforced polypropylene	Chevrolet impala (2000 model)	Rear shelf trim panels	[31]
Flax fiber-reinforced polypropylene	Heavy trucks	Freightliner century COE C-2	[31]
Coconut fibers natural rubber latex	Mercedes benz (A-class)	Seats	[31]

2.2 Aircraft Interiors

Aerospace interior components consist of both visible and invisible parts. Invisible items such as supporting structures, blankets, insulation, wiring and ducting, and visible parts such as windows, closets, bag racks, stowage bins, sidewalls, ceilings, lavatories, seats and flooring. Polymers form the major products of interiors including adhesives, sealant, foams, textile fibers (carpets or fabrics), honeycomb sandwich composites and molded shapes or sheet. Items known as payload parts, e.g. passengers' clothing, magazines, newspapers, cargo and luggage, are crucial to be considered for fire issues, but since the control of fire resistance for these items is very hard to achieve, they have not been taken into account in this area of research [32].

The materials used in interior components are required to be light and acceptable for cosmetic requirements as well as possessing fire-resistant properties. However, no composite material has been likely recorded to be optimal and show the incapability of toxic products and generating smoke, in addition to non-flammability. Besides, the requirements of each part probably confine the application of materials which must be considered in terms of fire-related characteristics.

Calamitous fire cases have happened in post-crash accidents while in-flight fires also have been caused.

In this study, accessible zones within the aircraft interiors for in-flight fires have not been taken into account since the fire can be immediately extinguished by trained flight crew using extinguishing equipment, and, of course, warning systems along with early detection are often well designed. But, inaccessible fire areas are very difficult to be extinguished, and maybe flight takes a long time to land and evacuate the passengers. Therefore, materials with long-term fireworthiness which generate exceptionally low levels of flammability are required to be employed for inaccessible aircraft interiors that are the target of this area of research [32, 33]. The adequate time for passengers to evacuate an aircraft in a post-crash fire scenario is imperative. The passengers would only survive if they leave the aircraft prior to any exposure to toxic, smoke and heat source from fire. The aforementioned scenarios can cause physical and mental impairment as well as visual obscuration.

2.3 Requirements and design for interior components of aircraft

The aircraft interiors are defined as every part which is inside of the pressurized shell of the fuselage. Part 25 of the regulatory requirements of FAR, which applies to interior parts, falls in FAR 25.855, baggage compartment or cargo, and FAR 25.853, compartment interiors [34]. The focus of this study would be to meet the requirements of cabin liners such as partitions, ceilings, lavatory, stowage bins, upper sidewall, lower sidewall and ducting materials. Figure 2-2 shows the interior cabin liner parts.

The interior cabin liner components would be designed to satisfy the requirements of the manufactures, airline crew and passengers, the airlines, other regulatory agencies and the FAA. The design criteria of interiors' requirements are emanated from the above-mentioned groups. Particularly, the fire safety criteria are recommended by FAA regulatory.

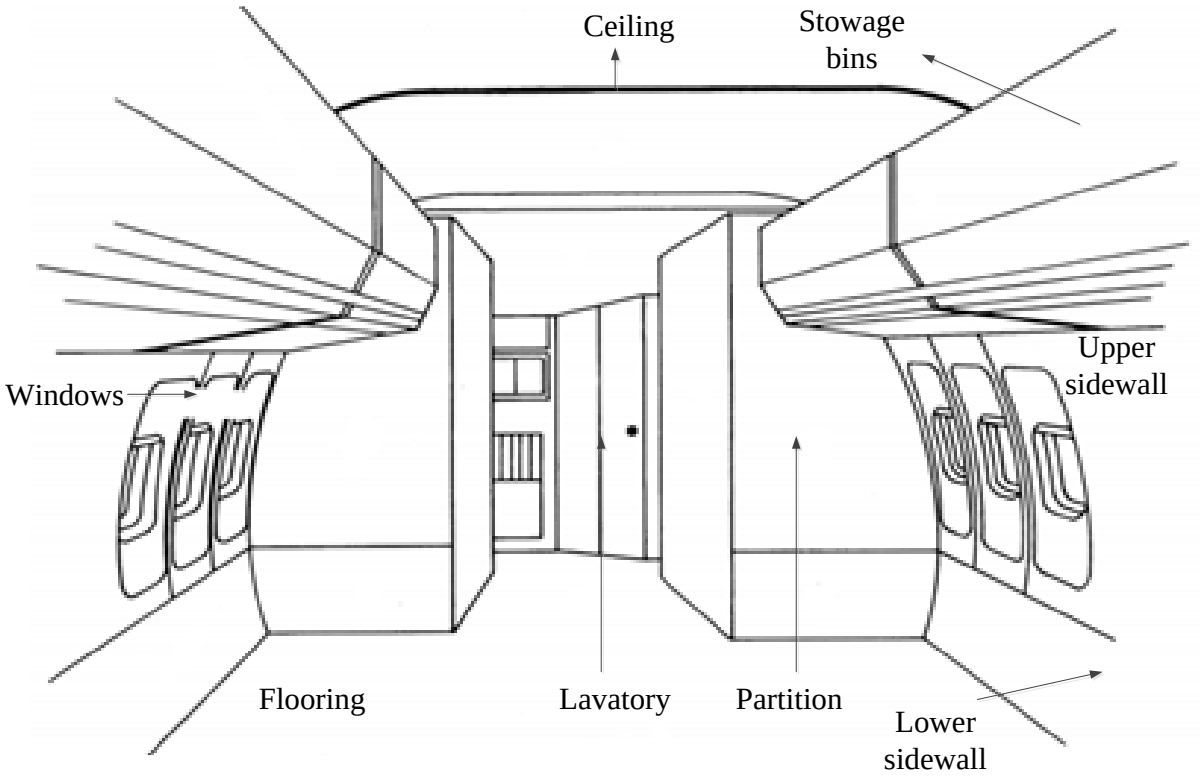


Figure 2-2 Schematic view of airplane cabin [34].

2.3.1 Aircraft materials and interior panel structures

Sandwich structures are normally used in the interior aerospace industry while some monolithic laminate can also be employed. The advantage of the sandwich construction is its high stiffness and strength to weight ratio along with a multitude of design possibilities to customize the end

properties. Depending on application, various panels with different decorative coverings, core, adhesives and face sheets can be employed [32-34]. Some panels for specific applications are shown in Figure 2-3 (FAR 25.853(a) and (a-1) are required to be met for these panels).

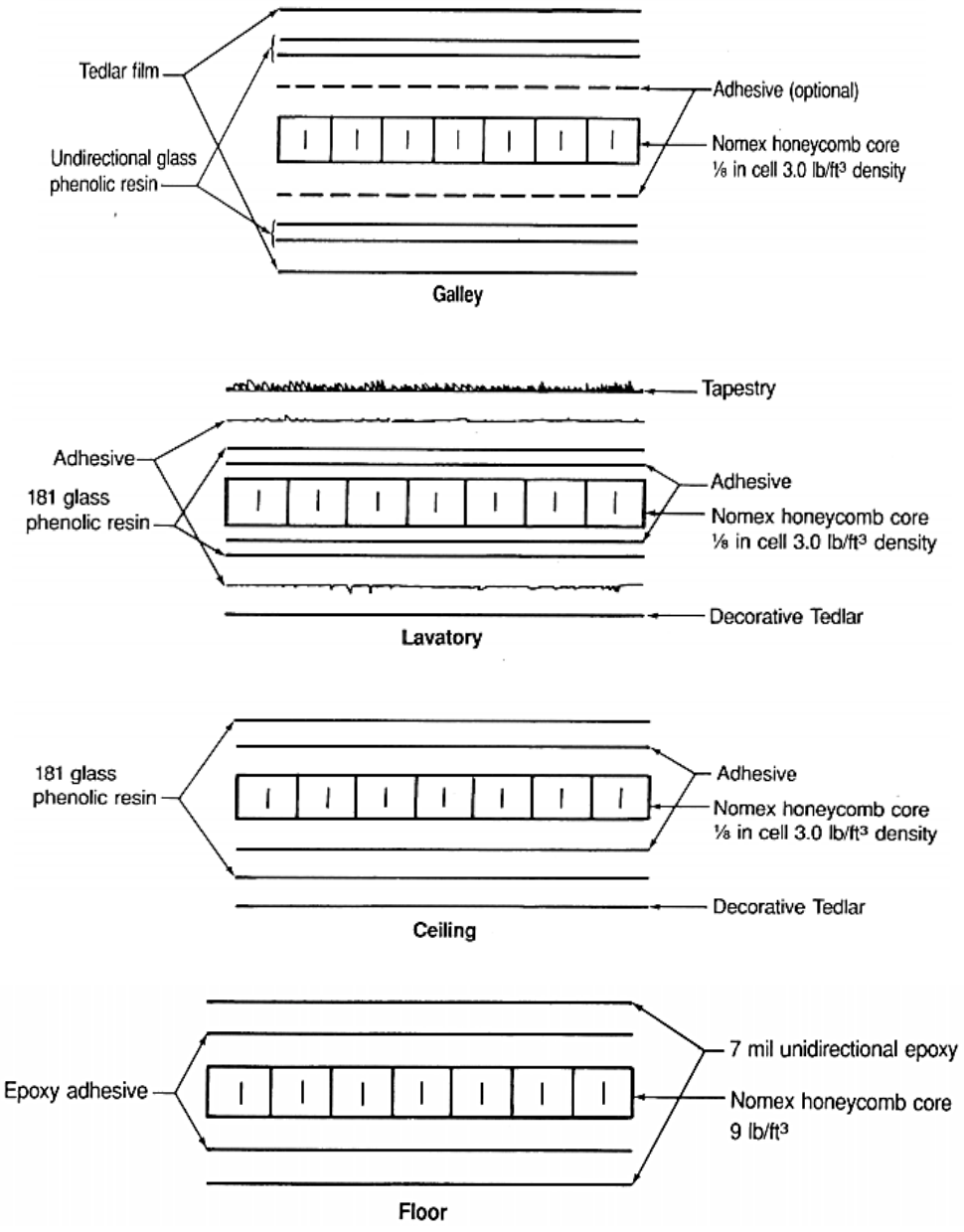


Figure 2-3 Typical cabin panel installation [33].

Ceiling and vertical surfaces are currently made of sandwich panels from a Nomex polyaramid core and face sheets of carbon fiber or fiberglass reinforcement and phenolic resin. A combination of fiber and resin can provide a face sheet. Commonly woven and unidirectional fiber reinforcing materials have been used to configure the face sheets. Fibers are required to possess suitable fire resistance and high strength. Traditional fiber materials such as carbon/graphic fibers and aromatic polyamides have depicted very high strength to weight ratio but are more expensive. Fiber glass is a lower cost alternative which is favorable for most common application with lower strength and modulus requirements. Table 2-2 shows the common material's types applied to different aircraft interior components.

Table 2-2 Materials applied in current aircraft interiors [32].

Applications	Materials
Air ducts	Glass/phenolic, epoxy, or polyester for large ducts
Passenger service units	Carbon or glass/phenolic
Stowage bins	Carbon or glass/phenolic/Nomex honeycomb
Partitions	Glass or carbon/phenolic/Nomex honeycomb
Overhead stowage bins	Carbon or glass/phenolic/Nomex honeycomb and edge urethane foam layer and reinforcement
Upper sidewall panel	Carbon or glass/phenolic
Lower sidewall panel	Carbon or glass/phenolic/Nomex honeycomb
Floor and floor covering	Carbon or glass/epoxy or phenolic/Nomex honeycomb floor panels

In the middle 1960s epoxy resins were broadly employed in various applications. By the start of 1970s phenolic resins were utilized as well. Although they usually include lower strength but low smoke emissions and fire resistance are of its good characteristics. Where presence of phenolic

resin is not obtainable and/or higher strength is needed for a particular application, epoxy resin is used [34].

2.3.2 Fire-resistant criteria

The wider part of FAA regulatory requirements, to a great extent, is on flammability, particularly for interior furnishings. The parameters for interior cabin liners involve the flame time, burn length, drip flame time, smoke density, heat release rate and total heat release, as shown in Table 2-3, as well as toxicity. Other interior components including cargo liners and seats are required to meet the kerosene oil burners of the type employed in furnaces (home heating sort) which is quite a stringent method. The available criteria belong to the interior cabin furnishings involving stowage bins, partitions, ceilings and sidewalls.

Table 2-3 Flammability criteria for partitions, ceilings, lavatory, stowage bins, flooring, upper sidewall, and lower sidewall (cabin liners).

Test method	Specification	FAA acceptance requirements
Smoke test	National Bureau of Standards (NBS) smoke chamber	Less than specific optical density* of 200 for the period of a four-minute test
Heat release*	Ohio State University calorimeter	Less than total of 65 kW. min/m^2 - for the duration of the first two minutes Less than peak rate of 65 kW/ m^2 - in the course of a five-minute test
Flammability	[(1)]12 s vertical Bunsen burner	3-second > drip extinguishing time 15-second > sample extinguishing time 152 mm > burn length

* Specific optical density: The amount of smoke generated per unit area (a dimensionless measure) according to light transmittance measurement.

* Heat release (total): The amount of energy emitted by the sample when burned.

* Heat release rate (peak rate): Highest heat energy emitted by the specimen when burning most severely.

(1) 60 s vertical Bunsen burner test requirements are mentioned in “Section 2.3.2.2”, which is of the requirements of panels whereas 12 s vertical Bunsen burner test is the only FAA test method required to be conducted for air ducting materials.

2.3.2.1 Ohio State University (OSU) heat release testing

Ohio State University test is a quantitative technique to analyze the way a specimen burns. The samples pushed into the burning combustion so that the rate of heat release (RHR) can be measured for products of the composite specimen [35].

Based on FAR 25.853 (a-1) or ASTM E906, this apparatus has been recommended and widely employed for measurement of the heat release of aircraft interior parts. Major aircraft companies including Boeing, Douglas, Daimler-Benz Aerospace, British Aerospace and Airbus are being obliged to employ this test documentation [15, 32]. According to heat release criteria, when heat flux of 35 kWm^{-2} is applied to the sample, an average total heat release is required to be less than 65 kW. min. m^{-2} during the first two minutes of running, and within the five minutes of experiment an average maximum heat release must be below 65 $kW.m^{-2}$ [36]. The specimen is required to insert horizontally in the chamber where a constant flow of air passes. The sample's thickness must be less than 45 mm, and the length and width needs to be 150 mm × 150 mm.

In order to measure the heat release rate and/or intensity of combustion, other methods have also been utilized. The instruments used for these methods are cone calorimeter, bomb calorimeter, limit oxygen index (LOI) and pyrolysis combustion flow calorimeter (PCFC) [15]. Bomb calorimeter was used in the current research study.

2.3.2.2 Resistance of materials to flame (as stated in Federal Aviation Regulation, FAR 25.853 and 25.855)

The vertical Bunsen burner test is carried out to measure the burn length, drip flame time and flame time of specimens. The definition and measuring method of each parameter is shown in Table 2-4.

Table 2-4 Definition and measuring method of burn length, drip flame time, flame time and ignition time.

Burn length (mm)	The distance from the original sample edge to the farthest proof of damage to the test sample. The damage places are owing to the combustion of that parts including parts of embrittlement, charring or partial consumption but not areas where material has melted away or shrunk from the heat nor including areas discoloured, warped, stained, or sooted.
Drip flame time (s)	The time in which flaming material lasts to flame after dropping from the sample to the bed of chamber. Three conditions might happen. First, on the condition no material drops from the sample, drip flame time is reported 0 s with the notation "No Drip". Second, if more than one drip fall, longest flaming drip is reported as the drip flame time. Third, once subsequent flaming drips reignite earlier drips which are flamed, the sum of all flaming drip time is reported as the drip flame time.
Flame time (s)	The time the sample continues to flame after the Bunsen burner flame is taken off from the beneath the sample.
Ignition time (s)	The time the burner flame is applied to the sample; either 12 or 60 s is acceptable for a particular part.

At least three samples are required to be tested, and samples must be rectangular (75 mm by 305 mm with required thickness). The flame height will be adjusted 38 mm and the sample is inserted with its lower edge, 19 mm higher than the level of the top of the burner. The flame for 12 or 60 seconds is employed, as considered, and then removed by either turning off the burner or moving the burner 76 mm (at least) from the sample. Depending on the ignition time, different conditions become acceptable as follows (

Table 2-5).

Table 2-5 The flammability requirements of FAR 25.853 (a) and FAR 25.853 (b) for cabin materials [34].

Ignition time (s)	12 s- FAR 25.853 (b)	60 s- FAR 25.853 (a)
Average Flame time (s)	below 15	below 15
Drip flame time (s)	below 3	below 5

Average Burn length (mm)	below 152	below 203

2.3.2.3 Testing for Smoke and toxicity assessment

This test is required to be done in National Bureau of Standards (NBS) chamber. Smoke optical density has to be less than 200 (dimensionless) for the period of four minutes. Furthermore, the limit value (parts per million, ppm) for toxicity has been specified by Airbus with the technical specification norm of ABD 0031. Table 2-6 shows the limit value of each toxic gas.

Table 2-6 The limit values for toxic gases (Airbus specifications) as collected from pinfa association.

Toxic gas	Limit value (ppm)
CO	1000
NO/NO_2	100
H_2S/SO_2	100
HCN	150
HCI	150
HF	100

2.3.3 Lab scale mechanical standards of interior aircraft components

Table 2-7 displays the values of different mechanical performances, collected from aircraft manufacturers, which define the requirements of aircraft interiors based on ASTM standards. Thermoplastics and advanced thermosetting materials have been used for the production of interior parts. Major aircraft companies such as BASF Aerospace Materials, EVONIK industries, Gurit, KYDEX, Sabic Innovative Plastics, etc are producing the aircraft interiors with these performances. The requirements of Federation Aviation Regulation of 25.853 paragraphs (a), (c) and (d) have been met for the aircraft parts.

The thicknesses of 0.71 to 12.70 mm can be fabricated for different interior components, which is dependent upon the interior application, aircraft manufacturer and aircraft model. The materials which can meet these requirements possess the capability to be employed in interior components including window reveals, tray tables, toilet shrouds, side wall panels, passenger service units, molding strips, lightening housings, life vest shrouds, lavatory floor pans, instrument panels, galley parts, escape slide pack boards, air ducts, bulkhead laminates and armrests.

Table 2-7 Minimum requirements of lab scale mechanical properties for aircraft interior furnishings) based on ASTM standards. Compilation from major aircraft companies [37-51].

Mechanical properties	Value
Tensile strength (MPa)	Not less than 23
Elongation (%)	Not less than 1
Flexural strength (MPa)	Not less than 63
Modulus of elasticity (GPa)	Not less than 2.22
Notched Izod Impact (for composites with the thickness > 3mm)	Not less than 53 J/m

2.3.4 The most probable parts to be fabricated from natural fibre composite

Considering the dimension, design and payload of aircraft interior components, natural fiber composites potentially can be used as composite skin for ceilings, sidewalls, partitions, galleys and lavatories. These aircraft parts consist of one or two layers of skin on top and at the bottom of a honeycomb structure. Therefore, composite skins that are capable of meeting the flammability, thermal and mechanical requirements of FAA and major manufacturer companies could possibly be considered by aircraft manufacturers for constructions of the relevant cabin panels. The interior components including placards, passenger service units, covers and air ducts which do not require to have honeycomb sandwich structures are also capable of being produced using natural fiber composites that meet the aircraft requirements.

The requisite to decrease fabrication costs has applied excessive pressures on aircraft interior designers to create production systems with ease of assembly and manufacturing. Natural fibers can be used as two different forms including chopped fibers and mat. Based on the type of fiber reinforcement, various fabrication techniques can be employed. On the condition that fiber mats are used to fabricate the composites, any types of resin infusion or vacuum technique that is capable of infusing the resin mixed with other fillers is favorable. On the other hand, chopped fibers composites can be effectively fabricated using compression molding. It is worth noting that if the additives or fillers possess large particle size, compression molding method is desirable as fillers get stuck in the tubing system (spiral and PVC tubes) and fiber mat during infusion process. For the fabrication of conventional carbon or glass fibre reinforced composite to be used for aircraft interiors as composite skin or as component, compression molding, casting, hydroforming, filament winding, vacuum based techniques, pultrusion, composite lamination which is followed by press curing have been employed [52].

2.4 Characteristics of oil palm and natural fibers

2.4.1 Physico-mechanical properties of natural fibers, their potentials and drawbacks

In comparison with synthetic reinforcing materials such as carbon or glass, natural fibers have numerous merits as well as drawbacks, as shown in Table 2-8.

Oil palm fibers, a form of lignocellulosic material, are renewable, plentiful and from natural resources, are becoming vital for the improvement of sustainable world economy [53]. Besides, oil palm fibers bear suitable tensile strength owing to solidity of the cellulose composition [54]. By using these fibers, one can substitute them for synthetic fibres and decrease the dependency on

this kind of fibres. Furthermore, compared to other food resources such as sugar cane and corn, oil palm is potentially available at lower cost due to being a waste crop in nature and also known as an alternative sustainable biosource [55-57]. It has been reported that 30 million metric tons of oil palm as waste biomass material have been harvested in the globe and nearly five million hectares of oil palm planted in 2011 in Malaysia [58]. Oil palm trees include empty fruit bunches (EFBs), fruit mesocrap, frund and trunk. The fibers can be exploited from each of these resources. The by-product EFB fibers are superior in terms of cost and accessibility. Thus, EFBs have the greater potential of being used in environmental friendly polymeric composites. Availability of EFB in large amount not just is important, but also possessing the lowest density even as compared to other natural fibers indicates a crucial importance for aerospace application (Table 2-9). Lower weight must be always taken into account in the aerospace's designs.

Table 2-8 Merits and drawbacks of crop fibers over traditional inorganic fibers as reinforcement in a polymeric material [31, 59-65].

Advantages	Disadvantages
Higher specific strength and stiffness than glass	Price variation due to agricultural politics or even harvest outcomes
Non-toxicity	Weak flame resistance
Lower energy cost	Poorer durability
No skin issues such as rashes and irritation	Limited maximum manufacturing temperature
Recovering calorific value as terminating its life cycle, especially compared to glass	Weak moisture property which leads to the swelling of natural fibers
Helpful role to global carbon budget	Different quality due to diverse whether condition
Suitable thermal and Insolation properties	Weaker mechanical strengths particularly impact
Good acoustic insolation and electrical resistance	Weak bonding between fiber and matrix
Easy production in terms of cost	-
Renewable nature	-
Higher biodegradability	-
Global availability	-
Less abrasiveness for manufacturing equipment	-

Generally light composite materials possess the highest usage in different applications, particularly in aerospace and automotive industry. Therefore, fibers' density plays a key role in designing and fabricating the composites. Table 2-9 provides a comparison of density and mechanical properties among various fibers.

Table 2-9 Comparison of the density and mechanical properties among different fibers and thermoset material [19, 66-75].

Fiber type/thermoset	Density (g/cm^3)	Density difference between oil palm and others (%)	Young's modulus (GPa)	Tensile strength (MPa)	Elongation at failure (%)
Kevlar49	1.44	+21.87	131	3600-4100	2.8
Carbon	1.8	+37.5	131	4000	2.8
Boron	2.6	+56.73	-	-	-
E-Glass	2.7	+58.33	73	1200	2.5
Oil palm	0.7-1.55	0	0.57-9	50-400	4-18
Hemp	1.48	+23.98	70	690	1.6
Tencel	1.55	+27.41	-	-	-
Flax	1.50	+25	50	345-1035	2.7-3.2
Talc	2.75	+59.09	-	-	-
Sisal	1.45	+22.41	9.2-22	155-635	2-2.5
Jute	1.30	+13.46	26.5	393-773	1.5-1.8
Spider Silk	1.30	+13.46	30	1300-2000	28-30
Coir	1.2	+6.25	4-6	175	10
Cotton	1.55	+27.41	5.5-12.5	287-597	7-8
Bamboo	0.85	-	11-32	140-800	2.5-3.7
Kenaf	1.4	+19.64	14.5-53	223-930	1.5-2.7
Thermoset	1.30	+13.46	-	-	-

2.4.2 Characteristics of EFB fiber

Empty fruit bunch (EFB) is preferred against other oil palm tree products due to its cost and availability as 73 % of FEBs are yielded up to fibers [11, 12]. 13-25 wt % lignin, 2-14 wt % extractives and 17-34 % hemicelluloses are existed in oil palm fibers [2, 4, 5]. There is always an interaction between the existing moisture and hydroxyl groups of fibers. The main interactions take place between moisture and hemicelluloses. The more a lignocellulosic fiber attracts

absorption the faster it loosens the structural stability, and causes poor bonding in composite. Therefore, it is desirable to remove the hemicellulose component from fiber through chemical treatment. As removal of lignin and hemicellulose accomplishes, the cellulose content increases [6].

Weathering can cause degradation reaction in most natural reinforcing materials. UV rays deform the interface in the oil palm fibers, especially where the lignin molecules exist. Due to the UV light, photo degradation reaction also causes discoloration in composites through chemical reactions in lignin [76]. The reason of degradation and poor bonding between polymer matrix and fiber is the presence of hemicellulose, pectin and lignin in the EFBs. Owing to these reasons, various forms of chemical surface treatments have been applied to enhance the performance of natural fibers in composites, which will be discussed in the next section. Table 2-10 and Table 2-11 report the contents of palm oil fibers and its physical and mechanical properties, respectively. The EFB density and its cellulose content are of good characteristics of this type of natural fiber.

Table 2-10 Oil pam fiber contents [77].

Constituents	Range
Cellulose (%)	42.7–65
Lignin (%)	13.2–25.31
Hemicellulose (%)	17.1–33.5
Holocellulose (%)	68.3–86.3
Ash content (%)	1.3–6.04
Extractives in hot water (100 °C) (%)	2.8–14.79
Solubles in cold water (30 °C) (%)	8–11.46
Alkali soluble (%)	14.5–31.17
Alfa-cellulose (%)	41.9–60.6
Alcohol–benzene solubility (%)	2.7–12
Pentosan (%)	17.8–20.3
Arabinose (%)	2.5
Xylose (%)	33.1
Mannose (%)	1.3
Galactose (%)	1.0
Glucose (%)	66.4
Silica (EDAX) (%)	1.8
Copper (g/g)	0.8
Calcium (g/g)	2.8
Manganese (g/g)	7.4
Iron (g/g)	10.0
Sodium (g/g)	11.0

Table 2-11 Physical and mechanical characteristics of oil palm fiber [77].

Property	Range
Diameter (μm)	150–500
Microfibrillar angle (°)	46
Density (g/cm^3)	0.7–1.55
Tensile strength (MPa)	50–400
Young's modulus (GPa)	0.57–9
Elongation at break (%)	4–18
Tensile strain (%)	13.71
Length-weighted fiber length (mm)	0.99
Cell-wall thickness (μm)	3.38
Fiber coarseness (mg/m)	1.37
Fines (<0.2 mm) (%)	27.6
Rigidity index, $(T/D)^3 \times 10^{-4}$	55.43

2.4.2.1 Comparison of different surface treatments for EFB fibers

To optimize and develop the performances of fiber reinforced composites, chemical modification of fiber plays a key role in enhancing the adhesion between fiber/matrix interfaces. Efficient surface treatment eliminates the original wax and deposits from fiber and increases wetting properties, thereby enhancing the mechanical characteristics of composite. Modifying the fibers can benefit topological nature, thermodynamic specifications and chemical surface reactions [78, 79]. Several commonly-used fiber treatments were reviewed and introduced below.

Fiber surface treatments have been conducted for the optimization of oil palm reinforcing materials. The most effective treatment led to the best chemical and physical modification is largely attributed to alkali treatment [80]. It was shown that alkali treatment decreased the fiber's weight by 22% whereas up to 6% fiber weight reduction was reported for silane treatment [81]. The thermal decomposition temperatures of untreated EFB and alkali treated fiber were measured 325 °C and 350 °C, respectively. Figure 2-4 shows a summary of the effect of several fiber surface pretreatment on EFB (OPF refers to EFB fiber in the figure).

Treatments		Effect on oil palm fibre
Mercerization	→	Amorphous waxy cuticle layer leaches out.
Latex coating	→	Partially masks the pores on the fiber surface.
γ irradiation	→	Partially eliminates the porous structure of the fiber and causes microlevel disintegration. It degrades mechanical properties considerably.
Silane treatment	→	Imparts a coating on fiber surface.
Toluene diisocyanate (TDI)	→	Makes fiber surface irregular as particles are adhered to surface.
Acetylation	→	Removes waxy layer from the surface and makes the fiber hydrophobic.
Peroxide treatment	→	Fibrillation is observed due to leaching out of waxes, gums and pectic substances.
Permanganate treatment	→	Changes the colour and makes fibers soft. Porous structure is observed after treatment.
Acrylation	→	Imparts a coating on fiber surface and removes pits containing silica bodies and keeps surface irregular. It improves mechanical properties of fibers.
Silane treatment	→	Keeps the fiber surface undulating and improves mechanical properties
Titanate treatment	→	Smoothens fiber surface.
Alkali treatment	→	Makes the surface pores wider and fiber become thinner due to dissolution of natural and artificial impurities.
Benzoylation	→	Imparts a rough surface to the fibers and makes pores prominent, which helps improving the mechanical interlocking with matrix resin.
Oil extraction	→	Imparts bright colour to the fiber. Removal of oil layer exposes surface pits and makes surface coarse.

Figure 2-4 The influence of different types of treatment on the EFB fiber [77].

2.5 The properties of EFB and natural fiber based composites

2.5.1 The effects of natural fiber treatment on the mechanical and thermal properties

Thermal and mechanical characteristics of composites used in aerospace parts are of crucial importance. Table 2-12 shows the effect of different types of natural fiber treatment on the thermomechanical properties of composites. For areca fiber reinforced composite materials with different polymers including epoxy, urea formaldehyde and melamine formaldehyde, it was observed that [82] the mechanical properties of alkali treated fiber composite including impact strength and flexural strength increased in comparison to untreated ones. Besides epoxy based composite demonstrated higher mechanical properties compared to other polymer composites used.

One type of chemical treatment which improved the thermal properties of coconut fibre PP, coconut fibre PLA and jute fibre PP composites was Diammonium phosphate (DAP) treatment, however, it was found to reduce the mechanical performances [21] , as a summary of results is depicted in Table 2-12. DAP of 5 wt% was considered as the best concentration for reducing the weight loss and linear burning rate. For coconut PLA and coconut PP composites, flexural strength decreased from about 42 to 41 MPa and approximately 31 to 24 MPa, respectively, with the incorporation of 5 wt% DAP treated fiber. The values reduced from approximately 19 to 11 MPa and about 12.5 to 10 MPa for tensile strength of coconut fiber PLA and PP composites, respectively, while flexural modulus increased from about 2.3 to 3.1 GPa for PLA composite and from around 1.49 to 1.59 GPa for PP composite. Besides, the mass loss rate and burning decomposition rate decreased for both PLA and PP coconut composites. Weight loss rate decreased from about 1.22 to 0.88 gr/min for PP coconut composite with the DAP treated fibers and also decomposition rate decreased from almost 26 to 15 mm/min. For coconut fiber PLA,

weight loss rate reduced from approximately 2.2 to 0.6 gr/min and decomposition rate decreased from about 25 to 15 mm/min. Similarly, flexural strength of jute fiber PP composite decreased from approximately 48 to 34 MPa with DAP treated jute fiber. Likewise, tensile strength reduced from around 31 to 12.5 MPa while flexural strength remained constant. Increased thermal performances were observed with the reduction in weight loss rate from almost 26 to 18 mm/min and decomposition rate from about 1 to 0.8 gr/min in comparison to those of untreated fiber composites. The improved flame retardancy after fibre treatment is due to the creation of ammonia and phosphoric acid on the fibre surface that promote protective char formation. The reduction in mechanical properties of composites containing DAP treated fibre was explained by the incompatibility of PP with DAP on the fibre surface. The SEM micrographs of DAP treated fibres reinforced PP and PLA composites showed fibre breakage, which is attributed to the reduced internal bonding of fibres with the incorporation of DAP flame retardants.

Table 2-12 Varying mechanical and thermal properties of palm and other natural fibers composites due to different fiber treatments (comparison between treated and untreated fibers composites).

Treatment	Natural composite	Bending strength	Flexural strength (MPa)	Impact strength ($J.m^{-2}$)	Tensile strength (MPa)	Fracture toughness	Flexural modulus (GPa)	Thermal properties	Ref.
Alkaline	Flax-epoxy	increase Up to 30%	-			-	-	-	[83]
Alkaline (potassium hydroxide 10% solution)	Areca-resin	-	Significant increase for 3 different fiber resins including epoxy, malmine urea formaldehyde and urea formaldehyde	Significant increase for 3 different fiber resins including epoxy, malmine urea formaldehyde and urea formaldehyde	-	-	-	-	[82]
Silane	Bombyx mori silk fibre composite	-	-		-	Increase	-	-	[67]
Alkaline	Kenaf 48wt% - epoxy	-	-		-	-	-	Decrease in decomposition temp. from 378 to 373 ºC and char	[84]
Enzyme modified (mixture of lipase, laccase and xylanase)	Palm 30wt%-PLA or PP	-	20% or 27% increase	-	15% or 18% increase	-	-	Improved deflection temp.7 or 15 ºC	[85]
Simultaneous alkaline and ultrasonic	Palm-PLA	-	-	Improved from almost 12.5 to 18.5	Improved from almost 51 to 63	-	-	Improved the degradation temp. from 330.5 to 350.7 ºC	[86]
Isocyanate	Palm-Polyurethane (PU)	-	Improved from almost 56 to 75	Improved from almost 9 to 12.5	Improved from 21 to 22.5	-	-	-	[87]

Coupling agent (maleated polypropylene (MAPP))	Craft wood-PP	-	-	Improved from almost 5.6 to 6.1	Improved from almost 39 to 41	-	-	Higher thermal stability and crystallinity (from 37.2% to 42.8%)	[88]
Diammonium phosphates (DAP)	Coconut fiber-PP or PLA	-	Decreased (value is discussed)	-	Decreased (value is discussed)	-	Improved (value is discussed)	Improved mass loss and burning decomposition rate (value is discussed)	[21]
Diammonium phosphates (DAP)	Jute fiber-PP	-	Decreased (value is discussed)	-	Decreased (value is discussed)	-	No change	Improved mass loss and burning decomposition rate (value is discussed)	[21]

Palm fibers were treated for an hour with different NaOH concentrations of 5 wt%, 10 wt% and 15 wt%, and produced the palm-rubber composites with 35% fiber mass fraction [89]. The highest values of mechanical properties were obtained for the composite reinforced with 5 wt% alkali treated fiber. Elongations at break were measured about 730 %, 690 % and 670 % for the composites with sodium hydroxide treated fibers of 5%, 10% and 15%, respectively. Additionally, the tear strengths of approximately 30.42, 28.49 and 25.50 kN/m, tensile strengths of 9.95, 9.61 and 8.86 MPa, and tensile modulus of 1.92, 1.85 and 1.80 GPa were obtained for 5%, 10% and 15% alkali fiber treated formulations, respectively. In another study [90] as displayed in Table 2-13, higher mechanical performances of composites attained with alkali treated fiber over silane treated fiber.

Table 2-13 Comparison of mechanical properties between the palm/sisal rubber composites reinforced with either optimal alkali treated (4 wt% concentration) fibers or silane treated fibers [90].

Treatment	Composite	Tensile strength (MPa)	Elongation at break (%)	Swelling index	Hardness (Shore A)	tear strength (N/mm)
Alkaline	Palm/sisal rubber	10.6	466	166 (Better)	83	55
Silane	Palm/sisal rubber	10	440	280.7 (Worse)	65	47

2.5.2 The effects of fiber type on thermal stability and the effect of fiber fraction on mechanical properties of composite

When high temperature of approximately 260 ºC applies to the natural fiber composite, first dehydration occurs followed by oxidative decomposition leading to quick weight loss conforming to the char formation at higher temperatures [88]. Fei Yao et al. [5] that studied the thermal properties of different natural fibers such as bast, agriculture residue, bamboo and wood

fiber found that the fibers decomposed at temperature range between 215 ºC and 310 º C corresponding to the activation energy of 160-170 kJ/mol. A comparison of thermal degradation temperature among different natural fibers as well as degradation temperature of EFB fibre PLA composite are shown in

Table 2-14. Another study [91] revealed that increasing the doum fiber in polyethylene polymer resulted in a slight decrease in thermal stability of the composite. Also it was shown that [91] doum fiber polyethylene composite attained maximum flexural modulus at 20 %wt fiber and Young's modulus at 30 %wt fiber. Alexander Naughton et al. [92], which conducted a research on hemp fibre polyester composite, indicated that increasing the amount of fiber improved the thermal characteristics of char residue. Besides, composites with higher thickness and greater wt% of hemp fibre improved the fire resistivity of the composite material. Thermogravimetric analysis [84] showed that kenaf epoxy composite presented greater thermal and charring stability with higher wt% of kenaf fiber.

Table 2-14 Thermal degradation temperatures of different natural fibers and EFB fiber composite.

Natural fiber	Degradation temperature (ºC)	Reference
Kenaf	297-434	[84]
Bamboo	250-420	[84]
Resole, sisal, reed and water hyacinth	290-490	[84]
Bast, agriculture residue, bamboo and wood fiber	215-310	[84]
Raw EFB fiber –PLA	330.5	[86]

The effects of palm fiber mass fraction on mechanical properties of different types of polymer composites are tabulated in Table 2-15. Depending on the nature of fiber and polymers, various optimum fiber mass fractions were observed. The effect of various wt% of palm fiber in PLA

composites was studied and found that 30 wt% palm fiber showed the highest tensile strength and modulus compared to 10 wt%, 20 wt% and 40 wt% , attributed to better interfacial bonding between fiber and polymer matrix [86]. Another research [93] conducted on palm-epoxy composite exhibited that tensile strength increased from about 46.1 to 47.78 MPa with reduction in fiber loading from 55 wt% to 35 wt% .

In a separate study, it was observed that 20 wt% palm fiber presented the highest mechanical properties of palm fiber phenol resin composite in terms of hardness, flexural modulus and impact energy as compared to other fractions of 0 wt%, 10 wt% and 30 wt% [94]. For palm rubber composite [89] investigated for different fiber loadings of 5 wt%, 10 wt%, 20 wt%, 35 wt% and 50 wt%, it was discovered that 5 wt% fiber exhibited higher tensile properties in the longitudinal direction. A study on sugarcane bagasse [95] showed that 20 wt% fiber had the greatest mechanical properties compared to other fractions of 0 wt%, 5 wt% and 10 wt%.

Table 2-15 The impact of fiber mass fractions on the mechanical properties of natural fiber composites.

Composite	Fiber mass fractions (wt %)	Mass fraction with higher mechanical properties (wt %)	Mechanical results investigated	Ref.
Palm-PLA	0-10-20-30-40	30	Tensile strength, modulus	[86]
Palm-epoxy	35-55	35	tensile strength	[93]
Palm-phenol resin	0-10-20-30	20	Hardness, impact, flexural modulus	[94]
Palm-rubber	5-10-20-35-50	5	Tensile modulus, tensile strength	[89]
Sugarcane bagasse-PP	0-5-10-20	20	Tensile modulus, flexural strength and modulus, impact strength	[95]

2.6 Polymeric Materials currently used for aircraft interiors: Thermosets vs. thermoplastics

It is highly recommended [33] that manufacturing methods for future interiors are required to be developed in such a way that composites and plastics can be fabricated at a (1) very low pressure as well as (2) temperature. One of the excellent benefits of thermosetting polymer is their capability of fabricating composite at low pressures and low (processing) temperatures (typically below 100 ºC) due to their low viscosity (0.1-10 Pa.s) prior to crosslinking and polymerization. In comparison with thermoplastic matrix, a thermoset matrix is more active with oil palm fiber (natural fiber) contents such as hemicellulose, cellulose and lignin leading to higher wetting capacity between the interface of fiber and matrix, thereby improving the interfacial shear strength for thermoset composites [77]. A standard manufacturing method in the aerospace industry is employing liquid composite moulding method which is feasible by the means of thermosets. On the other hand, the processing viscosity and temperature for thermoplastics are 100-10000 Pa.s and ca. 200 ºC <, respectively, which considers an issue for natural fiber composites. Figure 2-5 shows the selection process of thermoset material for the current study. High processing temperature can significantly reduce the thermo-mechanical behaviors of natural fibers, particularly at the temperatures which thermoplastics need to be processed. Furthermore, it is worth noting that currently thermosets including epoxy and phenol resins are of the main polymeric materials that employ in the fibre reinforced polymeric composites as the components of cabin parts, as illustrated in section 2.3.1. Table 2-16 indicate the general difference between thermoset and thermoplastic matrix, and the advantages and disadvantages of thermosets and thermoplastics based on aerospace usages [96] are shown in Table 2-17,

Table 2-18 and Table 2-19. Thermosets resins are typically mixed with a suitable coupling agent

to provide a low viscosity liquid. Then, curing can be speeded by applying heat to the resin contents. But, thermoplastics show high viscosity. They do not cure on heating. On heating, their molecules just melt and are capable of reprocessing. Despite of many studies conducted on thermoplastics, thermosets have been used for high performance applications.

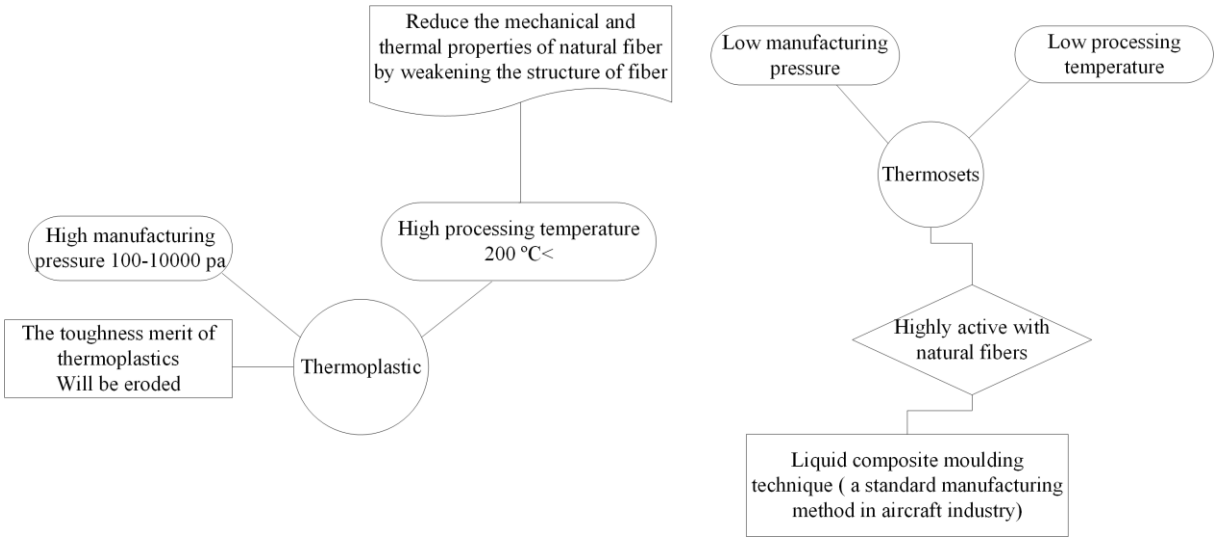


Figure 2-5 Justification of polymer type selection for this study.

Table 2-16 Comparision between thermoset and thermoplastic properties [96].

Thermosets	Thermoplastics
Great resistance to solvent	For organic solvents in some cases, limited resistance
Moisture absorption characteristics	Little moisture absorption characteristics
Possibility of processing in very low viscosity	Highly viscous
Irreversible processing	Reversible processing
Fracture energy is low	Fracture energy is high
Strain to failure is low	Strain to failure is high
Existence of chemical reactions as cured	No cure required, non-reacting

Table 2-17 Advantages and disadvantages of thermosets [96].

Advantages	Disadvantages
Creep resistance	Refrigeration is vital due to limited storage life
Practicable resin-liquid manufacturing	Cure duration is long 1-2 hours or more
High formability for complex forms	Long time required for processing
Suitable fiber wetting	Moisture absorption properties
Low processing temperature	-

Table 2-18 Merits and drawbacks of thermoplastics [96].

Merits	Drawbacks
Great delamination resistance	Weak tack and drapability
Without refrigeration, unrestricted shelf time	Creep properties
Fast processing	High processing pressure and temperature
Possible reprocessing for post-formable	Low resistance to solvent
Reusable scrap	-

Table 2-19 Thermosets vs. thermoplastics in aero-grade industry.

Thermosets advantages over thermoplastics:
• Cheaper and more cost-efficient to produce (due to lower pressure and processing temperature involved) • Toughness cannot be considered as thermoplastic advantages since it will be eroded

2.6.1 Epoxy thermoset

Among thermoset resins, epoxy is amongst the most widely used in aerospace industries owing to its low shrinkage, high mechanical and chemical properties, and sufficient adhesion to most fibers. They are not only applied for fabrication of composites, but also function as prominent adhesives and coating for most materials. Since epoxy resin has a low viscosity prior to curing, employing resin forming technique such as vacuum resin infusion is highly suitable. It has been showed that higher curing temperature tends to increase the T_g (glass transition temperature) of the cured epoxy. Epoxies treated at 180 °C and 120 °C showed dry service temperatures of 150 °C and 100-130

°C, respectively [96]. The major benefits of epoxies are summarized as follows:

- capability to optimize the epoxy resin for particular properties by formulation (treatments)
- ability to adjust the toughness
- its low volatile thereby increasing the safety
- good thermal resistance, dimensional stability, chemical resistance and low shrinkage, adhesion and processing versatility.

On the other hand, a few disadvantages of epoxy in comparison with polyesters are high cost of aerospace epoxy resin, moisture absorbing characteristic, relatively higher viscosity and slower cure, limited resistance to phenol and organic acids and low temperature performance [96].

2.6.2 Phenolic resin (PF) in aircraft interiors

PF resin is one of the thermoset materials used in char, flame and smoke resistant applications for aerospace interior components. During curing PF could react with large shrinkage and the cured thermoset is generally highly brittle. PFs are highly resistant to elevated temperature and also have excellent fire resistant properties under high heat fluxes and flames. The protection takes place when a surface layer of porous carbon is formed to slow down the burning process. PFs usually use for interior parts where non-structural application with smoke and fire retardant properties is required compared to that of mechanical properties. The physical and mechanical properties of phenol formaldehyde resin is shown in Table 2-20. In some applications, PF can be replaced with thermoplastic resin where higher mechanical properties are required. Thermoplastics could be processed with ease through thermoforming albeit its higher cost which must be taken into consideration. Three important points which must be taken into account when using phenol resins are as follows:

- the phenolic resins possess lower mechanical properties than other resins such as epoxy

owing to the presence of void contents in matrix

- the resin color is mostly dark brown
- high pressure is required for its fabrication.

Table 2-20 Typical Physical, chemical and mechanical properties of phenol formaldehyde resin (resole type) [97].

Liquid resin	
Appearance	Deep brown colour
Viscosity (cps)	18–22 s. on Ford cup B4
Water tolerance	1:8
Solid content (%)	50±1
Cured resin	
Density (g/cc)	1.3
Tensile strength (MPa)	10
Young's modulus (MPa)	375
Elongation at break (%)	2
Flexural strength (MPa)	10
Flexural modulus (MPa)	1875
Izod impact strength (kJ/m^2)	20

Table 2-21 compares the advantages and drawbacks of the most commonly used thermosets for aircraft industry. As epoxy resins naturally possess high mechanical properties, great compatibility with FR additives and no pre-requisite to be produced at high pressure, this type of thermoset was opted for the liquid casting process in this work. The mechanical performances of phenol resin are not sufficient by nature to be used for natural fiber composites in order to be considered for the considered interior components of aircraft such as panels, ceiling and sidewalls. Phenol resins are normally reinforced with glass or carbon fibre to create sufficient strength as composites. The high production pressure is not favorable for manufacturing as well. Hence, the resolution was made to enhance the flammability and thermal behaviors of natural fibre epoxy thermoset based composites.

For tensile properties of NF reinforced phenolic composites, Marliana et al. [98] reported the

tensile strength and modulus of 20 wt% kenaf fibre phenolic composites are about 4 MPa and 0.63 GPa, respectively. Peng et al. [99] attained the tensile strength and strain of 22.4 MPa and 2.9 % for sisal fibre phenolic composites. Oliveira et al. [100] studied sisal fibre reinforced phenolic composites, and figured out that flexural strength of phenolic thermoset and sisal fibre (30 wt%) phenolic composite was approximately 15 MPa and 63 MPa, respectively. Similarly, Bu et al. [101] obtained the flexural strength of 69.9 MPa for sisal fibre phenolic composites.

These mechanical values are normally higher for NF reinforced epoxy composites, e.g. the tensile strength and modulus of 30 wt% woven fibre epoxy composites were recorded 66.5 MPa and 3.26 GPa, respectively, and the flexural strength and modulus were obtained 92.79 MPa and 4.91 GPa [11]. This shows higher mechanical properties of NF epoxy composites than those of phenolic counterparts.

Table 2-21. General properties of epoxy vs. phenol resins [96].

	Epoxy	Phenol resin
Tensile, flexural and impact properties	higher	Lower
Manufacturing issue	long cure	1.high pressure is required for composite fabrication 2. prone to create voids in the composite
Resin colour	no colour/yellowish	dark brown
Thermal properties	good	high

2.6.3 Recently used thermoplastics for aircraft interiors

Recently different types of thermoplastic materials such as ABS, polycarbonate, Divinycell F, Elastollan thermoplastic polyurethane (TPU), polyphenylsulfone (PPSU), KYDEX thermoplastic sheets, etc. have been used for several components of aircraft interior parts without the presence

of fiber as reinforcement. These interior aircraft components have been fabricated by major aircraft manufacturers.

2.7 Flame retardants

Flame retardants have been used to improve the thermal and fire resistant performances of thermosets, thermoplastics and composites. They can be categorized into organic and inorganic compounds based on the elements and chemical formulas (hydroxides, metallic oxides boron, nitrogen, phosphorous, chlorine and bromine) which are present in their structures. Figure 2-6 indicates the different types of FRs.

For inorganic FRs, the following properties are expected to take place. Most of them act in condensed phase by decomposing endothermically. They either release carbon dioxide or water, both of which contribute to the inhibition of fire. The fire heat can be absorbed by means of such reactions. The char reside inhibits the penetration of heat into the area, leading to the fire extinction. Many inorganic FRs promote char and act as smoke suppressant, and all dilute the fire zone. Metal compounds such as metal hydroxides and antimony compounds, boron compounds such as sodium borate and boric acid, and phosphorous containing compounds such as ammonium polyphosphate are of the most widely used inorganic FRs. Organic FRs can be categorized into organohalogens and organophosphorus compounds. The halogenated FRs are either bromine or chlorine. Brominated FRs are very effective and show more flame resistivity than chlorine counterparts. Halogen based FRs pose several environmental disadvantages that led to the limitation of their usage in different applications. For organophosphorus FRs, phosphate esters are the most commonly employed organophosphorus FRs. Amongst the halogenated organophosphorus compounds, halogenated phosphate esters were widely used.

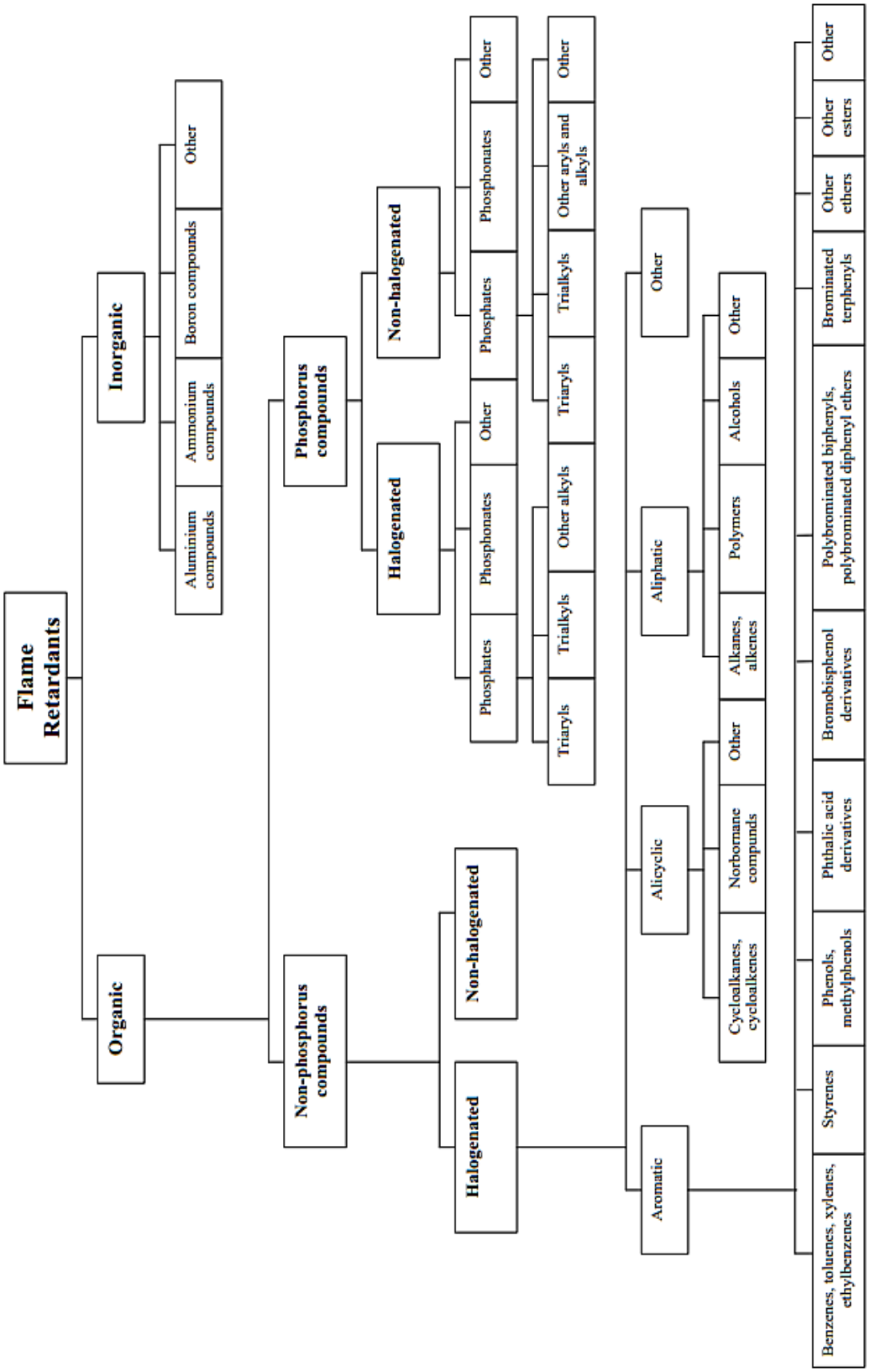


Figure 2-6 Detailed categories of flame retardants [102] .

Zinc borate (ZB) is a type of inorganic FRs required to be used with other flame retardants since this FR is a synergist. Zinc stannate (ZS) and Zinc hydroxystannate (ZHS) are of other inorganic non-toxic synergists. Antimony trioxide as an inorganic synergist can only be beneficial when blended with other halogenated FRs. Such combination offers the benefit of reducing the quantity of halogenated FRs being incorporated in polymer matrix. Ammonium phosphate (APP), on the other hand, is a dehydrating compound, which leads to a swelling (or intumescent) mechanism upon fire. APP catalyzes the dehydration reaction of other compounds through a swelling mechanism. Besides dehydration, APP also participates in the formation of residual char leading to its larger usage (Figure 2-7). In the swelling mechanisms, low heat spread, more carbon concentration, thick char film and high viscosity of melt of decomposed polymer are amongst the reasons that contribute to the reduction in the smoke and gases as well as flammability [103].

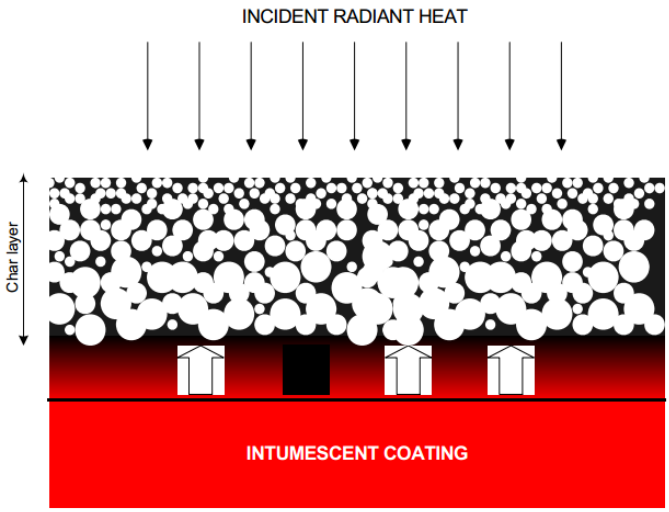


Figure 2-7 Swelling system when polymer is exposed to fire in the presence of APP (the figure was quoted from Norwegian Pollution Control Authority or SFT).

Red phosphorus provides flame retardancy thanks to the creation of phosphorous-oxygen links as well as formation of a heat shield on the surface of the polymers. The main weaknesses of this flame retardant are the creation of phosphine gas, which is toxic, during long storage and ignition and also its red color which causes polymer discoloration.

Alumina Trihydrate (ATH) acts as flame retardant partially owing the reduction of the volatile gases by formation of water molecules through dehydroxylation and partially contributing to a heat sink effect. When ATH thermally degrades above 200 ºC, alumina forms on the surface which is a heat-insulating barrier that inhibits more fire spread to the inner space of the polymers. Typically, in order to attain desirable flame retardant characteristics, a large amount of ATH is needed. The loading level of ATH can be decreased with appropriate spreading in the polymer, modification of surface and proper size of particles. Magnesium hydroxide (MDH) has similar properties and reactions as ATH whereas the thermal degradation of MDH is greater, approximately 325 °C.

2.8 Flammability and smoke properties of natural fiber composites

Fire retardants additives offer different materials i.e. thermosets, thermoplastics, textiles and rubbers the flame retardancy to diminish or delay the process of combustion. Each stage of self-sustaining polymer composite burning cycle (as seen in Figure 2-8) can be terminated by FRs, resulting in quenching of the fire or decreasing of the burning rate [16-18, 104-110].

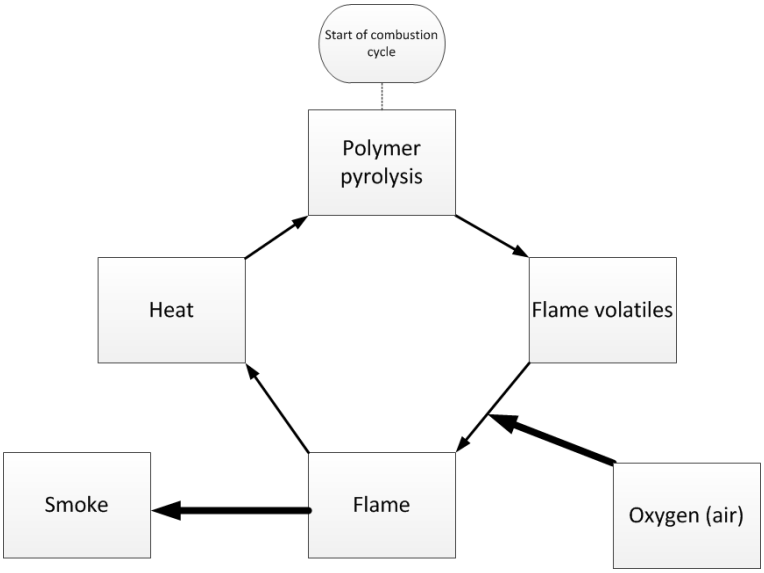


Figure 2-8 Self-sustaining polymer composite burning cycle [110].

Methods to overcome the flames or the combustion rate can be categorized as: first, reducing the heat feedback to the material to prohibit more pyrolysis (last stage on the top left side of figure); second, introducing constituent into the polymers which releases effective fire inhibitors i.e. APP agent (flame stage); third, the separation of fire from the atmosphere or air supply; forth, reducing the combustible volatiles with the modification of the pyrolysis process, which occurs with the formation of a thermal barrier between the flame and polymer to form a charred layer (commencement of cycle). Numerous FRs have been developed for composites and polymers. A number of them are appropriate for fiber reinforcement composites [111]. Chemicals for instance, melamine cyanurate, and aluminum trihydroxide (ATH) [112], boric acid with magnesium hydroxide [113], ammonium polyphosphate with expandable graphite [114, 115], ammonium phosphate (APP) [112, 116] and diamond phosphate (DAP) [117, 118] have been added into the thermoplastics or thermoset resins to upgrade the fire retardant characteristic of the composites.

Some common approaches have been employed to introduce FRs to composites such as modification or impregnation of fibers with FRs prior to manufacturing process or coating of the composite with FRs at the finishing step [13, 119]. In addition, the most common method is to mix fire retardant, polymer and/or fibers during processing [111].

2.8.1 Flame retardants for natural fiber reinforced polymer composite

Various properties of smoke and flammability are controlled by numerous factors as follows: (1) nature of polymer matrix, (2) nature of natural fiber, (3) bonding between fiber and polymer and (4) structure of polymer composite [13, 90, 120-122].

Ammonium polyphosphate (APP) as flame retardant was incorporated into polybutylene succinate (PBS), and led to the phosphorylation of flax fiber and hot hydrolysis of polymer [4] , but created lower thermal stability, as shown in Table 2-22. The role of flame retardant was to generate a protective layer thanks to the fiber structure protection and the charring of the polymer. Consequently, the peak of heat released rate reduced considerably due to the applied flame retardant. Table 2-22 and Table 2-23 displays the flammability properties (including pHRR (peak of heat release rate), TTI (time to ignition), EHC (effective heat combustion), MARHE (maximum average of heat emission), mass residue and thermal degradation temperature (T_d) of flax fibre polymer composite in the presence of 5 % APP flame retardants. The composite fabrication process first commenced with the addition of APP to the polymer, and then an internal mixer was employed to blend the mixture of fiber and polymer. Finally, materials were compressed in a mold. Moreover, in this research the significance of lignin in improving the flame retardancy was emphasized. In the other study [123], drip flame properties of ramie fiber PLA composite reduced when the microencapsulated ammonium polyphosphate was used as flame retardant.

Table 2-22 TGA results for biocomposites [4].

Biocomposites	Mass Res at 700 °C (%)	$T^{\circ}_{20\%}$ (°C)
PBS	0.75	370
95PBS5APP	5	346
70PBS30fl	6.8	358
65PBS5APP-30fl	14	317

Table 2-23 Cone calorimetry results of composites [4].

Biocomposites	TTI (s)	pHRR (kW/m^2)	EHC (kJ/g)	MARHE (kW/m^2)	Mass Res (%)
PBS	150	485	21.0	213.8	0
95PBS5APP	86	614	19.7	238.7	4.7
70PBS30fl	61	270	19.5	211.4	5.5
65PBS5APP-30fl	55	208	16.8	127.4	17

In another study [124] 25 % chopped flax fibre was reinforced to PLA/TPS (thermoplastic starch) bio-matrices. In order to improve the flammability resistivity of this biocomposite a new phosphorous-silane (PSil), acted as an agent for surface treatment, and glycerol phosphate (GP), as a plasticizer of starch with fire retardant properties, were blended together. The most effective flammability reduction was recorded when addition of 10 wt% APP was applied to the biocomposite. The observations showed a 40 % decrease of heat emission, high value of LOI (33 vol%) and best rating of UL 94 classification (V-0). Higher values of LOI (%) show greater flame resistivity. Table 2-24 and Table 2-25 show the flammability and smoke generation recorded for the biocomposite. The peak of heat release rate (pkHRR), TTI, total heat release (tHR) and mass residue were measured using calorimetry tests.

Table 2-24 LOI and UL-94 classification results [124].

	UL-94 classification	LOI (vol%)
PLA/TPS	HB	21
PLA/TPS-GP	HB	23
PLA/TPS/flax	HB	20
PLA/TPS-GP/flax	HB	21
PLA/TPS/flax-PSil	HB	23
PLA/TPS-GP/flax-PSil	HB	24
PLA/TPS-GP/flax-PSil + APP	V−0	33

Table 2-25 The calorimetry test results of the biocomposites [124].

	TTI (s)	pkHRR (kW/m^2)	tHR (MJ/m^2)	Residual mass (%)
PLA/TPS	33	774	105.4	0
PLA/TPS-GP	29	623	100.0	4
PLA/TPS/flax	34	410	98.1	5
PLA/TPS-GP/flax	28	270	90.3	6
PLA/TPS/flax-PSil	29	310	91.0	9
PLA/TPS-GP/flax-PSil	29	285	81.0	10
PLA/TPS-GP/flax-PSil + APP	34	149	57.5	24

Dhanushka et al. [125] reinforced 30 % hemp fiber into PLA polymer which contained multi-walled carbon nanotubes (MWCNT) and sepiolite nanoclay (Sep) as flame retardants. Compared to the PLA ternary system which was based on sepiolite nanoclay and multi-walled carbon nanotubes, the addition of hemp fibers reduced the total smoke release and amount of CO, and increased the residual mass. However, the peak heat release rate, total heat release and amount of CO_2 increased. The values obtained from cone calorimetry study are presented in Table 2-26.

Table 2-26 The results obtained from cone calorimetry tests [125].

Sample	Peak HRR (kW/m^2)	Total heat release (MJ/m^2)	Total smoke release (m^2/m^2)	Mean CO_2 (kg/kg)	Mean CO (kg/kg)	Residual mass (wt.%)
PLA	485	104	5	150	4.6	1.6
PLA/hemp	361	120	26	1.58	0.02	3.5
PLA ternary nanocomposite	265	115	112	0.82	0.03	3.5
PLA ternary nanocomposite/ hemp	340	122	57	1.57	0.02	10

Alhuthali et al. [126] considered 40% recycled cellulose fiber (RCF) to be reinforced separately into vinyl-ester polymer (VER) and vinyl-ester nanoclay composite using electrical mixer. Among the pure polymer, fiber reinforced polymer and fiber reinforced nanocaly (NC) composite the latter, nanocomposite, proved to possess greater flame retardancy and thermal stability, followed by cellulose reinforced polymer composite (Table 2-27). Nanoclay contributed to reduction of the flammability of the composite system by acting as both fire insulating agent and also processing the role of a mass transport barrier for decomposition of volatile products [127-129]. Furthermore, the formation of char improves by the addition of nanoclay [130, 131].

Table 2-27 The results of flammability test [126].

Sample	Burning out time (s)	Ignition time (s)	Fire spreading speed (mm/s)
VER	92	3.2	0.109
VER/RCF	98	3.53	0.097
VER/RCF/1%NC	102	4.03	0.102
VER/RCF/3%NC	104	4.24	0.098
VER/RCF/5%NC	110	4.6	0.091

In another study, the effect of the addition of banana natural fiber and nanoclay on the MA grafted PP (M-g-PP) polymer was investigated [132]. Melt interaction was used to fabricate nanocomposite, where melt blending was employed to mix the fibers into nanocomposite, and then the mixture was compression-molded. The composite system named OPP had the constituents of MA-g-PP, clay and PP with the concentration of 5 w%, 3 w% and 92 w%, respectively. 10 wt%, 20 wt%, 30 wt% and 40 wt% banana fiber was added to 3 wt% of nanoclay and 5 wt% of MA-g-PP to produce composites. In terms of flammability, HRR significantly decreased in the presence of clay filler compared to PP polymer (Table 2-28). One reason is attributed to a rise in absorbing radiations because of the nanoclay aspect ratio which is high or the alteration in thermal properties, and the other one is that the nanoclay acted as a barrier owing to providing the modification of degradation condition in the matrix. For banana fiber reinforced composites, the incorporation of natural fibers was found to increase the mass loss and HRR compared to the nanocomposite (OPP). 10 wt% fiber nanocomposite presented the lowest total heat release, HRR and total smoke release relative to that of 20 wt% and 30 wt% fiber reinforced nanocomposites.

Table 2-28 The results of cone calorimetry study for PP, OPP (nanoclay filled PP composite) and nanocomposites reinforced with 10 wt%, 20 wt% and 30 wt% fiber [132].

Description	PP	OPP	BRPP-10	BRPP-20	BRPP-30
Time to ignition (s)	30	36	28	27	26
Time of flameout (s)	561	855	719	648	615
Total heat release (MJ/m^2)	100.5	107.3	121.7	137.4	141.5
Mass lost (g)	30.8	31	32.5	32.2	32.6
HRR (kW/m^2)	2498.2	748.3	926.4	1136.77	1256.2
Total smoke release (m^2/m^2)	1298.8	1164.5	1581.9	1746.5	1612.7
SEA (m^2/kg)	445.87	519.61	304.1	322.24	360.42

Numerous flame retardants were incorporated into thermoset and thermoplastic polymers reinforced with natural fiber, and increasing addition of FRs was shown to enhance the flame resistivity and thermal properties of composites using vertical burner test, TGA experiment,

calorimetery study, LOI, UL rate test, etc. [9, 11, 15, 98, 133-162]. However, Ohio State University calorimeter and National Bureau of Standard smoke chamber tests are required to be conducted in order to evaluate the possibility of employing natural fiber reinforced polymeric composite flame retarded with suitable FRs in aircraft interiors. Despite enhancing the flame retardancy and thermal behaviors, increasing FRs can lead to a drop in the mechanical properties.

The flame resistance and thermal properties of thermosets material such as polyesters and epoxy can be enhanced using phosphorus and phosphorus-halogen compounds, halogenated mixtures with the addition of antimony oxide, and aluminum oxide trihydrate [163]. Aromatic bromine has been used in commercial applications, but its high corrosiveness and toxicity are the disadvantages of this flame retardant when charred. Owing to the environmental disadvantages posed by halogen compounds, this study focused only on non-halogenated flame retardants comprising of phosphorous, boron and aluminum compounds.

A list of suitable halogen-free flame retardants that have been used for interior components of aviation, car, bus, rail vehicles and ship is shown in Table 2-29. As highlighted, APP and ATH are being widely used to produce effective FR systems for all epoxy and other types of resins in all the mentioned parts of interiors. In addition, zinc borate is used in flame retardant systems and, is a known synergetic agent and smouldering suppressant.

Table 2-29 Suitable halogen-free flame retardants (HFFR) for various resins and polymers used for interior components of car, bus, rail vehicles, ship and aviation. (pinfa association [164])

Application	Polymer	HFFR
Flooring	PVC	ATH, isopropylated phosphate ester, CDP, zinc borate
	Polyolefins	MDH, ATH, intumescent systems, new phosphonates
	Epoxy	ATH, APP, intumescents, ethylene diamine phosphate, melamine borate, DOPO
	Phenolic resins	Melamine borate, phosphate esters
	Urethane elastomers	Aluminium phosphinate, melamine cyanurate, TPP, CDP, APP, melamine phosphate, melamine polyphosphate
	Elastomers	ATH, MDH, P-based
Ceilings Sidewalls Panels Structural parts	UP resin	ATH, APP, EDAP, intumescent systems, DMPP
	VE resin	ATH, APP
	Acrylate resin	ATH, APP, intumescent systems
	EP resin	ATH, APP, intumescent systems, DMPP, DOPO, cyclic phosphonate
	Phenolic resins	Melamine borate, phosphate esters
Dashboard Instruments	PC	Sulphonates
	ABS	TPP, RDP, and BDP
Instrument panels	PC/ABS	TPP, RDP, and BDP
Instrument cluster housing Speaker grilles Gear knobs	TPU	APP, metal phosphinate, melamine cyanurate, melamine polyphosphates, TPP, CDP, zinc borate
Console parts Trunk tailgates	TPE	Metal phosphinate +N-synergist, intumescent systems
Steering wheels Air ducts	Polyamide, nylon	Melamine cyanurate metal phosphinate +N-synergist
Tubing	Polyolefin	Intumescent systems
Door trim / handle	Reinforced PP	Intumescent systems
Pillar claddings Door pockets	RIM	APP, ATH, melamine phosphate, melamine polyphosphate, intumescent systems
Door panels Chairs Other interior devices	UPR	ATH, APP, EDAP, melamine phosphate, DMPP, intumescent systems
Insulation materials	r-PUR	P-polyols, DMPP, APP, TEP
	PIR	RP, DMPP, APP, TEP
Coatings	2K-PU, epoxy, acrylates	ATH, phosphate ester, APP
Sealants (flame-retarded and/or fire-resistant)	PUR, acrylic, epoxy, elastomers, PVC	ATH, APP, RP, EDAP, melamine phosphate and -pyrophosphate, melamine polyphosphate, phosphate esters, melamine borate, zinc borate

2.8.2 Expandable graphite as flame retardant in composites

Expandable graphite (EG) is a halogen free intumescent flame retardant, which is water insoluble and environment friendly. Graphite flake consists of stacked layers of graphene sheets with the hexagonal sp^2 hybridized carbon lattice [165, 166]. Its carbon atoms arranged in a 2D structure are covalently bonded together through van der Waals forces which are weak. Nitric acid and/or sulphuric acid as blowing agent are intercalated into the crystal carbon layers of graphite structure. In the event of heat, such intercalated graphite flakes are capable of exfoliation along c-axis. EG expands in the condensed phase and decreases the smoke density. The oxidization of EG occurs upon endothermic combustion at high temperatures. The chemical reaction between EG and sulfuric acid is shown below:

$$2\ H_2SO_4 + C \rightarrow 2\ H_2O \uparrow + 2SO_2 \uparrow + CO_2 \uparrow \quad (1)$$

Graphite intercalation compound exfoliates rapidly and forms worm-like structure with a very low density of 0.006 g cm^{-3}, which acts as an insulating barrier on the burning surface to inhibit the mass and heat transfer [167]. Recently expandable graphite have been focused as material which can significantly improve the flame retardancy [168].

The effect of expandable graphite (EG) was reported from a recent work [166], and it was found that the incorporation of 24 wt% EG into a 50 wt% wood-recycled polypropylene increased the LOI value significantly. Kuranska et al. [165] produced bio-based polyurethane-polyisocyanurate (PUR-PIR) foam composites with 150 and 250 isocyanate indices. They used two techniques to attain bio-polyols: epoxidation with transesterification (ROPtr) and opening oxirane rings (ROPep) with triethanolamine. In order to improve the flame retardancy of composites, EG with the concentrations of 3 wt%, 6 wt% and 9 wt% was used. Oxygen index of composites increased at higher amount of EG particles for composites with varying isocyanate index (Figure 2-9).

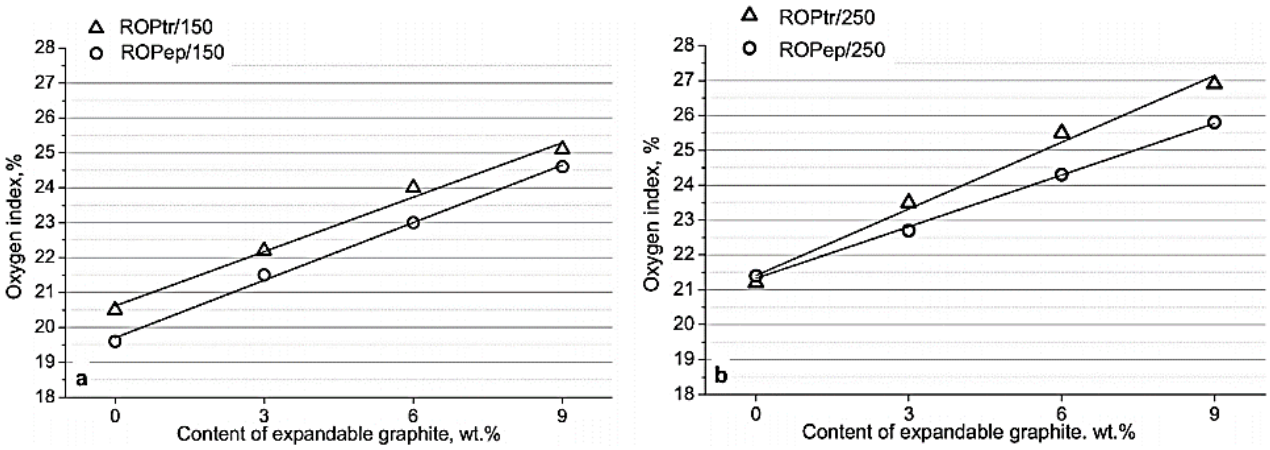


Figure 2-9 The impact of EG particles on oxygen index percentage of PUR-PIR foam composites with different isocyanate index (150 and 250) [165].

Cone calorimeter test was used to characterize the flame performance of PUR-PIR composites, and the parameters including heat release rate (HRR), time to ignition (TTI), peak of the heat release rate (p-HRR), total heat release (HRR), total smoke release (TSR), heat release rate (TTP) and maximum average rate of the heat emission (MARHE) were obtained. As shown in Table 2-30, HRR, p-HRR, HRR, TSR and MARHE reduced remarkably with increased loading of EG particles. TTI did not show any special trend with the inclusion of EG and generally TTP decreased with increasing concentration of EG particles. For example, the value of p-HRR decreased from 240 kW/m^2 to 136 kW/m^2 with the addition of 9 wt% EG into ROPep/150 composite as well as a significant reduction in released smoke from 560 m^2/m^2 to 288 m^2/m^2 was experienced. For the symbols mentioned in Table 2-30, the numbers of 150 and 250 show isocyanate index, and the last numbers (i.e. 3, 6 and 9) after slash indicate the weight percentage of EG in the composites.

Table 2-30 Cone calorimeter test results of PUR-PIR foam composites and the effect of EG on flammability parameters [165].

Symbol	TTI (s)	THR (MJ/m^2)	p-HRR (kW/m^2)	TTP (s)	av-HRR (kW/m^2)	TSR (m^2/m^2)	MARHE (kW/m^2)
ROPep/150	3	19.8	240	30	64.9	560	177.7
ROPep/150/3	2	18.0	205	20	61.0	452	144.4
ROPep/150/6	3	17.3	165	20	58.5	341	112.6
ROPep/150/9	3	15.7	136	20	53.2	288	87.7
ROPtr/150	3	18.0	233	50	59.1	522	164.7
ROPtr/150/3	3	18.5	216	60	62.6	559	145.9
ROPtr/150/6	2	19.5	152	20	66.1	406	119.1
ROPtr/150/9	4	18.0	142	15	60.9	270	96.6
ROPep/250	3	15.4	157	25	51.1	404	102.4
ROPep/250/3	4	15.9	155	20	54.0	337	95.6
ROPep/250/6	3	15.8	138	15	53.5	285	91.5
ROPep/250/9	4	14.3	118	20	48.4	204	76.3
ROPtr/250	3	18.6	176	30	60.8	485	134.9
ROPtr/250/3	4	18.7	150	20	63.3	372	103.7
ROPtr/250/6	3	17.3	131	20	58.8	291	88.2
ROPtr/250/9	4	14.4	129	20	48.7	260	80.1

TGA results showed that thermal degradation temperatures at 5%, 25% and 50% mass loss did not change significantly whereas the mass residue at 800 °C improved with addition of EG particles (Table 2-31).

Table 2-31 TGA results of foam based composites varying expandable graphite [165].

Symbol	$T_{5\%}$ (°C)	$T_{25\%}$ (°C)	$T_{50\%}$ (°C)	Residue at 800 °C (%)
ROPep/150	283	337	408	17.4
ROPep/150/3	280	336	407	19.9
ROPep/150/6	283	336	412	22.3
ROPep/150/9	280	337	446	34.7
ROPtr/150	263	340	415	15.3
ROPtr/150/3	262	340	413	15.0
ROPtr/150/6	266	344	422	22.0
ROPtr/150/9	263	337	445	33.9
ROPep/250	292	350	420	25.1
ROPep/250/3	283	338	416	23.7
ROPep/250/6	283	338	422	27.5
ROPep/250/9	263	336	474	37.7
ROPtr/250	280	353	421	23.8
ROPtr/250/3	281	351	426	25.9
ROPtr/250/6	280	349	428	27.8
ROPtr/250/9	268	355	622	30.2

Yang et al. [169] investigated the effect of 10-20 wt% EG particles on epoxy resin and found that lower values of HRR and p-HRR were obtained from the cone calorimeter measurements with the incorporation of EG particles. Liu et al. [170] studied EG filled high impact polystyrene (HIPS) with UL-94 and LOI tests, as shown in Table 2-32. The amount of expandable graphite (wt%) is displayed after EG in the table. V-0 rating attained for the composite filled with 50 wt% EG and this formulation indicated highest value of LOI (28.7%) relative to other composites.

Table 2-32 UL-94 and LOI results of polystyrene flame retarded by EG [170].

Samples	UL-94	LOI (%)
Pure HIPS	No Rating	18.1
HIPS/EG20	No Rating	21.9
HIPS/EG40	V-1	27.6
HIPS/EG50	V-0	28.7

Laachachi et al. [171] studied the effect of incorporating 5 to 50 wt% of EG on the flammability properties of epoxy resin. From cone calorimeter measurements, TTI, pHRR and THR were recorded, as shown in Figure 2-10. TTI rose with increasing content of EG particles in the composites, followed by a steady enhancement of p-HRR with increasing incorporation of EG up to 25 wt% and then a sudden drop of p-HRR with the addition of 50 wt% EG. The THR values reduced with increasing addition of EG particles except for 15 wt% EG loaded formulation.

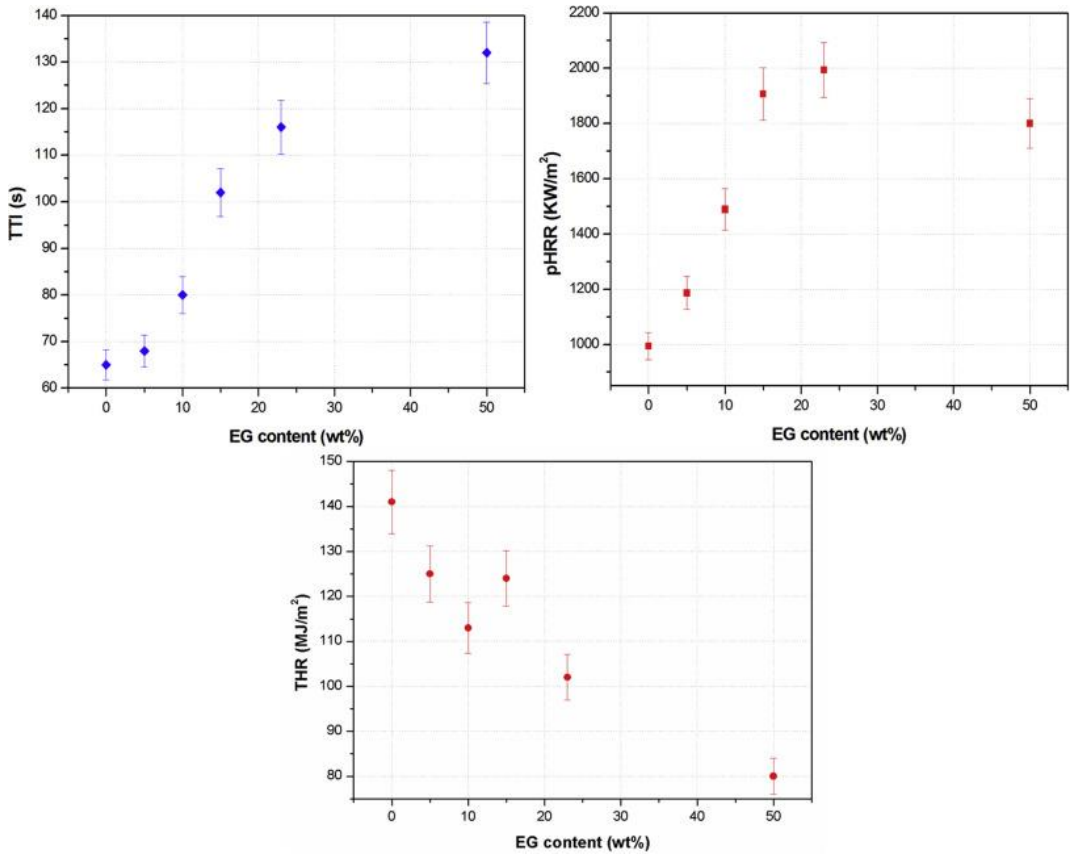


Figure 2-10 Cone calorimeter measurements of time to ignition (TTI), peak of heat release rate (p-HRR) and total of heat release (THR) for epoxy resin flame retarded with 5-50 wt% of EG [170].

Bai et al. [172] produced a composite with 40 g polypropylene grafted with 9 g of m-isopropenyl-α,α-dimethylbenzyl-isocyanate (m-TMI-g-PP) and reinforced with 60 g wood flour. The tested results of the composite were compared with another composite with the same amount of constituents as well as 25 g EG particles. With regards to mechanical behaviors, the tensile strength (MPa), elastic modulus (GPa), elongation to break (%), flexural strength (MPa) and notched impact strength (kJ/m^2) reduced with the incorporation of 25 g EG from 26.2, 249.2, 17.9, 60.2 and 2.3 to 21.3, 177.3, 15.9, 51 and 1.9, respectively. However, the thermal behavior and flame retardancy improved with the addition of EG. The values of LOI%, UL-94 rating and char residue

at 800 °C from TGA test demonstrated remarkably enhancement. The p-HRR and THR values from cone calorimeter test reduced noticeably, and ignition time (IT) improved significantly.

Several types of EG with different expansion ratios and pH levels, as displayed in Table 2-33 [173], were incorporated into magnesium hydroxide (MDH) filled ethylene vinyl acetate (EVA) to produce the composites shown in Table 2-34. From the LOI and UL-94 (Table 2-34) as well as the cone calorimeter results (Table 2-35), it was observed that higher expansion ratio of EG particles increased the LOI value, provided the V-0 level, reduced the effective heat of combustion and enhanced the time to ignition whereas the variations in pH of EG particles did not provide any specific trends. Therefore, EG particles with higher expansion ratio, which is 510 ml/g, was used in the current work, included in chapter 5. The expansion ratio is defined as the volume of EG produced per gram of graphite product, which is measured in litre per gram. (The grams of graphite needed to produce 1L of EG.)

Table 2-33 The physical and chemical properties of different types of EGs.

Type	A	B	C	D
Size (mesh)	50	80	100	> 100
Expansion ratio	330	220	120	100
pH	8.20	9.52	3.92	7.59

Table 2-34 The EVA formulations loaded with several types of EG show different flammability characteristics.

Symbol	Formulations		Flammability	
	MH (phr)	EG (phr)	LOI (%)	UL-94
$M_{120}A_{10}$	120	10(A)	44	V-0
$M_{120}B_{10}$	120	10(B)	39	V-0
$M_{120}C_{10}$	120	10(C)	35	Fail
$M_{120}D_{10}$	120	10(D)	35	Fail

Table 2-35 The effective heat of combustion (EHC) and time to ignition (IT) obtained from cone calorimeter test.

Sample	M_{130}	$M_{120}A_{10}$	$M_{120}B_{10}$	$M_{120}C_{10}$	$M_{120}D_{10}$
Average EHC (MJ/kg)	17.85	8.69	10.66	15.2	13.51
IT (s)	114	219	93	99	96

Literature studies on the effect of EG on flammability reduction, thermal and mechanical properties enhancement for epoxy resins reinforced with natural fibers are generally lacking, in particular those employed oil palm EFB fibers as reinforcing agent.

2.9 Federation Aviation Regulation testing

2.9.1 Vertical Bunsen burner experiment

Chai et al. [10] set up a vertical Bunsen burn experiment which was similar to FAR 25.853 60s, as presented in Figure 2-11. The specimens measuring 70 mm × 290 mm were vertically positioned. Two different types of twill weaves (TW_1 and TW_2) and one unidirectional (UNI) flax fibers were used to produce three different natural fibre based epoxy composites. In addition, the glass fibers of plain weave (PW), twill weave (TW) and unidirectional were used as reinforcement to produce three variant of glass fibre epoxy composites. Fiber fraction ranging from 37 to 39 wt% with thickness of 6.2 to 6.6 mm were fabricated using resin infusion molding.

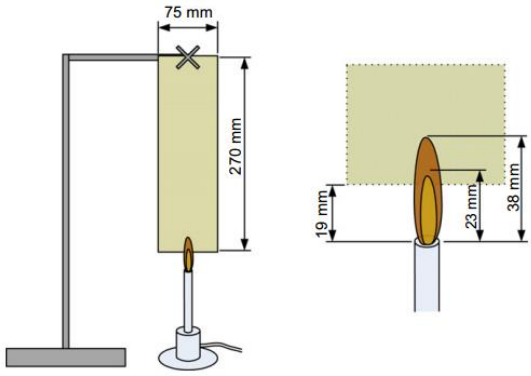


Figure 2-11 Flame adjustment and the specimen positioned for vertical Bunsen burner test [10].

Figure 2-12 shows that the flax fiber reinforced epoxy composite specimens burned intensely compared to that of glass fiber epoxy composites owing to the progressive degradation of fiber structure as well as the nature of natural fiber that acts as fuel source. The combustion process and pyrolysis were faster and greater in natural fiber composite. Natural fiber composite twisted and shrunk along the length and width whereas the glass fiber samples maintained their initial shape. As shown in Table 2-36, larger mass loss was observed in flax fiber epoxy composite than that of glass fibre reinforced formulations.

Table 2-36 The results of vertical burner tests for the epoxy composites reinforced with flax and glass fibres [10].

Fibre type	Glass			Flax		
	UNI	PW	TW	UNI	TW (1)	TW (2)
Total burn time/s	500	560	575	510	515	743
Initial mass/g	228.8	224.4	222.1	169.5	177.1	170.9
Final mass/g	155.5	147.5	140.9	14.3	19.7	37.7
Mass lost/g	73.3	76.9	81.2	155.2	157.4	133.2



Figure 2-12 The specimens still burning after 180 s. a) TW_2 natural fiber, b) TW_1 natural fiber, c) UNI natural fiber, d) TW glass, e) PW glass and UNI glass fibre composite specimens [10].

It can be concluded that natural fiber composite itself does not have the potential to meet the safety requirements of aircraft interiors. The presence of compatible FRs can contribute to the enhancement of their flame resistivity. However, a series of comprehensive flammability tests is required to be carried out to ensure that materials are capable of being utilized in the interior parts. Vertical Bunsen burner, Ohio State university calorimeter and National Bureau of Standard smoke chamber requirements of FAR standards are required for validation. Results obtained from these two mentioned tests were not found to be reported for natural fiber reinforced composites, to the best of author's knowledge.

2.10 Nomex honeycomb panels using composite skins

For the aircraft interiors components including ceilings, partitions, galleys, closets and lavatories, a Nomex honeycomb core is bonded to glass or carbon fiber reinforced composite skins on both

sides of the core. The epoxy adhesive film, prepreg materials and pre-impregnated skins are of main methods to adhere the honeycomb core to composite skins. The Nomex honeycomb core used for aircraft interior components is made of phenolic resin impregnated aramid paper required to possess the cell size of 3.175 mm. The recent (last four years) publications on Nomex honeycomb core bonded to composite skins are shown in Table 2-37. The reports highlighted that panels were fabricated for application in public transport industries and not any specific parts of vehicles were highlighted. The skins are generally made of composites with phenolic or epoxy resin reinforced with carbon or glass fiber. All the parts of composite panels used for aircraft interiors including Nomex honeycomb and composite skins must meet the safety requirements of airplane interior standards (FAA). The detailed properties of honeycomb panels are further discussed in section 6.1.

Table 2-37 Summary of the recent researches on Nomex core panels with composite skins.

Stabilized compressive strength (MPa)	Core material/adhesive properties	Composite skins	Cell size (mm)	Density (kg/m^3)	Ref.
1.72 (ASTM C 365)	Hexagonal Nomex	Carbon fiber epoxy	3.2	48	[174, 175]
Compression tests were conducted after tensile test	Hexagonal Nomex/ Epoxy adhesive film	Glass fiber epoxy	4.8	32	[176, 177]
Compression tests were conducted after tensile test	Hexagonal Nomex/ Epoxy adhesive film	Glass fiber epoxy	4.8	64	[176, 177]
2.08 (ASTM C 365)	Hexagonal Nomex/prepreg material (autoclave molding)	E-glass fiber phenolic resin	3.175	48	[178-180]
0.8 (ASTM C 365)	hexagonal Nomex/Epoxy adhesive film in an autoclave	Carbon/bismaleimide (resin) composite	4.76	32	[181]

2.11 Summary

Currently, most of the ceilings, partitions, lavatories, galleys and sidewalls are comprised of sandwich panels fabricated from a Nomex honeycomb core and synthetic fibre based polymer composite skins, in particular sheets of phenolic or epoxy resin reinforced with fiberglass or carbon fibers. The top surfaces are covered with highly formable decorative thermoplastic films that are printed in a variety of complex patterns and colors and are embossed in a wide selection of textures and gloss levels. Various parts of stowage bins, air ducts, windows and insolation have also been fabricated with the composites that met the aircraft interior requirements without the honeycomb core in the structure. However, the world's focus on lowering carbon footprints and increasing sustainable credentials of materials are particularly pertinent in the aerospace sector. The unrelenting passion of sustainability has led to an expanding search for high performance, renewable fibers reinforced composites with affordable cost. There has been numerous development reported on the potential of replacing synthetic fibers with natural fibers sourced from plants, crops, animals, agro waste and other natural resources such as oil palm, coconut, coir, bamboo, sugarcane, pineapple, wheat straw, rice husk, banana, sisal, cordenka, flax, hemp, kenaf, cotton, betelnut, etc. [27-29, 182] with majority targeted on non-structural automotive components and general household utilities [183-187]. However, the challenges of producing palm based fiber composite fit for aircraft interiors are its ease of biodegradability and combustibility as well as difficulty in removal of the residual oil content which hinders optimum adhesion between fiber and matrix. From the current data published in the field of natural fiber composites, it can be revealed that appropriate polymeric matrix with effective treatment of natural fiber offers the potential to meet the lab scale mechanical properties of aircraft interiors as composite component or composite skin of Nomex honeycomb core, however, safety factors including flammability,

heat release, smoke and toxicity, which are the main elements of FAA standards, are generally lacking in terms of investigation carried out according to FAR specifications. Besides, very few publications were reported to evaluate the flammability and mechanical properties of Nomex honeycomb panels with natural fiber composite skins.

The current challenge, in order to meet the requirements of aircraft interior parts, is to fabricate composites with approved mechanical characteristics [188-190] as well as effective flame retardancy [190-192]. The summary of selection criteria for choosing materials and methodology is outlined as follows:

1- EFB fibers as a natural fiber not only are widely available in Malaysia, but also comparatively show lower density relative to other types of natural fibers, which form the main driver for component growth of aircraft interiors.

2- As discussed in Section 2.8, higher concentrations of flame retardants improve the flame resistivity, smoke and thermal behaviors of composite materials. Various flame retardants have been employed that among which APP has been widely used due its effectiveness at low concentration compared to other flame retardants [193, 194]. ATH and ZB were also widely used in transport industries for fabrication of composites. Depending upon polymer type and the required application, compatible and proper flame retardants are required to be considered. As demonstrated in Table 2-29, the application of numerous FRs for the interior parts of car, bus, rail vehicles, ship and aviation is highlighted. The most widely used flame retardants that showed potential for use with epoxy polymer and other resin based systems are APP and ATH. Zinc borate as a synergistic material has also been used with epoxy resin as the interior components as well. Expandable graphite as an effective flame retardant with several expansion ratios and pH levels was previously investigated,

and concluded that higher expansion ratio of EG creates greater flame resistivity. In the current study, EG particles with the expansion ratio of 510 ml/g was used.

3- Despite the fact that increasing the amount of FRs in composites enhance the flame retardancy of composites, they may deteriorate the mechanical properties. Therefore, the lowest amount of FRs that are capable of meeting the requirements is taken into account. The attempt is to apply less than 20 wt% flame retardants to refrain from significant reduction in the mechanical properties. In the current work, the maximum amount of flame retardant to be incorporated into composites is 15 wt%.

4- After obtaining the optimum formulations from FR and expandable graphite filled composites, it is crucial to improve their mechanical properties via chemical fiber treatment. As discussed in Section 2.5, natural fiber treatment is capable of enhancing the mechanical properties of the composite. Alkali treatment improves the interfacial adhesion between polymer and natural fiber by eliminating the wax and deposits from the surface of natural fibers.

5- Thermosets do not require high temperatures during pre-cured fabrication of composite and are highly compatible with natural fibers. The processing temperature of thermoplastic is about 200 °C<, which tends to damage the structure of EFB fibers as well as lowers the thermal performances of natural fibers. Epoxy resin is selected due to higher mechanical properties in comparison to phenol resin and also it is not necessary to use high pressure for the fabrication of epoxy based composites. The fire resistivity of epoxy composites can be effectively enhanced by the inclusion of suitable flame retardants.

6- In order to meet the requirements of FAA, aircraft agencies and aerospace manufacturers, the flammability behaviors as well as mechanical performances must be investigated. In

this study, the flammability tests (vertical Bunsen burner experiment including FAR part 25.853-b and 25.853-a) as well as other lab scale mechanical testing experiments were performed. However, two more instruments are required to evaluate the performance of composite materials for use as interior components of aircraft. Ohio State University calorimeter that measures the amount of heat release and National Bureau of Standards (NBS) smoke chamber machine that measures the specific optical density. These analyses could not be outsourced for conducting experiments in the current work due to several limitations. To compensate for Ohio State University calorimeter, the bomb calorimetry study was conducted to measure the gross heat of combustion. But, no equivalent value is available to convert the values to an equivalent of heat release value from Ohio State University calorimeter test.

In addition to that, few other tests such as thermogravimetric analysis (TGA), field emission scanning electron microscope (FESEM), and energy dispersive spectroscopy (EDX) were carried out for the palm fiber reinforced FR filled composites and formulations with expandable graphite. Besides, combined confocal Raman spectroscopy and atomic force microscopy (AFM) and furnace test were performed for expandable graphite particles. Dynamic thermal mechanical analysis (DMA) was also conducted for the EG filled composites. Finally, the mechanical and flammability performances of Nomex honeycomb panels with the natural fiber composite skins were analyzed.

Chapter 3

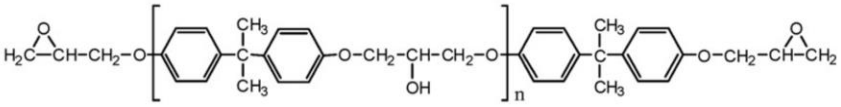
3. Methodology

3.1 Materials

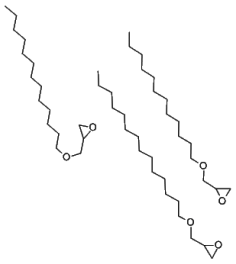
Alumina Trihydrate (ATH) of Hydral PGS-SD grade with median particle size of 1 μm in diameter, specific gravity of 2.42 g/m^3, pH value of 9~10 and decomposition temperature of 220 °C and Zinc Borate 400 grade (ZB) with particle size of 3-5 μm and specific gravity of 2.67 g/m^3 and temperature of dehydration of 290 °C was provided by J.M. Huber Corporation (Malaysia). ZB had zinc oxide (ZnO) content of 37~40 %, borate oxide (B_2O_3) of 47~49 % and water (H_2O) quantity of 13~15.5%. Ammonium polyphosphate (APP) phase II powder of grade Exolit AP 422 (degree of polymerization greater than 1000) with decomposition temperature of more than 275 °C, density (at 25 °C) of 1.9 g/m^3, particle size of less than 50 μm, distribution particle size of more than 95 wt%, pH value of 5.5~7.5, phosphorous content of 31~32 % w/w and nitrogen content of 14~15 % w/w was provided by Clariant (Singapore) Pte Ltd. An ambient cure two-part epoxide resin system Ultimeg 2020 were provided by AEV Asia Sdn Bhd (Malaysia). The viscosity of mixture of epoxy (Ultimeg 2020 base) and hardener (Ultimeg 2020 hardener) at 25 °C was measured 0.2- 0.6 Pa.s and had the specific gravity of 1.1. The chemical structure of the epoxy and hardener is shown in Figure 3-1. Pulverized palm empty fruit bunch fiber (hereinafter stated as EFB) was purchased from Szetech Engineering Sdn. Bhd. The EFB fiber had an average length in the range of 10- 20 mm and bundle diameter of 100 - 200 μm (Figure 3-2 (a) and (b)). Another type of EFB fibers with 1-3 mm in length was supplied by PolyComposite Sdn Bhd. The average density and diameter of the EFB fibres were 1.07 g/cm^3 and 100-400 μm, respectively (Figure 3-2 (c)). Sodium hydroxide with minimum 99% alkalimetric titration used for the chemical treatment

of EFB fibers was purchased from R&M Chemicals. Resin infusion equipment and tools were supplied by (Easy Composites Ltd) and a water based formaldehyde-free cross-linked acrylate binding agent, Acrodur DS 3530, was supplied by BASF Malaysia Sdn. Bhd. The binder had approximately the solid content of 50 %, pH value of 3.5 and viscosity of 150~300 mPa.s. The chemical structure of Acrodur DS 3530 is illustrated in Figure 3-3 .Expandable graphite (EG) was supplied by Qingdao Kropfmuehl Graphite Co. Ltd. with carbon content and expansion ratio of 99.1% and 510 ml/g, respectively. Ash content and moisture were measured 0.9% and 0.34%. 80% of EG particles showed the particle size of more than 300 µm, 1.2% below 150 µm while the remaining 18.8% fell in between the two size, as shown in Figure 3-4, and the pH value of particles was recorded between 3 and 6. The aerospace grade Nomex honeycomb with the density of 29 kg/m^3 was supplied by Easy Composite Ltd. The Nomex honeycomb had the thickness of 2 mm and cell size of 3.2 mm.

Component A. Epoxy resin (Ultimeg 2020)

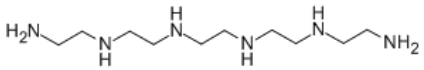


Diglycidyl ether of bisphenol A, DGEBA (CAS No. 25068-38-6)

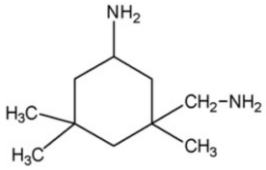


Alkyl glycidyl ether (CAS number: 68609-97-2)

Component B. Ultimeg 2020 hardener



3,6,9,12-tetra-azatetradecamethylenediamine (CAS number: 4067-16-7)



Isophorone diamine (CAS number: 2855-13-2)

Figure 3-1 Chemical structure of epoxy compounds and amines [195].

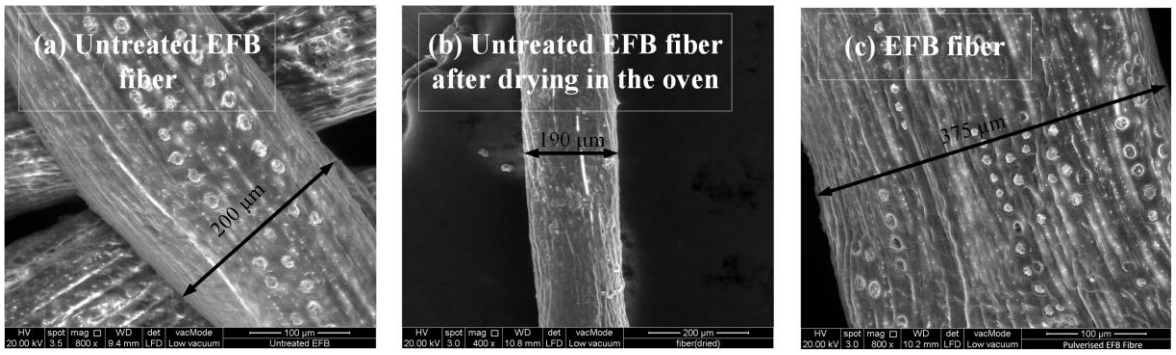


Figure 3-2 SEM micrographs of (a) untreated EFB fiber, (b) untreated EFB fiber after drying in the oven, which were purchased from Szetech Engineering Sdn. Bhd. and (c) EFB fiber provided from PolyComposie Sdn Bhd.

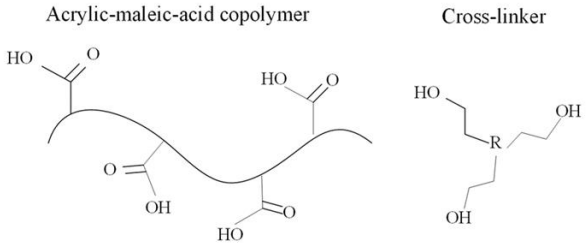


Figure 3-3 The chemical structure of Acrodur DS 3530.

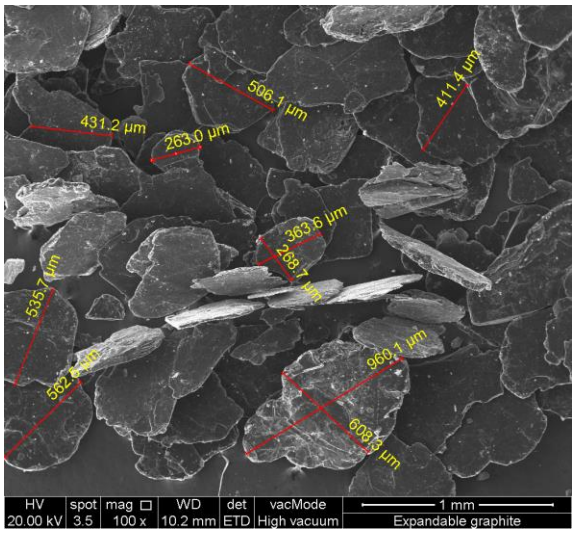


Figure 3-4 SEM micrograph depicts the particle size of expandable graphite.

3.2 Fiber mat fabrication

Randomly-orientated EFB fibers were dispersed in a water-binder suspension of 10:1 (v/v) ratio to form a mat in a customized sieve (180mm × 320mm) with the mesh size of 1.5mm × 2mm. Fiber length of 10-20 mm was chosen to avoid fiber entanglement and to encourage even distribution of fiber during mat fabrication [196]. The sieve was then taken out where draining of water took place. The fiber mat was then flipped upside down onto pieces of dry cloth, and another layer of dry cloth was placed on top of the fiber mat to absorb residual water from both sides. The bonded mat was shifted to metal plates with blotting papers on top and bottom of the mat. A load of 15 kg (equal to 2.6 kPa) was then applied on top of the fiber mat for 10 minutes to press out the remaining water and to produce a mat with an even thickness of 1 mm. Fully soaked blotting papers were replaced with new ones and pressed with the same weight until the mat was visibly dried. The dried fiber mat was subsequently placed within a convection oven maintained at 100°C for 4 hours with an applied top loading of 4kg while measurements were taken to ensure the fiber mat

showed no further weight loss due to moisture evaporation. The dried fiber mat was further kept dry within the oven at a lower temperature of 70 °C for 24 hours (The fiber mat showed the weight of 20 g with negligible variation as in the most cases the fiber mats indicated the same weight.) until resin infusion was to be carried out. The fiber mat was dried under selected temperature to ensure that the structure and properties were not damaged by the extreme temperature. Figure 3-5 shows the mat fabrication process from scratch.

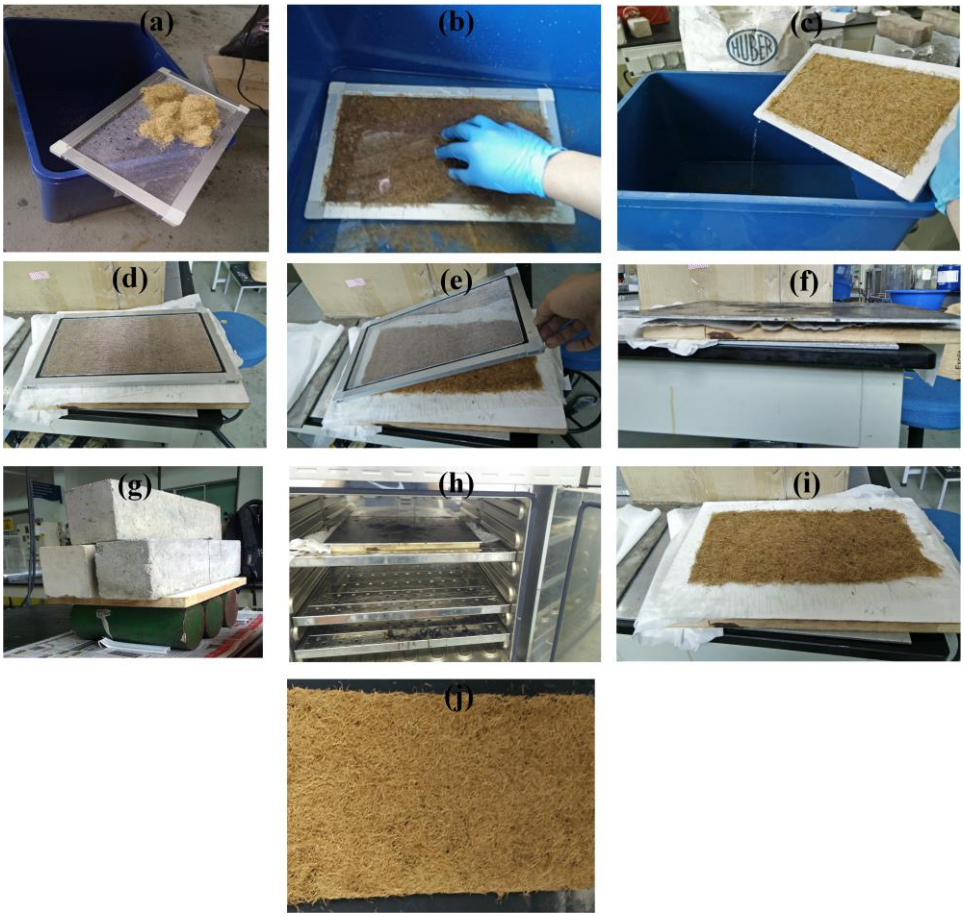


Figure 3-5 Mat fabrication process. (a) preparation of the required amount of fiber, (b) fiber soaking and dispersion, (c) draining the water, (d) filtered mat was shifted to plates with blotting papers, (e) sieve removal, (f) the fiber mat was placed between the metal plates, (g) the required load was applied, (h) the mat with an applied weight on top of it was placed in a convection oven, (i) removal of fiber mat from oven and (j) an evenly distributed EFB fiber mat.

3.3 FRs- based composite fabrications

3.3.1 Initial set up

The fabrication process of FR loaded EFB composite is illustrated in Figure 3-6 and Figure 3-7. A summary is outlined. In the first stage, a PVC plate was sprayed with a silicone release agent. Then gum tape was applied around the perimeter of the mold and the EFB fiber mat was placed onto the mold, as shown in Figure 3-7 (b). A layer of peel-ply was positioned on the EFB mat (Figure 3-7 (c)). This was followed by an infusion mesh that helped the resin to flow and distribute through the mold. Subsequently an infusion spiral and resin feed silicone connector was fitted to the vacuum system. Then vacuum line silicon connector was positioned and the bagging film was stuck to the gum tape. Resin feed hose was connected to the bag and another PVC hose was firmly connected to the bag through vacuum line. An infusion line clamp was used to close the resin feed line and, as a result, evacuating air from the vacuum system. At the stage where full vacuum was achieved, the sealed bag was left for 15 minutes to ensure there is not any leakage.

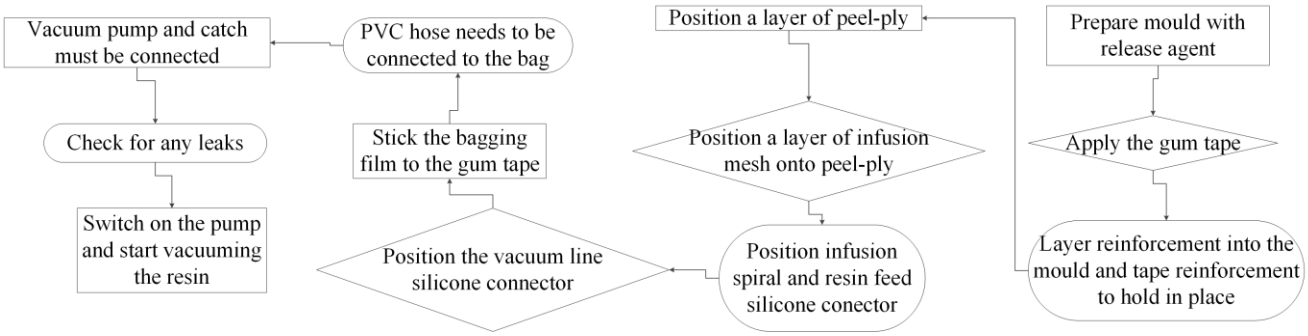


Figure 3-6 Fabrication process using resin infusion technique.

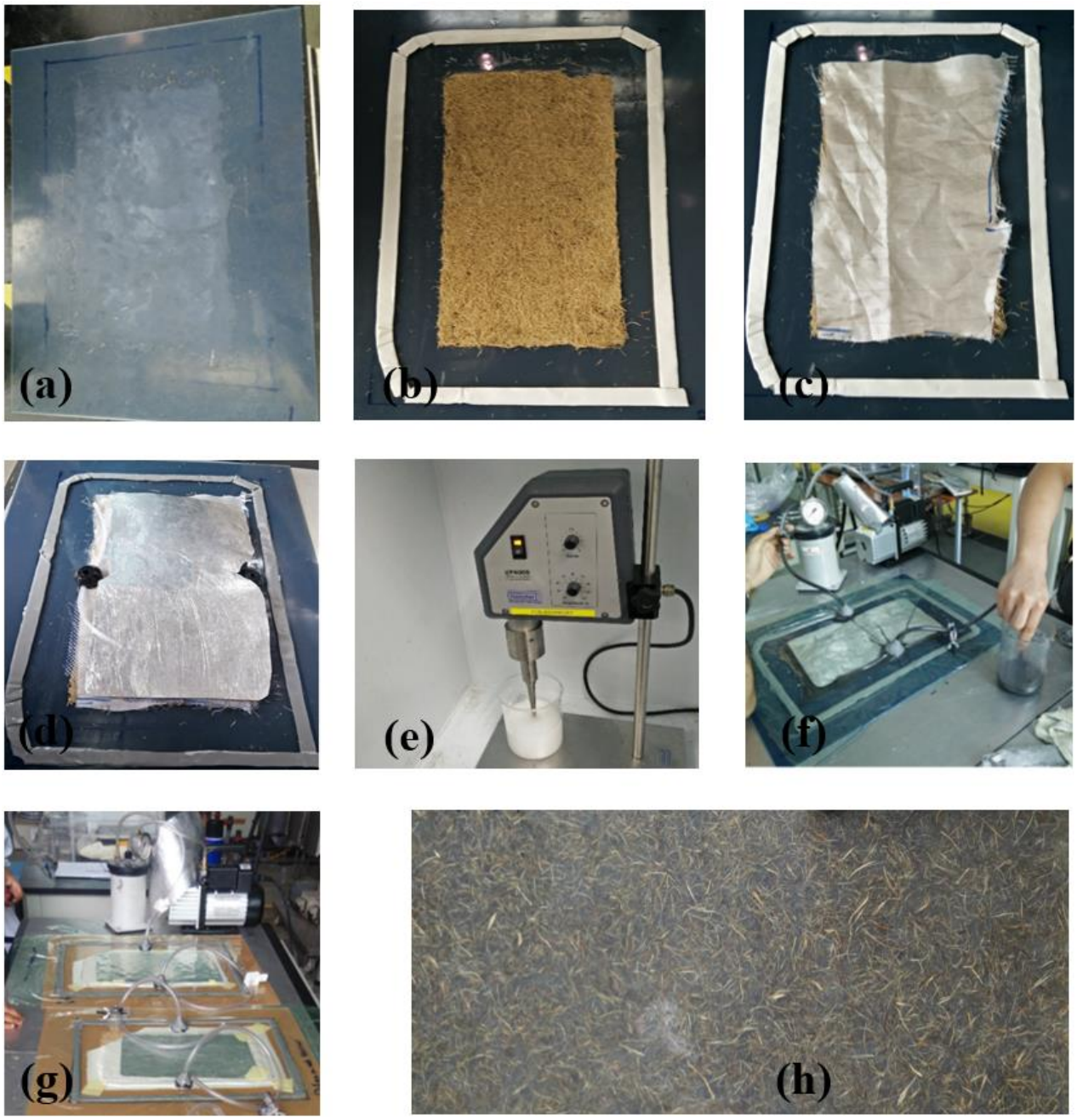


Figure 3-7 Composite fabrication process. (a) plastic mould, (b) applying the gum tape and placing the EFB fiber mat, (c) laying the infusion mesh and peel ply, (d) laying the aluminum foil, (e) sonication process, (f) resin infusion, (g) curing for 24 hours and (h) a near view of composite.

3.3.2 Resin infusion

Prior to resin infusion process, pre-determined quantity of FRs were added into the epoxy resin and approximately 15 minutes of ultrasonication was applied using a UP400S Ultrasonicator from Hielscher Ultrasonics GmbH (Figure 3-7 (e)) at a frequency of 24 kHz and 50% amplitude until homogeneous dispersion was observed. Fabricated palm fiber mat (explained in 3.2 Section) was then laid on top of a PVC mold and resin infusion process was to be conducted as follows: After vacuuming out the air from the infusion area via a vacuum pump and no leakage was observed, hardener was added into the sonicated mixture at a weight ratio of 5:1 (epoxy: hardener). The mixture was then infused throughout the fiber mat in the mold at the vacuum pressure level of -1 bar. The curing process of EFB reinforced epoxy composite took place under room temperature for 24 hours. The final product of FR additive composites is depicted in Figure 3-7 (h). The combination of neat epoxy and EFB fiber, as control composite, were also prepared for comparison purpose. Also, two of the formulations (treated control and optimum) fabricated with alkali treated fibers in order to compare their mechanical properties. The formulations fabricated are shown in Table 3-1. The number in front of abbreviations represents the amount of constituents (in percentage) by weight in the composites.

Table 3-1 Sample designation (The concentration of constituents is shown by wt%).

composites	ATH	APP	ZB	Fiber	Treated fiber	Epoxy
E100	-	-	-	-	-	100
$E_{82}F_{18}$ (control)	-	-	-	18	-	82
Treated control	-	-	-	-	18	82
$CATH_5$	5	-	-	18	-	77
$CATH_{10}$	10	-	-	18	-	72
$CATH_{15}$	15	-	-	18	-	67
$CAPP_5$	-	5	-	18	-	77
$CAPP_{10}$	-	10	-	18	-	72
$CAPP_{15}$	-	15	-	18	-	67
$CATH_5APP_{10}$	5	10	-	18	-	67
$CATH_{10}APP_5$	10	5	-	18	-	67
CZB_5	-	-	5	18	-	77
CZB_{10}	-	-	10	18	-	72
CZB_{15}	-	-	15	18	-	67
$CATH_5ZB_{10}$	5	-	10	18	-	67
$CATH_{10}ZB_5$	10	-	5	18	-	67
$CAPP_{10}ZB_5$	-	10	5	18	-	67
$CAPP_5ZB_{10}$	-	5	10	18	-	67
$TATH_5APP_{10}$	5	10	-	-	18	67

3.4 Fiber treatment

For the composites fabricated by resin infusion technique, two formulations (treated control and optimum) were made with treated EFB fiber for the evaluation of changes in mechanical properties. The pre-treatment was conducted as follows: Sodium hydroxide (NaOH) solution was prepared with a 5 wt% concentration. The required amount of EFB fibers were immersed in alkaline aqueous solution (the initial pH of solution, measured by Metrohm-827 pH lab, was around 10.7) for period of 24 h at ambient temperature, and subsequently were thoroughly washed with distilled water until the complete elimination of traces of NaOH (until the pH value dropped

to approximately 7 in pH meter). Fibers were then dried for 24 h in an oven maintained at 70 °C. The process of fiber alkali treatment is shown in Figure 3-8.

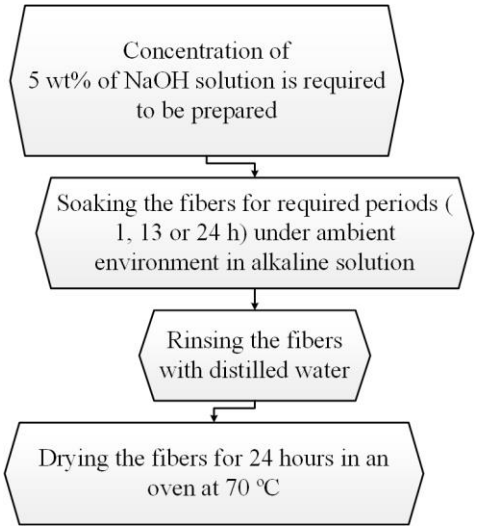


Figure 3-8 The process of EFB fiber chemical treatment.

3.5 Preparation of EG filled EFB epoxy composites and formulations with EG coating

The EFB fibers and EG platelets were oven dried for 24 hours at 70 °C and 100°C, respectively, prior to the composite fabrication. EG-filled EFB epoxy composites were produced by mixing measured quantity of EG and subsequently EFB fibers into epoxy resin at ambient temperature. The mixture of EG and epoxy were mixed with the aid of a mechanical stirrer with a constant revolution of 1000 rpm for 30 minutes, followed by ultra-sonication with amplitude of 50% and the frequency of 24 kHz for the period of 15 minutes to achieve a homogenous dispersion in the epoxy matrix. EFB fibers of 20 wt% with the length of 1-3 mm were added into the mixture to soak for 5 minutes while the mixture was shaking in a shaker incubator with the speed of 150 rpm at ambient temperature. Hardener was then added at appropriate ratio and mixed for 2 minutes. The process of transferring the mixture had to be gentle to prevent air being induced into the

composites. The mix spread across the mold manually and left for 30 min in order to achieve partial cured state. Afterwards, a top plate was gently placed to close the mold. All these steps were applied to eliminate void formation. The mixture was degassed for 15 minutes in a catch pot connected to a vacuum pump prior to compression molding. The mixtures were poured into a matching mold with the thickness of 2 mm. Composites were cured for 24 hours under the compression loading of 17 kPa (on the projected area of 200mm × 120mm) at ambient temperature. It is worth noting that the weight of mixture of composite was calculated according to density of constituents used. Slightly higher amount of the volume of mold was considered for the mixture. The densities used for epoxy polymer, EG and EFB fiber were 1.11 (as per manufacturer specifications) , 2.2 [197] and 1.07 g/cm^3 (measured by the author), respectively. The formulations prepared with their respective wt% from compression molding technique were stated in Table 3-2.

Table 3-2 Sample designation (values represent wt %).

Formulations	Epoxy	EFB fibers	Treated EFB fiber	EG
E100	100	0	-	0
Control (C)	80	20	-	0
CEG3	77	20	-	3
CEG5	75	20	-	5
CEG7	73	20	-	7
EG5	75	-	20	5
*Coating3	97	-	-	3
*Coating5	95	-	-	5

*Both sides of the control were coated with the mixture (epoxy and EG).

Moreover, two formulations with EG coating were fabricated to evaluate their performances in the Bunsen burner test. Expandable graphite at 3 wt% and 5 wt% were added into the epoxy resin and the mixture was first dispersed manually and then mixed with the aid of ultra-sonication for 15

mins with similar frequency and amplitude used for the composite fabrication. The stoichiometric ratio of hardener was incorporated to the mixture and stirred for 2 mins prior to degassing for 10 minutes. Subsequently, the mixture of epoxy/EG was applied by brushing on the surface of 20 wt% EFB fiber reinforced composite in two steps. Initially, a layer of coating was applied on the surface of the composite and allowed to cure for 24 h. Then, the second layer of coating was brushed to provide a suitable surface finish and to obtain an approximately 0.5 mm coating on each surface of composite. The thickness was measured using a digital vernier caliper.

In order to investigate the effect of fiber pretreatment on mechanical properties of EFB fiber reinforced EG filled composites, one additional formulation (EG5) was produced using the alkali treated fibers. The fibers were soaked in an aqueous NaOH solution with the concentration of 5 wt% for 24 h at room temperature and then rinsed with the distilled water until they reverted to the neutral pH value. Figure 3-9 shows several pictures of composites fabricated

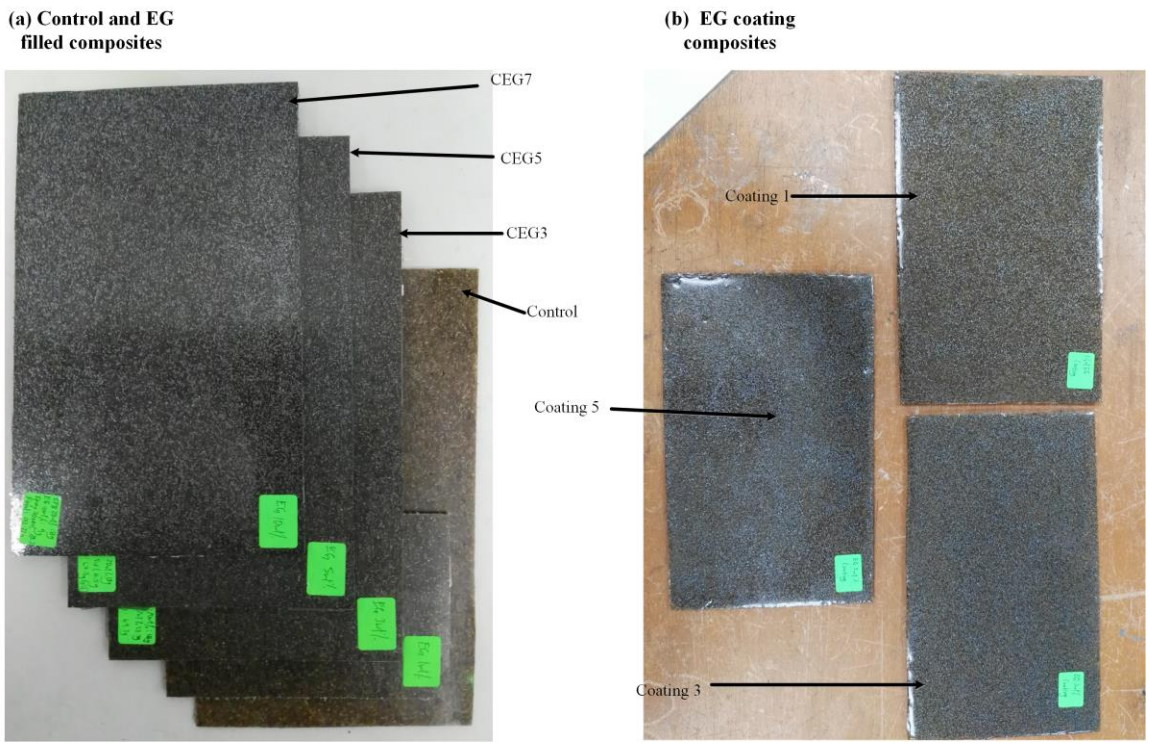


Figure 3-9 (a) control and EG filled composites and (b) EG coating composites.

3.6 Characterization

3.6.1 Vertical Bunsen burner test

The vertical Bunsen burner test was carried out in accordance with Federal Aviation Regulation (FAR) part 25.853-b (equivalent to ASTM F 501, Daimler-Benz Aerospace ATS 1000.001, Douglas DMS 1511, Boeing BSS 7230 F2, British Aerospace BACM 1555A and Airbus ATS 1000.001) [34] to determine flammability characteristic of the materials. Three specimens measuring 152.5 mm × 37.5 mm × 2 mm, equivalent to half of the standard FAR specified dimension, were tested. The specimens were held vertically via a lab stand and flamed for 12 seconds using methane fuel supplied by Bunsen burner placed directly under the specimen. The total flame time, mass loss percentage, burn length and drip flame time were measured to analyze the flammability properties. For formulations which met the vertical Bunsen burner test

requirements, a series of full size specimens (305 mm × 75 mm) was used and tested. The same results in terms of total flame time, drip flame time and burned length were obtained.

For honeycomb specimens and panel specimens, a series of full size specimens (305 mm × 75 mm) in accordance with FAR-25.853 (b) was used and tested. Three of the optimum formulations that could meet the FAR-25.853 (b) specifications, were tested against FAR-25.853 (a) (equivalent to ASTM F 501, Daimler-Benz Aerospace ATS 1000.001, Douglas DMS 1510, Boeing BSS 7230 F1, British Aerospace BACM 1551A and Airbus ATS 1000.001), [34] which is the vertical Bunsen burner experiment with the ignition time of 60 s.

It is worth mentioning that to evaluate the potential of composite materials to be used for aircraft interiors, all the requirements of FAA, aircraft agencies and aerospace manufacturers must be met. On top of vertical Bunsen burner test, two more tests are required to investigate the possibility of composite materials for use in aerospace cabin parts. Ohio State University calorimeter and NBS smoke chamber tests are crucial to measure the heat release and the specific optical density, respectively. However, these two instruments could not be outsourced in Malaysia and several countries in the current work. To compensate for Ohio State University calorimeter, bomb calorimeter test was carried out to measure the gross heat of combustion. However, no equivalent formula is available to convert the gross heat of combustion value to an equivalent of heat release value from Ohio State University calorimeter test. It is necessary to collaborate with aircraft manufacturers in order to analyze all the requirements of each particular manufacturer and also it helps increase the chance of access to those above-mentioned instruments.

3.6.2 Bomb calorimeter

Bomb calorimeter was used to validate the heat capacity of compounds prompted by control composite, FRs additive and EG filled formulations. Gross heat of combustion was measured by PARR 6100 bomb calorimeter according to ASTM D-240 standard [198]. 2 L of water was contained in the metal bucket where the specimen was placed and gradually bomb charged with O_2 to 30 atm (3 MPa) at ambient temperature. Sample weight of 0.8 to 1g was placed in a cylindrical crucible and the specimen was linked to the fused wire for combustion to occur. At least two samples for each formulation were tested and the average measurements were computed. Figure 3-10 depicts the picture of equipment used to evaluate the ignitibility performance of composites.

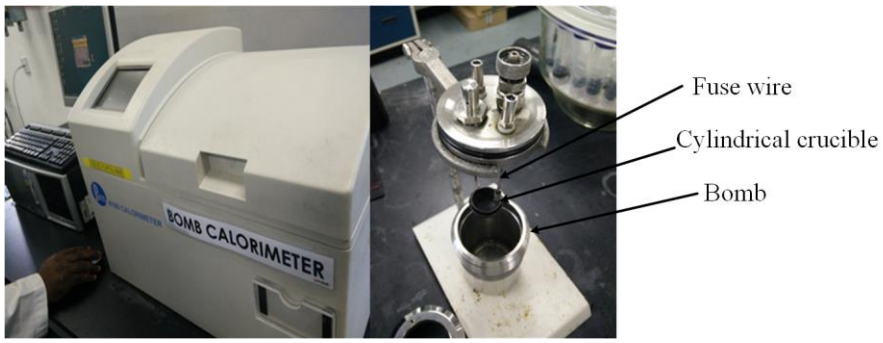


Figure 3-10. Bomb Calorimeter equipment.

3.6.3 Thermogravimetric analysis

The thermal stability was evaluated with the aid of a TGA 1 STARe system (Mettler Toledo) Q500 instrument. Specimen of approximately 10-15mg in weight was placed in an open alumina pan under nitrogen flow rate of 50 ml/min and heated from ambient (30˚C) to 600˚C at a heating rate of 20˚C/min. The char residual and thermal degradation temperature (T_d) were calculated.

The thermal degradation EG filled composites and formulations fabricated by compression molding was studied in an alumina pan with a lid, which has a hole on top, due to expansion of EG, under similar flow rate and heating rate. The EG filled formulations were heated in N_2 environment from 30 to 700 ˚C.



Figure 3-11. TGA testing instrument.

3.6.4 Dynamic thermal mechanical analysis

Dynamic thermal mechanical measurements were conducted on a PerklinElmer DMA 8000 instrument. The frequency was set to 1 Hz and the temperature increased from 30 ˚C to 100 ˚C at a ramping rate of 3 ˚C/min. The single cantilever mode was used for the sample dimension of 25 mm × 7 mm × 2 mm. This mode of test was used as proposed by Perklin Elmer as the best choice and since it is the ideal mode for the sample geometry with the thickness of 2 mm. The DMA equipment is shown in Figure 3-12. The test was conducted to measure the storage modulus (E′) and loss factor (Tan δ) of epoxy, control and EG loaded formulations.

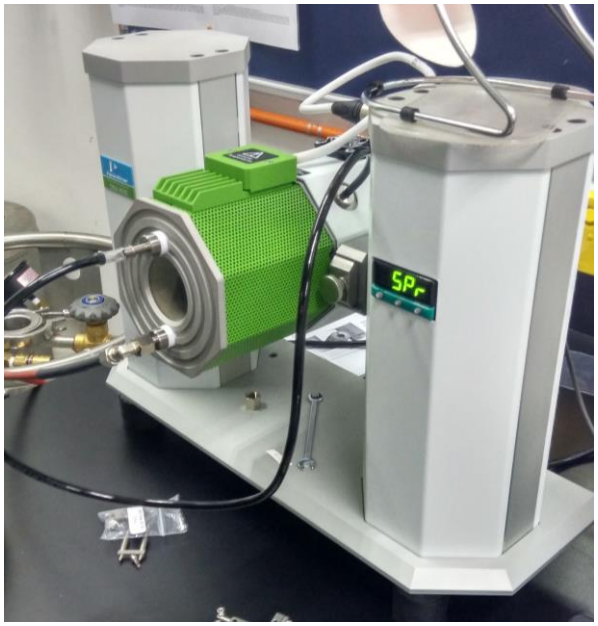


Figure 3-12 DMA instrument.

3.6.5 Fourier Transformed Infrared spectroscopy (FTIR) analysis

FTIR was conducted to analyze changes in chemical compositions of fibers after treatments. About 3 mg of EFB fibers was crushed using a centrifugal ball mill and mixed with potassium bromide (KBr) and then compressed into a disk of Perkin-Elmer FTIR spectrophotometer. IR spectrum was recorded by co-adding 5 scans at the resolution of 3 cm^{-1} in the frequency range of 4000-400 cm^{-1}. From the results obtained, the effectiveness of chemical treatment was determined by analysis of the peak absorbance. The steps to prepare the material and the last stage, which is placing the mixture inside the instrument, are shown in Figure 3-13.

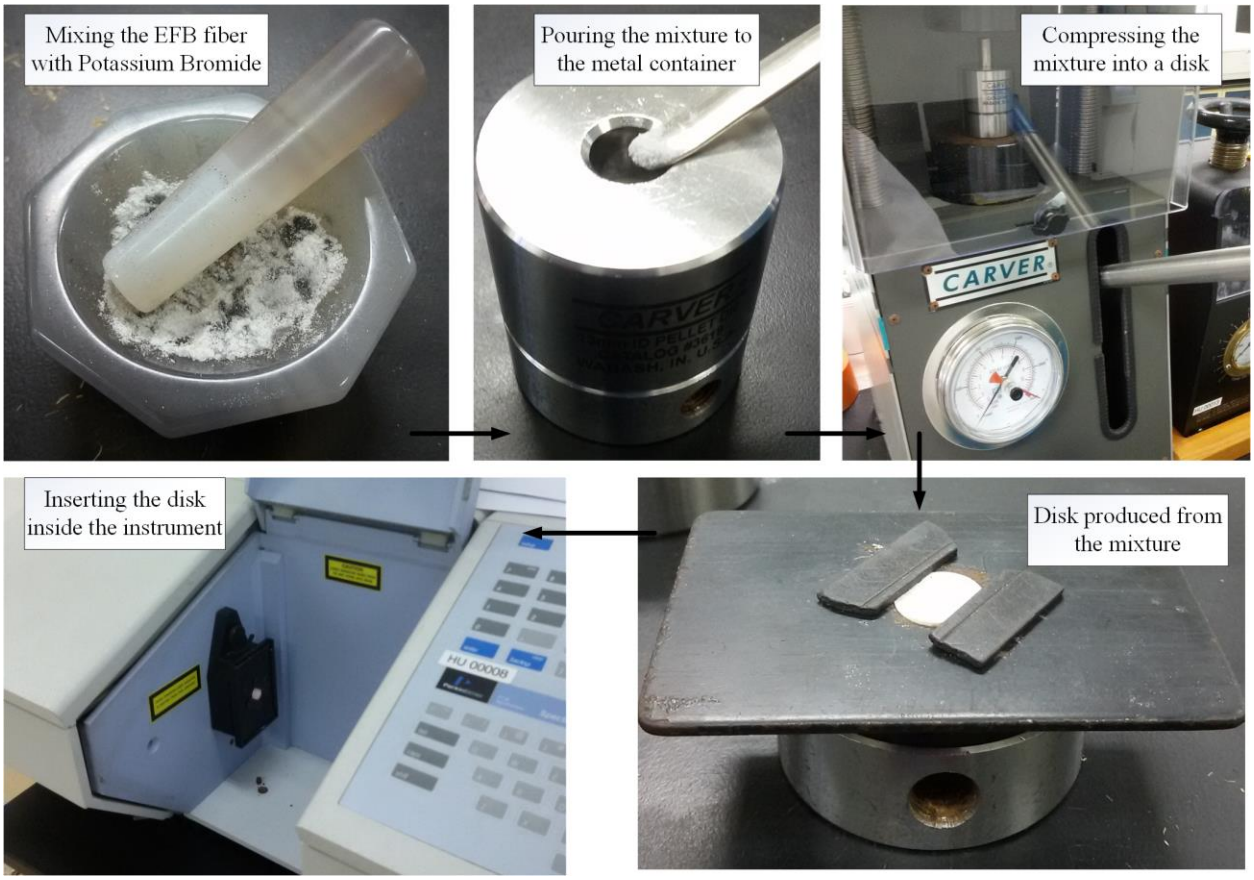


Figure 3-13 Preparation procedure of FTIR test.

3.6.6 Tensile testing

Rectangular specimens of 120 × 20 × 2 mm^3 (that were cut using a band saw machine) were tested with the aid of a Llyod Instruments LR50k testing machine in accordance to ASTM D3039 [199] at a crosshead speed of 2 mm/min and the load-cell of 5kN was used. Five specimens of each formulation were tested using a gauge length of 60 mm and the mean value was recorded. Figure 3-14 depicts several fractured tensile specimens right after experiment.

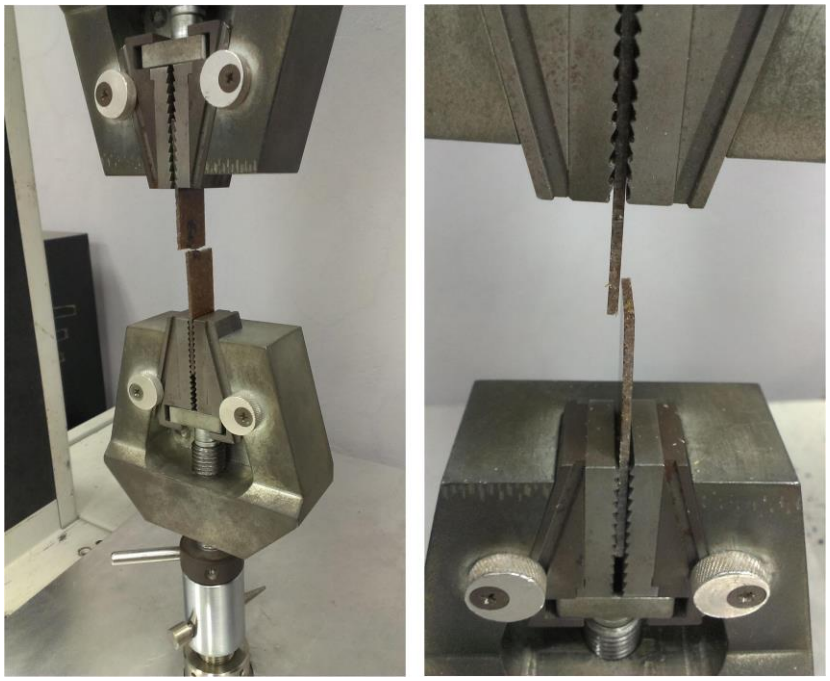


Figure 3-14 Fractured tensile samples right after tensile testing.

3.6.7 Flexural testing

Rectangular specimens of 100 × 20 × 2 mm^3 were tested using a Llyod Instruments LR50k testing machine in a three point bending mode with a span length of 60 mm in accordance to ASTM D790 [200], as shown in Figure 3-15. Crosshead speed of 5 mm/min and load-cell of 5kN were used. Five specimens of each formulation were tested and the mean values were used to analyze the flexural strength and strain of the various formulations.

The flexural properties of Nomex honeycomb sandwiched panels were evaluated by 3 point bending tests in accordance with ASTM C393 [201] where the speed for crosshead was 6 mm/min and the specimen size was 200 mm × 75 mm × 6 mm. The support span was set to 150 mm. More information regarding the detailed test and fabrication of honeycomb panels with the composite skins is described in Chapter 6.



Figure 3-15 A composite sample fractured under a three point bending load.

3.6.8 Compression test

Flat-wise stabilized compressive tests was conducted in accordance with ASTM C365M standard [202] to evaluate the out-of-plane crushing performances of Nomex honeycomb sandwich panel. The Llyod Instruments LR50k testing machine was used to conduct the tests on specimens measuring 50 mm × 50 mm (length × width). The thickness of Nomex honeycomb and sandwich panel was 2 mm and 6 mm, respectively. The moveable head installed on top moves downward to apply the load to the specimen through the loading plate. A spherical seat was fixed to the stationary head to remove probable eccentric load. The specimens were compressed with the cross head speed of 0.5 mm/min. The five specimens of each sandwich panel were tested and values of compressive properties were recorded.

3.6.9 Plate shear test

Transvers shear experiments were carried out according to ASTM C273 [203] with the aid of Llyod Instruments LR50k testing machine. The specimen size of 150 mm (length) × 50 mm (width) was used and the tensile loading rate of 0.5 mm/min was applied to the samples. The tests

were conducted in L (ribbon direction) and W (transverse to the ribbon) directions, and four specimens were tested for each direction. Plate shear properties of honeycomb core in L and W directions were recorded when a shear force is applied parallel to the L-W plane.

3.6.10 Field emission scanning electron microscopy (FESEM)

SEM was carried out on FEI Quanta 400F FESEM microscope at the increasing voltage of 20kV. The SEM micrograph of the untreated fibers, treated fibers and composites' fractured surfaces was scanned to observe the deposits removal from fibers after treatment as well as adhesion, dispersion and load transfer between the fiber, FRs, EG particles and epoxy matrix.

3.6.11 Energy dispersive spectroscopy (EDX)

Energy dispersive spectroscopy study was performed using the same FESEM instrument. The elemental composition of residual char attained after the Bunsen burner and TGA tests were observed and analyzed. The EDX tests were conducted for the CAPP10ATH5 (optimum FR based composite), EG particles and EG filled composites.

EDX evaluations were also carried out to determine amount of the elements in EFB fibers. The weight percentage of carbon and oxygen in fibers prior to and after chemical treatments were evaluated.

3.6.12 Furnace test

In order to investigate the expansion temperature, char structure and char expansion of expandable graphite, EG flakes were placed in a Carbolite furnace (CWF 12/65/550 model, as shown in Figure 3-16) preheated at different temperatures of 100 °C, 150 °C, 200 °C and 300 °C. The EG particles were maintained for the duration of 10 s and then withdrawn.



Figure 3-16 The furnace used for the tests.

3.6.13 Coupled confocal Raman and AFM (atomic force microscopy) Microscopy

Microstructure of expandable and expanded graphite was investigated by Confocal Raman spectroscopy on a WITec Confocal Raman Microscope coupled with an AFM (Model alpha300RA) at ambient temperature. The instrument had excitation wavelength of 532 nm and the laser power was delivered to 18 mW. The specimens were placed on a 3 axis piezoelectric-controlled stage. High spatial resolution of microscopy is due to the piezoelectric scanning table that allows 3-D displacements in 3 nm steps. High resolution micrographs of Raman profile mapping were conducted to study the differences between expandable and expanded graphite and to understand how the structure of expandable graphite changes after combustion in order to protect the underlying layers of substrate.

Chapter 4

4. Thermal and mechanical properties of flame retardant filled EFB reinforced epoxy composite

4.1 Introduction

In the event of fire, an intumescent ammonium polyphosphate (APP) agitated by the heat source eliminate ammonia (NH_3) and water while forming ultraphosphate (PO_4) which could act as a protective layer against fire propagation. Alumina trihydrate **(**ATH) on the other hand undergoes endothermic dehydration upon fire, releasing water vapor which function as diluent for the combustible gases with concurrent formation of a thermally stable ceramic alumina (Al_2O_3) that serve as an insulating layer against heat and mass transfer [204, 205]. For zinc borate (ZB) based fillers, they promote charring and cross-linking of materials [206-210]. Furthermore, when ZB is used with other fillers as synergistic particles, they encourage the generation of low melting glass, leading to the formation of an inorganic char barrier [211-213]. In the endothermal reactions, they also dilute the combustible gases and discharge bound water. It was reported that boron acts as an inhibitor of carbon ignition and ZB acts as a smoke suppressant [214].

Introduction of NF into neat polymers (epoxy and biopolymers) reduced the heat release and enhanced flame retardant performances relative to those of the pure matrices [9, 140, 215], and incorporation of small loading level of FR could further reduce the flammability of biocomposite at the cost of a slight drop in mechanical properties. E.g. the addition of 30 wt% kenaf fibre into Poly(3-hydroxybutyrate-co-3-hydroxyvalerate) (PHBV biopolymer) decreased the pHRR from 1713 to 809 kW/m^2, CO yield decrease from 0.04 to 0.02 (kg/kg),fire growth rate index decreased from 61.3 to 32.3 kW/m^{2}s and residue increased from 0.2 to 0.8 wt% [140]. Kenaf fibres formed

an insulating layer that protected the bulk of substrate during combustion by inhibiting the penetration of flammable gases and heat. Kenaf fibre acted as a carbonized agent, promoting a network of cavities and holes impacting the combustion process and the release of volatile gases. Few reports (flax fibre/nylon polyamide PA6 and Polybutylene Terephthalate (PBT)/actilox and exolite FR [137], sisal fibre/PP/APP and ZB [216]) have been published on the simultaneous enhancement of flammability, thermal stability and mechanical properties of NF based composites using FRs and no previous studies were conducted to investigate the effect of FRs on the fire resistivity of the palm empty fruit bunch (EFB) fiber reinforced epoxy based composite. This work aimed to study the combined effects of APP/ATH/EFB fiber, APP/ZB/EFB fiber as well as ZB/ATH/EFB fiber on flame resistivity and thermal performance of the resulting epoxy based composite by means of a series of characterizations to obtain the optimized compositions of the constituent loadings.

Alkali chemical treatment was conducted on the EFB fibers. This method is the most extensively used treatment owing to its effectiveness, low cost and convenience of use [217, 218]. The morphological, structural, thermal, moisture properties and chemical compositions were studied through SEM, EDX, FTIR and TGA. The alkali treatment leads to increased percentage of cellulose content and thermal characteristics as well as reduced moisture content relative to those of untreated fibers. The effects of the addition of IFRs (one of the optimum formulations of FRs) and chemical fiber treatment on the mechanical properties of EFB fiber epoxy composite were investigated. The composites were analyzed using tensile and flexural testing. Detailed morphological investigation was conducted to study the dispersion of FR particles and the bonding between fiber and epoxy matrix within the composites.

4.2 Flammability and thermal properties of the FR filled EFB epoxy composites

4.2.1 Flammability of FR filled EFB epoxy composite

The control composite (E82F18), refer to Table 3-1, was fabricated to provide proper comparisons with the ATH/APP loaded formulations. The results of vertical Bunsen burner 12 s test recorded in terms of drip flame time, total flame time and mass loss (wt%) are shown in Figure 4-1. Incorporation of ATH into EFB fiber reinforced epoxy composite did not reduce the burning resistivity, as compared to that of the control (E82F18), in terms of drip flame time and total flame time. All of the ATH-filled composites burned intensely and brightly with severe dripping. Adding more ATH fillers reduced the total flame time, with increasing of drip flame time. ATH does not promote cross-linking on combustion and also ATH particles induce low mechanical properties (due to poor bonding between matrix and ATH), both of which are the factors that created easier and more dripping. Specimens burned off completely and no burn length was recorded (100 % total mass loss). With increasing loading of APP, the total flame time slightly reduced. The lower total flame time and no dripping phenomenon were detected for all APP filled composites relative to those of formulations containing ATH. This is probably due to the degradation of APP that leads to the formation of a strong char barrier which limits heat and mass transfer, with release of ammonia and water which dilutes the gaseous phase. Suardana and Lim [21] found that degradation of APP generates phosphoric acid which could interacts with the hydroxyl group of natural fiber to form phosphorous esters. This ester acts as catalyzes for dehydration of fibers, leading to the formation of a carbonaceous structure with reduction of vapor phase composition and released energy. CAPP10 showed 5% lesser mass loss than that of CAPP5 and displayed 12% reduction in the mass loss compared to that of CAPP15. Similar optimum concentration of APP particle in the range of 3-20 wt% was achieved at 10~12 wt% by Castrovinci et. al [219]. The

flame resistivity of APP at higher loading (>10 wt.%) tends to be lower, implying that APP can affect either positively or negatively depending on the optimum loading. All composites loaded singly with APP burned off with full burn length.

APP is much more effective than ATH in flame resisting composites. It was observed that [219] inclusion of 60 wt% ATH was required to achieve similar flame resistivity effect attained with 10-12 wt% APP. However, composites with higher concentration of ATH were prone to significant drop in mechanical properties.

Exceptionally, when 10 wt% APP and 5 wt% ATH were introduced into the EFB reinforced epoxy composite, a synergistic effect took place that created self-extinguishing properties upon the removal of Bunsen burner. 0 s drip flame time, slight total mass loss and burn length of less than 10 mm were obtained for this composite. However, formulation with 10 wt% ATH and 5 wt% APP could not establish self-extinguishing behavior and total mass loss was approximately 50 wt% but zero drip flame was still maintained. The synergistic effect of the combined APP and ATH is discussed in the following discussion.

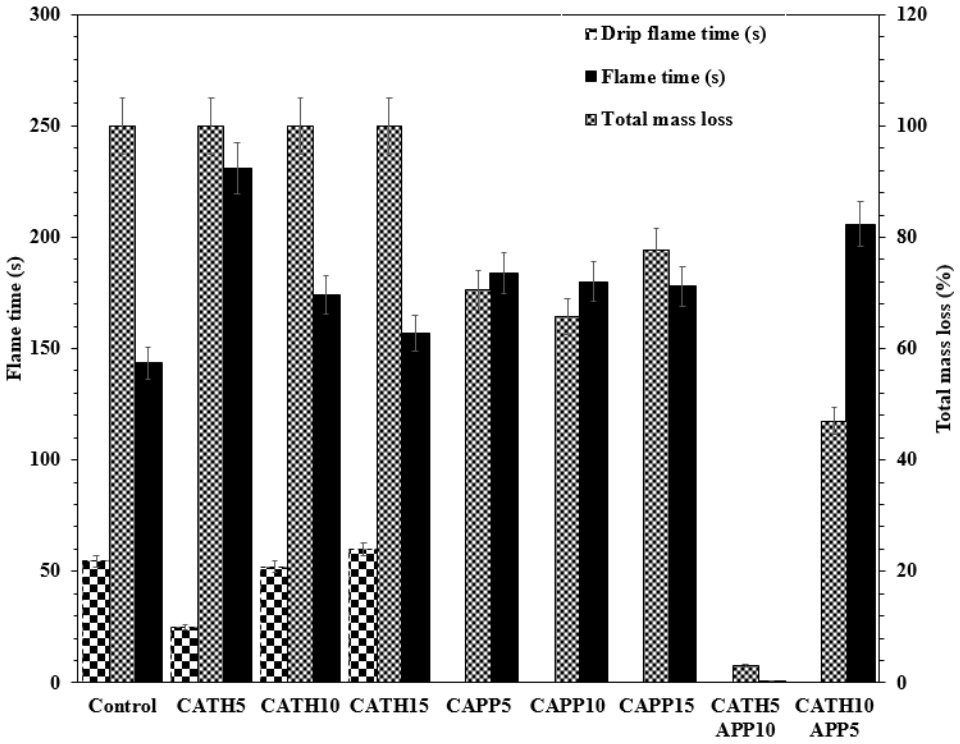


Figure 4-1 The results of vertical Bunsen burner testing for the control specimen and the composite specimens filled with FR.

Thermal reactions of ammonium polyphosphate/aluminum trihydrate mixture:

The chemical structures of APP and ATH are shown in Figure 4-2 and the following equations (Figure 4-3 and Figure 4-4) [219] depict the chemical reactions occurring during the thermal degradation between APP and ATH. The interactions show the flammability performance of the APP/ATH mixture acting as a FR system. The chemical reactions took place over a varying range of temperatures.

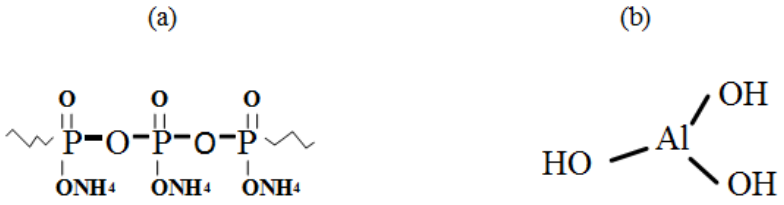


Figure 4-2 The chemical structures of APP (a) and ATH (b) [219].

The chemical reaction first occurred between APP (NH_4PO_3) and hydroxyl groups (−OH) of ATH at a temperature lower than 400°C (Figure 4-3). This resulted in the formation of aluminum phosphate with generation of water and ammonia (NH_3) out of ammonium salt (NH_4). These reactions kept repeating until aluminum metaphosphate ($(Al(PO_3)_3)n$) was formed.

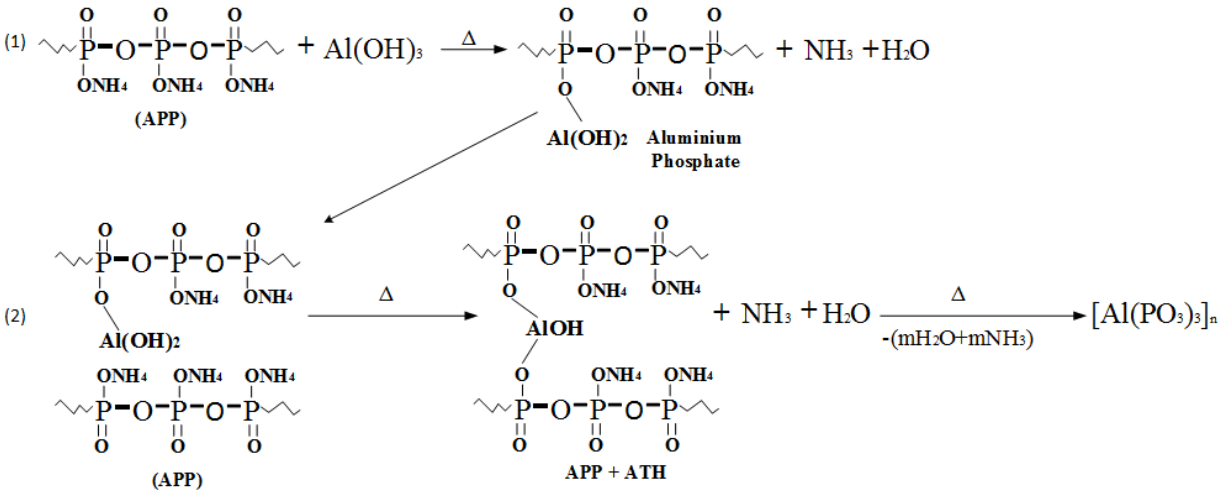


Figure 4-3 Reactions between ATH and APP [219].

At higher temperature, further reactions took place forming aluminum orthophosphate ($AlPO_4$) from the long chain polyphosphate as well as releasing ammonia and water (Figure 4-4).

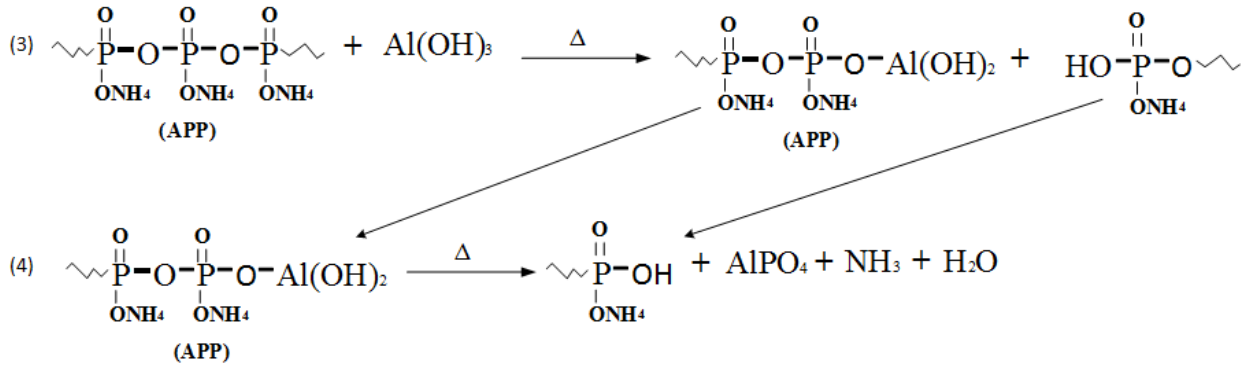


Figure 4-4. Reactions between ATH and APP at elevated temperatures [219].

The combined effect of APP/ATH contributed to an improved fire extinguishing behavior due to a number of factors. Firstly, the generation of aluminum phosphate prevents the evaporation of phosphorous volatility. Secondly, the basicity of ATH that furnish protons exchange and an easier evolution of water and ammonia gas. Thirdly, the crystalline form of Al- P-O alters the glassy ultraphosphate structure by which gases can readily escape the solid surface [219].

Flammability of composites:

Figure 4-5 and Figure 4-6 show the structure of specimens containing APP and APP/ATH upon completion of the flammability tests. The samples with ATH-based additive burned more vigorously than the specimens loaded with APP and no mass residue was left in the clamp of lab stand. All the burned parts of ATH loaded samples fell down on the tray placed under the samples and ATH filled specimens could not retain the structure. This is owing to the greater flame resistivity of APP than that of ATH as this filler could not adequately confine the pyrolysis process and volatile gases liberation during the fire, expediting the combustion progression and increasingly deteriorating the structure.

As seen in Figure 4-5, the bulk structure was maintained in APP filled specimens. The hybrid of ATH and APP exhibited its synergistic effect where inclusion of 5% APP and 10% ATH (in CATH10APP5 formulation) prevented the drip of flame. When the replacement was changed to the optimum value of 10% APP and 5% ATH (in CATH5APP10 formulation), self-extinguishing properties were observed (Figure 4-6). This specimen burned for < 1s upon removal of Bunsen burner after 12 s of continuous exposure to direct flame and created zero drip flame and a burn length of less than 1 cm and mass loss of less than 3%.

It would be noteworthy to add that pieces of control sample broke off on the burning edge of specimen and subsequently dropped while this phenomenon did not occur for all the specimens containing ATH and APP. This shows the effectiveness of APP and the hybrid of APP/ATH on the NF-reinforced epoxy composites.

It requires to highlight that, for the control formulation, the structure of specimens deteriorated vigorously with the liberation of volatile gases upon fire whereas increasing addition of APP and ATH was visually observed to reduce the amount of gases emitted from burning part of specimens. The smoke was largely lesser with the presence of APP/ATH hybrid, particularly for CATH5APP10 due the synergistic effect of APP and ATH at this ratio.

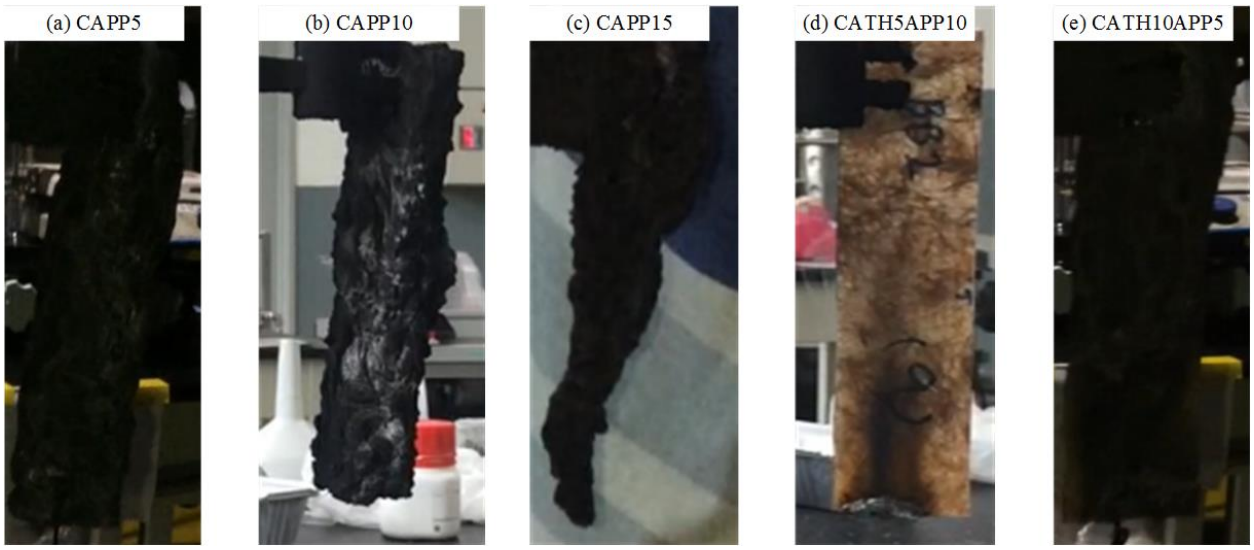


Figure 4-5. The test samples of (a) CAPP5, (b) CAPP10, (c) CAPP15, (d) CATH5APP10 and (e) CATH10APP5 composites after vertical Bunsen burner experiment.



Figure 4-6 The intumescent char of CATH5APP10 after vertical Bunsen burner test.

Figure 4-7, Figure 4-8 and Figure 4-9 present the results of the inclusion of ZB, hybrid of ATH/ZB and hybrid of APP/ZB attained from the vertical Bunsen burner 12 s testing experiment. The composites containing ZB particles, ATH/ZB hybrid formulations and CAPP5ZB10 showed a reduction in the mass loss by approximately 31-35 % compared to the control and decreased the

drip flame time to 0 s in comparison to that of the control. ZB additive significantly affected the drip flame time as its incorporation at each level of loading led to a zero dripping. 15% ZB-loaded formulation was found to perform the best in terms of reduced total flame time in comparison with ZB filled composites, CAPP5ZB10 and formulations with ATH/ZB hybrid, and this formulation along with CZB5ATH10, CZB10ATH5 and CAPP5ZB10 composites created the lowest mass loss with regards to the composites loaded singly with ZB particles, ascribed to higher incorporated FR. CZB15 showed slightly lower mass loss relative to CZB5ATH10, CZB10ATH5 and CAPP5ZB10. The more incessant reduction in the total flame time and mass loss percentage of ZB containing composites exhibited the effectiveness of this intumescent flame retardant (IFR) upon its incremental incorporation. ZB particles, after its thermal degradation, perform both releasing water in gas and condensed states which dilutes the combustible gases and forming a vitreous protective film (B_2O_3) in the burning zone.

Exceptionally, the addition of APP and ZB particles at 10 wt% and 5 wt%, respectively, was found to create a synergistic effect and self-extinguished the flame with 0 s flame time, 0 s drip flame time and the burn length less than 1 cm after withdrawing the Bunsen burner (Figure 4-9). As observed from CATH5APP10 composite and current result, to produce the highest efficiency in self-extinguishing the fire, the synergism between FR particles can contribute significantly.

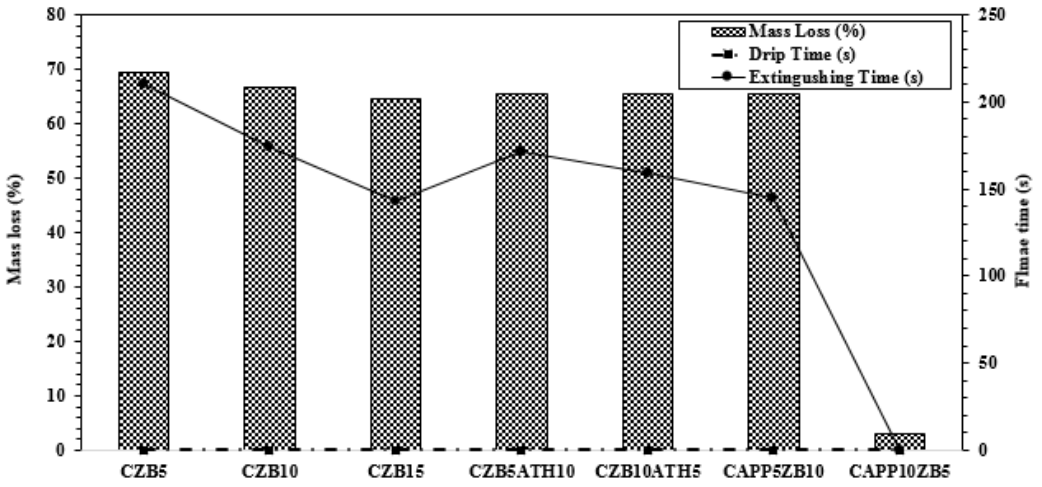


Figure 4-7. Bunsen burner results of formulations containing ZB, hybrid of ZB/ATH and hybrid of APP/ZB.

Thermal reactions of ammonium polyphosphate/zinc borate mixture [220]:

APP and ZB particles do not react at the temperature of 260 °C. APP initiates to decompose at this temperature as shown in equations (5) and (6) whereas ZB does not undergo the thermal decomposition. Firstly, ammonium polyphosphate (APP) particles yield evolving ammonia and polyphosphoric acid at approximately 250 °C (equations (5)).

(5) $[NH_4PO_3]n \rightarrow nNH_3 + [HPO_3]n$

Secondly, by increasing the temperature, in the 360~420°C range, an intumescence process takes place when the char and ammonia are formed and the water is released due to the reactions of the carbonaceous compound with the polyphosphoric acid (equations (6)).

(6) $carbon\ source + [HPO_3]n$

$$\rightarrow C\ (phosphocarbonaceous\ structure\ or\ char) + [H_3PO_4]$$

From the temperature of 290 °C, the decomposition of ZB begins and an amorphous product was formed, as displayed in equations (7).

(7) $2ZnO, 3B_2O_3, 3H_2O \rightarrow 2ZnO, 3B_2O_3 + 3H_2O$

Between 300 and 415 °C, a reaction between the decomposed products of APP and ZB starts which produces BPO_4 species. BPO_4 compound can be generated in two plausible ways, as described in equations (8) and (9), suggested by Samyn et al. [220].

(8) $2ZnO, 3B_2O_3 + 10[HPO_3]n \rightarrow 2ZnO + (n-6)/4P_4O_{10} + n/2H_2O + 6BPO_4$

(9) $2ZnO, 3B_2O_3 + 10\ H_3PO_4 \rightarrow 2ZnO + P_4O_{10} + 15H_2O + 6BPO_4$

At around 580 °C, the zinc orthophosphate ($Zn_3(PO_4)_2$ compound) was formed due to the reaction between P_4O_{10} and zinc oxide (these two compounds were produced in the previous process), as displayed in equation (10) .

(10) $0.5P_4O_{10} + 3ZnO \rightarrow Zn_3(PO_4)_2$

The $Zn_3(PO_4)_2$ compound melting at approximately 1050 °C yields P_2O_4 and zinc oxide.

(11) $Zn_3(PO_4)_2 \rightarrow P_2O_5 + 3ZnO$

Then, the formation of the zinc pyrophosphate occurs owing to the reactions between P_2O_4 and ZnO (equation (12)).

(12) $3\ P_2O_5 + 2ZnO \rightarrow Zn_2P_2O_7$

Also, the borophosphate and the zinc orthophosphate can react to yield the B_2O_3 compound and zinc pyrophosphate as indicated in equation 13.

(13) $2BPO_4 + 2Zn_3(PO_4)_2 \rightarrow B_2O_3 + 3Zn_2P_2O_7$

The creation of zinc phosphate and borophosphate (BPO_4) contributes to stabilize phosphorous species and provides this synergy between APP and ZB.

The burnt residue of ZB incorporated samples is shown in Figure 4-8 and Figure 4-9. When ZB particles were introduced into formulations, the tendency to sustain the original structure was induced at each level of loading concentration. The composites containing ZB swelled along the length and width, and twisted marginally in the direction of its vertical axis. Also, it was observed that the smoke produced from formulations containing 15 wt% FRs was visibly lesser than other composites.

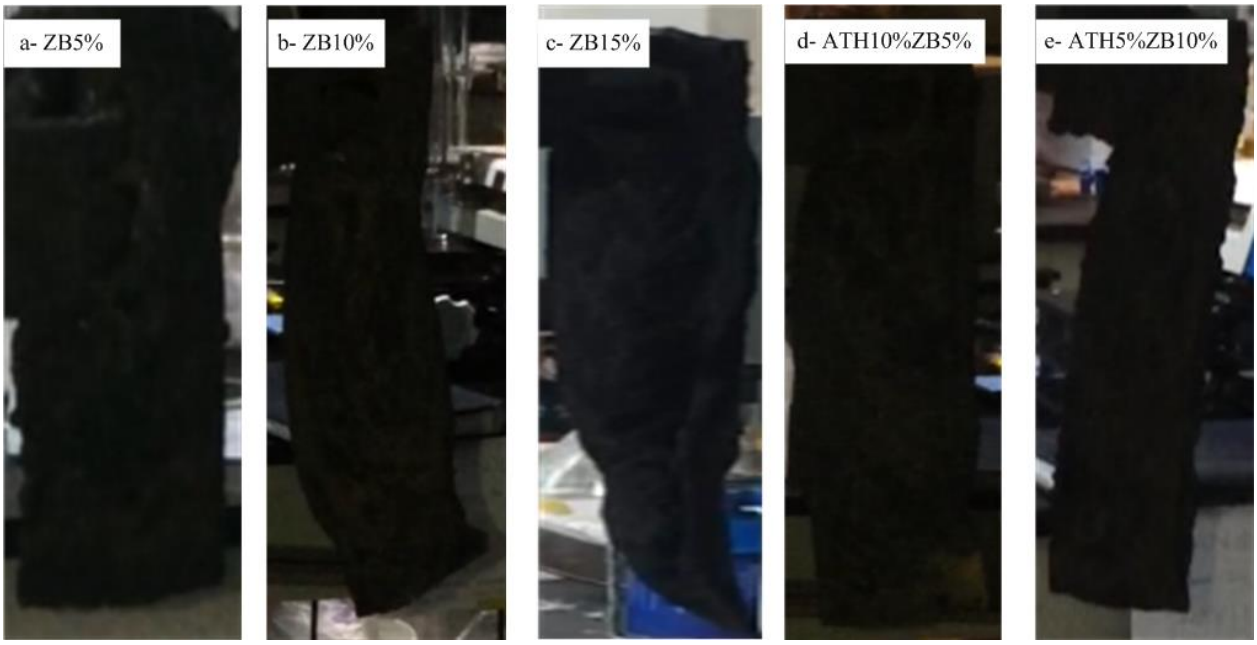


Figure 4-8 Images of burnt FR-based composites after veritcal Bunsen burner tests. (a) CZB5, (b) CZB10, (c) CZB15, (d) CATH10ZB5 and (e) CATH5ZB10.

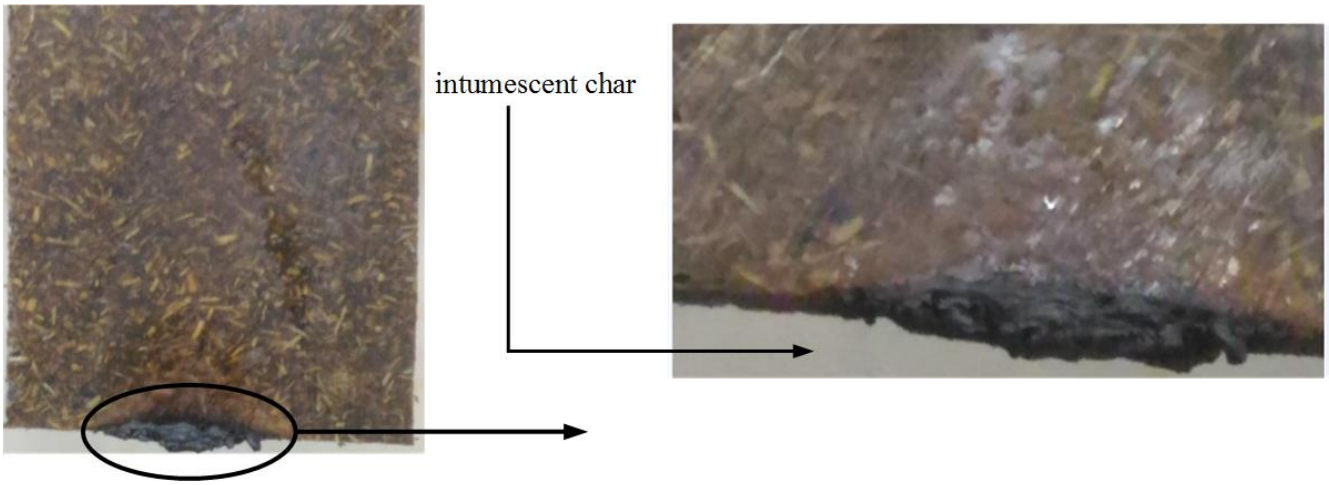


Figure 4-9 The intumescent char of CAPP10ZB5 after vertical Bunsen burner test.

In summary, it was observed that APP and ZB individually are capable of enhancing the flame resistant properties including drip flame time, total flame time and mass loss more than ATH filled composites. The synergistic effect of APP at 10 wt% with either ATH or ZB at 5wt% was observed to produce the greatest flame retardancy compared to other formulations coupled with two types of FRs as well as composites flame retarded singly. Both CATH5APP10 and CAPP10ZB5 show no total flame time and no drip flame time, and their burn length was very similar (around 3 mm).

4.2.2 Heat release properties of FR filled EFB epoxy composites

The bomb calorimetry testing was used to investigate the heat of combustion of the reaction between the sample and oxygen measured based on the changes in temperature of the water. The gross heat (GH) of combustion evaluated by the bomb calorimetry exhibits the combustibility of samples.

Table 4-1 presents the GH of E100, control and composites containing ATH, APP and hybrids of APP/ATH. Pure epoxy burned wildly when subjected to combustion, with GH of 35.36 (MJ/kg). When EFB fiber was introduced into pure epoxy, a large drop in the GH, ≈ 11.02% was observed, which is in agreement with those reported in literature [13]. This can be attributed to lesser gross heat of combustion of EFB fibre than that of the neat epoxy.

Walters et al. (40) tested two grades of epoxy, the novolac (CAS number: 028064-14-4) and the bisphenol-A epoxy (CAS number: 001675-54-3), and GH values of 31.37 MJ/kg and 32.50 MJ/kg were attained, respectively. The gross heat of combustion per unit of mass can be calculated by the ratio of the molar heat of combustion (ΔH_c, kJ/mol) of the sample over the molecular weight (M_p, g/mol) of polymeric sample. The decreased GH with the addition of natural fibre is ascribed to the reduction of $\Delta H_c / M_p$ ratio. It is worth mentioning that the molar heat of combustion is obtained by subtraction of the molar heat of formation of polymeric sample (ΔH_f of sample) from the molar heats of formation of the products (ΔH_f of water and CO_2). It was reported that GH of palm EFB fibre, palm oil mesocarp fibre and palm shell is 17.46, 18.09 and 19.58 MJ/kg, respectively [221]. GH of empty fruit bunch from date palm tree was recorded approximately 19 MJ/kg [222]. GH of 11 different branches of tropical trees were investigated in another study and highlighted that the values are in in the range from 18.7 to 21.3 MJ/kg [223]. The GH of these natural resources show considerably lesser values than that of epoxy resins.

The incorporation of ATH or APP into epoxy/EFB fiber led to a reduction in GH. APP demonstrated 3.83% decrease in combustion performance of EFB fiber reinforced epoxy composite at low loading (5 wt%). Upon the addition of 10% APP, the GH reduced by 6.91%

relative to that of the control, which is due to lesser heat of combustion of APP particles. APP generates water and ammonia which mitigates the gaseous state.

The flame resistant effect for the composites containing APP reached optimum when 10 wt% APP was added. The same trend of heat release was recorded [219] when 3 to 20 wt% of APP was incorporated into polymeric formulations, the greatest flame resistivity was observed in formulations containing 10-12 wt% APP. This signifies the dual flame retardancy impact of APP on polymeric composite that can be either enhancing or dropping depending on the amount of APP, which requires further investigation.

The incremental introduction of ATH could further slowdown the heat release of combustion. This FR decomposes during combustion, generating water in the vapor state through pyrolysis and alumina (Al_2O_3). The water leads to an endothermic process, which removes the heat from the underlying layers. The Al_2O_3 layer also acts as a shielding barrier against the transfer of heat and mass.

The hybrid of APP and ATH tested ($CATH_5APP_{10}$ and $CATH_{10}APP_5$) recorded the lowest GH as compared to that of E100, control, APP filled and ATH filled composites, with 13.9% drop relative to that of the control, implying the synergetic effect as evaluated in this work, in agreement with results from Bunsen burner analysis. The hybrid of APP and ATH resulted in a thermally stable surface shielding with aluminum orthophosphate (Al-P-O_4) crystalline compounds rather than the ultraphosphate, and more complete elimination of ammonia and water which enhance the thermal surface shielding of composites.

Table 4-1 The gross heat of combustion of E100, control and composite samples filled with FR from bomb calorimeter experiment.

Formulations	Gross Heat (MJ/kg)	Decrement of GH from the control composite (%)
E_{100}	35.36	11.02
Control	31.85	0.00
$CATH_5$	30.55	-4.08
$CATH_{10}$	30.00	-5.81
$CATH_{15}$	28.56	-10.34
$CAPP_5$	30.63	-3.83
$CAPP_{10}$	29.65	-6.91
$CAPP_{15}$	31.50	-1.09
$CATH_5$ APP_{10}	27.41	-13.95
$CATH_{10}$ APP_5	27.40	-13.96

Table 4-2 presents the GH values of the ZB, ATH/ZB and ZB/APP hybrid samples and their decrements from the control. Based on the results obtained, greater improvements in fire resistance are correlated to a higher amount of flame retardant additive due to the liberation of non-combustible products of FRs. This phenomenon occurs owing to a heat absorption mechanism and also the production of a charred protective layer on the flammable surface. The barrier layer inhibits the heat or mass transmission between the condensed state and combustion zone [224, 225]. The progressive decline in GH was observed when the ZB additive concentration increased from 0% to 15%. Composite with 15% ZB loading was found to drop the GH by about 11.72 % compared to the control, presenting the least GH performance compared to the formulations flame retarded singly with ZB and composites loaded with the hybrids of ATH/ZB. In general, all the composite systems with 15% FR loading and formulation containing 10% ZB could lower the GH by minimum 10% relative to the control.

The hybrids of APP and ZB was observed to create the lowest values of GH, in comparison to other formulations, with 13.43% and 14.59% reduction relative to the control sample. The synergy that creates between APP and ZB is the reason of this enhancement in the decrease of GH, which

is in accordance with vertical Bunsen burner results. Other formulations containing 15 wt% ZB, 15 wt% APP, 15 wt% ATH and 15 wt% hybrids of ZB/ATH were not observed to provide lower values of GH than that of APP/ZB hybrid counterparts.

Table 4-2 Gross heat of formulations.

Sample	Gross heat (MJ/kg)	Decrement of GH from the control (%)
Control	31.85	0
CZB5	31.04	-2.55
CZB10	28.63	-10.12
CZB15	28.12	-11.72
CZB5ATH10	28.31	-11.13
CZB10ATH5	28.21	-11.43
CAPP5ZB10	27.57	-13.43
CAPP10ZB5	27.20	-14.59

Generally, increasing addition of FRs contributed to the reduced gross heat of combustion, however, the synergy between constituents can further enhance the heat release reduction of composites. The values of GH for CATH5APP10 and CAPP10ZB5 were very close, 27.41 and 27.20 MJ/kg, respectively.

4.2.3 Thermal properties of FRs filled EFB epoxy composite

The TGA testing of control, ATH loaded composites, APP loaded formulations and hybrid composites was conducted in nitrogen atmosphere as composite pyrolysis upon combustion is described by the decomposition of an anaerobe system [226], illustrated in Table 4-3 and Figure 4-10.

The composites containing FR started to break down at approximately 300°C owing to the thermal degradation of epoxy resin. The major weight loss started at approximately 315°C and sustained for at least another 100 °C. Incorporation of APP was observed to enhance the char residue content, where a hybrid of 10 wt% APP and 5 wt% ATH resulted in the highest recording. This can be ascribed to the degradation of APP in the presence of ATH formed aluminum orthophosphate and aluminum metaphosphate. However, APP addition to the composites reduced the thermal degradation temperature (T_d) since APP releases water upon thermal degradation [116, 227] and contributed to a premature degradation of epoxy as a result of hot water hydrolysis. Besides, the second reason of reduced thermal degradation temperature is owing to the presence of phosphate groups, which decomposes earlier to generate thermal char [228, 229]. Similar fashion of lower T_d was observed when APP was incorporated into epoxy [230], and PP [231]. The same trend of higher post combustion mass residual with increasing APP loading was reported in the work of Dorez et al. [4] and Wen et al. [232]. Fiber phosphorylation (as shown in Figure 4-11) and degradation at low temperature (250 °C) [233, 234] initiated along with the matrix decomposition. APP interacts with both the polymer matrix and natural fiber, and mainly fiber lignin content [235], leading to the formation of shielding charred barrier for mass and heat transfer. The existence of phosphate groups in the structure of APP relatively lowers the thermal decomposition temperature and subsequently forms a protective charred layer which retards the epoxy degradation [228, 229, 236].

With increased loading of ATH, the mass residue and thermal stability improved when heated, which can be attributed to its decomposition into water vapor due to endothermic reaction and conversion to the thermally stable aluminum oxide ($2Al(OH)_3 \rightarrow Al_2O_3 + 3H_2O$) that demonstrates a very high melting temperature of 2054 °C [226].

Synergistic effect was detected when the combined ATH/APP was used, where enhanced mass residue was recorded with approximately 87.53% and 57% for CATH5APP10 and CATH10APP5 relative to that of the control, respectively. The T_d, which was computed at 50 wt% mass loss, was not affected due to the presence of APP in the mixtures. The same synergetic effect was observed in the Bunsen burner and bomb calorimetry analyses.

Table 4-3 TGA results of the control and formulations loaded with APP and ATH.

Formulations	Char Residual at $T_{600°C}$ (wt%)	T_d (◦C) at 50 wt% mass loss
Control	15.56	385.87
$CATH_5$	20.47	383.37
$CATH_{10}$	21.20	388.56
$CATH_{15}$	22.16	389.39
$CAPP_5$	21.41	376.78
$CAPP_{10}$	22.20	358.04
$CAPP_{15}$	19.50	376.03
$CATH_5APP_{10}$	29.18	368.20
$CATH_{10}APP_5$	24.43	368.43

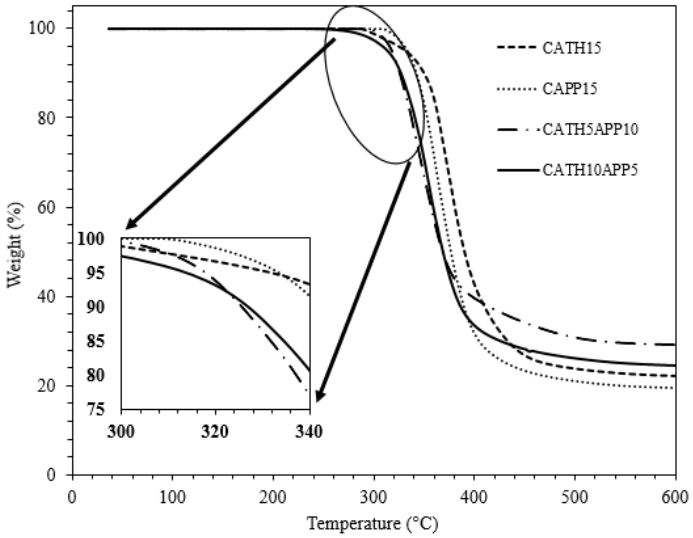


Figure 4-10. The degradation behaviors of the selected formulations containing APP and ATH.

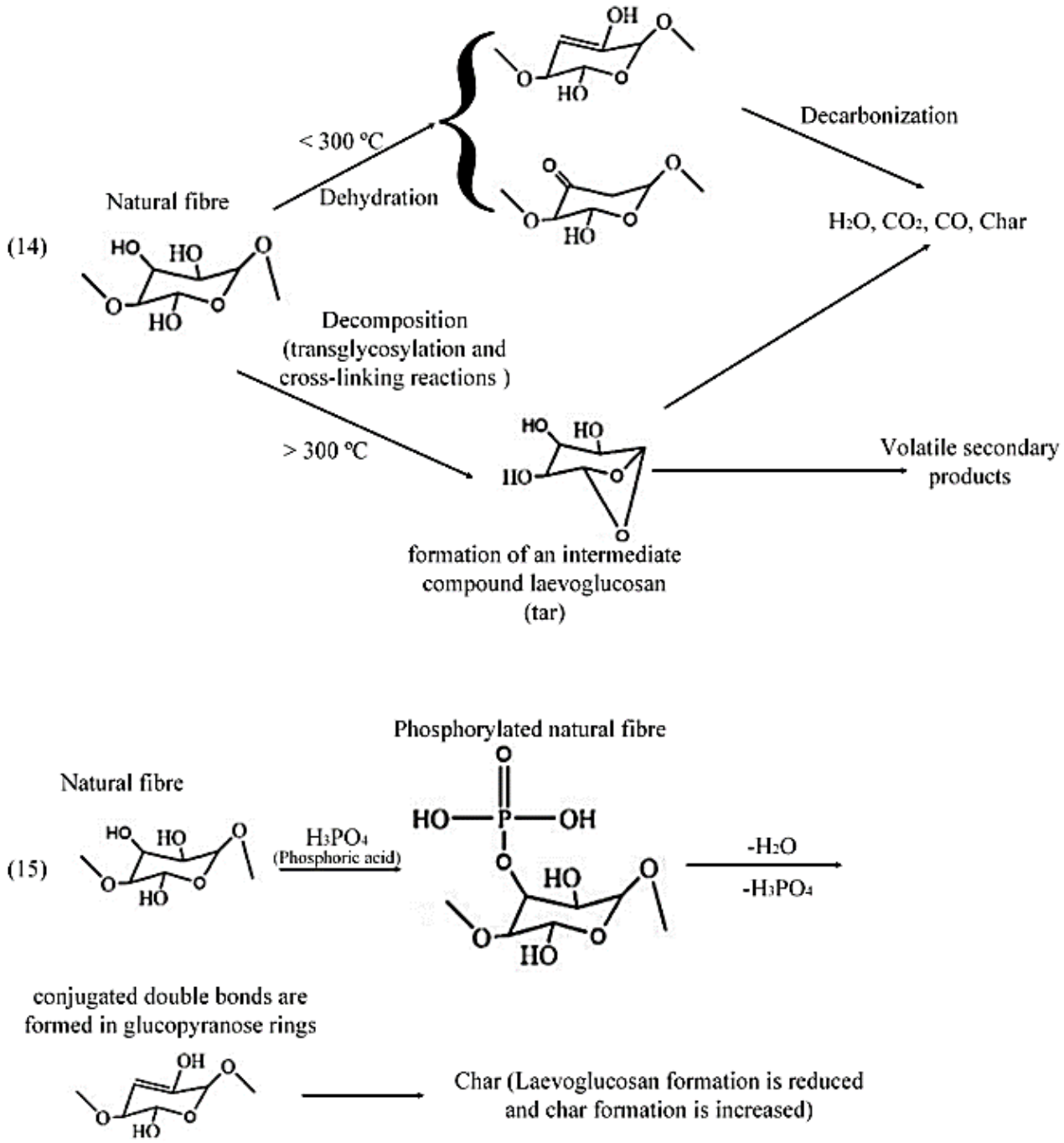


Figure 4-11 Reaction 14 illustrates the charring mechanism of natural fibre without APP and reaction 15 shows the charring process with the presence of APP (fibre phosphorylation) [233, 237].

Thermal stability of ZB, ZB/ATH and ZB/APP filled composites was characterized from the residual content and thermal degradation temperature created via the thermal decomposition. The TGA results of the composites tested in nitrogen atmosphere are depicted in Figure 4-12 and

Table 4-4. The thermal degradation temperature at 50 % mass loss and residual mass of formulations were measured. The char formation increased with incremental addition of FRs loading and the amount of solid content was proportional to the FRs concentration of the formulations, and thermal stability improved especially at higher FR loading. The residue obtained from CZB15, compared to the control, improved significantly by 124.7%. It shows that higher improvement in thermal stability and mass residue of formulations was directly influenced by the presence of ZB as 15 wt% loading provided the greatest values in comparison to those of other formulations. It was evidenced that ZB releases 15% water by weight when heated from 290 to 450 °C [238], which leads to an increase in the thermal resistance of ZB-based composites. The water vapor released from the FRs due to the thermal breakdown of material can act dually by both diluting the concentrated volatile generated which is due to the oxidizable pyrolysis and absorbing the heat to decrease the temperature in the burning zone, thereby promoting the formation of char.

In addition to that, the thermal degradation temperature at 50 wt% mass loss (T_d) of FR filled composites enhanced relative to the control, and CZB15 showed the highest T_d of 404.69 °C. The hybrid formulations showed slightly lesser values of residual mass and T_d than the composite with 15% ZB. For the hybrid samples, the composites containing greater amount of ZB provided the enhanced mass residue and T_d. It can be determined that ZB filled composites produced higher thermal stability than that of its ATH and APP counterparts, as compared with the previous data. Since the ZB particles are more effective in enhancing the flame retardancy than ATH fillers, ZB/ATH hybrid composites (CZB5ATH10 and CZB10ATH5) showed slightly lesser values of

residual mass and T_d than those of the composite with 15 wt% ZB. The mass residue and T_d of CAPP10ZB5 and CAPP5ZB10 reduced slightly relative to those of CZB15, attributed to the presence of APP additives in the composites. The reduction in the thermal degradation temperature of composites containing APP is owing to the water release and early degradation of phosphate groups, which the latter contributes to the char formation. APP fillers affect the thermal behavior of natural fibres and produce the fibre phosphorylation at lower temperatures during the decomposition.

Table 4-4. TGA results of the control and formulations containing ZB.

Sample	Residual mass at T_{600} °C (%)	T_d (°C)
Control	15.56	385.87
CZB5	27.92	389.49
CZB10	32.59	400.03
CZB15	34.96	404.69
CZB5ATH10	30.94	397.85
CZB10ATH5	33.12	401.31
CAPP5ZB10	34.45	401.10
CAPP10ZB5	32.29	398.32

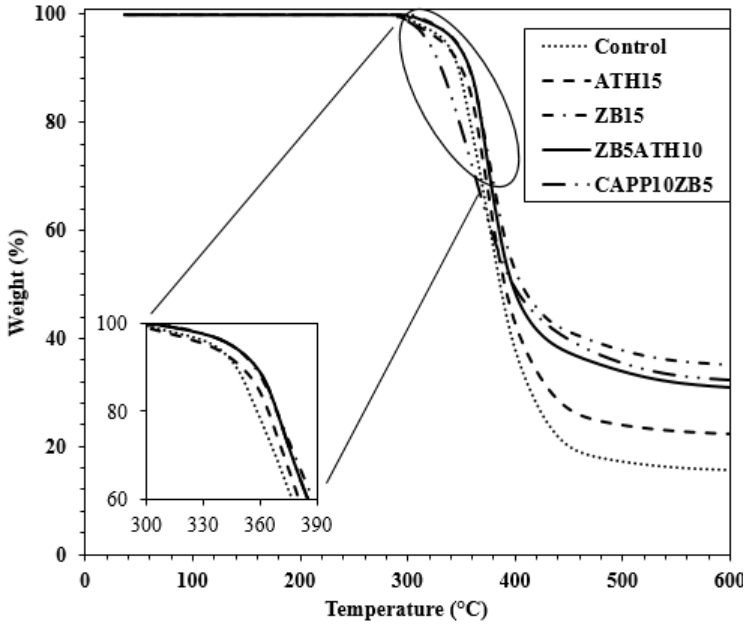


Figure 4-12. Thermogravimetric analysis (TGA) curves of the control and composites containing ZB.

In summary, the inclusion of ZB particles in the composites was found to provide higher char residue content and thermal degradation temperature than other composites flame retarded by APP, ATH and hybrid of FRs (at the same weight percentage of FRs).

4.2.4 EDX study

The EDX analysis tests were carried out on one of the optimum FR based formulations (CATH5APP10) and its TGA char was investigated as well. The micrographs indicate the uniform distribution of FRs on EFB fibers (after burning) and the matrix, as shown in Figure 4-13. Figure 4-13(a) illustrates the microstructure of residue (spectrum is magnified on fiber) after TGA test whereas the other images exhibit the whole fractured surface of sample taken at several sample areas (Figure 4-13(b, c and d)). The agglomerates were not observed that implies the efficient spread of various phases. For the char structure (Figure 4-13(a)), a closed and compact residual

layer was formed and this carbonaceous char structure restricts the diffusion of volatile gases and heat into the substrate. Nitrogen gas within FRs helped enhance the flame retardancy of composite by increasing the cohesion of char residue [239]. No cracks or opening was observed in the network of char layer and the protective char was densely packed. This is due to the mechanical interlocking between the FRs, fibers and polymer matrix [240], which leads to a more effective char barrier in insulating mass and heat transfer from burning surface to the substrate. The EDX analysis detected the peaks that are present in the char corresponding to carbon (C), oxygen (O), aluminum (Al) and phosphorous (P). C, Al and P were present in the char owing to "EFB fiber and epoxy", ATH and APP, respectively (Figure 4-13(a)). These elements were also detected on different fractured surfaces of CATH5APP10 (Figure 4-13(b, c and d), but with lesser C, Al and P content. This suggests that after thermal decomposition larger amount of carbon, aluminum and phosphorous elements remained within the sample. After burning the amount of oxygen reduced compared to that of unburned samples (Figure 4-13(b, c and d). The largest amount of element that was present in both char and the unburnt sample was carbon attributed to the presence of EFB fiber and epoxy polymer.

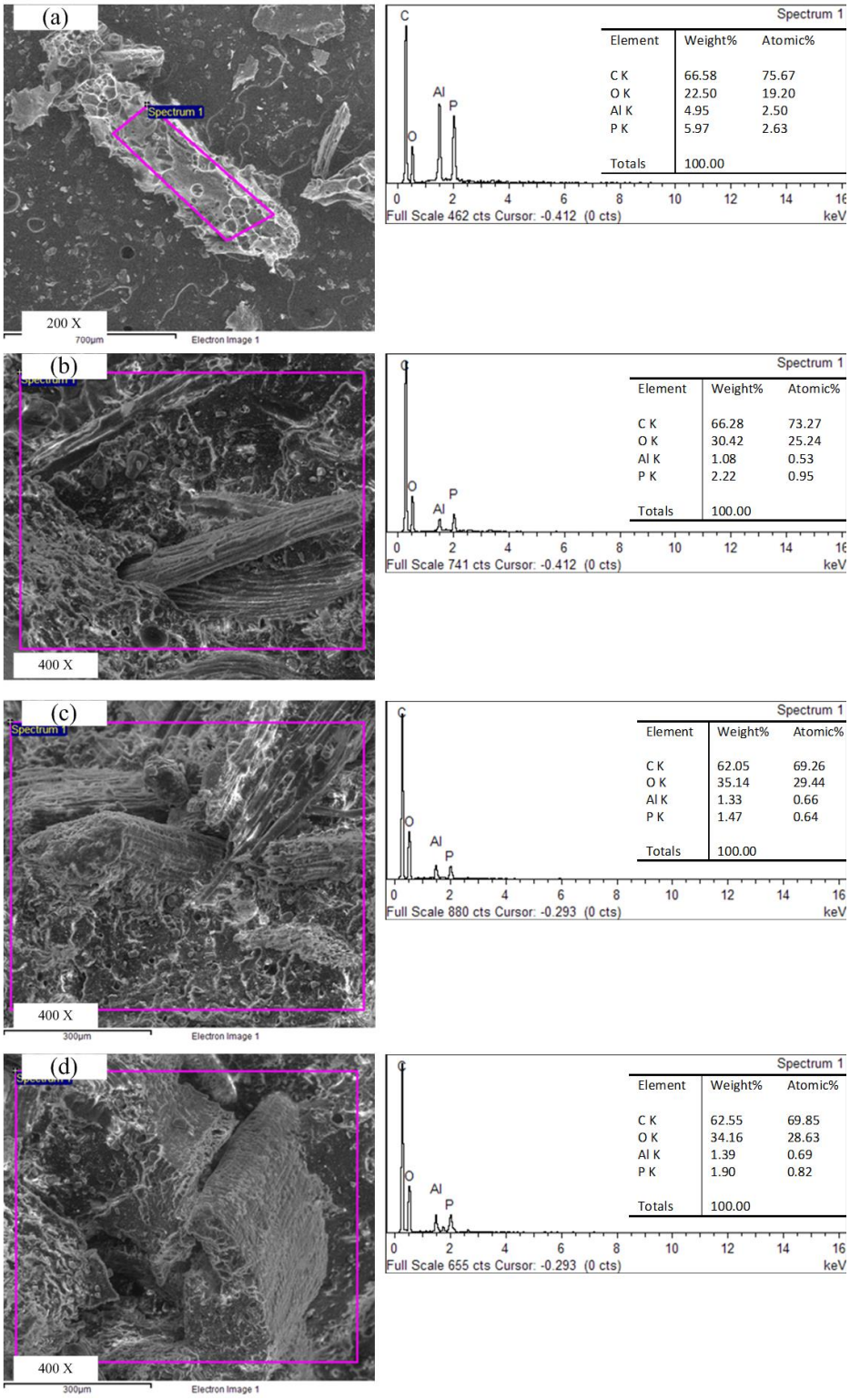


Figure 4-13 EDX analysis of CATH5APP10 sample. (a) spectrum magnified on the fiber after TGA test, (b, c and d) the spectrum magnified on all sample surface.

To elucidate the relationship between the intumescent char and FR (APP/ZB) behavior, the microstructure of CAPP10ZB5 prior to and after 60 s vertical Bunsen burner test was examined by EDX/SEM and compared with the char residue of the control, which dripped on the floor after the burner test.

As illustrated in Figure 4-14, the char of APP10ZB5 formed a compact, smooth, homogenous, intumescent and continuous surface, which led to the inhibition of gas diffusion, heat and mass transfer.

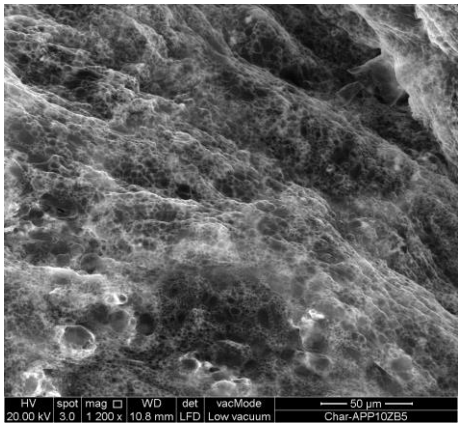


Figure 4-14. SEM micrographs of intumescent char of CAPP10ZB5 in different areas at magnifications of 1200 ×.

The presence of particles on the surface of intumescent char was observed, and the elements are determined by EDX Figure 4-15. C, O, B, Zn, P and N were the existing elements in the structure of the char, which implies the presence of different compounds comprising of all above-mentioned elements, in particular zinc phosphate and borophosphate, forming an intumescent char with more crosslink network. The char network, which is highly cross-linked owing to the presence of B based compounds, possessed sufficient mechanical performance and inhibited the transfer of heat and mass into the bulk of substrate, thereby resulting in the enhancement of flame retardancy.

Presence of N, which exists in APP, contributed to the enhancement of the fire resistivity by increasing the cohesion of char residue [239].

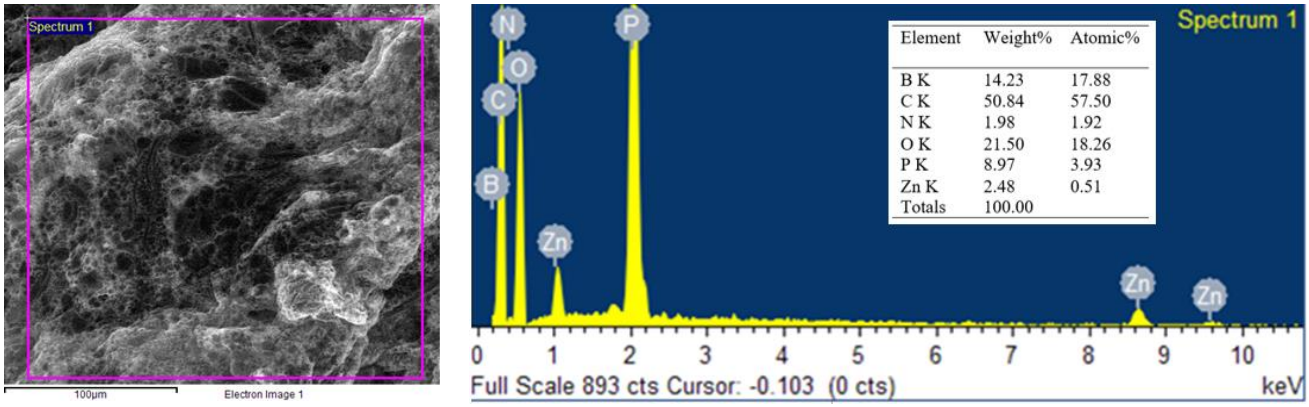
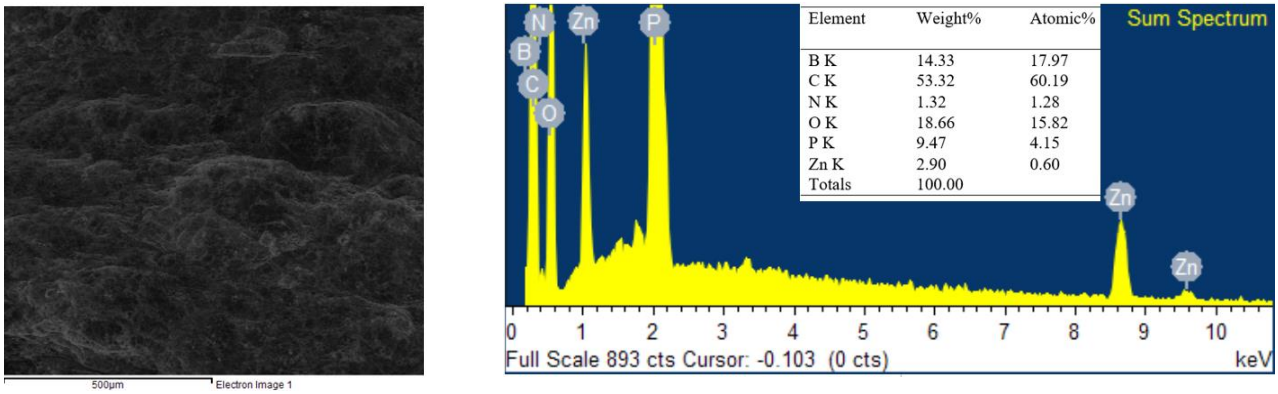


Figure 4-15. EDX of the intumescent char of CAPP10ZB5 and presence of elements.

A comparison between APP10ZB5 sample prior to and after combustion (Figure 4-16 and Figure 4-17) infers that the elements were distributed uniformly on the fractured surface and intumescent char without agglomerates. Moreover, it could be found that B, O, P and Zn contents of the char are higher than those of fractured sample whereas C content was lesser. This is due to the promotion of zinc phosphate and borophosphate on the microstructure surface of intumescent residue at elevated temperature, and improvement of crosslinking network upon flame.



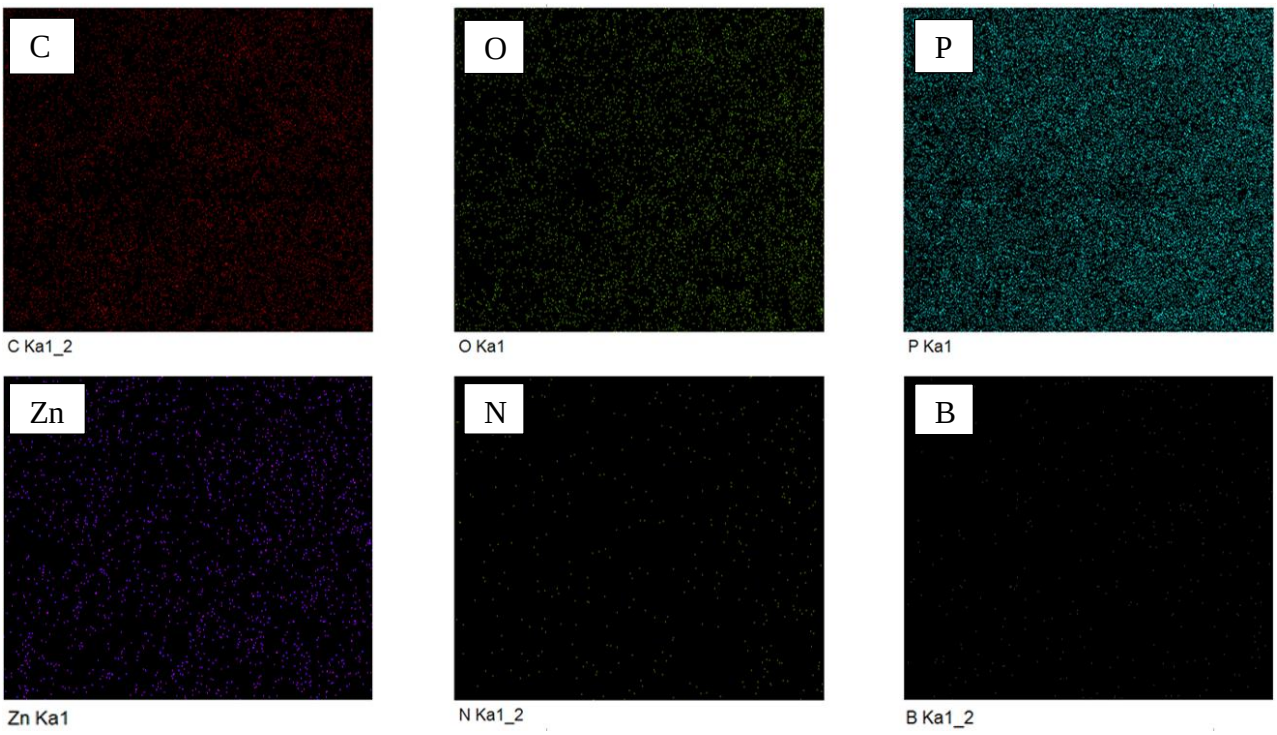
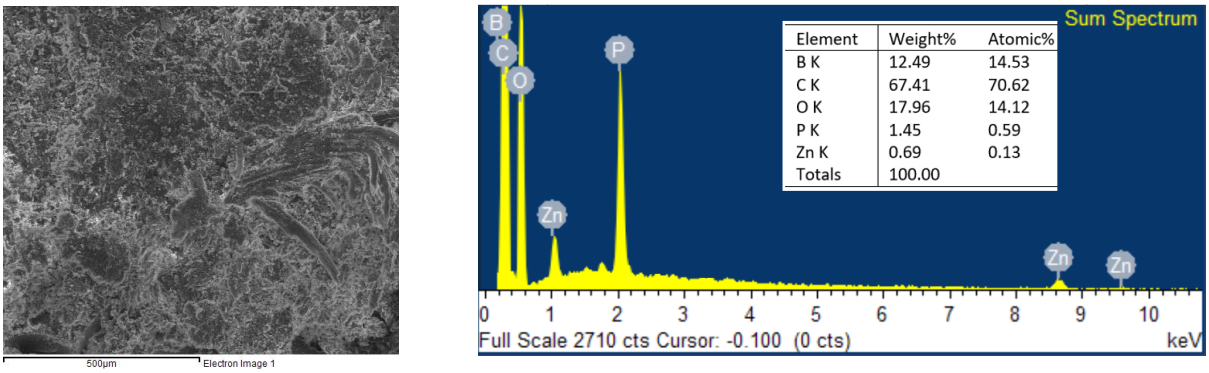


Figure 4-16. The mapping of dispersion of the elements on the intumescent char surface (CAPP10ZB5) shown in this image.



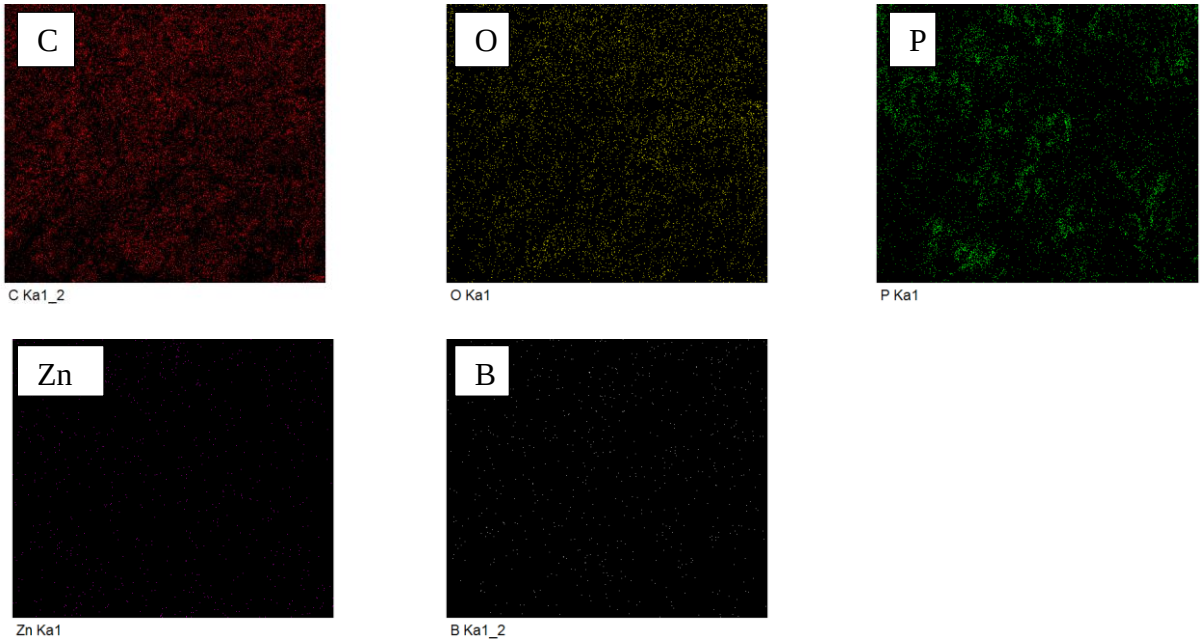


Figure 4-17. EDX analysis and the mapping of dispersion of different elements in CAPP10ZB5 composite prior to the combustion.

The char residue of the control illustrated some holes and cavities on the surface of the residue (Figure 4-18) due to inadequate generation of char upon fire. The micro-sized porous caused a pathway for penetration of pyrolysis volatiles, oxygen and transmission of heat and mass into the bulk of substrate. This is owing to the weak mechanical structure of char without FR particles.

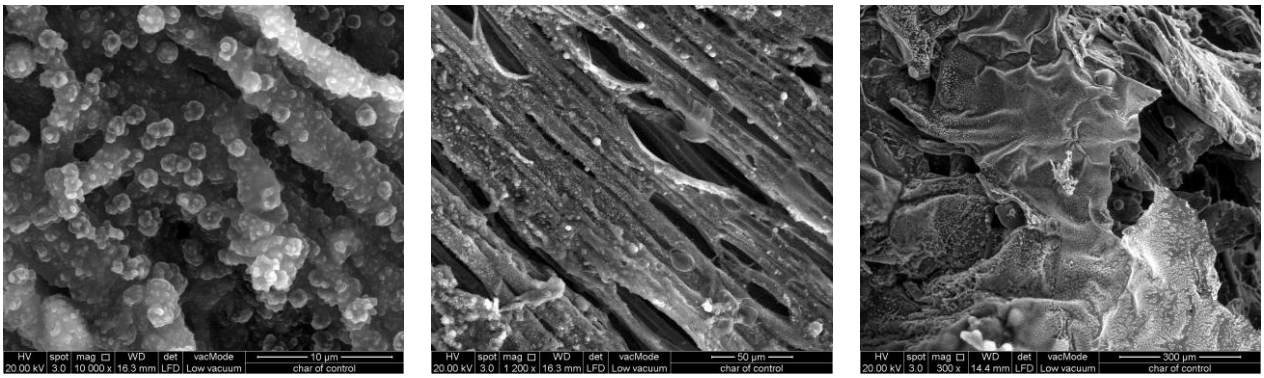


Figure 4-18. SEM micrographs of char residue of the control in different areas at magnifications of 10000 ×, 1200× and 300×.

4.2.5 Morphological features of composites

The SEM micrographs of fractured surface of the control, ATH-loaded, 10 wt% APP and CATH10APP5 are exhibited in Figure 4-19. Homogenous distribution of flame retardants was observed in SEM micrographs. The mechanical properties can be affected by the physical characteristics of the polymer, types of additive, additive concentration and filler dimension, distribution and shape. The surface interaction between filler and polymer matrix plays a key factor in the fracture mechanism and crystalline behavior of the polymer, both of which directly influence the mechanical properties of the formulations [241].

No additive is present in the control sample (Figure 4-19-a) whereas increasing addition of ATH particles is visible, as shown in Figure 4-19-b, c and d. For the composite containing 10 wt% APP content, the particles can be observed in Figure 4-19-e. The FR fillers are visible in CATH10APP5 formulation (Figure 4-19-f). The fibres and FR particles mixed within epoxy matrix are shown by yellow ellipses and red arrows in Figure 4-19, respectively.

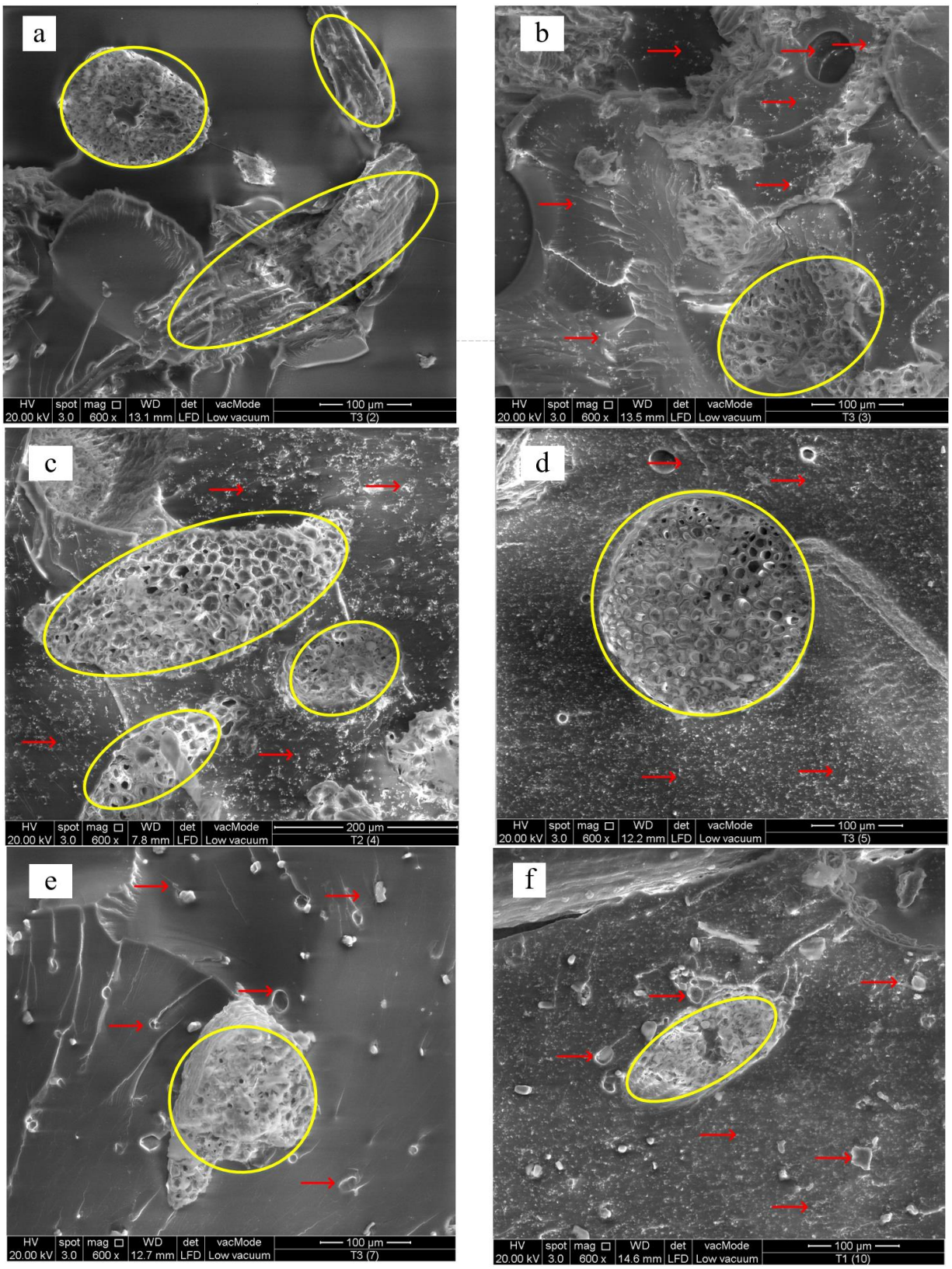


Figure 4-19. Morphology of (a) fiber/epoxy (control), (b) CATH5, (c) CATH10, (d) CATH15, (e) CAPP10 and (f) CAPP5ATH10 at 600 X.

SEM images of fractured surface taken from varying composites (namely: (a) ZB5, (b) ZB10, (c), ZB15 and (d) ATH5ZB10) are illustrated in Figure 4-20. The micrographs exhibited a good linkage between matrix and fiber. The SEM images showed good distribution and dispersion of FRs in the epoxy matrix where increasing presence of FR particles are clearly visible, as shown in Figure 4-20 (c), (d) and (e).

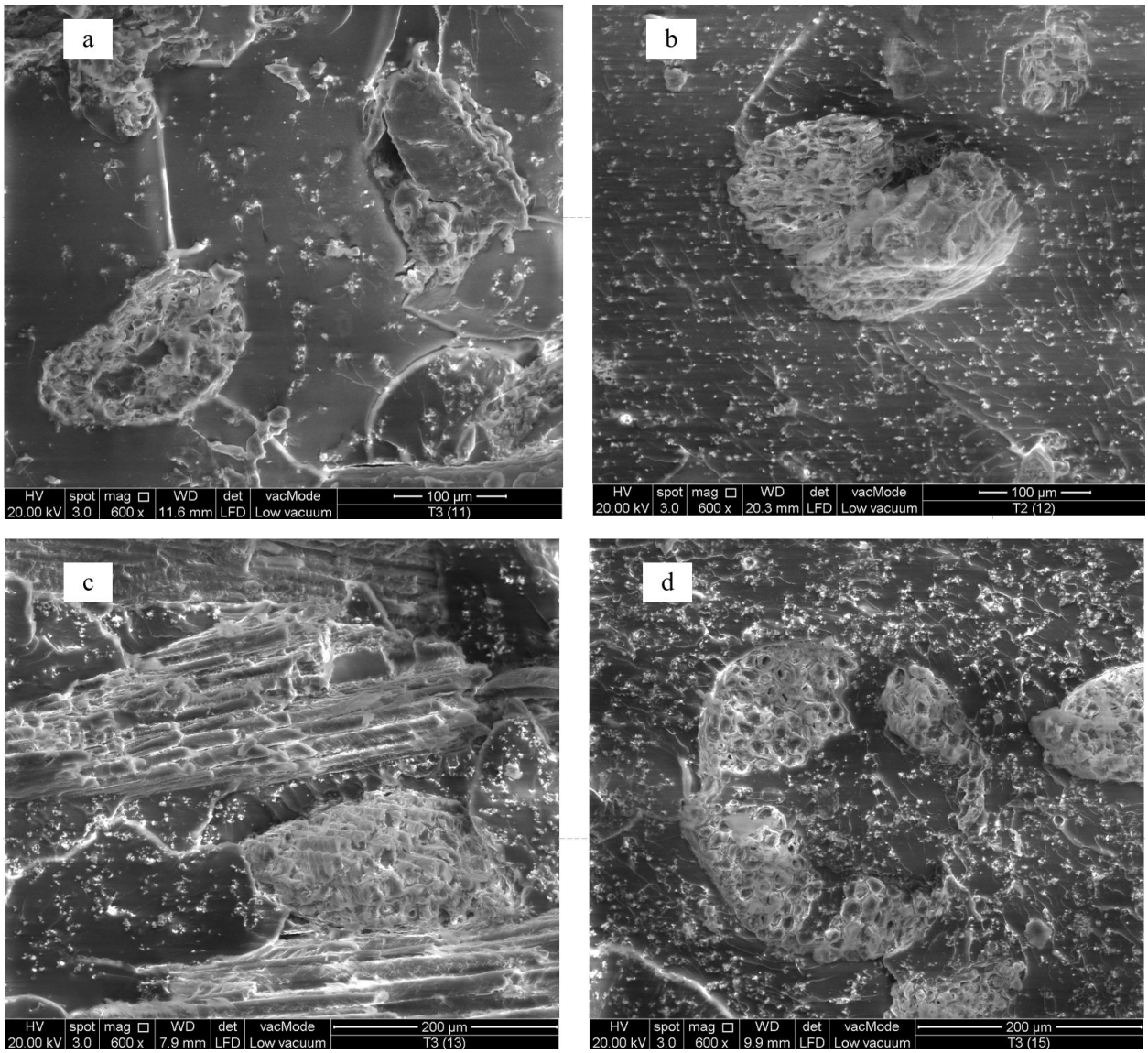


Figure 4-20 SEM micrographs of (a) CZB5, (b) CZB10, (c) CZB15 and (d) CATH5ZB10.

4.3 Comparative Thermal and Physical Investigation of Chemically Treated and Untreated Oil Palm EFB Fiber

4.3.1 Evaluation of fiber surface morphology

It is crucial to evaluate the modifications in the surface morphology of fibers in order to investigate their adhesion with polymer matrix in composite materials. SEM micrographs of untreated fibers and 5% alkali treated fibers for the soaking period of 24 h are displayed in Figure 4-21. For untreated fibers, no fiber fibrillation was observed but a compact and smooth surface. However, alkali treatment distinguished a regular, rough and clean surfaces in the treated EFB fibers (Figure 4-21 (b), relative to that of raw fiber (Figure 4-21 (a)), attributed to the decrease of impurities. The fiber treatment leads to a reduction of the diameter owing to the elimination of a numerous portion of natural oils, waxy substances, lignin and hemicellulose. All these could result in larger number of reaction sites of EFB cellulose with polymer matrix. The reaction between NaOH solution and fibers with their hydroxyl groups during a mercerization treatment is shown as follows [2] :

(16) $NaOH + FiberCell - OH \rightarrow H_2O + FiberCell - O^- Na^+ + impurities$

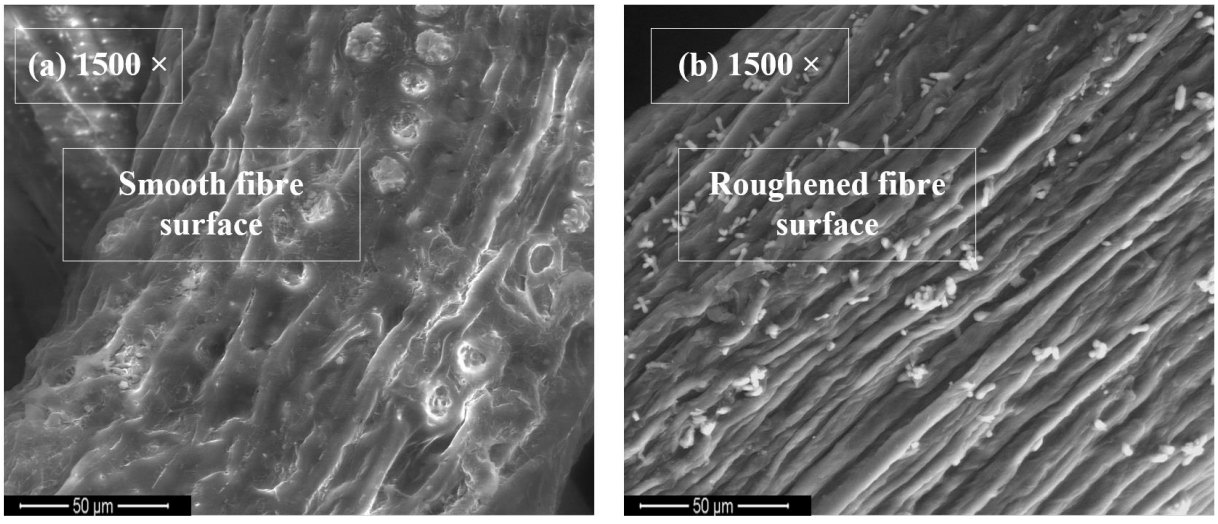


Figure 4-21 SEM micrographs of (a) untreated EFB fibre, (b) 5% alkali treated EFB fibre.

4.3.2 EDX study of EFB fibers

The EDX tests of untreated and treated EFB fibres were conducted, as the observations are shown in Figure 4-22. The amount of elements in the fibers on the selected spectrums were obtained. It was observed that almost the same amount of C (48 wt%) and O (51 wt%) were present in both types of fibres. A small quantity of impurity (Si) was found in the untreated EFB fibre (Figure 4-22-a), which was then removed after the chemical treatment (Figure 4-22-b). This indicates the positive effect of EFB fibre alkaline treatment.

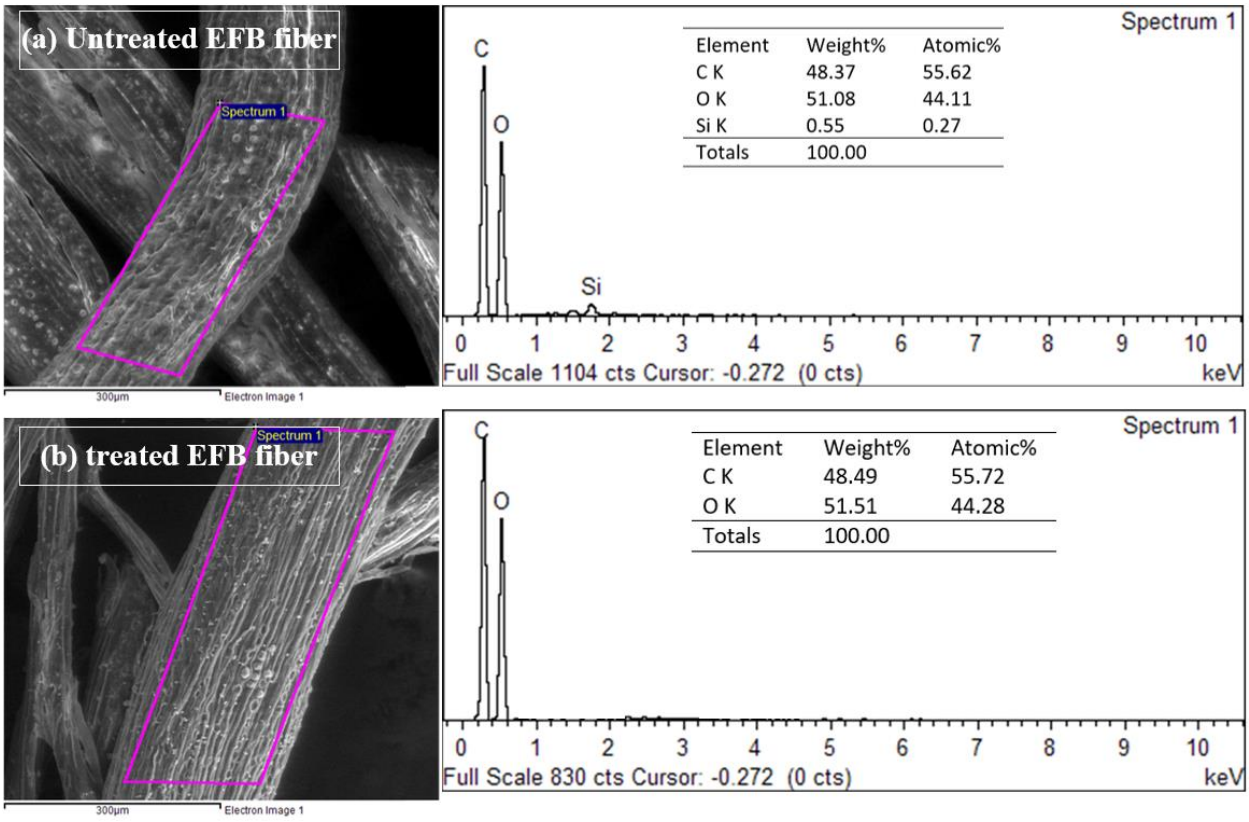


Figure 4-22 The EDX results of (a) alkaline treated fiber, (b) untreated fiber.

4.3.3 FTIR study

In order to investigate the effect of treatment on the raw fiber, FTIR was carried out to study chemical compositions of EFB fibers before and after 5% alkali treatment. Figure 4-23 displays FTIR spectra of untreated and treated EFB fibers. The peak observed at 3442 cm^{-1} indicates hydrogen bonded −OH stretching [242]. The absorbance of –OH diminishes substantially from 0.34 in untreated fibers to 0.05 in alkali treated fibers. The peak found at 2868 cm^{-1} denotes the C−H stretching from CH_2 and CH present in hemicellulose and cellulose. This implies that the C−H stretching absorbance reduces in EFB treated fibers. The C−H stretching detected at the peak of 2348 cm^{-1} is for polysaccharide chains [243], which reduced in the treated fibers. The absorbance peak at 1743 cm^{-1}, which was found to reduce in EFB alkali treated fiber, is for ester group in hemicellulose and C=O band with carboxyl [244]. The absorbance peak at 1580 cm^{-1} is explained by the water content of fiber, which decreased significantly after chemical treatment [245]. The peak observed at 1242 cm^{-1} is attributed to the C−O stretching vibration of the acetyl group present in lignin [246]. This peak reduced with the alkali treatment of the EFB fibers. The absorbance peak at 1151 cm^{-1} signifies C−O−C stretching vibration of the pyranose ring in polysaccharides [247], which was observed to drop in treated fibers. The glucosidic bond was observed at the absorbance peaks of 834 cm^{-1} and 897 cm^{-1} [248]. The Si−O bonding present in the bands ranging from 421.33 cm^{-1} to 567.54 cm^{-1} [249] lowered in alkali treated fiber. Hence, a large amount of lignin and hemicellulose was eliminated due to the chemical treatment as the absorbance peaks decreased markedly due to the mechanism of chemical treatment.

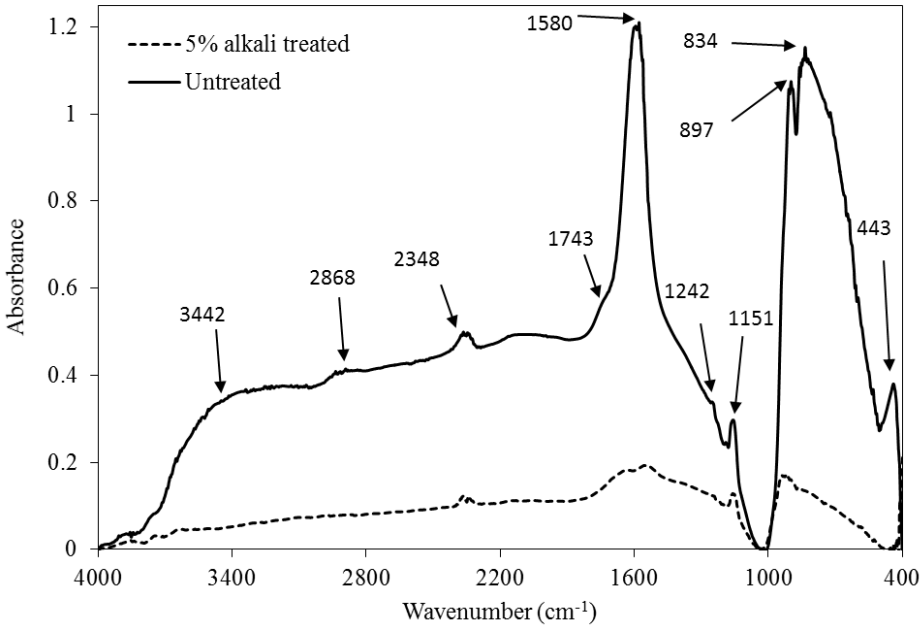


Figure 4-23 FTIR spectra of untreated and alkali treated EFB fiber.

4.3.4 Thermal stability

TGA was used to evaluate the thermal stability of treated and untreated EFB fibers. The decomposition kinetics was measured with the aid of TGA results. The results are shown in Figure 4-24, Figure 4-25 and Table 4-5. At first, all untreated and treated EFB fibers lost a small quantity of mass between 30 °C and 170 °C owing to the evaporation of moisture. Untreated fibers initiated to decompose at around 270 °C whereas alkali treated fibers initiated to decompose at about 285 °C. The greater resistance of alkali treated EFB fiber to thermal degradation is attributed to the elimination of hemicellulose, waxy substances and lignin after treatment of fiber [250]. The second stage of thermal degradation occurred in the 220-350 °C temperature range. The degradation stage is ascribed by the decomposition of hemicellulose and cellulose substances [251]. Third stage is the decomposition of lignin occurred in a broader temperature range of 200-

600° C [252]. Table 4-5 presents the onset degradation temperature (T_{onset}) at 5% weight loss, thermal decomposition temperature at 20 wt% weight loss (T_{20}) and residual weight of samples at 600 °C. The results show that the alkali treatment of fibers significantly increased the T_{onset} and T_{20} relative to the untreated sample. Moreover, alkali treated fibers show higher amount of char at 600 °C by approximately 1.08 % increase compared to that of untreated one, attributed to the removal of hemicellulose and deposits after the EFB alkaline treatment.

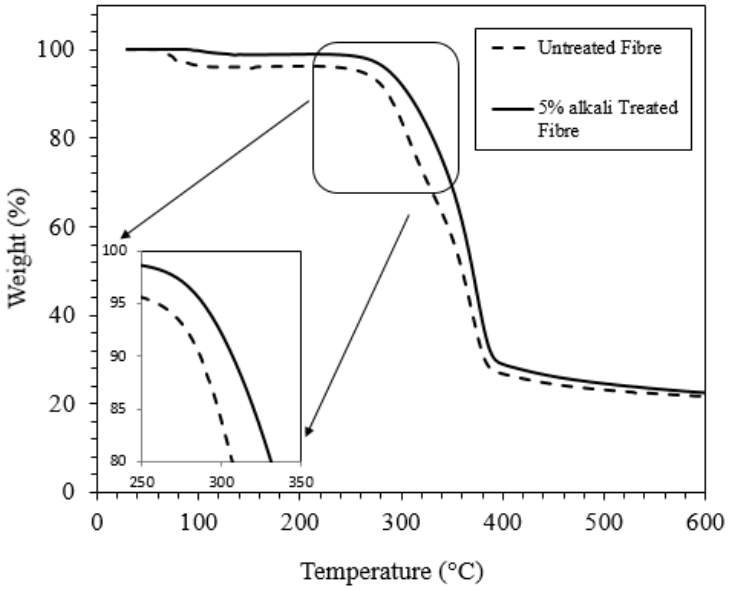


Figure 4-24 TGA analysis of untreated and treated fibres.

Table 4-5 T_{onset} (°C) at 5 wt%, T_{20}, T_{max} and residual weight (%) at 600 °C.

	Untreated fiber	Alkali treated
T_{onset} (°C) at 5 wt%	261	300
T (°C) at 20 wt%	307	346
T_{max} (°C)	363.33	378.33
Residual weight (%) at 600 °C	21.77	22.85

After the water vaporization of fibers, two shoulder peaks were observed for untreated fibers. First, at 306 °C, which is corresponding to the thermal decomposition of pectin, glycosidic bonds of cellulose and hemicellulose. The first peak was not found in alkali treated fibers owing to the removal of those substances after chemical treatment while the major peaks at 378.33 °C (T_{max}) and 363.33°C (T_{max}) were detected for alkali treated and untreated fibers, respectively (Table 4-5). These peaks are due to the thermal decomposition of α-cellulose, which is why alkali treated fiber possessed higher degradation temperature. It can be concluded that the chemical treatments increased the thermal stability of EFB fibers by eliminating the non-cellulose substances.

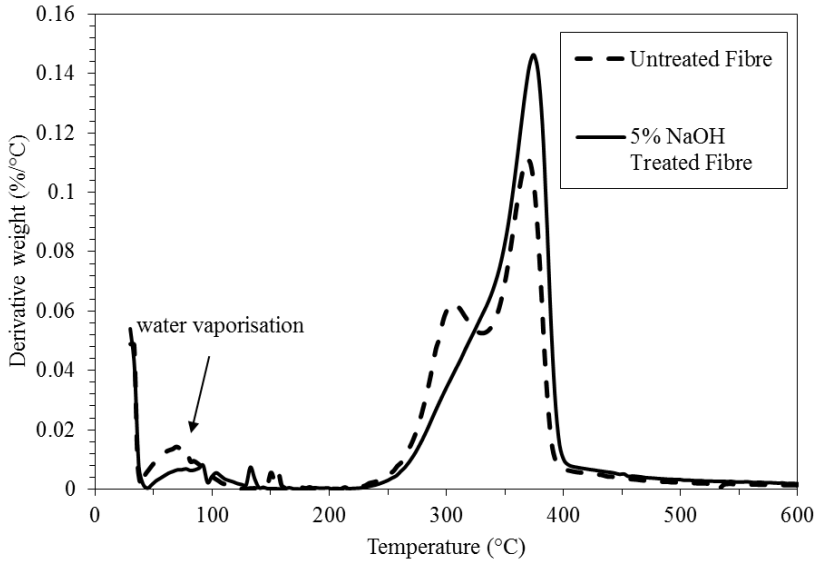


Figure 4-25 DTG curves of untreated and treated fibers.

4.4 Mechanical characterizations of EFB fiber composites and formulations containing optimum flame retardants

4.4.1 Tensile properties

The tensile strength, strain and Young's modulus of untreated EFB reinforced composite (control), alkali treated EFB fiber reinforced composite (treated control), ATH/APP filled composites with/without chemical treatment of EFB fibers (TATH5APP10/CATH5APP10, respectively) and CAPP10ZB5 are shown in Figure 4-26 and Figure 4-27, respectively. The untreated EFB fiber reinforced composite (control) presented the tensile strength of 33.89 MPa and elongation to break of 4 %. The inclusion of 15 wt% FRs (APP/ATH) reduced the ultimate tensile strength and elongation to break by approximately 17% and 22% compared to the control, respectively. APP particles were revealed to markedly grow moisture uptake and decreased mechanical performances in wood- polymer composites [253]. In general, it has been formerly found that intumescent composites decrease the tensile behaviors of the formulation relative to the neat polymer matrix [234, 254-257]. The reduction in strength and elongation to break of composites filled with ATH particles is due to poor intermolecular forces amongst ATH, matrix and other constituents (such as fiber) [258].

When the composites fabricated with alkali treated EFB fibers, all tensile properties enhanced over that of formulations reinforced with untreated EFB fibers. The utmost value of tensile stress and strain were revealed for treated EFB fiber reinforced epoxy with 42.38 MPa and 6.63 %, respectively. Compared to the FR filled composite reinforced with untreated fibers, the FR filled composite reinforced with alkali treated fibers exhibited approximately 10 % and 8 % increase in tensile strength and elongation to break, respectively. The improvements in tensile strength and ductility were due to elimination of substantial deposits such as lignin, wax and hemicellulose after

treatment. This contributes to strong matrix-fiber interfacial adhesion by increasing the interfacial area of contact between the fiber and matrix. CAPP10ZB5 presented similar values of strength and elongation to break to CATH5APP10 (Figure 4-26-b). The failure mode of composites depict in Figure 4-28. SEM images exhibited slight fiber debonding in the interface of fiber and matrix, as shown by red arrows in Figure 4-28-a and Figure 4-28-c, in composites reinforced with untreated EFB fibers. This mode of failure suggests the ineffective load transfer between the untreated EFB fiber and matrix. This performance was not observed for fractured surface of treated fiber composites (Figure 4-28-b and Figure 4-28-d). As presented by red ellipses, the failure was mainly characterized by fiber breakage. It is evident that matrix adhered to the treated fiber. This behavior confirms that alkali treatment provided strong adhesion between treated EFB fiber and matrix.

As illustrated in Figure 4-27, the Young's modulus slightly increased with the addition of FRs into the control (CATH5APP10, CAPP10ZB5 and TATH5APP10), with the greatest being 3.53 GPa for alkali treated fiber composite containing FRs. The Young's modulus of formulations reinforced with treated fibers enhanced over that of untreated fiber reinforced formulations. The improvement in Young's modulus corresponded to alkali treatment is ascribed by enhanced bonding between the matrix and fibers, indicating that loads transferred sufficiently from the matrix to fibers.

Fractured surfaces of tensile samples were scanned under SEM to examine distribution and dispersion of FR particles as well as bonding between the EFB fiber and epoxy matrix, as shown in Figure 4-28, within EFB/epoxy composite. The EFB fibers were distributed homogeneity within epoxy matrix and no obvious void content was observed. SEM images revealed that flame retardant particles distributed homogeneously within the epoxy matrix (several particles are highlighted by yellow circles in Figure 4-28-c and Figure 4-28-d). The interfacial interactions within polymer matrix are influenced by the presence of FR particles. Flame retardants can change

both the crystalline behavior of polymer matrix and the micro-mechanism of failure process [241]. In this case, particles negatively affected the mechanical properties of composites.

When the alkali treated fibers were used to produce composites, the values of mechanical properties increased, attributed to the strong adhesion between epoxy matrix and fibre. The improved interfacial wettability helps enhance the load transfer from the polymer matrix to the EFB fiber.

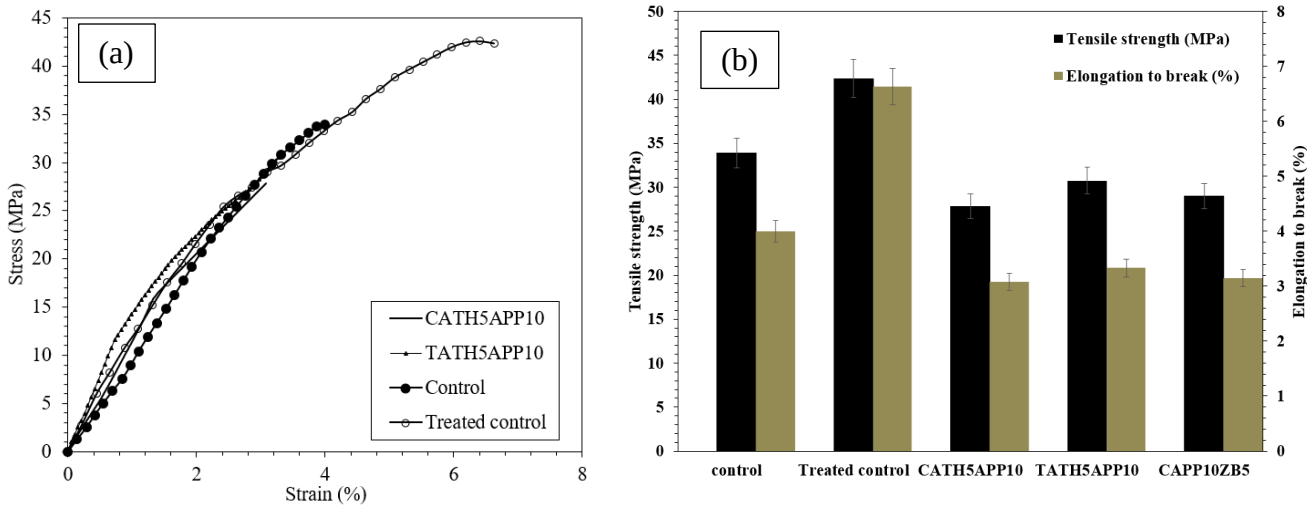


Figure 4-26 (a) The stress-strain curves and (b) tensile strength and strain of formulations.

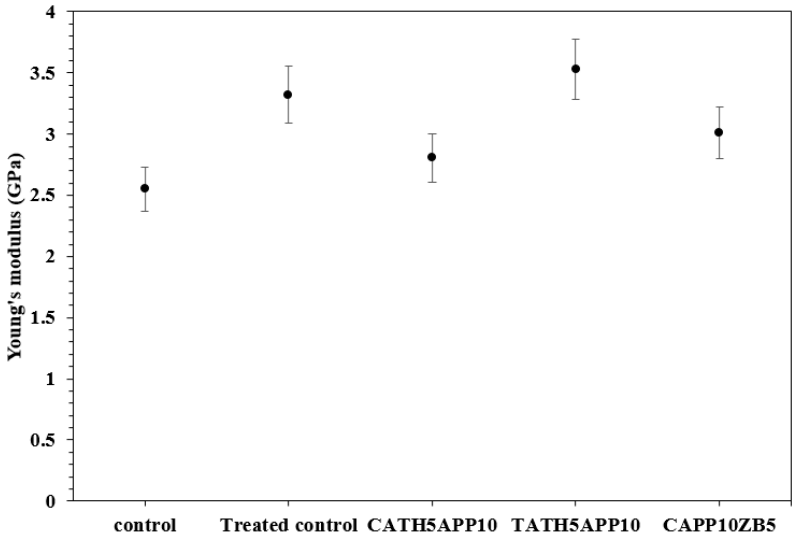


Figure 4-27 The Young's modulus of formulations.

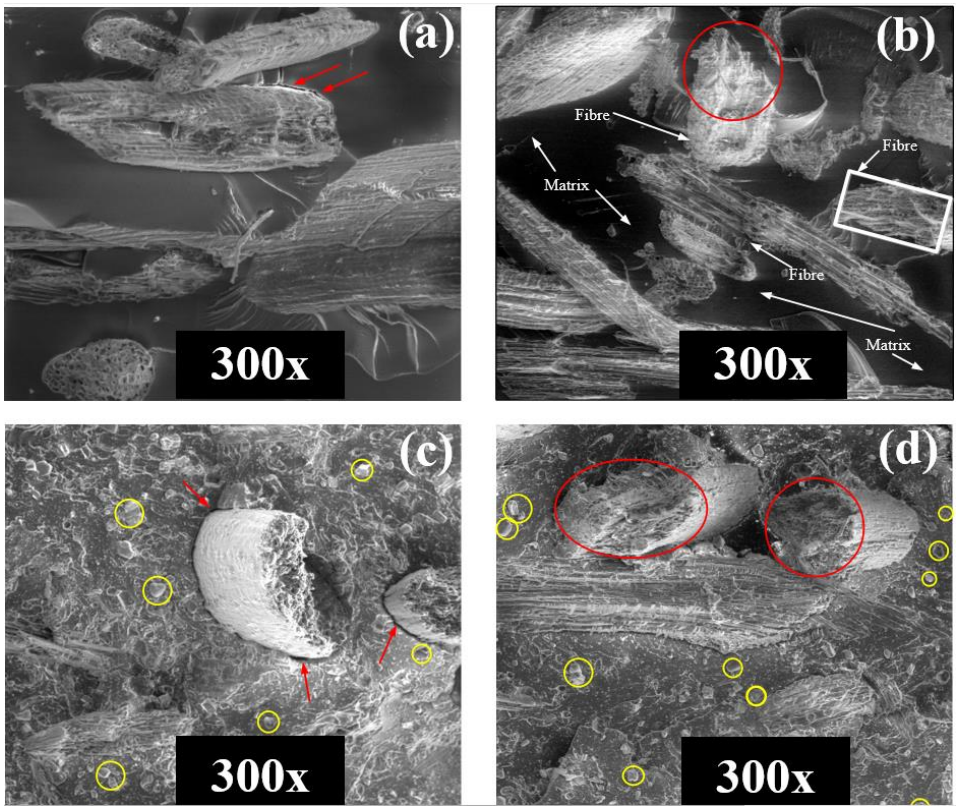


Figure 4-28 SEM micrographs of (a) control, (b) treated control, (c) CATH5APP10 and (d) TATH5APP10.

4.4.2 Flexural properties

The flexural properties of formulations are displayed in Figure 4-29 and the trends of flexural properties are similar to those of tensile strength, strain and modulus. It was found that flexural strength and strain of composites with treated and untreated EFB fibers reduced with the incorporation of flame retardants. This shows that the intermolecular bonding between the constituents broke easily under flexure, implying that flame retardants act as impurities and reduce the matrix continuity [11] (as observed in Figure 4-28).

In order to improve the flexural properties, the fiber alkali treatment was conducted and the composites with treated EFB fibers exhibited higher values of flexural properties. The flexural strength, strain and modulus improved by approximately 5%, 13% and 5%, respectively, for treated fiber composite compared to that of composite reinforced with untreated fibers. For FR filled formulation (CATH5APP10), similar trend in increased flexural properties achieved with the incorporation of alkali treated fibers (TATH5APP10). The increment in flexural stress, strain and modulus was calculated about 7%, 11% and 5%, respectively, for FR filled composite with treated fibers (TATHAPP10) relative to those of untreated formulation containing FR (CATHAPP10). CAPP10AZB5 and CATH5APP10 demonstrated similar values of flexural strain and modulus while flexural strength was higher for CAPP10AZB5. The flexural modulus increased slightly with the inclusion of FRs.

The increase in flexural properties of treated EFB fiber composites, compared to those of untreated ones, could be attributed to the enhanced interfacial bonding of the treated EFB fibers with the epoxy matrix. During fabrication process, the epoxy matrix penetrates easier into the treated fiber

bundles [259]. This phenomenon occurs due to the removal of traces of waxy layers on the surface of fiber with the aid of alkali treatment.

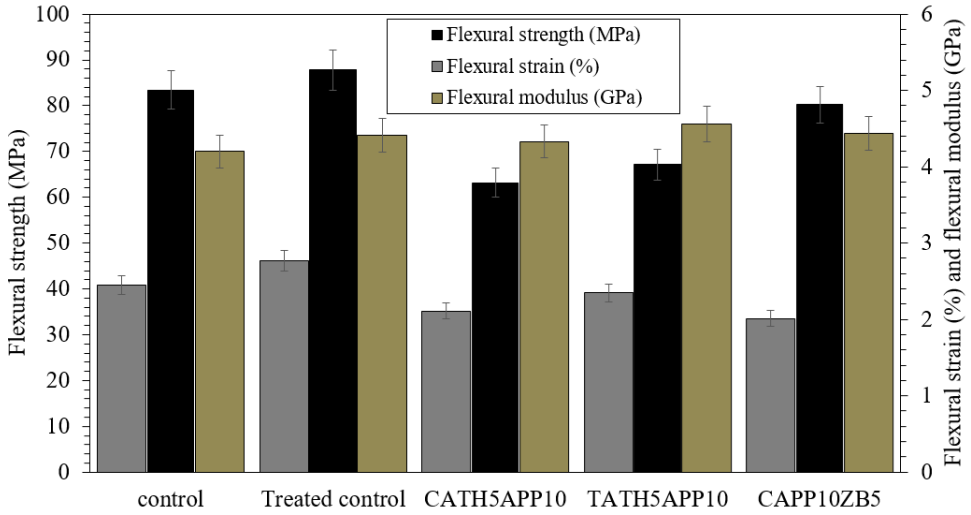


Figure 4-29 The flexural properties of formulations.

4.5 Summary

The effective amounts of IFRs required to provide the best flame retardancy behaviors of EFB-based epoxy composites were examined. The hybrid of 10 wt% APP and 5 wt% ATH as well the hybrid of 10 wt% APP and 5 wt% ZB (due to the formation of borophosphate (BPO_4) and zinc phosphate which contributes to stabilize phosphorous species) were the formulations which could meet the aircraft interior requirements in terms of vertical Bunsen burner test. The rest of the formulations that were investigated failed the Bunsen burner test. It was observed that ATH typically required a greater concentration (between 50 and 60% wt.%) to create an acceptable FR-based systems [260] , but increasing ATH concentration evidently deteriorates the mechanical characteristics. The incorporation of APP was found to reduce the degradation temperature,

however APP depicted the capability of an enhanced charring, as revealed in TGA, ascribed to the formation of NF phosphorylation, 0 drip flame time and reduced GH. Introducing FRs, either ATH or APP alone, showed much lower mass residue and flame retardant behaviors than those of the ATH/APP coupled systems. This depicted the establishment of synergistic effect, which can be attributed to the effect of ATH and APP mixture upon combustion that besides water, forms two different shielding systems including a ceramic metal oxide and aluminum orthophosphate with more complete elimination of ammonia and water in the vapor phase. The CZB10, CZB15, CZB10ATH5 and CAPP5ZB10 formulations were observed to perform satisfactory in the TGA tests with the thermal stability and mass residue of higher than 400 °C and 32%, respectively. The incorporation of ZB particles individually was found to provide a great influence on the thermal resistivity of EFB reinforced epoxy composites. The GH values of lower 27.60 MJ/kg was found for the coupled composite systems including CATH5APP10, CATH10APP5, CAPP10ZB5 and CAPP5ZB10.

Pulverized EFB fibers were treated with NaOH solution followed by neutralizing the fibers. The surface morphology and evaluation of amount of elements present in the fibers were conducted by SEM and EDX analysis. Treated and untreated fibers were also tested through FTIR and TGA. Elimination of lignin and hemicellulose led to the increase of cellulose percentage. SEM images showed that alkali treated fibers possessed a rougher surface as well as finer fiber than untreated fibers. EDX indicated the removal of impurity after alkaline treatment. FTIR spectroscopy analysis indicated the removal of lignin and hemicellulose from the interfibrillar regions in NaOH treated fiber compared to the untreated fiber. TGA revealed greater thermal stability and lower moisture content of alkali treated fiber than untreated ones. These suggest the elimination of hemicellulose and partial elimination of lignin in alkali treated fibers.

Mechanical testing analysis showed that tensile strength, elongation to break, flexural strength and flexural strain reduced with the incorporation of FRs (APP/ATH and APP/ZB) whereas modulus of elasticity and flexural modulus slightly increased. When the EFB fibers were treated in 5 wt% NaOH solution, the mechanical properties of untreated control and TATH5APP10 enhanced compared to those of control and CATH5APP10, respectively. The composites containing 5 wt% ATH-10 wt% APP as well as 10 wt% APP-5 wt% ZB were observed to meet the minimum lab-scale mechanical requirements, in terms of tensile strength, elongation to break, tensile modulus and flexural strength, for aircraft interior furnishings. SEM images revealed the fiber breakage failure of composites with treated fiber while the mode of failure for untreated fiber formulations were fiber debonding. SEM micrographs illustrated that FR particles dispersed well within the epoxy matrix, however, the particles acted as stress concentration zone, resulting in the reduced mechanical properties.

All in all, two more flammability tests are required to evaluate the suitability of using the optimum formulations (CATH5APP10 and CAPP10ZB5) for aircraft interiors in terms of flammability tests in accordance with FAR requirements. The tests are National Bureau of Standards (NBS) smoke chamber in order to measure the smoke density and Ohio State University (OSU) calorimeter to measure total heat release and peak heat release rate. These two instruments could not be located in Malaysia and several other countries, thus it is suggested that these tests be carried out with the aid of major aircraft companies abroad as part of the future work. Additionally, each aircraft manufacturer has its own requirements which must be taken into consideration. E.g. in regards to the mechanical tests, there are particular mechanical tests, which is conducted in each aircraft manufacturer company, that each aircraft interior composite and component is required to meet its related criteria. This highlights the importance of collaboration with an aerospace manufacturer in

order to perform all the required tests and optimize the formulations by the incorporation of flame retardant additives, treatment of the fibres and using suitable fabrication technique. It is worth mentioning that the potential exists as natural fibre reinforced composites, which is highlighted earlier, have been utilizing in the interior parts of several branded automobiles.

In the following chapter, the effect of expandable graphite (EG) as a FR on the flammability, thermal and mechanical properties of EFB filled epoxy composite was investigated. Chapter 5 explained the function of EG on the event of fire and thermal conditions, and how EG particles provided a thermal barrier.

Chapter 5

5. Expandable graphite filled EFB fibre reinforced epoxy composite

5.1 Introduction

Natural fiber reinforced epoxy composites are highly flammable due to the presence of natural fibers and epoxy resin, which are both combustible in nature [98]. In order to be used for aerospace industry, and enable to meet their stringent requirements, developing a flame retarding and thermally stable natural fiber reinforced composites as well as strong mechanical properties has become highly desirable. A wide range of varying flame retardants such as intumescent flame retardants and halogen based materials have been employed to improve the thermal resistivity and fire retardancy of polymer composites thus far [99, 261]. To attain the desired levels of thermal and fire resistance, concentrations with higher than 25 wt% additives are commonly necessary to be applied, which unavoidably causes low levels of mechanical performances [262, 263]. Therefore, a material with highly flame resistance characteristics is required to be used for natural fiber reinforced polymeric composites to provide sufficient fire retardancy at low concentration. Recently, several studies were conducted on the effects of expandable graphite (EG) on the wood polypropylene composites [166], polyurethane- polyisocyanurate foam composites [165] and epoxy based composites [169], and it was observed that increasing addition of EG particles significantly enhanced the thermal stability and decreased flammability properties of composites. This could highlight the potential of EG as an effective flame retardant, which still needs to be investigated and evaluated in the required flame resistant composite systems.

EG, known as an intumescent flame retardant material, is categorized as a type of graphite flake and possesses layers of hexagonal carbon structure. A distinctive flame retardant characteristic of

EG is that sulfuric acid (H_2SO_4) is intercalated between its crystalline structure (carbon layers). At alleviated temperature, the EG gets oxidized, as shown in equation 1 [165], because of a redox process on reaction with H_2SO_4 and forms evolved gases including CO_2, H_2O and SO_2. These gases help dilute the heat and O_2 concentrated near the fire zone, in the case of thermal decomposition.

$$C + 2\,H_2SO_4 \rightarrow CO_2\uparrow + 2\,H_2O\uparrow + 2SO_2\uparrow \quad (1)$$

The blowing effect of evolved gases that is escaping through the EG leads to an increase in the volume of EG, resulting in an irreversible worm-like structure in EG filled materials, which exfoliates perpendicular to the carbon layers. This char suffocates the flame and hinders the transfer of heat and mass from the underlying substrate. The char also is capable of acting as a physical barrier to diffuse oxygen and heat from the burning zone. Due to a dearth of O_2 created by abovementioned protections, flame spread becomes difficult [264-266]. Figure 5-1 illustrates the way EG acts in the event of fire.

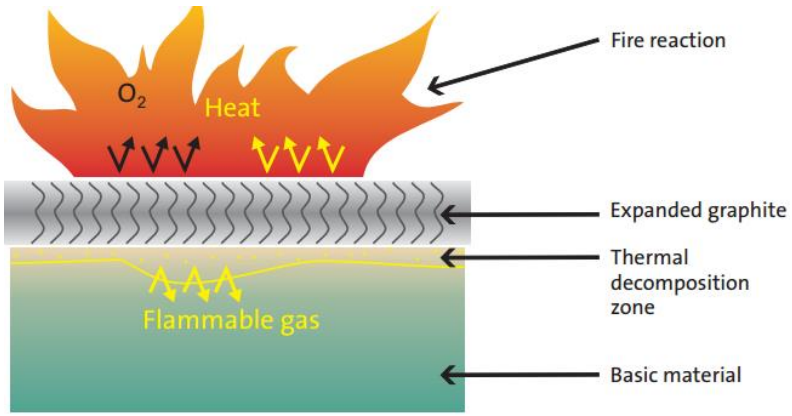


Figure 5-1. Protection of expandable graphite for material during fire [267].

EG not only possesses the flame retarding effect, but also has no-smoke production and low toxicity [268-270]. EG decreases the smoke density as it works mainly in the condensed phase [165]. However, the amount of EG must be controlled in the interior components due to the presence of CO_2 and SO_2 gases. Each aircraft interior manufacturer has its own requirements for the toxic gases released upon combustion, which the minimum quantity of each toxic gas must be met. This requires the appropriate formulation of composites in order to meet all the flammability, thermal and smoke properties simultaneously for each respective aircraft manufacturer.

The aim of this research study was to evaluate the impacts of EG particles in terms of filler and intumescent coating on the flame resistivity, char expansion, char composition, heat shielding, char morphology, gross heat of combustion, char residual weight and mechanical performances of EFB fiber reinforced epoxy.

5.2 Characterizations of expandable graphite

5.2.1 EG expansion analysis

Initially, the characterization of expandable graphite (EG) was conducted. SEM micrographs of expandable graphite after placing them in a furnace for the period of 10 s at the temperatures of 150 °C, 200 °C and 300 °C were shown in Figure 5-2. It was observed that EG exfoliation initiated only when heated at 300 °C. This indicates that most of intercalating substances degraded and formed gases (mainly CO_2 [271]) escaped from the interstices of EG, resulting in expanding the graphite layers. Figure 5-3 illustrates the EDX results of EG after thermal shock at 200 °C (prior to exfoliation) and 300 °C (after exfoliation). It was found out that EG heated at the temperature of 300 °C possessed higher amount of carbon and lesser concentration of oxygen than those of EG

heated at 200 °C. The weight percentage of carbon increased from 77.44% to 87.75% whereas oxygen weight percentage dropped from 20.81% to 10.83%. This proves that EG reacted and expanded at 300 °C and, as a result, higher quantity of oxygen burned and greater amount of carbon remained.

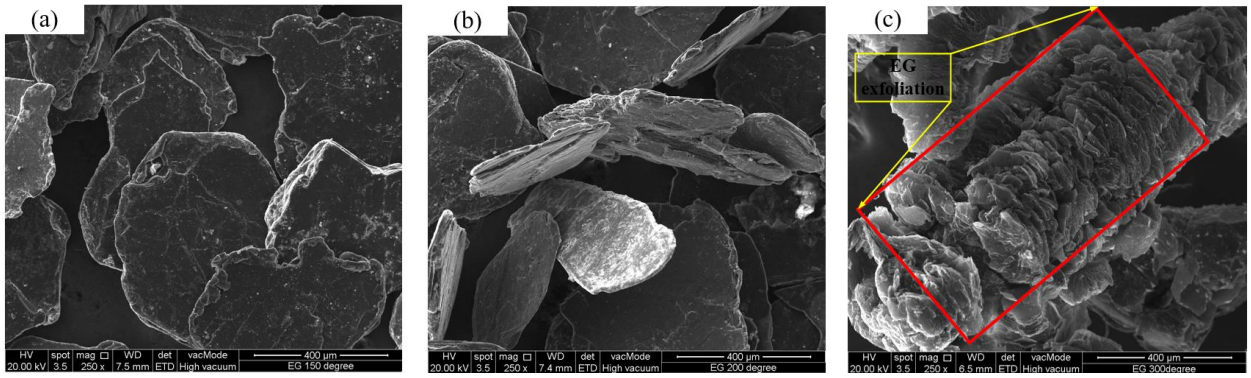


Figure 5-2 SEM images of expandable graphite at 150 °C, 200 °C (Mag 250X) and 300 °C (Mag 250X was used to illustrate a clearer image of the expansion).

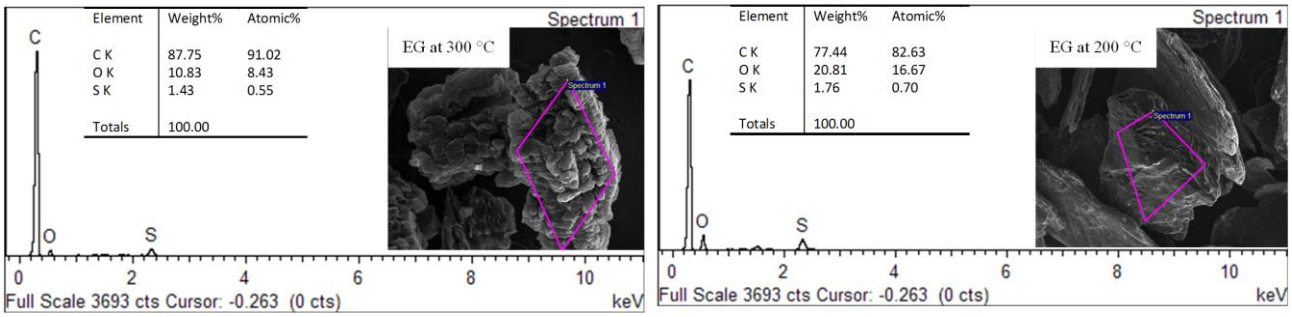


Figure 5-3 EDX results of EG heated at 300 °C and 200 °C (Mag 250X).

5.2.2 Diameter of expandable and expanded graphite

The virgin expandable graphite (EG), as received, was in the form of platelets with a diameter range of 263-608.30 μm, as shown in SEM micrographs in Figure 5-4, and according to the

supplier analysis the expansion ratio of 510 was recorded for this type of EG. After undergoing the thermal conditions caused by vertical Bunsen burner and TGA tests, as shown in Figure 5-4, expandable graphite expanded along the z-axis of EG and transformed to a vermicular structure. The loose and multi porous structure of exfoliated graphite was also witnessed in the micrographs. A similar diameter range to the virgin EG was observed in expanded graphite. Stacks of nano-graphite sheets formed in expanded graphite provided the multi-porous structure and galleries.

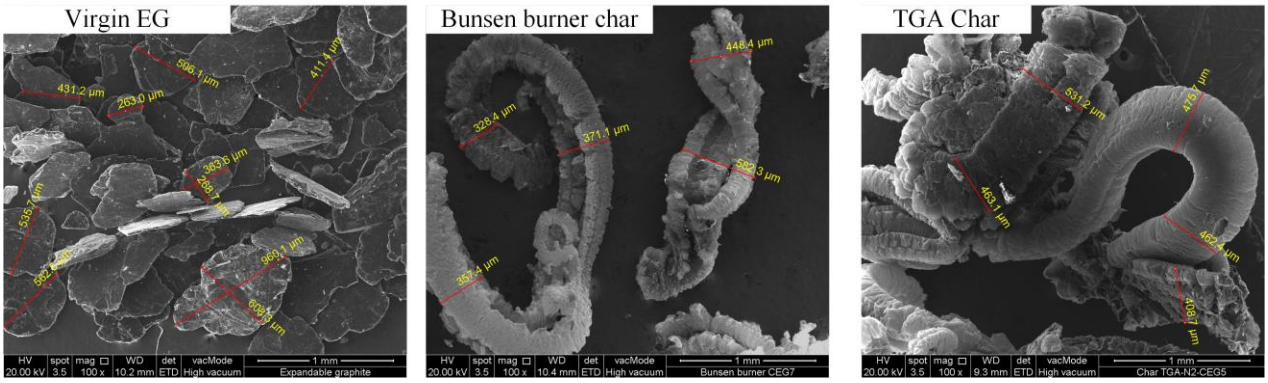


Figure 5-4 SEM micrographs of expandable graphite, expanded graphite from vertical Bunsen burner test and expanded graphite from TGA test (Mag 100X).

5.2.3 Flammability of EFB epoxy composites containing EG as filler and coating

The results of vertical Bunsen burner tests are shown in Table 5-1. The neat epoxy and the control burned fast and the fire reached the top of lab stand and clamp, thus resulting in failure of passing Federal Aviation Regulation (FAR) requirement. For neat epoxy, the total flame time (TFT) and drip flame time (DFT) were recorded 105 s and 50 s, respectively, and the entire length of specimen burned. Reinforcing EFB fibers into epoxy resin (Control composite) was observed not to help improve the fire resistivity as the entire specimen vigorously burned, and also TFT and DFT were

obtained 160 s and 72 s, respectively. No shielding barrier was formed by EFB fiber components to limit the heat and fuel transport, resulting in the increased flame time and drip flame time in comparison with the neat epoxy.

Incorporation of only 3% wt EG extinguished the flame, and could drop TFT as small as less than 1 second, stop dripping flame and reduce the specimen burned length (only 1 mm burned length). With the inclusion of 5 wt% and 7 wt% EG, both the TFT and DFT showed 0 second and the burned length was measure about 0 mm. This was attributed to the strong promotion of exfoliation of EG layers that occurred prior to the growth of ignition of EFB fibers and epoxy resin, which could effectively inhibit the transfer of gas and heat between the burning substrate and fire zone.

Figure 5-5 and Figure 5-6 exhibit images of EG filled composites after withdrawing the Bunsen burner and burning the specimens. The expanded graphite burned is clearly seen at the bottom of samples along the width (Figure 5-5) and thickness (Figure 5-6). The volume of burned part of EG greatly increased and the worm like structure that was formed suffocated the fire by limiting the mass and gas transfer from the composite to the heat source, inhibiting further degradation of underlying material. The worm like structure of graphite, acted as an effective thermal barrier against the flame source, could be observed in Figure 5-5 and Figure 5-6 after burning.

For EG coated composites, the results of Coating3 sample showed that 3 wt% EG on the surface of composite was not sufficient to decrease the TFT below 15 seconds and failed to meet the requirement. No DFT was recorded and the burned length was measured 1.8 mm, which led to a 1.79 wt% weight reduction. However, the addition of 5 wt% EG as coating was observed to meet the requirements (Table 5-1). The TFT and DFT were recorded 0 s and a burned length of 1 mm occurred. This signifies a minimum amount of EG particle is required to provide self-extinguishing properties. Figure 5-7 illustrates the images of burned coating5 sample at different views.

Expandable graphite expanded instantly and self-extinguished the flame right after withdrawing the burner.

With regard to the amount of smoke generation, a very large quantity of smoke was observed while E100 and C specimens were burning vigorously. The incorporation of EG particles reduced the smoke generation of composites in such a way that increasing addition of EG additives into the composite was observed to produce lesser amount of smoke. For coating3, (the quantity of EG particles was lesser than other composites containing EG) the specimen produced lesser amount of evolved smoke than E100 and C specimens, but more than other formulations containing EG. Coating5 released the smoke almost as much as CEG3. These observations agree with previous investigations which highlighted EG functions predominantly in the condensed phase thereby reducing the smoke density [165]. Other studies proved that EG possesses low toxicity and no-smoke production [268-270].

Table 5-1 The results of vertical Bunsen burner tests.

Formulations	Total Flame time (s)	Drip flame time (s)	Burn length (mm)	Mass loss (%)	FAR requirement of the test
E100	105	50	The entire length	100	Failed
C	160	72	The entire length	100	Failed
CEG3	0.5	0 (No Drip)	1	0.07	Passed
CEG5	0	0 (No Drip)	~0	0.05	Passed
CEG7	0	0 (No Drip)	~0	0.03	Passed
Coating3	33	0 (No Drip)	1.8	1.79	Failed
Coating5	0	0 (No Drip)	1	0.08	passed

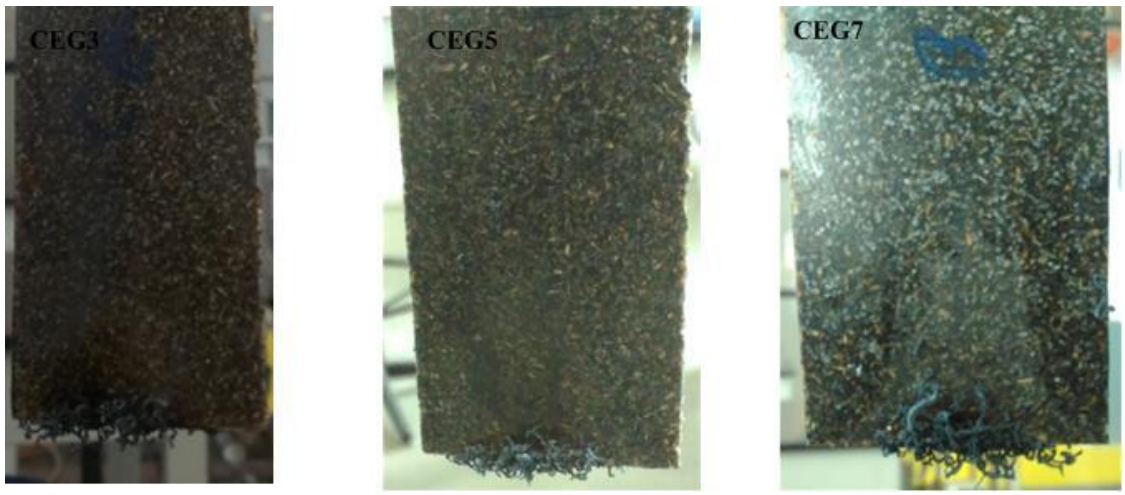


Figure 5-5 The CEG3, CEG5 and CEG7 specimens burned by vertical Bunsen burner test are shown along the width.

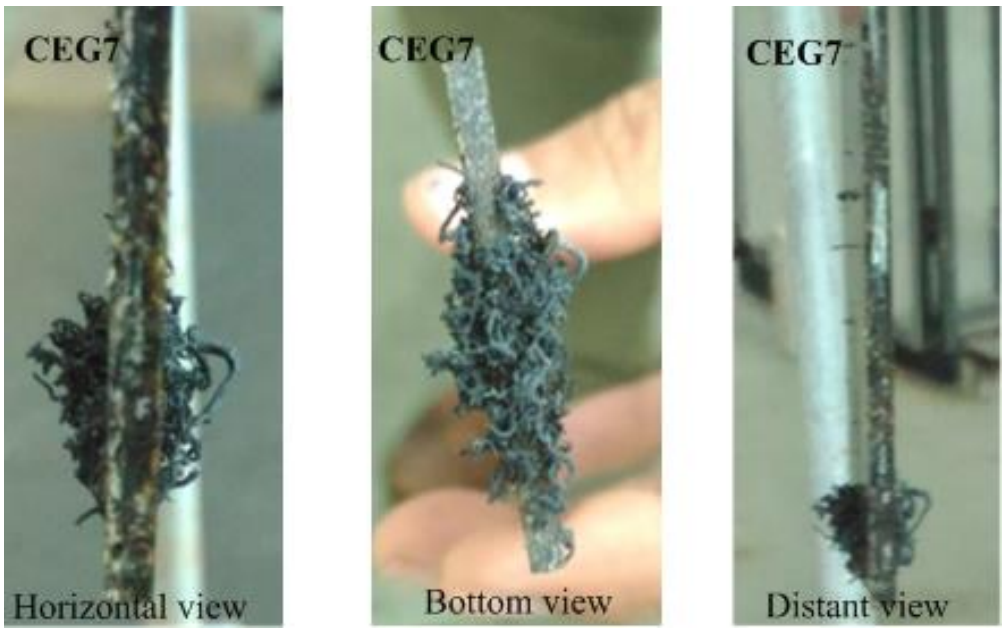


Figure 5-6 The CEG7 specimen burned by vertical Bunsen burner test are shown at different views along the thickness.



Figure 5-7 The images of coating5 sample at different views after Bunsen burner tests.

5.3 Heat release properties

The impact of varying concentration of EG in EFB reinforced composites on GH of combustion obtained with the aid of bomb calorimeter is displayed in Table 5-2. The effectiveness of a flame resistant system is obtained by its potential to decrease the GH of combustion.

The results that were attained revealed that the inclusion of EFB fiber into epoxy decreased the GH from 35.36 MJ/kg to 29.17 MJ/kg (by about 21%) and the GH further dropped with the incorporation of EG. Increasing addition of EG reduced GH, e.g. incorporation of 7% EG lowered the value of combustibility the most by 25.54% and 4.32% compared to the neat epoxy and control, respectively. This reduction is proportional to the concentration of EG introduced into formulations.

During the combustion, the control and EG filled composites formed a greater quality char layer due to the presence of EFB fibers and EG particles, which inhibited the oxygen and heat transfer to the bulk of matrix substrate, resulting in a reduced GH value. Also, EG, during heating, is capable of covering the surface of substrate and improving the stability and strength of the intumescent char [272].

Table 5-2. Gross heat of combustion for E100, C and EG filled formulations.

Formulations	Gross heat (MJ/kg)	Decrement of GH from the control composite (%)
E100	35.36	21.22
C	29.17	0
CEG3	28.96	-0.72
CEG5	28.36	-2.78
CEG7	27.91	-4.32

5.4 Thermal properties of EFB fibre epoxy composites containing EG as filler and coating

The thermal stability is a key parameter of materials that limits their usage in different applications. Hence, the thermal stability of produced formulations was investigated in nitrogen environment.

Formulations underwent two different thermal degradation stages of intumescence corresponding to the temperature range from 30 to 390 °C and formation of char and its decomposition at 390-700 °C, respectively, as shown in Figure 5-8.

During the first stage, EG initiated degradation, hence liberating carbon dioxide (CO_2), which possesses the flame extinguishing impact. Higher residual loss took place in the EG filled formulations at this stage, which indicated the main volume of gases spread into the environment. Subsequently, the EFB fiber and then epoxy was partially degraded in the formulations. Natural

fibers have the initial thermal decomposition in the 200-305°C temperature range, which is attributed to the degradation of the cleavage of glyosidic linkages of cellulose, pectin and hemicellulose that create 20% weight loss [20, 273-275]. The thermal decomposition is followed by the degradation of α-cellulose at the temperature range from 305°C to 370°C with 45.2% weight loss [275-277]. Various neat epoxies were observed to decompose thermally in the degradation range from 320 °C to 350 °C [278], at 335 °C [275] and at 372 °C [84].

In the second stage, the further thermal degradation of epoxy took place mainly in the first place, then followed by the degradation of EFB fiber in the composites. Lignin decomposes in a wide temperature range from 200 °C to 900 °C [20, 247, 274, 275, 279]. This long thermal decomposition temperature range of lignin is due to its complex structure that is aromatic with different branches [247, 275]. The char residue increased at 600 °C for E100, C, CEG3, CEG5 and CEG7 as compared to residue at 500 °C, and it further increased at 700 °C. Ultimate residual weight at 700 °C for E100, C, CEG3, CEG5 and CEG7 were 17.50, 18.47, 22.24, 27.29 and 28.31, respectively, as shown in Figure 5-8. Indeed, an utmost enhancement of 10.81% residual mass was attained between E100 and CEG7. Greater amount of residue improves the anti-oxidation degree in the char, allowing the char to resist greater temperatures intended for a longer period. The enhancement in residual weight was witnessed with the presence of EFB fiber and increase in EG wt%, which can be seen at various temperatures in

Table 5-3. This establishes that the worm-like, swollen, dense and continuous char was effectively generated in EG filled formulations to shield the undelaying substrate from thermal decomposition. The worm-like structure of char formed at about 300 °C was due to the expansion of EG particles.

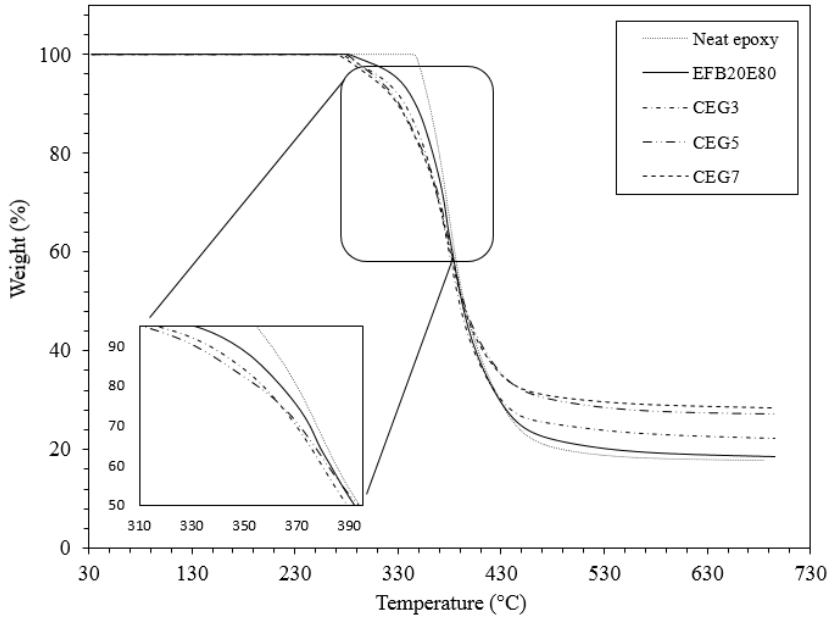


Figure 5-8. TGA results for formulations fabricated.

Table 5-3 Residual weight at varying weight temperatures.

		Mass residue (%)		
Formulations	Td (°C)	at 500 °C	at 600 °C	at 700 °C
E100	374.69	19.51	18	17.5
C	375.14	21.07	19.04	18.47
CEG3	379.41	24.60	22.89	22.24
CEG5	379.54	29.42	27.68	27.29
CEG7	379.60	30.13	28.78	28.31

DTG curves for E100, EFB20E80, CEG3, CEG5 and CEG7 are depicted in Figure 5-9. Inclusion of EG particles into EFB fiber reinforced composite shifted the thermal degradation temperature (T_d) to higher temperatures, as shown in

Table 5-3. Addition of EFB fiber and EG platelets provided higher T_d in comparison with neat epoxy. This is ascribed to enhanced matrix-fiber interactions [275, 280] and EG expansion that forms a worm-like barrier on top of the substrate [166]. Incorporation of different amount of EG enhanced the thermal degradation temperature of control sample from 375.14 °C to 379.50 (±0.10) °C. Expandable graphite contributed to the establishment of a higher char expanded during thermal process. Higher char generation can decrease the pyrolysis reactions, inhibit the formation of combustible gases and limit the thermal conductivity of burning substances [278, 281]. Increasing concentration of EG slightly improved the thermal degradation temperature of composites. CEG5 and CEG7 exhibited a lower weight loss rate compared to other formulations, suggesting the enhancement of thermal stability caused by higher concentration of EG.

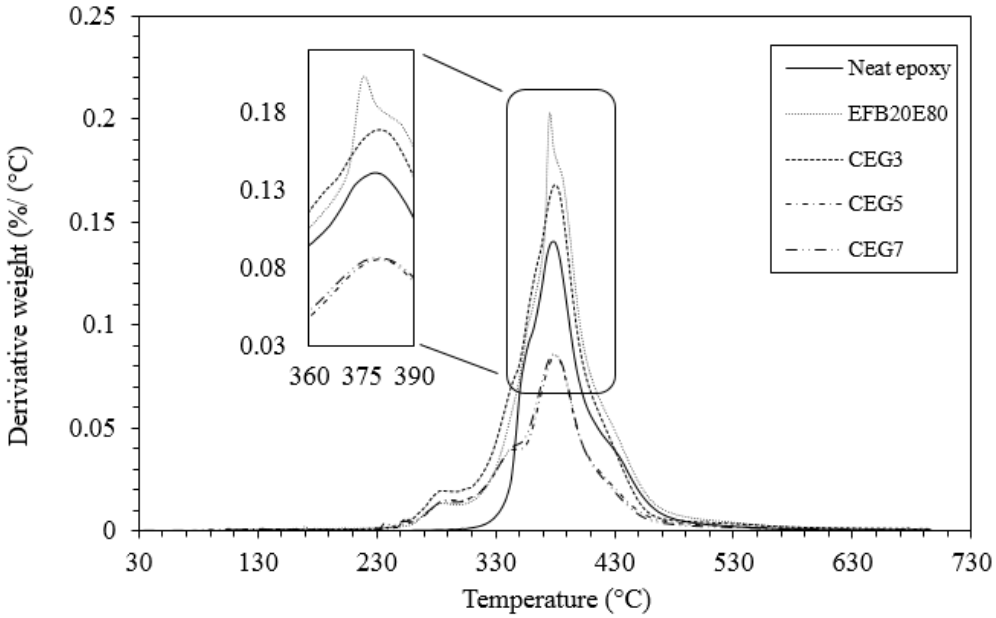


Figure 5-9 DTG curves for E100, EFB20E80, CEG3, CEG5 and CEG7.

5.5 DMA analysis

Figure 5-10 and Figure 5-11 show the storage modulus (E′) and loss factor (Tan δ) of epoxy, control,CEG3, CEG5 and CEG7 as a function of temperature varied from 30 °C to 100 °C, respectively. The storage modulus at 30 °C of samples was also measured and displayed in Figure 5-12. This analysis was carried out to measure the effect of EFB fibers and EG particles on the vicoelastic behavior of epoxy resin.

As seen in Figure 5-10, inclusion of EFB fibers into pure epoxy significantly increased E′ at glassy state region. The control composite showed higher storage modulus than that of other formulations. Increasing EG particles was found to lower the E′ compared to the control, however still higher than neat epoxy due to the EFB fibers reinforced in composites. At the temperature of 50 °C, the control composite and CEG7 showed approximately 65% and 33% rise over neat epoxy, respecitvely. With the increase of temperature, a gradual decrease in storage modulus attained and this was followed by an abrupt decrease in thermal transition temperature (T_g), attributed to the transision of samples from glassy to rubbery state. As the temperature increases, composites containing EG particles presented an early reduction in E′. The onset of T_g were around 54 °C , 53 °C and 51-52°C for neat epoxy, control and composites with EG particles, respectively.

Figure 5-11 indicated that the minimum loss factor in peaks was for the neat epoxy with the value of 0.74, and the Tan δ increased with the inclusion of EFB fiber and/or EG particles, the greatest being CEG7 with the highset Tan δ of 0.85. It suggests that EG and EFB fiber induced higher energy dissapiation than E100. The T_g can be obtained from the peak of damping co-efficient (loss factor). T_g increased by 1.65 °C with addition EFB fibers into pure epoxy and also composites with EG particles (CEG3 and CEG5) improved T_g by about 0.84 °C over neat epoxy. However, the further increament of EG concentration (CEG7) dropped the T_g of composite (64.72 °C) to nearly

similar value of neat epoxy. The thermal transition temperature explains the mobility level of matrix segments of polymer networks, e.i, a reduction in the mobility of polymeric chains can be correlated with the increment in T_g [271]. This explanation clarifies higher value of T_g in the control and EG filled composites than neat epoxy as the EFB fiber and EG particles constrained the mobility of micromolecules of epoxy polymer, which is ascribed by high amounts of fibers and fillers in composites.

As shown in Figure 5-12, due to good interfacial interaction between epoxy polymer and EFB fiber elastic modulus at 30 °C of control composite introduced the highest value in comparision with other formulations. Furthermore, the incorporation of EG particles dropped the modulus. This could be attributed to the lack of adhesion between epoxy matrix and EG particles. EFB fibres (similar to other NFs) possess high degree of permeability [9]and 20 wt% EFB mass fraction was the maximum amount that could be introduced into the composite. Therefore, there was not sufficient interfacial adhesion to create good bonding between epoxy matrix and EG fillers. Similarly, it was reported that the storage modulus reduced with the inclusion of EG into rigid polyurethane [269].

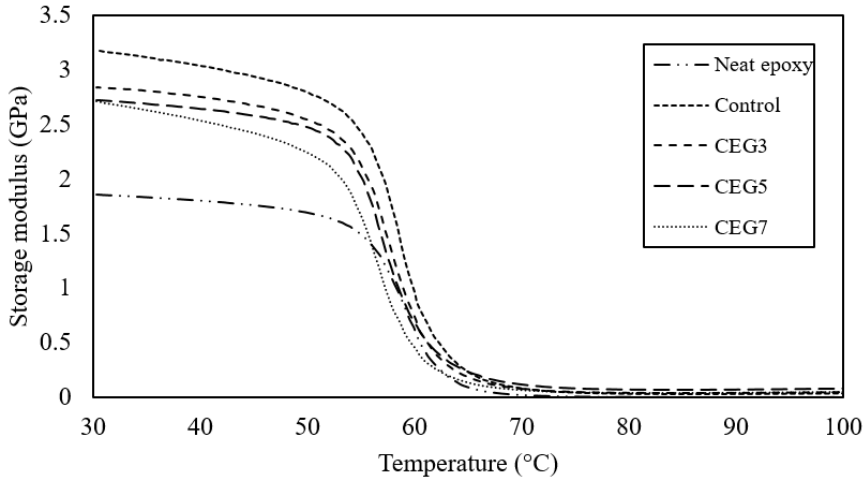


Figure 5-10 Storage modulus of formulations.

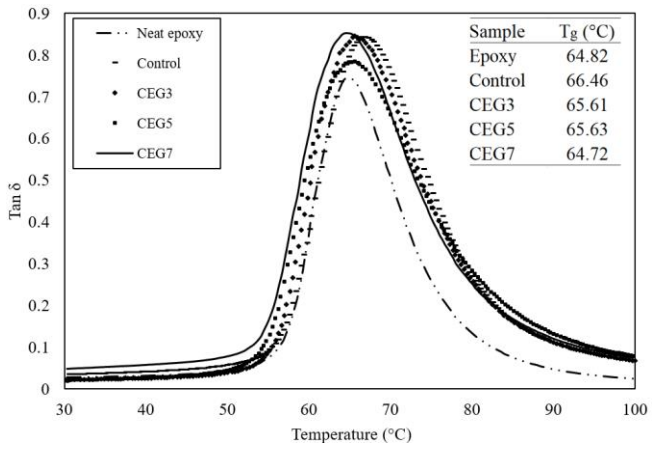


Figure 5-11 Loss factor of neat epoxy, control and EG filled composites.

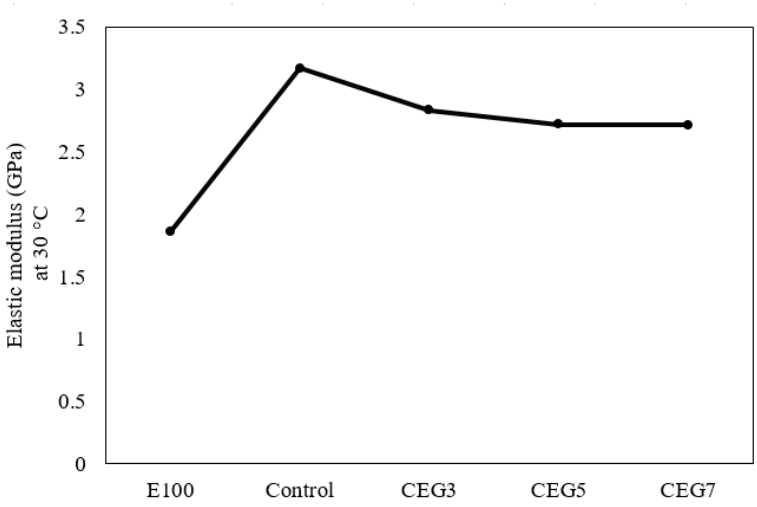


Figure 5-12 Elastic modulus of formulations at 30 °C.

5.6 Combined confocal Raman-AFM analysis

The burned composite specimens were first scanned and their weight-light images show in Figure 5-13. This test was conducted in order to compare the intumescent char formed after burning the specimen with the unburned surface of specimen. The unburned and burned parts of each specimen

observed are seperated by a dashed line. EG particles expanded after combustion and formed a protective swollen char residue. The expanded graphite obtained from the burner test was compared with expandable graphite using Raman spectra, AFM, surface topography and surface roughness in order to understand the way expandable graphite protects the composite in the event of fire.

Raman spectrum was used to evaluate the surface charactersitics of expandable and expanded graphite particles. Figure 5-14 depicts the charactersitic Raman G, D and 2D bands of expandable and expanded graphite particles prior to and after the burner test, respectively. The location of G peak, indicating the order state of graphitic (sp^2-bonded) carbon, was observed in the 1540-1620 cm^{-1} spectral range, and the location of sp^3-bonded carbon (disorder state, D peak) was found in the range from 1320 cm^{-1} to 1400 cm^{-1} [282-285]. For the spectral range between 2600 cm^{-1} and 2780 cm^{-1}, the carbon corresponding to the 2D peak located [283, 285]. Raman spectrum of expanded graphite shifted to the left compared to the expandable graphite spectrum, indicating that graphite particles tensioned after burning. This proves that expandable graphite shields the heat and mass transfer into the bulk of substrate on combustion, and after expansion at higher temperature stretches and exfoliates.

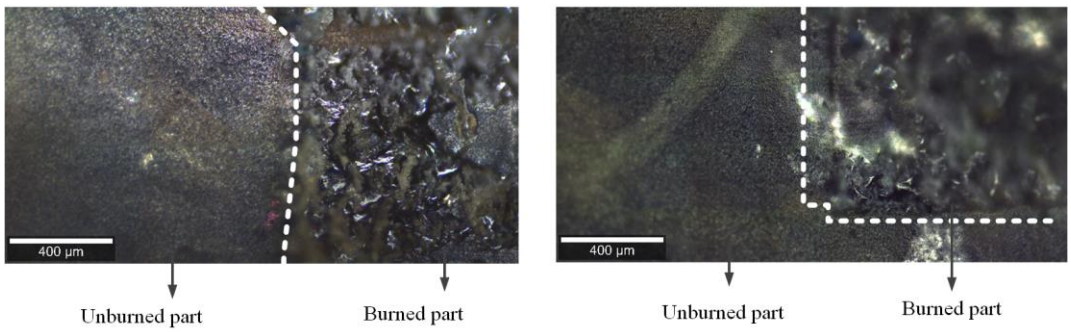


Figure 5-13 White-light images of unburned and burned composite specimens.

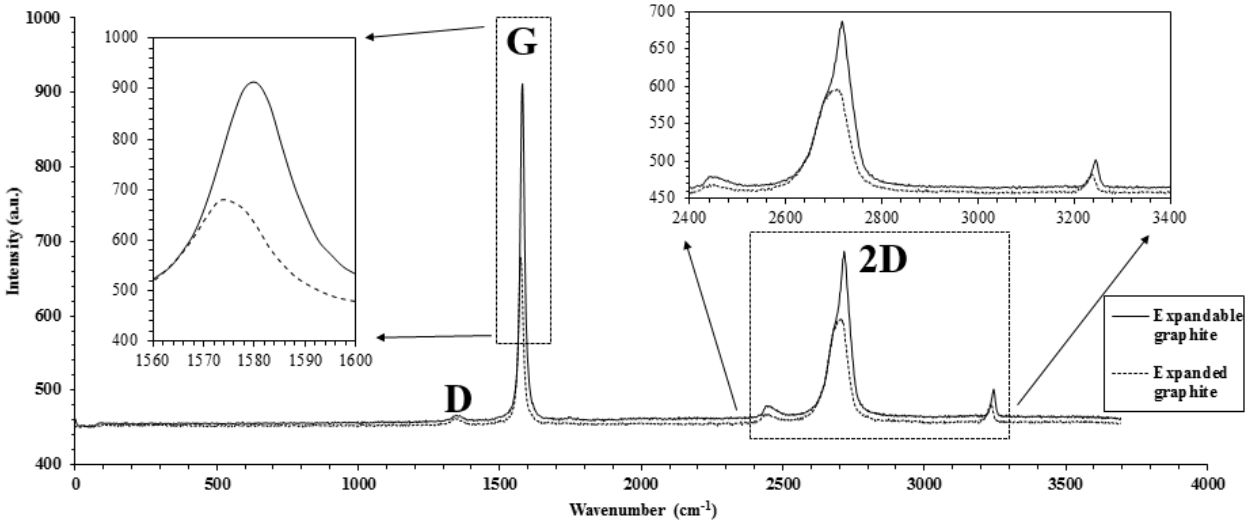


Figure 5-14 Raman spectra attained from expandable and expanded graphite particles.

AFM characterization was conducted to visualise the surface morphology of expandable and expanded graphite particles, and their white-light images and AFM phase images were obtained (as shown in Figure 5-15). The pristine graphite and burned graphite are evident in the white-light images (Figure 5-15-a and Figure 5-15-b). Upon combustion, EG particles (Figure 5-15-c) exfoliated, which led to the seperation of graphite layers as shown in Figure 5-15-d.

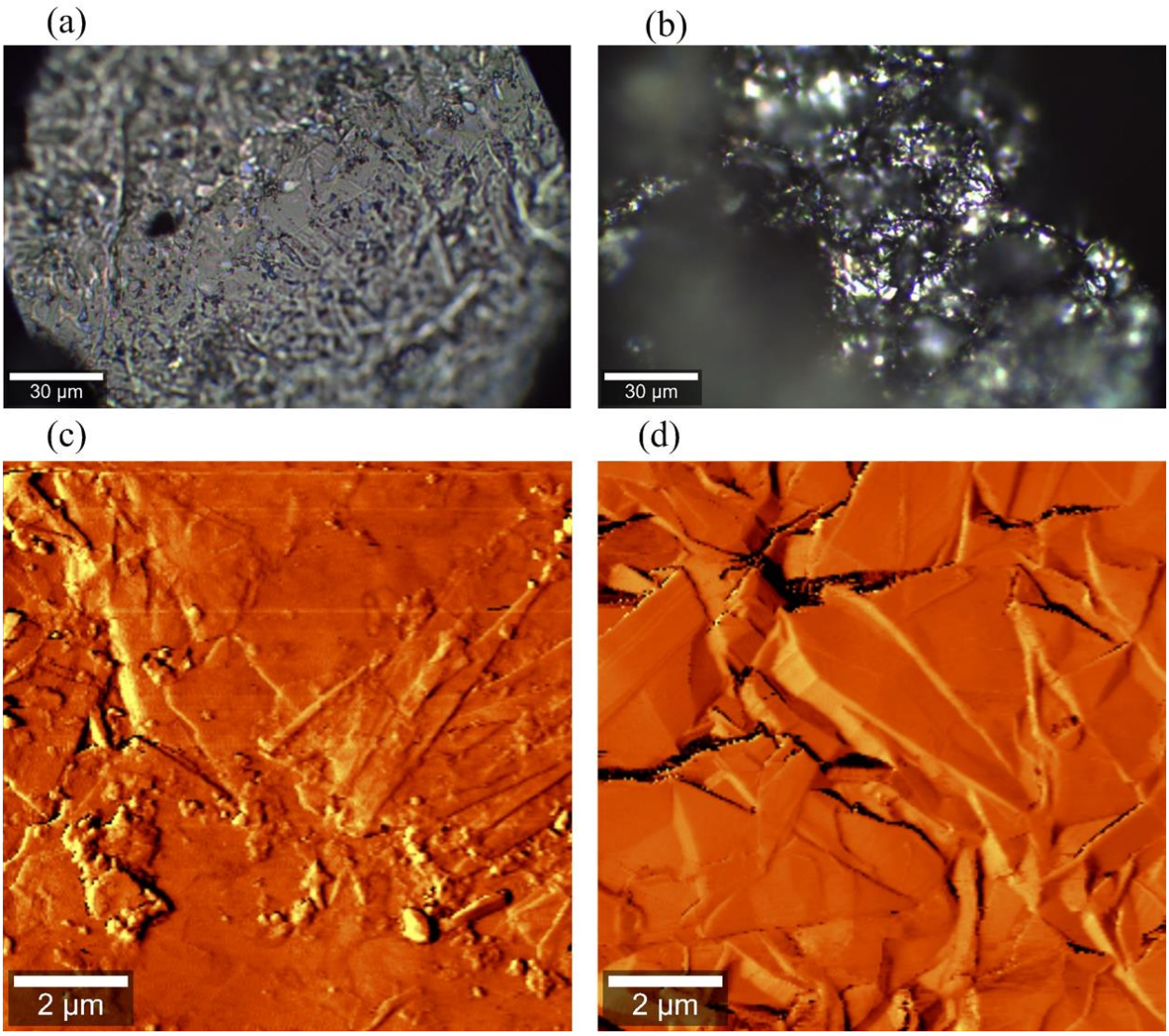


Figure 5-15 White-light images of (a) expandable graphite and (b) expanded graphite. AFM images of (c) expandable graphite and (d) expanded graphite.

AFM two dimensional (2-D) and three dimensional (3-D) surface topographies were observed by AFM microscopy, as depicted in Figure 5-16. The arrangements of physical features of expandable and expanded graphite were detected. The pristine expandable graphite (Figure 5-16- a and b) expanded in the event of heat and produced broad layers of graphite (Figure 5-16- c and d). Topology images of expandable graphite are denser whereas EG images are more transparent.

Surface roughness of particles are shown in Table 5-4. For the analyzed area of 99.2203 μm², the roughness surface average (SA) and roughness mean square (SQ) of graphite decreased from 238.88 nm to 169.71 nm and from 270.78 nm to 213.75 nm after expansion, respectively. This implies the smoother surface of graphite after exfoliation as expected due to the expansion of graphite layers and increased surface area [271, 282].

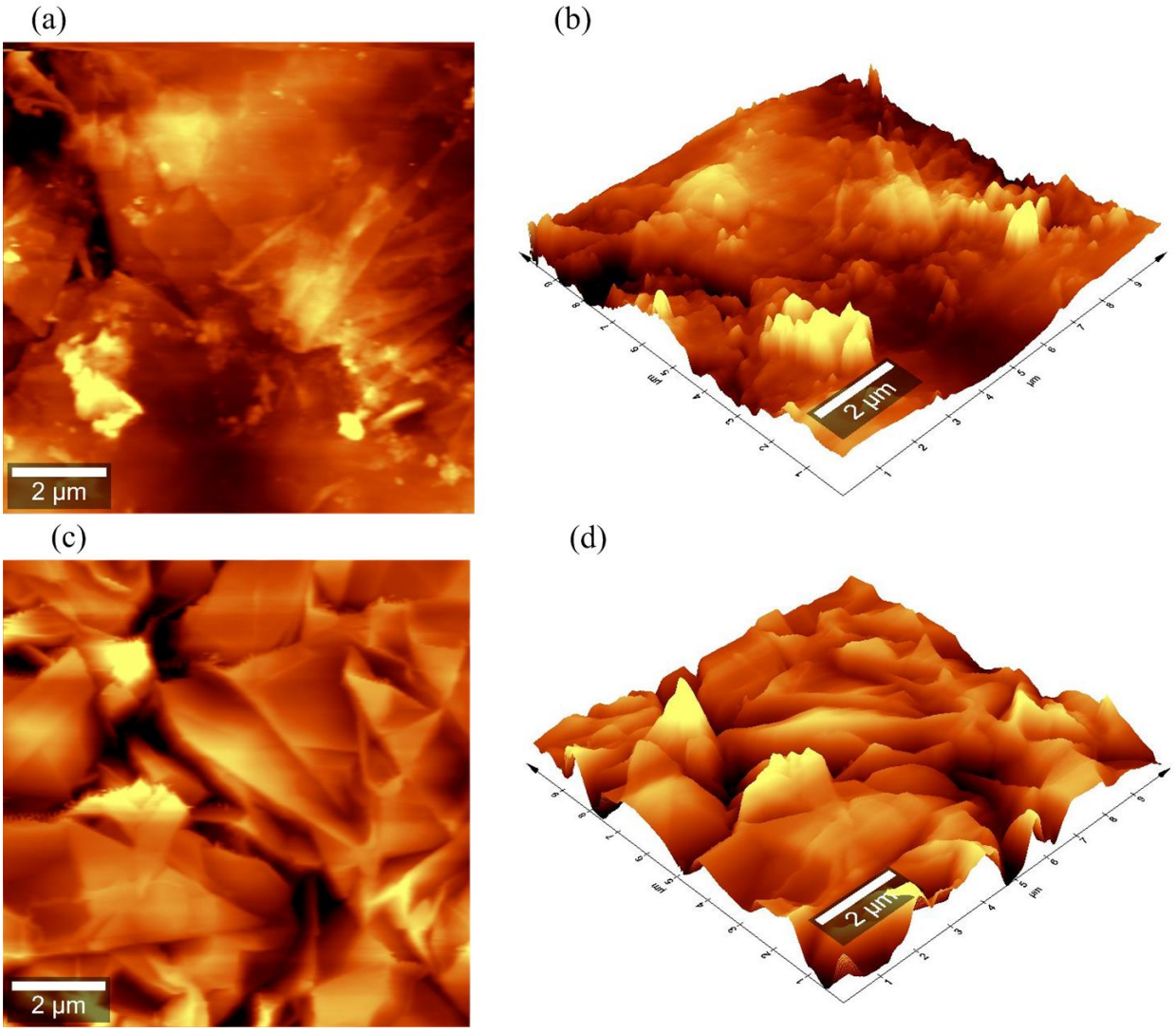


Figure 5-16 Topography images of expandable graphite (a) 2-D and (b) 3-D as well as expanded graphite (c) 2-D and (d) 3-D.

Table 5-4 Surface roughness of expandable and expanded graphite particles.

	Expandable graphite	Expanded graphite
Analyzed area (μm²)	99.2203	99.2203
True area (μm²)	102.894	124.475
Peak-peak (nm)	1167.94	1788.76
Roughness surface average (SA) (nm)	238.881	169.71
Roughness mean square (SQ) (nm)	270.784	213.752

5.7 EDX analysis

The microstructure of char layer attained after vertical Bunsen burner and TGA tests for CEG7 and CEG5 are displayed in Figure 5-17 and Figure 5-18. An expanded char generated during the thermal decomposition that acts as a barrier against gases and heat. Upon the event of fire, the expandable graphite in CEG7 expanded and formed a worm like structure of carbon layer, as illustrated in Figure 5-17-a. The residual structure of EFB fiber formed from degradation of CEG5 showed many cracks and large holes attributed to less condensed char or inadequate char generation [286] (Figure 5-18-a). With the presence of both EFB fibers and EG particles existed in composites, a multiporous and thick char with a homogenous and uniform cell-size distribution was formed as shown in Figure 5-18-c. This charred structure would be favorable as it retarded the heat and mass transfer into materials. The physical structure of residue plays a key role to provide a desired thermal resistivity. The homogenous, compact and dense structure of char are capable of promoting effective thermal insulation properties. The content (%) of carbon and oxygen almost remained similar for the char burned in air atmosphere and the sample tested under nitrogen in TGA. Generally, high weight percentage of carbon implies a strong degree of antioxidization for the residue at greater temperatures. The presence of S in the char residue is

attributed to the exfoliation of EG at high temperature, leading to the release of SO_2. The existence of small amount of K could be ascribed to the contamination of char residue in the alumina pan.

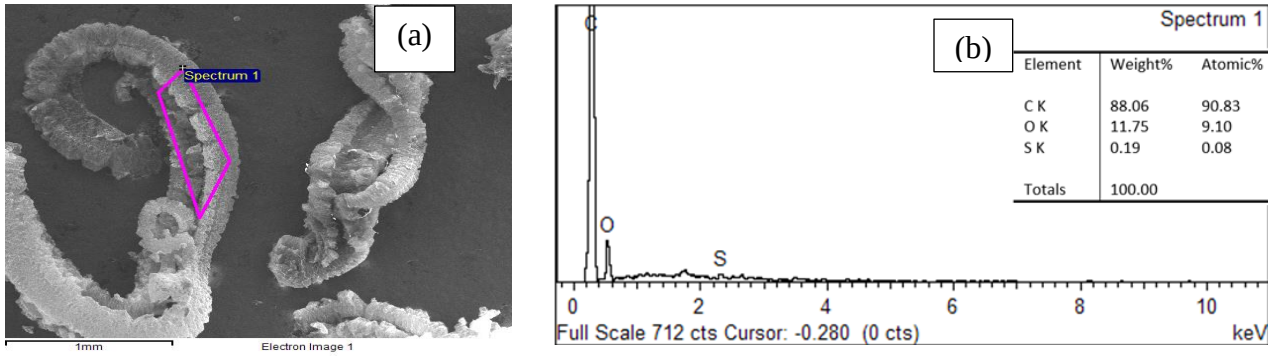


Figure 5-17. EDX analysis of char residue for CEG7 after vertical Bunsen burner test in the air atmosphere at 100X: (a) the selected spectrum, (b) elements in the char residue.

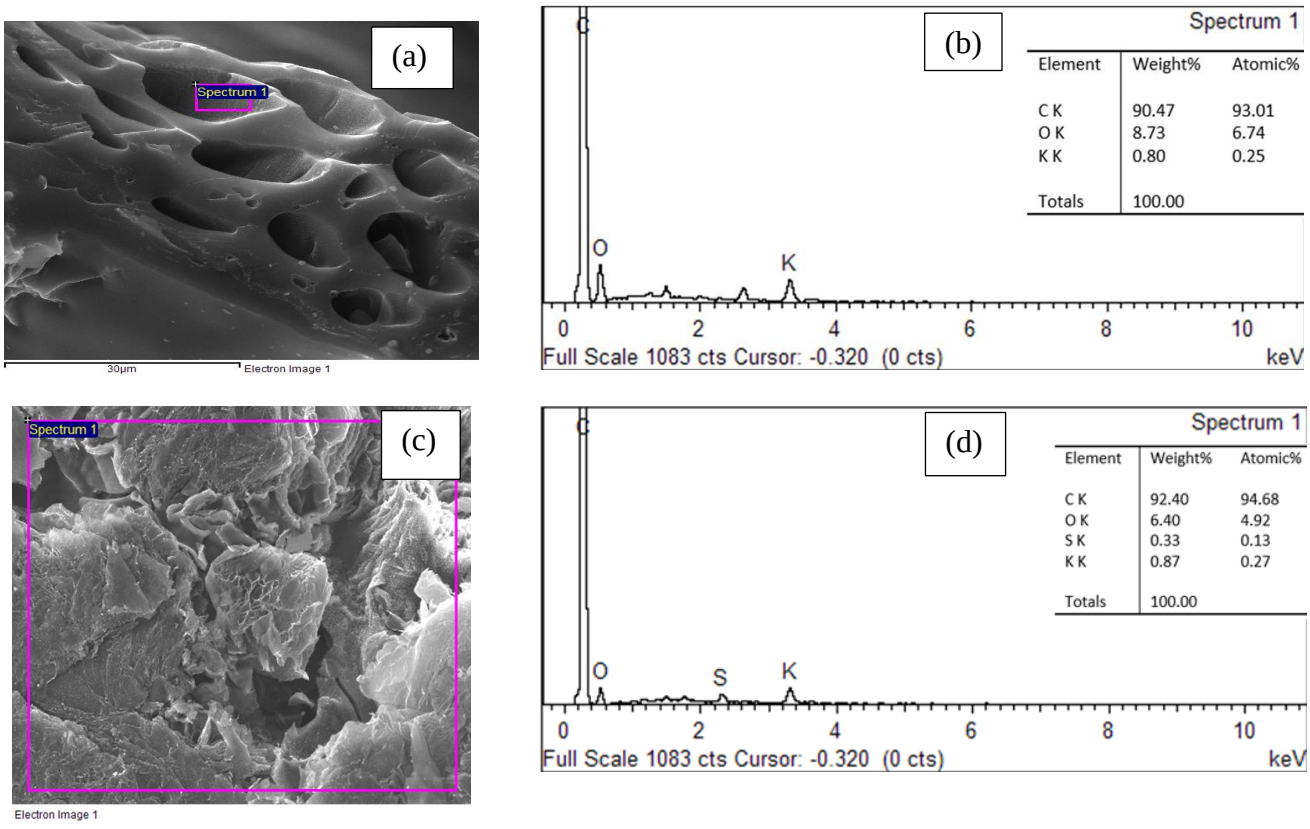


Figure 5-18. EDX analysis of char residue for CEG5 after TGA test in the N_2 atmosphere at (a, b) 5000 X and (c, d) 1000 X.

5.8 Morphology of composites

In order to investigate the bonding and dispersion of the EG and EFB fiber when added into epoxy resin at different concentration of EG, SEM was used. SEM micrographs of tensile fractured samples are presented in Figure 5-19 and Figure 5-20.

As displayed in Figure 5-19, a relatively strong interfacial bonding between epoxy and EFB fiber was observed, as highlighted with red arrows, which demonstrates good adhesion of EFB fibers with the epoxy when pulled under tension. The SEM images indicated no fiber debonding and or pull out in the fibrous regions and a breakage was formed during the tension, highlighted by yellow arrow. The abovementioned reasons suggest the positive effect of EFB fiber as reinforcement on improved mechanical properties of control composite relative to the neat epoxy.

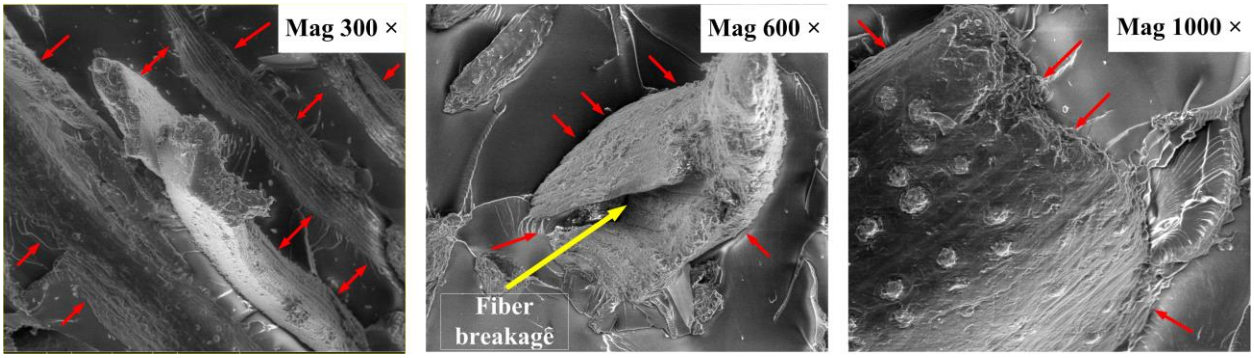


Figure 5-19 Micrographs of EFB20E80 at magnifications of 300×, 600× and 1000× after tensile test.

For the impact of varying EG to the EFB fiber reinforced composite on the microstructure and fracture surface of formulations, the tensile fractured surface of samples were scanned and are indicated in Figure 5-20. The interfacial adhesion of EFB fiber and EG fillers with epoxy resin

were illustrated by green and red ellipses, respectively. EFB fibers were observed to show good bonding with matrix and similar to control sample, fiber breakage was occurred (highlighted by yellow arrow) and no pull out was detected. Despite of fibers, it was found out that EG fillers were not capable of providing a strong interaction with matrix and micro-cracks were formed when the samples were pulled. (20 wt% weight fraction of EFB fibres were the maximum quantity that could be reinforced into the composite due to the high degree of wetting of NFs. EFB fibres tend to absorb the epoxy polymer, therefore, the interfacial bonding between EGs and epoxy matrix was not adequate.). This implies the lower mechanical properties of EG filled composites than those of the control. Increasing incorporation of EG particles worsened the interfacial wettability amongst constituents. River like structure of epoxy resin were also marked in the micrograph. For the composite reinforced with treated EFB fibers (EG5), as illustrated in Figure 5-20, it was observed that the fracture was chiefly characterized by the breakage of EFB fibers. Since the treated fibers were free of lignin, hemicellulose, wax and other surface deposits [287, 288], epoxy matrix was observed adhering to the EFB fibers, thereby providing stronger bonds between the EFB fibers and epoxy matrix.

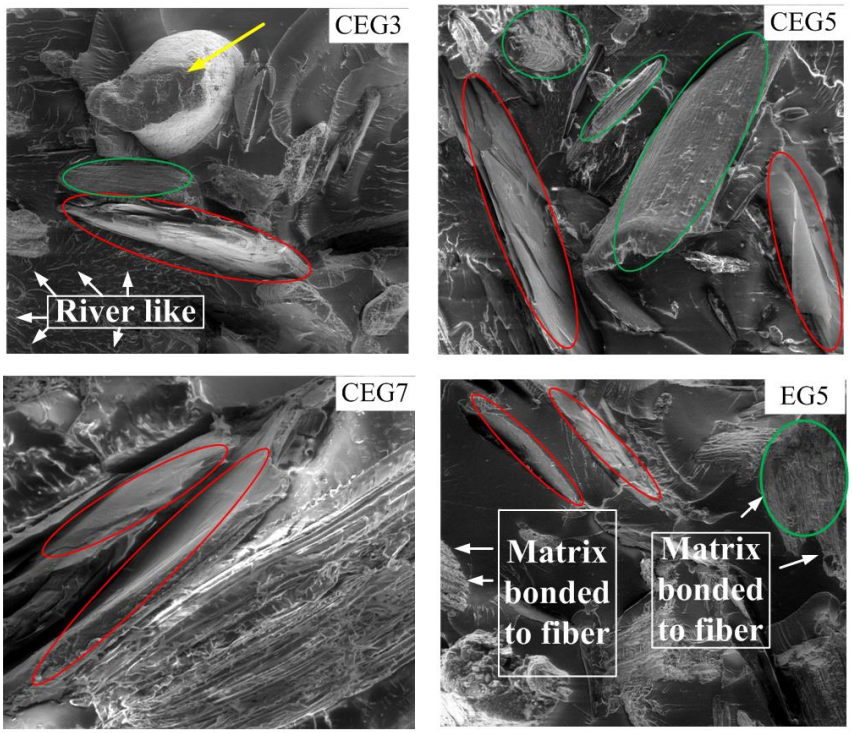


Figure 5-20. SEM micrographs of control, EG filled composites and EG5 at 300X.

5.9 Tensile properties

The tensile strength, Young's modulus and strain at break of E100, C, CEG3, CEG5, CEG7 and EG5 are shown in Figure 5-21 and Figure 5-22. Inclusion of 20 wt% EFB fiber into neat epoxy improved the tensile strength, i.e. 27.42% increase compared to that of E100.

As shown in Figure 5-21, any increase of EG in untreated EFB fiber composite reduced the tensile strength relative to control composite, but still higher than neat epoxy. This can be attributed to the tension load which did not transfer from epoxy matrix to EG particles owing to the lack of interfacial adhesion between polymeric matrix and EGs [289, 290]. This can also be observed from SEM images (Figure 5-20), attributed to the high degree of permeability of NFs that absorb the epoxy matrix [9], as highlighted previously. E.g. CEG7 showed 15.05% decrease in the tensile strength compared to that of the control. The tensile strength of formulation reinforced with alkali

EFB fibers (EG5) enhanced over that of the control, epoxy and untreated EFB fiber EG filled composites. The enhancement in tensile stress was calculated 24.77% relative to the control, which could be ascribed to stronger interfacial adhesion between the treated EFB fibers and resin matrix.

With regards to tensile strain, the incorporation of EFB fiber into the brittle epoxy enhanced the ductility of composites, as depicted in Figure 5-21. The elongation to break increased by 58.63% with the inclusion of EFB fiber into the epoxy. Any further incorporation of EG platelets dropped the elongation to break, with the greatest being CEG7 with 23.59% reduction as compared to the control. The elongation to break was found to increase by 51.26% with the usage of alkali treated EFB fiber in the EG5 relative to the control. The reduced strain with the increased concentration of EGs is due to the lack of bonding between EGs and polymer matrix [290], as observed from SEM micrographs (Figure 5-20).

The tensile modulus of all formulations is shown in Figure 5-22. The control exhibited 62.72% increase in the tensile modulus over that of E100 and tensile modulus improved by 28.80% in EG5 relative to that of the control. The maximum value of modulus was for the EG5 due to the presence of treated EFB fibers. Increasing the amount of EG particles in the untreated EFB fiber reinforced composites reduced the modulus. The results of Young's modulus are in accordance with the storage modulus, as obtained from DMA study. This drop implies the insufficient adhesion between the polymeric matrix and EGs [172, 289] as also depicted from SEM images (Figure 5-20). The same reduced trend in tensile moduli with the incorporation of EG into polymeric matrices was observed in other studies, cited as [172, 289].

It can be concluded that EG particles disturb the load transfer from polymer matrix to the EFB fibers, resulting in the reduced tensile properties, and also could not act as an effective

reinforcement to resist tensile loads to improve the mechanical behaviors. These properties were observed to improve with the incorporation of chemically treated natural fibers.

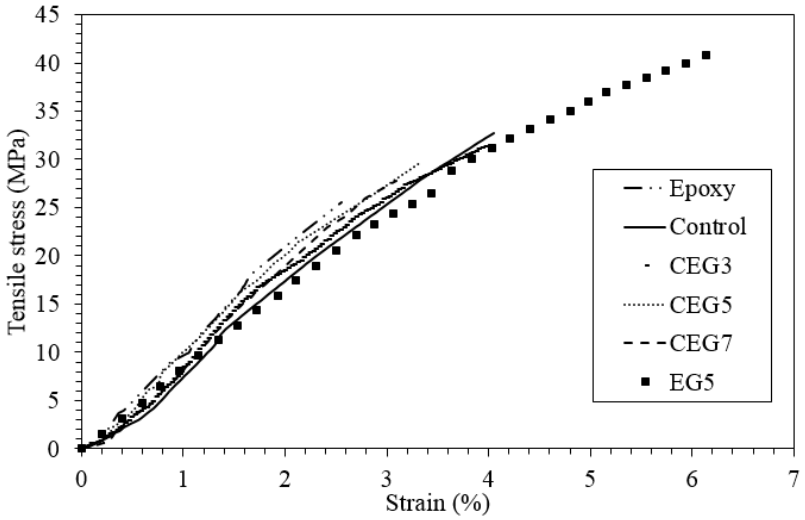


Figure 5-21 Tensile stress-strain curve of E100, C, CEG3, CEG5, CEG7 and EG5.

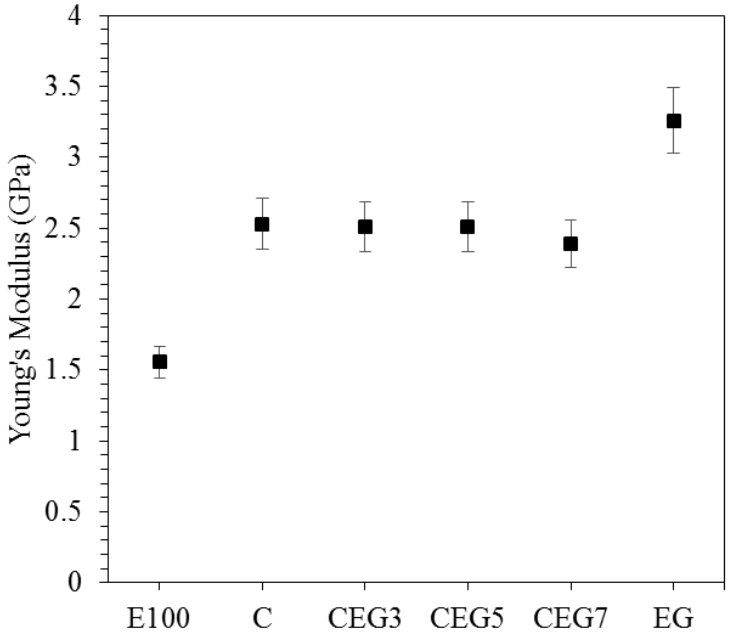


Figure 5-22 Young's modulus of E100, C, CEG3, CEG5, CEG7 and EG5.

5.10 Flexural properties

The flexural properties of neat epoxy, control, composites reinforced with varying wt% of EG concentrations and EG filled composite with alkali treated EFB fibers are shown in Figure 5-23. The trend of the flexural performances was similar to those of tensile properties. It was observed that the reinforcement of EFB fiber enhanced the flexural strength, strain and modulus when added into epoxy resin with the increment of 19.3%, 93.2% and 68.1 % for flexural strength, strain and modulus, respectively. Besides, every increase of EG concentration in EFB fiber reinforced composite dropped the flexural properties. The formulation reinforced with 7 wt% EG exhibited 8% and 34.3% and 15.1% reduction in flexural strength, strain and modulus relative to those of the control, respectively. The abovementioned variations (reduced flexural properties) could be ascribed to poorer interfacial interaction of EG flakes with epoxy polymer (as shown in SEM micrographs (Figure 5-20)), which limits the mobility of epoxy polymeric chains [172]. Similar decrease in flexural strength and modulus was found with the incorporation of EG particles into the NF polymeric composite [172]. The increase in flexural behavior of EG5 was associated to the presence of alkali treated fibers. The flexural strength, strain and modulus improved by approximately 2.2%, 20.8% and 4.6%, respectively, compared to those of control. This implies the positive effect of alkali treatment on the flexural properties similar to the tensile behaviors but to a lesser degree.

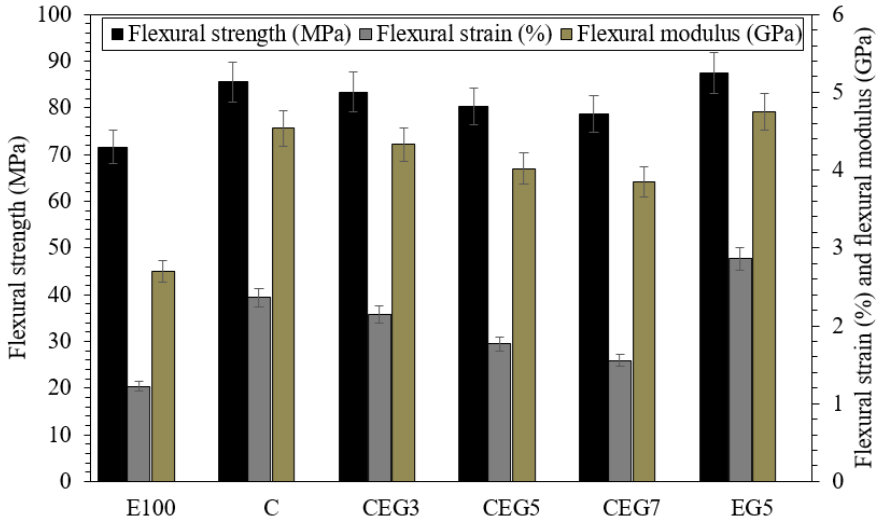


Figure 5-23 Flexural properties of formulations.

5.11 Summary

The flammability and thermal resistivity of EFB fiber reinforced epoxy composites were remarkably improved by the inclusion of EG particles as filler and EFB fibers, as proved by the vertical Bunsen burner, bomb calorimeter, TGA, confocal Raman-AFM, SEM, EDX tests and also characterization of EG. This was attributed to the exfoliation of graphite layers with the aid of generation of EFB fiber char in the case of a thermal condition, which could shield the heat and mass transfer into the bulk of material. The requirements of aircraft interior for vertical Bunsen burner were met by EG filled composites at each concentration used. For EG coating composites, the formulation with 5 wt% EG coating was found to meet the requirements of the Bunsen burner test. On the other hand, increasing incorporation of EG fillers reduced the mechanical properties relative to the control due to low level of interfacial adhesion between the EG and other constituents. However, reinforcing EFB fiber was observed to improve the mechanical properties relative to the neat epoxy, which could compensate the negative effect of EG fillers on mechanical

behaviors. The alkali treatment of EFB fibers improved the mechanical properties of EG filled composite further, even to higher values than the control. The control composite and all formulations filled with EG were in the acceptable range of mechanical performances for the aircraft application.

These EG filled composite systems were shown to provide cost-effective and feasible strategy to establish a thermally resistant composite material, which can be produced through an industrially simple processing technique as well as inexpensive expandable graphite and EFB fiber; however, the future work shall be to enhance the mechanical performances of EG filled epoxy composites.

Similar to CATH5APP10 and CAPP10ZB5, CEG7 was observed to meet the 12 s vertical Bunsen burner requirements with 0 s flame time, no drip flame time and negligible burn length. GH of combustion was measured less than 28 MJ/kg for all three formulations. Minimum lab scale tensile and flexural performances were found to be passed by the aforementioned composites.

Chapter 6

6. Nomex honeycomb panels with EFB composite skins

6.1 Introduction

Currently, carbon or glass fiber phenolic Nomex honeycomb panels have been utilized to produce the parts of aircraft interiors. Nomex core is used in aerospace applications due to its formability, strength to weight ratio, various cell sizes, fire resistance, low dielectric performances and good insulating behaviors. Sidewall panels, ceilings, partitions and over stowage bins are of instances of the applications of these sandwich panels in airplane [176, 178, 291, 292].

To improve the fuel consumption by reducing the weight and usage of environmental friendly fibers, synthetic fibers (carbon and glass fibers) can potentially be replaced with NFs. A decrease in mass of one structural interior component could result in weight savings in other parts or subsystems of aircraft, or lead to enhancing payload capacity and increasing fuel economy. However, safety factors are required to be considered to ensure that mechanical and flammability performances of components with the newly developed materials are capable of meeting the requirements. Aircraft interior components having honeycomb composite panels such as lower and upper panels, overhead stowage, partitions, galley, lavatories, stowage bins and ceiling are required to resist loads applied to them prior to, in-flight and after flight. The loads can be dynamic during turbulence and landing so that structural integrity and safety of commercial aircrafts need to be guaranteed. The materials used for the construction of a honeycomb panels including the composite skins and Nomex honeycomb are required to meet the FAR requirements as well, which is in terms of flammability and smoke performances. The ignitibility of natural fibre polymeric composites hinder their rapid development in aircraft components.

Composites with honeycomb structures present remarkable out-of-plane compression, energy absorption and shear performances for low weight, which is why they have been used for aircraft cabin parts, as some of these compartments are shown in Figure 6-1. Once Nomex honeycomb is collapsed, the support of Nomex to the composite sheets reduces substantially. This signifies the importance of honeycomb core's resistance to collapse under flatwise compressive loadings. These honeycomb composite structures consist of a very lightweight core separating two high strength and thin face sheets (Figure 6-2). The function of core is to increase the second moment of inertia and as a result, bending stiffness based on I-beam principle [293], as depicted in Figure 6-3. The core carries transverse shear and normal loads, and the face sheets mainly resist the compressive and tensile loads owing to bending forces. The role of skin/core adhesive is to rigidly join the parts of sandwich panel in order to act as one component to bear both high bending and torsional strength.

Every interior component used in aircraft cabin must meet the safety and mechanical requirements of FAA, other aircraft agencies or manufacturers. With regards to the safety, both face sheet and honeycomb core have to meet the flammability and thermal requirements. Nomex honeycomb used in aircraft interiors is made of phenolic resin bonded aramid paper and must meet the FAR 25.583. Phenolic resin is inherently flame resistant which, in a flame scenario, develops low levels of combustion produces and smoke in comparison to other types of resins such as polyester and epoxy. The composite skins are required to meet all FAR-part 25 requirements as well.

In spite of the great attention to honeycomb composite panels, no publications present information on mechanical and flammability properties of honeycomb panels with composite skins produced by reinforced natural fibers embedded in flame retardant or expandable graphite. To the best of author's knowledge, compressive, flexural and shear performances as well as vertical Bunsen

burner (12 s and 60 s) data for honeycomb panels containing Nomex honeycomb and EFB fiber (FR or EG filled) epoxy skins have not been reported so far.

To reliably anticipate the component safety in terms of structural stability and flame resistivity, understanding the performance of composite sandwich panels through compressive, flexural and shear tests and burner experiment has become essential particularly in aircraft interior parts as the role of composite skins and the Nomex honeycomb is to satisfy the structural and ignitibility safety. The compressive, flexural, shear, vertical Bunsen burner (12 s and 60s) and SEM tests were carried out to study the flammability and mechanical behaviors of composite sandwich structures. The modes of failure, structural response of the honeycomb core and panels, adhesion between the honeycomb core, adhesive and composite skins as well as their ignitibility were investigated.

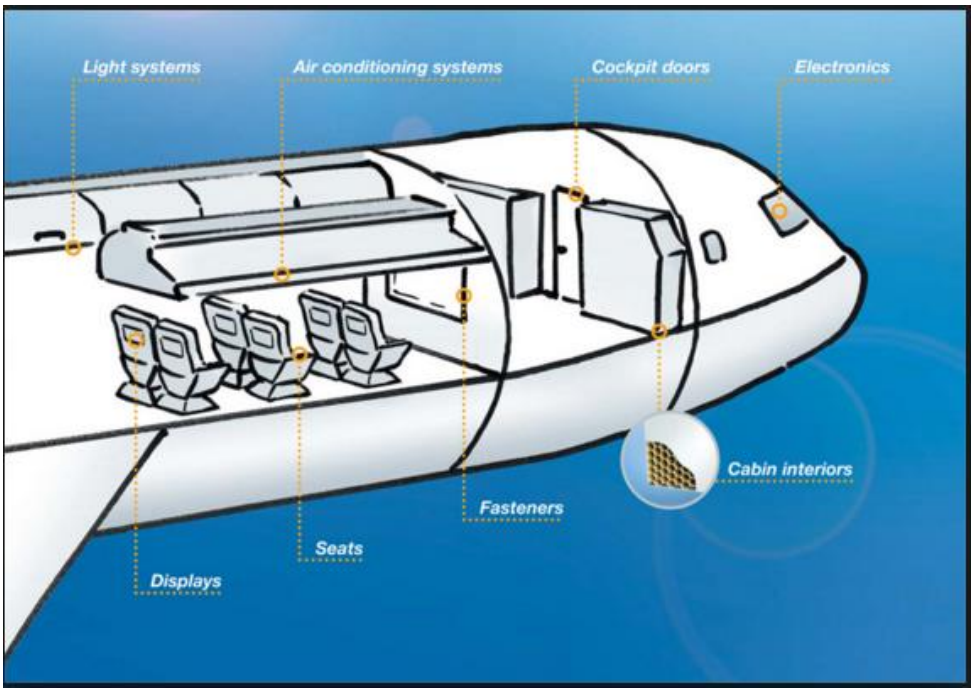


Figure 6-1 A few cabin parts made of honeycomb composites are exhibited (Source: Aerospace DELO).

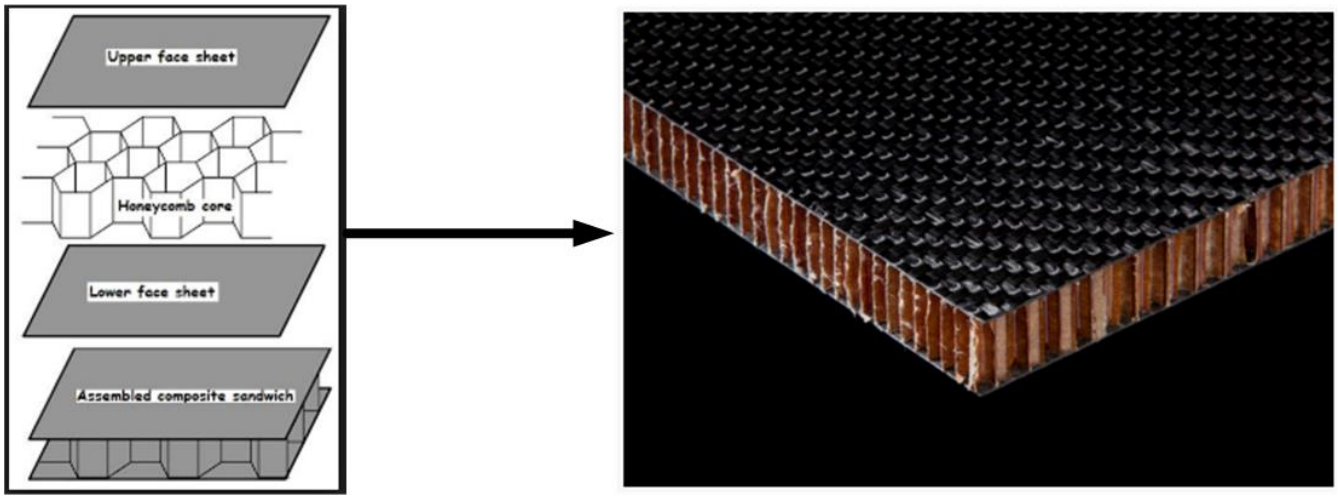


Figure 6-2 The core and face sheets of composite sandwich fabricated a sandwich panel (sources: NauticEXPO and Hexaflex).

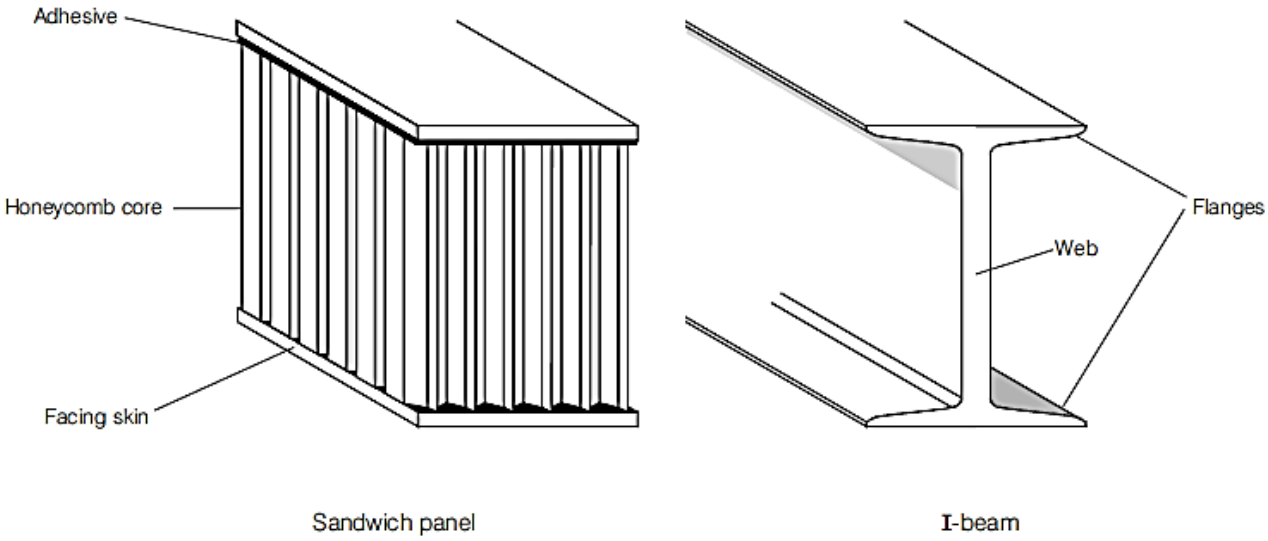


Figure 6-3 Principle of bending strength and second moment of inertia for honeycomb core composites (Source: STRESS EBOOK LLC.).

6.2 Fabrication of honeycomb panels

6.2.1 Preparation of face sheets of honeycomb panel

Composite skin sheets for the panels were fabricated using compression molding. The optimum percentage of APP and ATH was selected from the previous experiment to prepare the skins for one of the panels and the other composite honeycomb panel was produced using 7 wt% of EG particles in the skins. The APP and ATH possessed 10 wt% and 5 wt% in composite sheets, respectively, which was first mixed with epoxy for 2 minutes and then placed in an ultra-sonication with amplitude of 50% and the frequency of 20 kHz for the period of 15 minutes to achieve a homogenous dispersion in the epoxy. Subsequently, the pulverized alkali treated EFB fibers of 20 wt% with the length of 1-3 mm, which were oven dried for 24 hours at 70 °C prior to the composite fabrication, were added into the mixture of epoxy and flame retardants to soak for 5 minutes while the mixture was shaking in a shaker incubator with the speed of 150 rpm at ambient temperature. Hardener was then added at appropriate ratio and mixed for 2 minutes. The mixture was degassed for 15 minutes in a catch pot connected to a vacuum pump. Finally, the mixture of slightly higher amount of the mold volume was poured into a matching mold with the thickness of 2 mm and were cured for 24 hours under the compression loading of 17 kPa at ambient temperature.

Similar fabrication technique was employed for the fabrication of EG filled composite skins with one additional further mixing procedure prior to ultra-sonication of the mixture on a mechanical stirrer with the constant step rate of 1000 rpm for 30 mins. The formulation prepared with their respective wt% from compression molding technique is shown in Table 6-1.

Table 6-1 Formulations used for the fabrication of face sheets with their constituents by weight percentage (wt%).

Formulation of face sheets for the panels	Epoxy	fiber	APP	ATH	EG
Face sheets for sandwiched structure 1	65	20	10	5	-
Face sheets for sandwiched structure 2	73	20	-	-	7

6.2.2 Preparation of the sandwiched panels

The composite sandwich panel was prepared by bonding the two composite face sheets to honeycomb core using the brushing technique. As the thickness of aerospace grade core was 2 mm, the dipping method could easily fill up the cells of Nomex core with adhesive. The aerospace grade Nomex honeycomb had a density and cell size of 29 kg/m^3 and 3.2 mm, respectively. Firstly, a layer of the same epoxy grade used for the fabrication of composite skins with the weight of approximately 104.16 µg/mm^2 was brushed on one surface of the honeycomb core, and the core was carefully placed with the "L" direction (ribbon direction) along the primary direction on top of a composite skin to bond together using a top weight with the pressure of 4 kPa, which was largely smaller than the ultimate compressive stress of honeycomb core. The structure was left to cure for 24 hours at ambient temperature (Figure 6-4) prior to the bonding of the second face sheet on the other side of honeycomb core. Subsequently, the other side of Nomex honeycomb core was brushed with about 104.16 µg/mm^2 of epoxy and positioned on another skin. The pressure of 4 kPa was applied to the honeycomb structure until it cured fully after 24 h. Two sandwich panels were fabricated using two different types of composite skins, namely skin 1 and skin 2. Each sandwich panel possessed 6 mm thickness consisting of two composite skins with each 2 mm

thickness as well as a Nomex honeycomb core with the thickness of 2 mm, as shown in Figure 6-5.

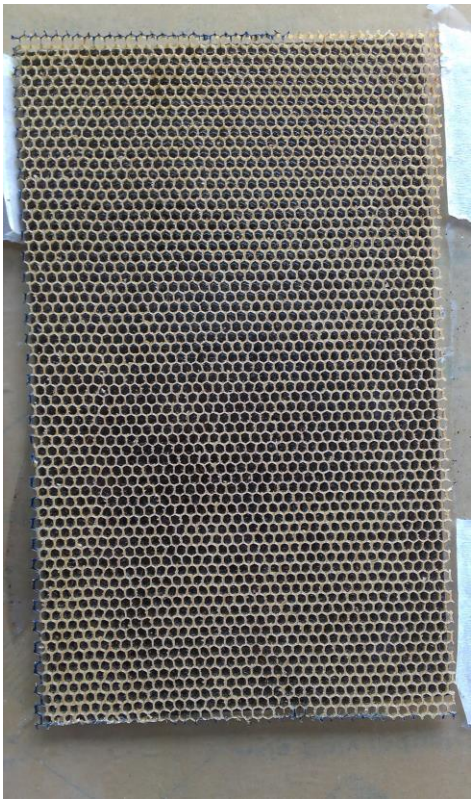


Figure 6-4 Bonding of honeycomb to one of the skins which is at the bottom of core.



Figure 6-5 The final product which is a honeycomb core panel with 6 mm thickness.

6.3 Characterizations of Nomex honeycomb sandwich structure

To evaluate the flexural response of composite sandwich panel and to provide the compressive and shear performances of the core, the compressive test for the Nomex core and sandwich structure, and three-point bending test for the composite panel were conducted.

6.3.1 Compressive properties

In order to design the sandwich panels, understanding of their compressive behaviors is crucial. Flat-wise stabilized compressive tests were performed to study the out-of-plane crushing performance of honeycomb sandwiched panels. The test set-up of honeycomb sandwiched structure subjected to the stabilized compressive loading is shown in Figure 6-6. Five honeycomb core coupons measuring 50 mm × 50 mm × 2 mm were bonded between two FR filled composite skins and another five core coupons of the same dimension were bonded between two EG filled composite skins. The specimen geometry and detailed deformation process are illustrated in Figure 6-7 and Figure 6-8, respectively. The specimens collapsed, crushed and then hardened during the deformation.

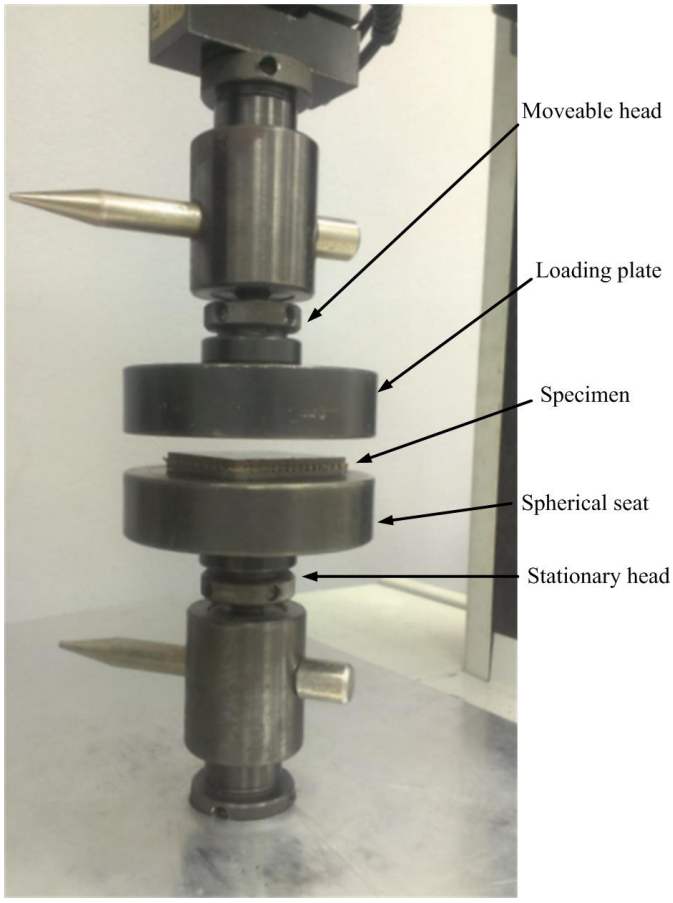


Figure 6-6 Test set-up of a honeycomb sandwich structure subjected to the stabilized compression.

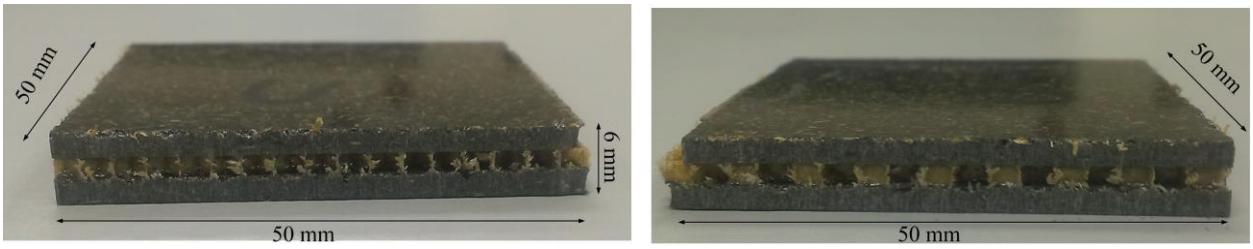


Figure 6-7 Specimen geometry of flat-wise stabilized compressive test at different views.

Figure 6-9 shows the elastic-plastic relationship between stabilized compressive stress and strain of sandwich structures, which includes three deformation stages. The first stage is the elastic region up to the stabilized compressive stress in the range of 0.88- 1.02 MPa for all the panels. The second stage consists of the collapse phase followed by crushing phase at almost constant crush stress

(plateau strength). The last one includes the densification region with the strain densification in the range of 71.6%-73.6% for all the panels, where the cells of honeycomb structure are completely compressed leading to a steep stress upsurge. As all 10 specimens of two different types of panels exhibited similar results, the curve of two specimens from each panel is illustrated in Figure 6-9.

The tests determined a range of values of stabilized compressive stress, crush strength and densification strain of the honeycomb panels, as shown in Table 6-2. As the same technique was used to bond the Nomex honeycomb core to the EFB fibre reinforced composite skins, and composite skins are rigid under compression, compressive results are the effect of compression of the core which are the same in terms of strength and modulus for both types of panels. The thickness of composite skins and Nomex honeycomb core do not affect the compressive properties. However, for the same cell size and thickness of honeycomb with different density, the compressive strength and modulus are higher for the core with higher density. For the same density and thickness, varying cell size does not significantly change the compressive strength and modulus [30, 294]. As highlighted previously, an aerospace grade honeycomb core possessing the specific density and cell size was used in this work.

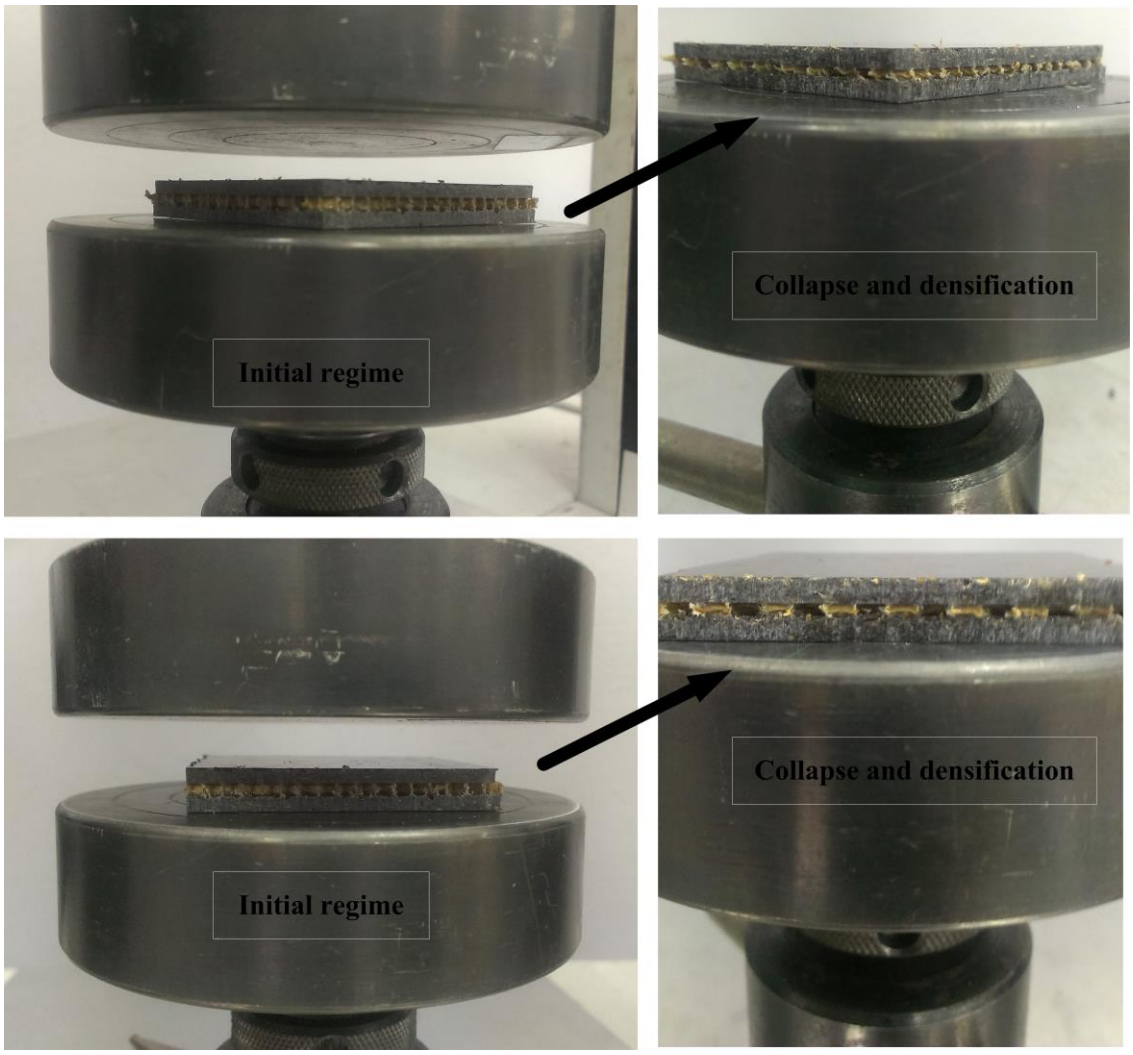


Figure 6-8 Deformation stages: Honeycomb panels prior to compressive test on the left images (initial regime) and honeycomb panels crushed after applying the load on the right side (crushing regime and densification).

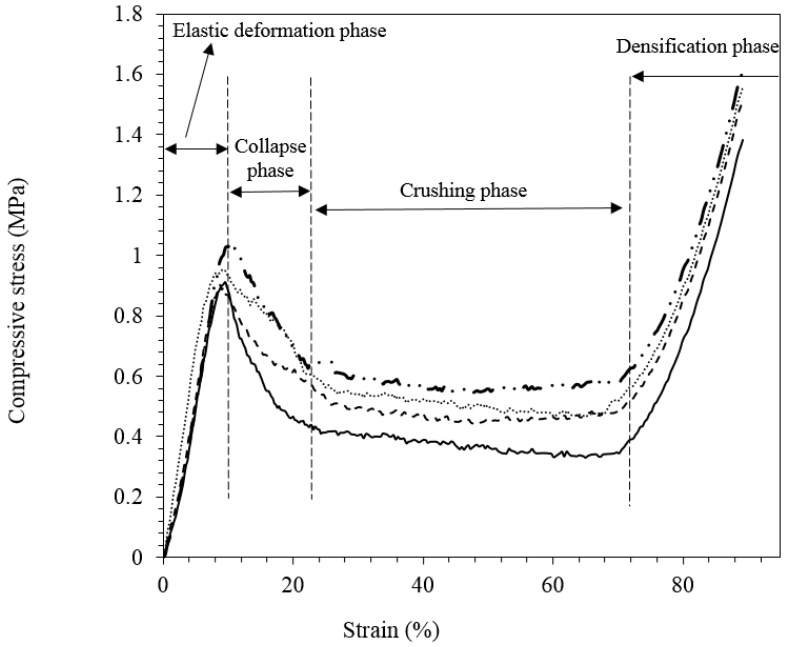


Figure 6-9 Flat-wise stabilized compressive stress-strain curves of 4 selected specimens of sandwich composite panels (all specimens from different panels show similar trends).

Table 6-2 Out-of-plane compression performances of honeycomb panels.

Compression properties	Values (range)
Stabilized compressive strength (MPa)	0.88- 1.02
Initial crush strength (MPa)	0.42- 0.60
Densification strain (%)	71.68- 73.68

6.3.2 Flexural properties of honeycomb core sandwich panels

Flexural performance of the sandwich panels with different skins was evaluated using three-point bending test mode. Figure 6-10 and Figure 6-11 show the bending stress-displacement behavior of Nomex honeycomb core panels with EG filled composite skins and FR filled composite skins,

respectively. Flexural behaviors of sandwich configuration were investigated in accordance to ASTM C393M [201]. The formula for facing flexural stress was found as:

$$\sigma = \frac{P_{max}\, S}{2\, t\, (d + c) b} \quad (1)$$

Where σ is the facing flexural stress, t is the thickness of composite skin (2 mm), S is span length (150 mm), P_{max} is the maximum applied load prior to failure, d is the sandwich thickness (6 mm), b is sandwich width (75 mm) and c is core thickness (2 mm).

The five sandwich panel specimens with EG composite skins broke at an ultimate fractured stress in the range from 97.45 MPa to 107.23 MPa (Figure 6-10-a). For honeycomb core panels with FR filled composite skins, the values of ultimate bending stress was in 90.14-99.50 MPa range (Figure 6-11-a). The lower range of maximum flexural strength in panels with FR filled skins can be attributed to higher amount of particles that are present in their composite skins than panels with EG skins. Composite containing FR had 15 % concentration of particles whereas in the other composite 7% of EG was introduced. These particles interfere the continuity of polymer matrix under flexure and reduce the bending properties of composites.

The failure of panels started with the initiation of crack at the bottom skin, and honeycomb core crushed until the complete fracture of this composite skin. Furthermore, while the upper skin bended parallel to the bottom skin, the upper skin fractured shortly after the failure of bottom skin. As shown in Figure 6-12 and Figure 6-13, the skins failure occurred in the middle of the specimen, and the top and bottom skins fractured with a small offset. Nomex honeycomb core crushed under the flexure as well.

It is worth highlighting that increasing the thickness of honeycomb core leads to the enhanced flexural strength [30].

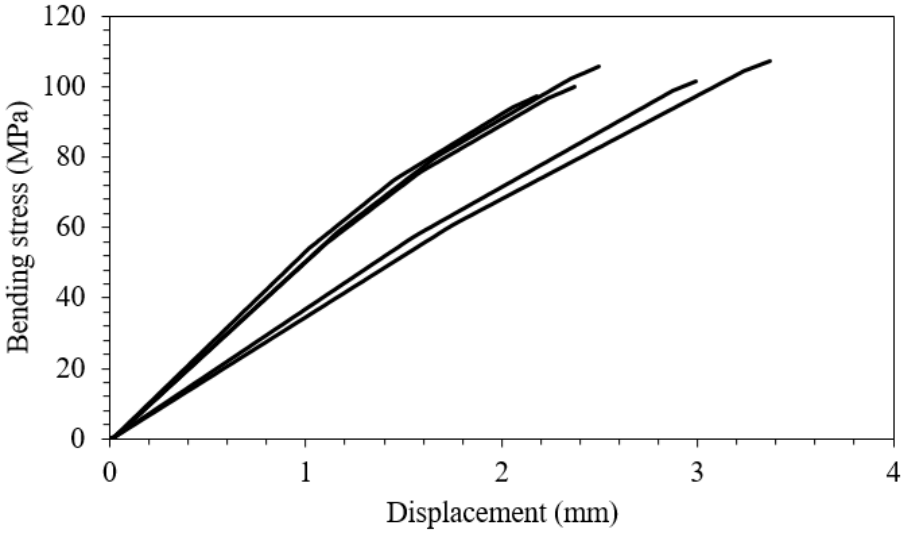


Figure 6-10 Bending stress-displacement curves of all panel specimens with EG filled skins.

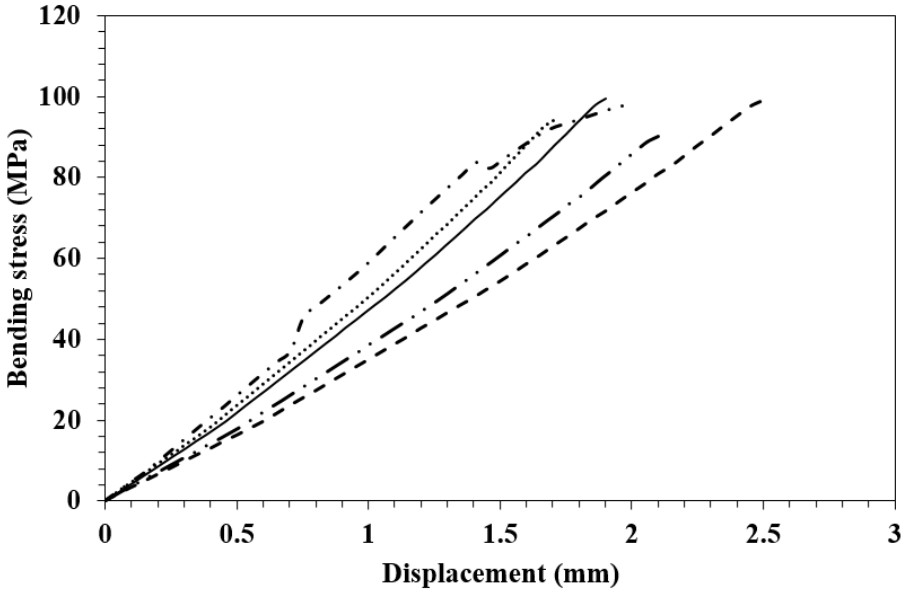


Figure 6-11 Bending stress-displacement curves of all panel specimens with FR filled skins.

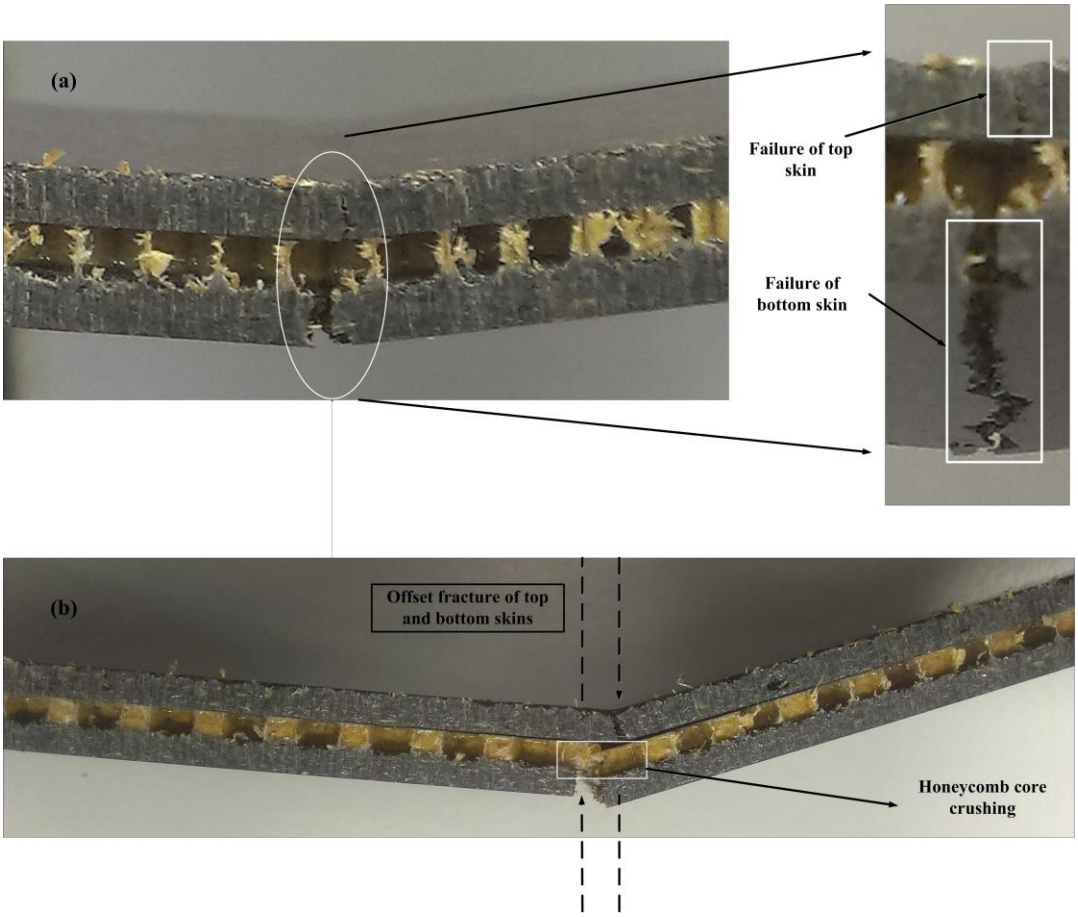


Figure 6-12 Failure mode of honeycomb sandwiched panel with EG filled composite skin.

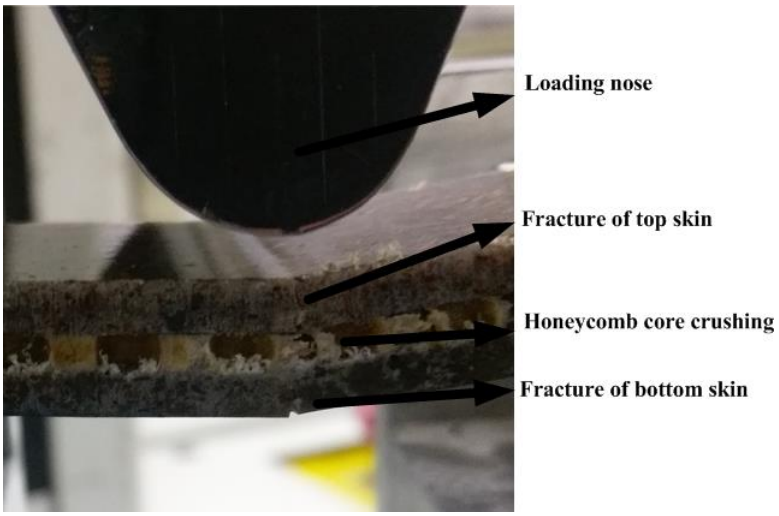


Figure 6-13 Failure mode of honeycomb core panel with FR filled composite skin.

6.3.3 Core shear ultimate stress from bending test

Nomex honeycomb shear performances were studied by bending experiments according to ASTM C393M. The core shear ultimate stress (τ) was calculated as follows:

$$\tau = \frac{P_{max}}{b\,(d + c)} \tag{2}$$

For sandwich configuration with EG filled facings, the core shear ultimate stress was found 2.73 MPa where P_{max}, b, d and c were 1638.08 N, 75 mm, 6 mm and 2 mm, respectively. τ was calculated 2.56 MPa for honeycomb core structure with FR loaded composite skins where P_{max}, b, d and c were 1538.30 N, 75 mm, 6 mm and 2 mm, respectively. The higher τ for the panel with EG skin is due to its greater P_{max}.

It was shown that the shear behavior of a honeycomb core is highly dependent upon the facing materials, facing thickness, core thickness and loading conditions, therefore, the shear values may vary remarkably from one series of test to another [30]. It is necessary to stress that honeycomb shear values attained from bending tests are greater than the values attained from plate shear tests [30]. E.g. skin thickness alone leads to large variations since the skins are able to take on shear forces besides what the honeycomb carries. Additionally, the skins are capable of carrying further shear forces after the core has yielded.

6.3.4 Bending stiffness

The sandwiched panel bending stiffness (D) was calculated by the following formula in accordance with ASTM D7250M [295], where E is the modulus of elasticity of the composite skins.

$$D = \frac{E\,(d^3 - c^3)\,b}{12} \tag{3}$$

For the panel with EG filled composite skins, D was calculated 4.36 Nm^2 where E was measured 3.36 GPa from the tensile test. In the absence of Nomex honeycomb core, the bending stiffness measured was 1.34 Nm^2. This indicates that bonding the Nomex honeycomb core to the EG-filled facings increased the bending stiffness by 3.25 times.

For the panel with the composite skins made of the hybrid of APP and ATH particles (composite skins had the elastic modulus of 3.53 GPa, as measured previously), D was calculated as 4.58 Nm^2. Structure without honeycomb core had the bending stiffness of 1.41 Nm^2. Thus, D enhanced by approximately 3.25 times in the case of the Nomex honeycomb core bonded to the composite skins as demonstrated in the current study.

Consequently, it was observed that utilization of the Nomex honeycomb core stiffens the sandwich structure with a negligible increase in its weight.

In order to compare the required weight of a composite beam to the sandwich panel with the same composite (beam) skins for the same values of bending stiffness, the bending stiffness of composite beams was calculated as follows:

$$D' = \frac{E\ b'\ t'^3}{12} \tag{4}$$

Where D′ is the bending stiffness of composite beam, E is the elastic modulus of composite beam, b′ is the width of composite beam and t′ is the thickness of composite beam. The calculations were made in such a way to achieve the same value of honeycomb panel bending stiffness for composite beams.

For an EG loaded composite beam having D′ of 4.36 Nm^2 (the same value of bending stiffness as panel containing EG filled composite skins), E of 3.36 GPa and b′ of 75 mm, the thickness of composite beam (t′) is required to be approximately 6 mm. This shows that by utilizing the panel containing two EG filled composite skins that each having thickness of 2 mm, an approximate weight reduction of 33.33 % can be achieved (the weight of honeycomb core and adhesive is negligible).

In regards to a composite beam loaded with FR additives, on the condition that a bending stiffness (D′) of 4.58 Nm^2 (the same value as bending stiffness of a panel with FR loaded composite skins) is required to achieve, having E and the width of FR loaded composite beam, 3.53 GPa and 75 mm, respectively, the required thickness is about 6 mm as well. Similar to previous type of panel, mentioned in previous paragraph, for the panel containing FR filled composite skins, the weight reduction was calculated to be around 33.33 %. This highlights the importance of honeycomb core in improvement of flexural stiffness without using a beam with higher weight. Greater thickness of honeycomb core enhances the stiffness of panels [30, 294].

6.3.5 Plate core shear properties

Plate shear tests were conducted in accordance with the ASTM standard C273 [203] and the experiments were performed in L and W directions for panels containing EG loaded composite skins (2 specimens) and FR filled composites skins (2 specimens). In this test, the secondary shear stresses are negligible [203, 296]. The dimensions of specimens were 150 mm × 50 mm and the loading rate was 0.5 mm/min. Both sides of specimens were bonded to a metal plate with the aid of ULTIMEG 2020 two parts epoxy resin which were cured in an oven at 70 °C. The set-up was performed in such a way that the line of action (or plane in which the force acts) of the direct

tension load passes along the diagonally opposite side of honeycomb core [203], as illustrated in Figure 6-14 (a). The shear stress can be calculated as follows:

$$\tau = \frac{P}{Lb} \tag{5}$$

Where τ is honeycomb shear strength, b is width of honeycomb (50 mm), L is the length of core (150 mm) and P is the load on specimen. The shear failure of honeycomb cells is exhibited in Figure 6-14 (b).

The results (Figure 6-15 and Figure 6-16.) show a linear elastic deformation, followed by a remarkable force reduction down to a strength plateau due to shear buckling. The strength plateau continued until the cell walls tore and then led to complete failure.

In regards to longitudinal transverse shear results, the strain-stress values reduced more obvious than W direction owing to buckling. Besides, the developing plateau finished at considerably lesser strain values than W direction results.

It is worth highlighting that the thickness of honeycomb core does not affect the plate core shear properties. For the same density of core, varying cell size does not considerably affect the plate core shear strength and modulus. However, the core shear strength and modulus improve with increased Nomex core density [30, 294].

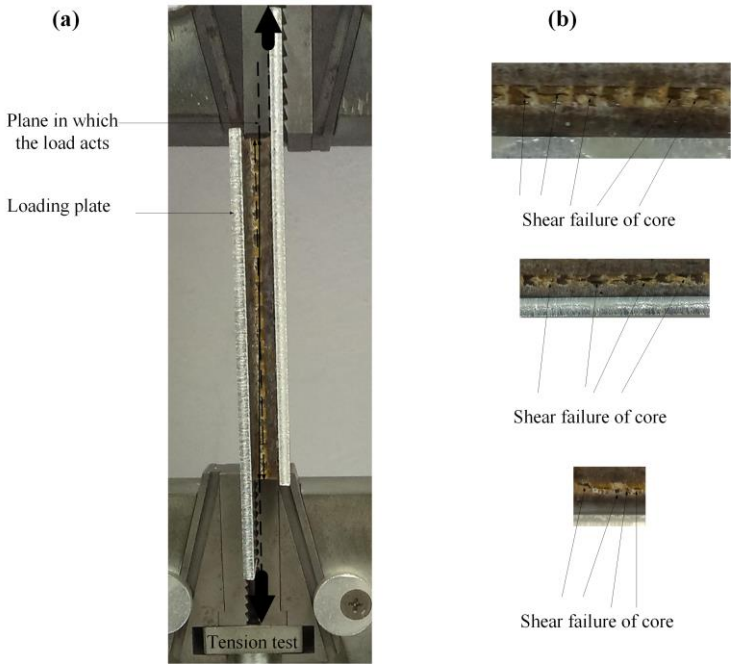


Figure 6-14 (a) Plate shear test conducted by employing force line of action and (b) shear failure of Nomex core at different areas.

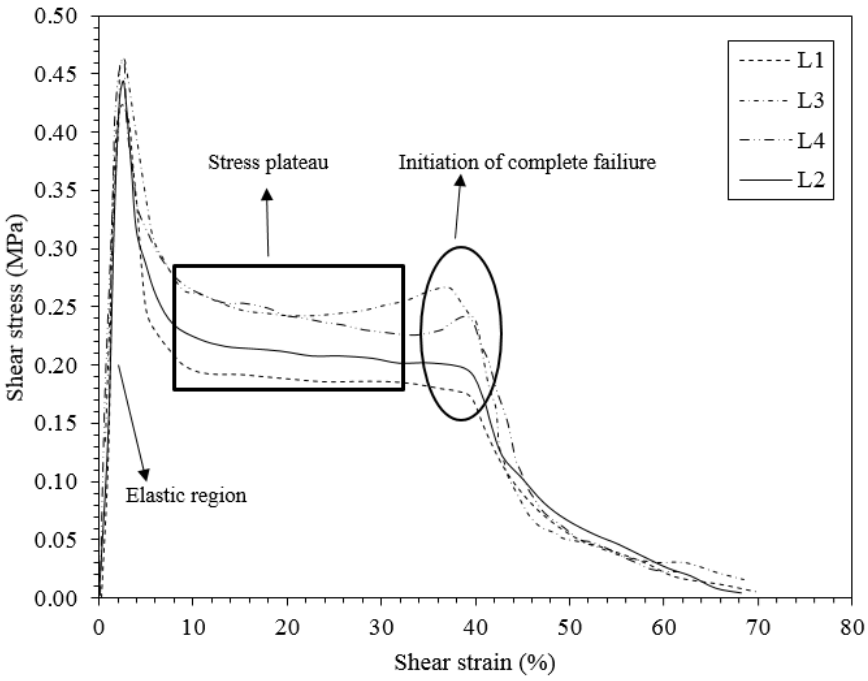


Figure 6-15 Shear stress-strain response where core was tensioned in its longitudinal direction.

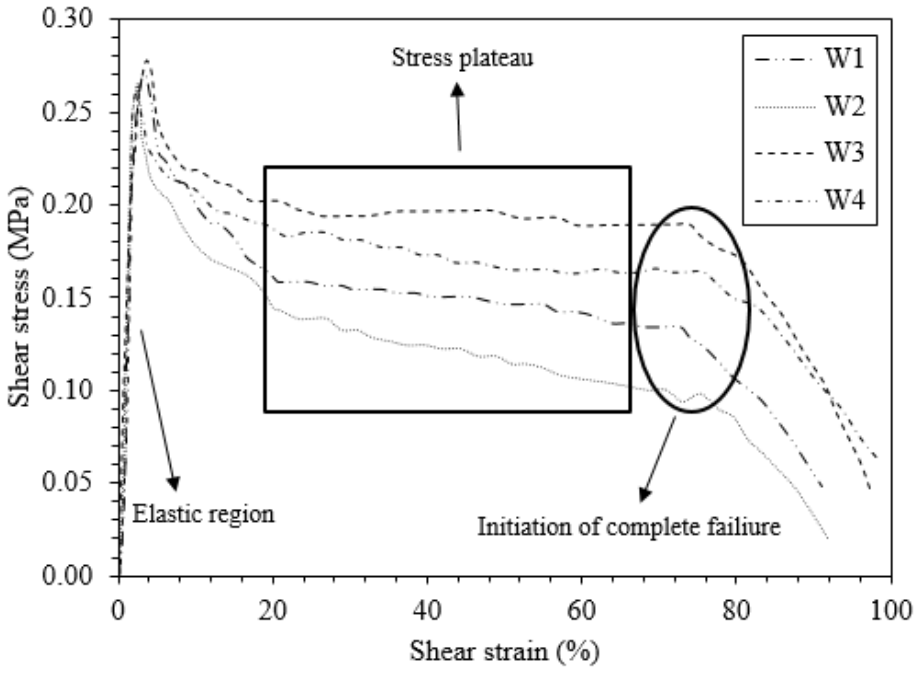


Figure 6-16 Shear stress-strain response where core was tensioned in its W direction.

6.3.6 Flammability of Nomex honeycomb panels with natural fibre based composite skins

Vertical Bunsen burner test V12 was conducted in accordance with FAR 25.853 (b) aviation standard to investigate the flammability of two types of panels with FR composite skins and EG composite skins as well as the Nomex honeycomb core. A Bunsen burner flame burning methane gas (with min 99% purity) was applied to the specimen holding vertically for 12 seconds. The rectangular specimens had the length and width of 305 and 75 mm, respectively. The detailed set-up and flame height are shown in Figure 6-17. The exhaust hood installed in the chamber helps to clear the smoke after each experiment.

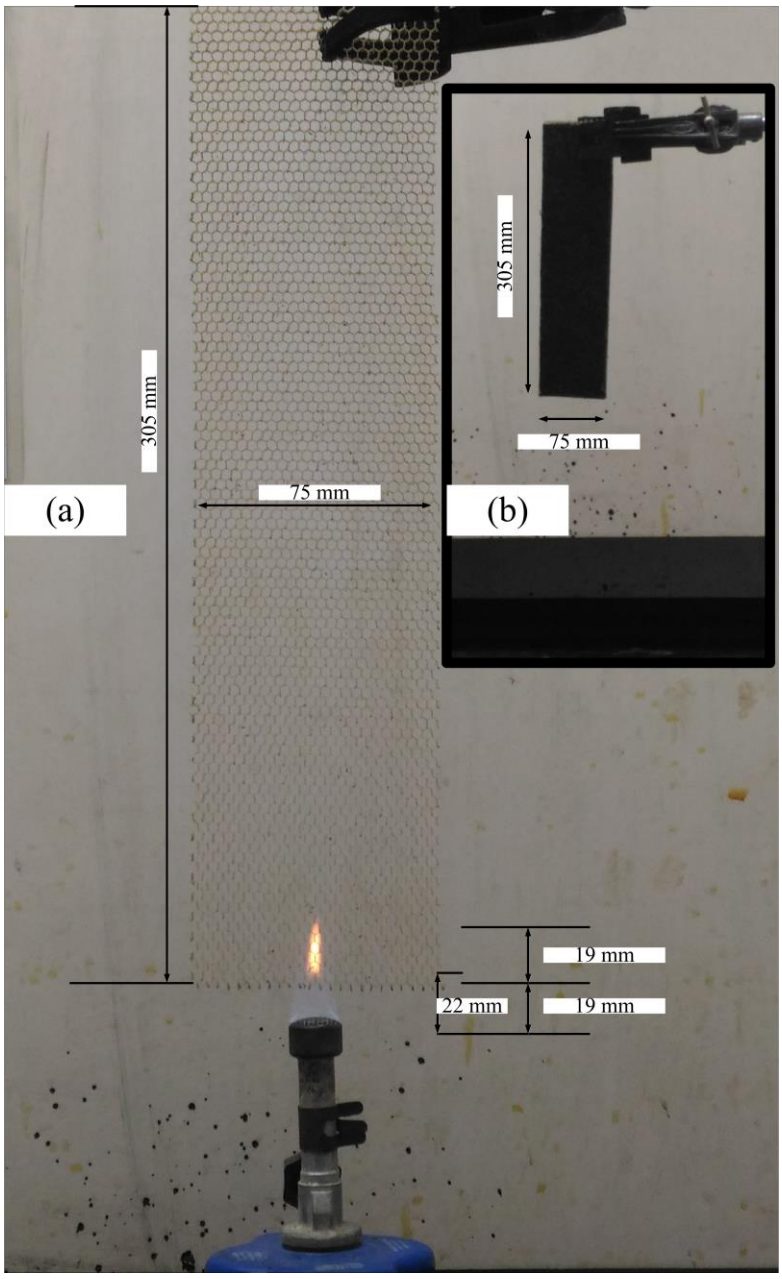


Figure 6-17 Detailed set-up of vertical burner test. Specimens located in a lab cabinet which has an exhaust hood: (a) Honeycomb core and (b) panel.

The results of vertical Bunsen burner tests are shown in Table 6-3. According to FAR 25.853 standard, all the structures were observed to meet the requirements of flammability in terms of flame time, drip flame time and burnt length. This is due to the presence of phenolic resin in Nomex

core as well as FRs and EG particles in the composite skins. 0 s flame time and no drip time were found for both types of panels, and their difference in the burn length and mass loss was negligible. Thicker Nomex honeycomb core and composite skins are capable of producing higher flame resistivity due to the presence of more phenolic resin and FRs in the protective char layer. However, each aircraft manufacturer has its own design criteria, e.g. thickness, width and length, for each respective panel.

Table 6-3 Vertical Bunsen burner results of different structures.

Structures	Flame time (s)	Drip flame time (s)	Burn length (mm)	Mass loss (%)	Requirement of the FAR test
Nomex honeycomb core	0	0 (No Drip)	50	3.03	Passed
Panel with FR skins	0	0 (No Drip)	~0	0.05	Passed
Panel with EG skins	0	0 (No Drip)	1.3	0.07	Passed

The vertical and front sections of specimens after burning are illustrated in Figure 6-18. The lower part of Nomex honeycomb specimen exposed to flame shrunk, discolored, stained, sooted and warped (Figure 6-18-(a) and (e)). Phenolic resin that is present in the honeycomb produces layers of porous carbon to slow down the process of combustion of the material. The char formed inhibits the flame spread, which is why no flame time and drip flame time were reported for the Nomex honeycomb specimen. For panel with EG filled composite skins, the EG particles exfoliated in the event of fire and hindered further ignition. They formed worm like char to protect the underlying layers of substrate (Figure 6-18-(b) and (e)). The protection for panel with FR filled composite occurred with the intumescent char. The char swollen shielded the panel's specimen from flame, as shown in Figure 6-18-(c) and (f).

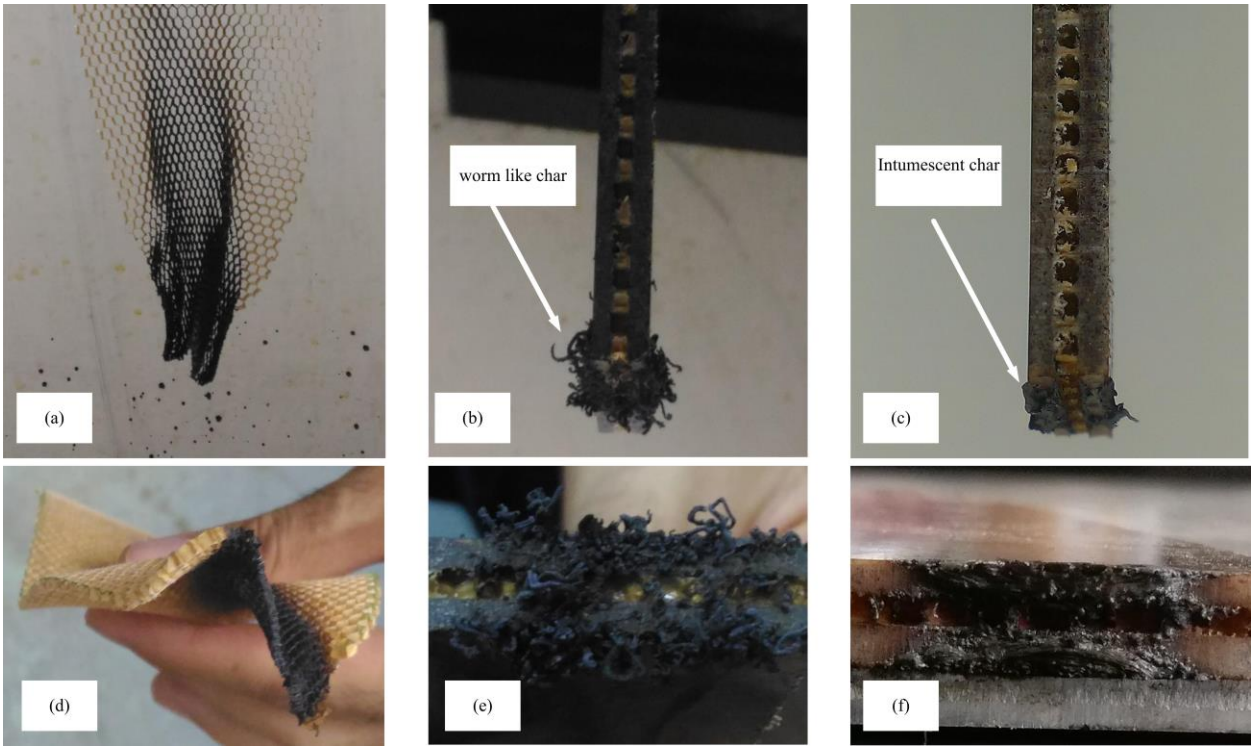


Figure 6-18 Vertical section of the specimens: (a) Nomex honeycomb core, (b) panel with EG filled composite skins and (c) panel with FR filled composite skins. Front section of specimens: (d) Nomex honeycomb core, (e) panel with EG filled composite skins and (f) panel with FR filled composite skins.

Figure 6-19-(a) illustrates the Nomex honeycomb burning and producing smoke when the flame was applied to the specimen. For all the honeycomb specimens, smoke produced and released during the first 7 s of applying the Bunsen burner flame. However, both types of panels released the smoke right after removing the burner from underneath the panels' specimens (Figure 6-19-(b) and (c)). The smoke lasted to release for about 5~6 s after withdrawing the Bunsen burner for both types of panels.

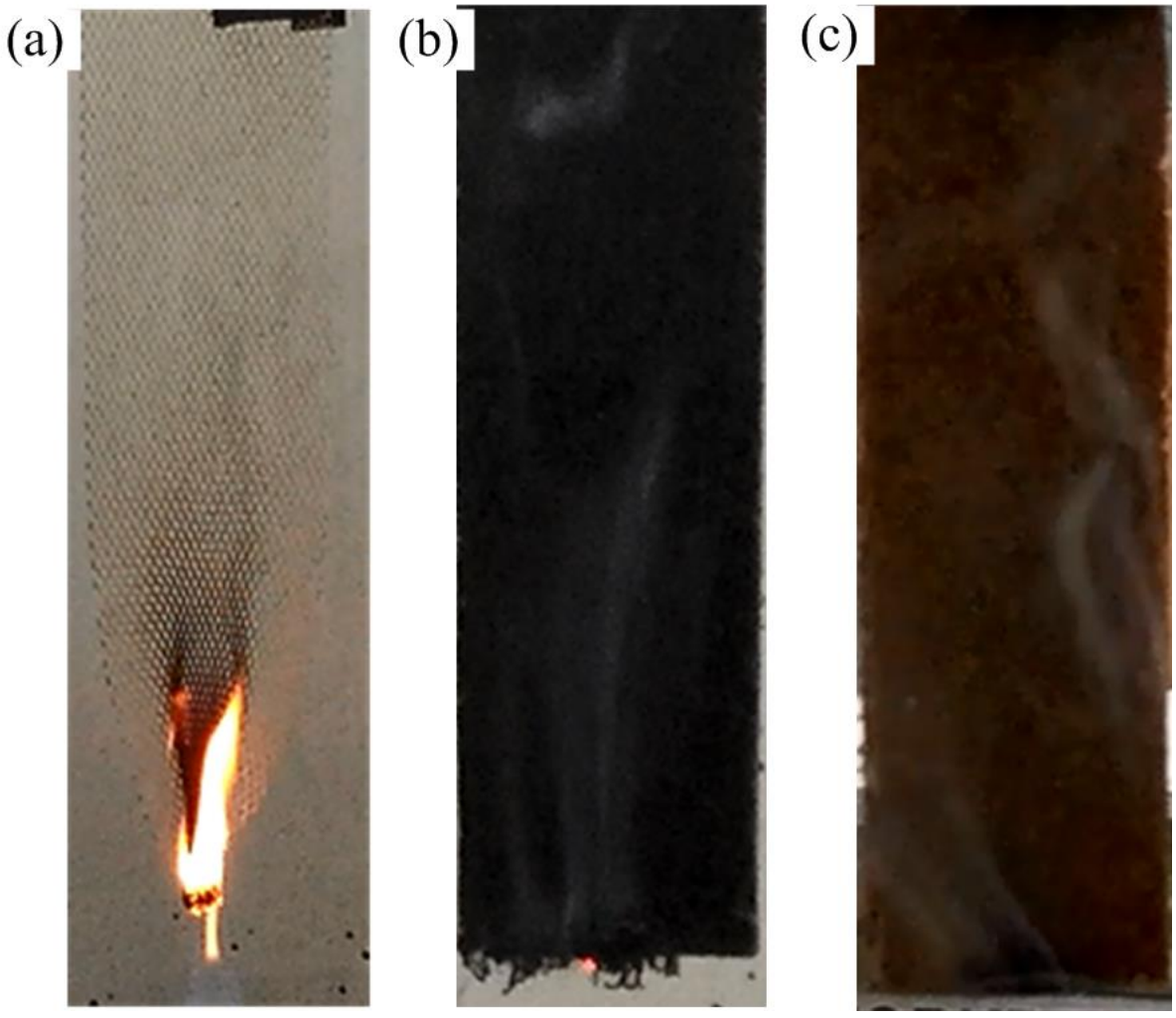


Figure 6-19 Smoke produced: (a) during the burning of Nomex honeycomb in the presence of Bunsen burner; and right after withdrawing the Bunsen burner from underneath (b) the EG panel's specimen and (c) FR panel's specimen.

To specifically utilize the composite skins and panels made of natural fibre composites for partitions, ceilings (interior ceiling panels), sidewalls (interior wall panels), structural flooring, large cabinet walls, galley structure and materials employed in the structure of stowage panels (except compartments used to stow small objects e.g. maps and magazines, and not including under-seat stowage compartments), the vertical Bunsen burner test with the flame time of 60 s in accordance with FAR 25.853 (a) must be used. Therefore, Nomex honeycomb core, EG7,

ATH5APP10 and APP10ZB5 composites, which were of the formulations that met 12s- FAR 25.853 (b) specifications (as discussed in chapter 4, 5 and 6), were tested. The composites were fabricated using the compression molding technique to be consistent in the analysis of this test. APP10ZB5 composite was produced similar to the fabrication of ATH5APP10 (FR) composite skin reinforced with 20 wt% treated EFB fibre (explained in the beginning of the current chapter). The EG7 formulation loaded with 7% EG was the same as EG filled composite skin. Three specimens from each formulation measuring 305 mm (length) × 75 mm (weight) underwent 60 s Bunsen burner flame and the results are tabulated in Table 6-4.

In accordance with FAR 25.853 (a), the average flame time, drip flame time and burn length are required to be below 15s, 5s and 203mm. Therefore, all the composites and Nomex honeycomb core successfully met the specifications of vertical Bunsen burner test. Formulations, treatments, and optimizations of natural fibre composites can further be conducted in collaboration with an aircraft manufacturer until the fulfillment of all the requirements such as heat release (from OSU calorimeter), smoke (from NBS chamber) and required mechanical performances. Amongst ATH5APP10, APP10ZB5 and EG7, the latter showed a few seconds of flame time, attributed to the lesser quantity of FR, i.e. 7 wt% EG particles.

Table 6-4 Vertical Bunsen burner results (60s test) of Nomex core and different optimum composites.

Structures	Flame time (s)	Drip flame time (s)	Burn length (mm)	Mass loss (%)	Requirement of the FAR test
Nomex honeycomb core	0	0 (No Drip)	65	3.10	Passed
ATH5APP10	0	0 (No Drip)	15~20	0.11	Passed
APP10ZB5	0	0 (No Drip)	25~30	0.29	Passed
CEG7	7	0 (No Drip)	20~25	0.31	Passed

The burned composite specimens after 60 s vertical Bunsen burner test are displayed in Figure 6-20. The composites containing FRs promoted the intumescent char that inhibited the progression

of heat and mass transfer into the bulk of substrate (Figure 6-20 (a) and (c)). For EG loaded formulation, the protection occurred by producing worm like expanded graphite, thereby insulating the fire from the underlying materials, as shown in Figure 6-20 (b).

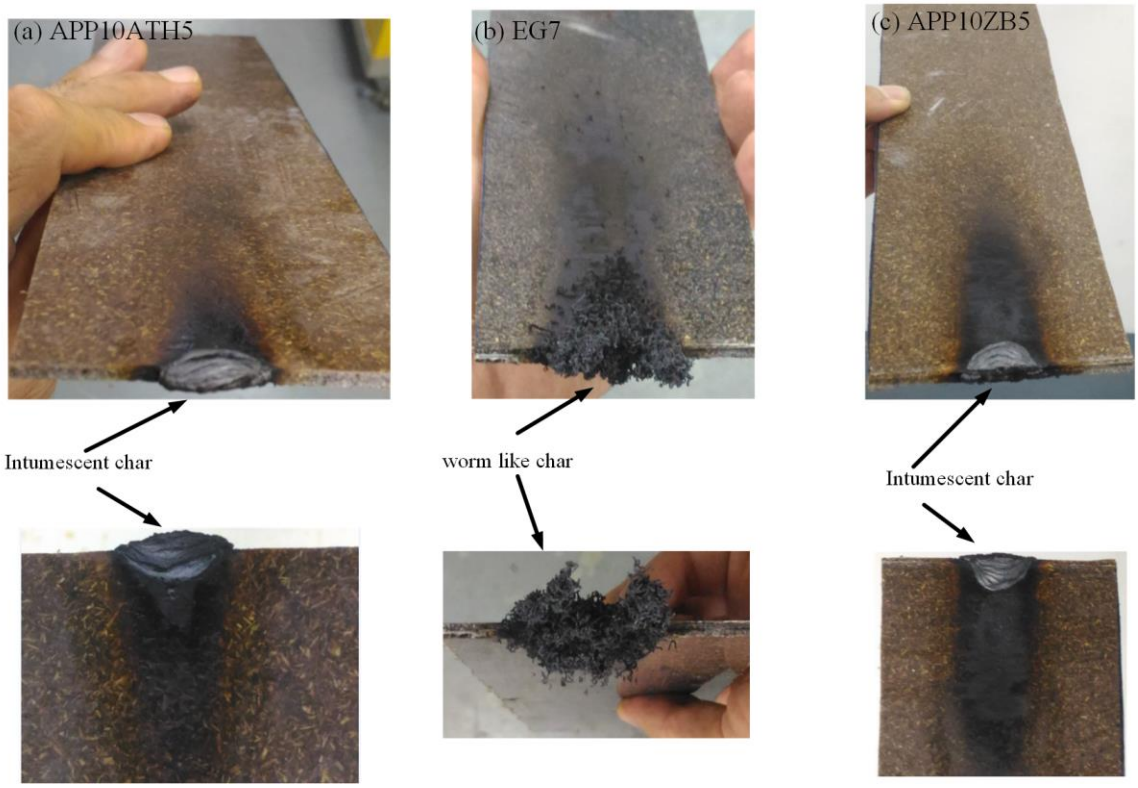


Figure 6-20 Different sections of the composite specimens including (a) ATH5APP10, (b) EG7 and (c) APP10ZB5 burned by applying 60 s Bunsen burner flame vertically.

For Nomex honeycomb, the smoke was only produced during the first 7 s of placing the Bunsen burner and no smoke was observed thereafter, due to the formation of the protective char layer by phenolic resin. The smoke released from the composites are shown in Figure 6-21. The specimens containing APP and ATH were visibly observed to produce constant amount of smoke from the burning zone after about 15 s exposure to the vertical Bunsen burner. The smoke continued after

withdrawing the burner for nearly another 12~14 s. For the composite specimens filled with APP and ZB, similar to APP10ATH5 specimens, the smoke was visibly observed after approximately 17 s from positioning the Bunsen burner beneath the specimens, and the smoke sustained for another 17 s after removing the Bunsen burner. When the composite specimens filled with EG were tested, considerably smaller amount of smoke was visibly observed relative to other two FR filled formulations. The smoke started after approximately 25 s of applying the burner and lasted for about 20 s after withdrawing the Bunsen burner.



Figure 6-21 (a) ATH5APP10 and (b) APP10ZB5 specimens produced visible smoke, (c) EG7 specimens showed lesser smoke.

6.3.7 SEM study

SEM micrographs of Nomex honeycomb core and panel without top EG filled composite skin are shown in Figure 6-22 and Figure 6-23, respectively. The Nomex honeycomb core is made of

phenolic resin bonded aramid paper and has the density of 29 kg/m^3. As observed in Figure 6-22-a, the nominal cell size of honeycomb core is 3.175, which is the nominal aerospace cell size for hexagonal Nomex core. Figure 6-22-b shows the hexagonal Nomex honeycomb core at lower magnification.

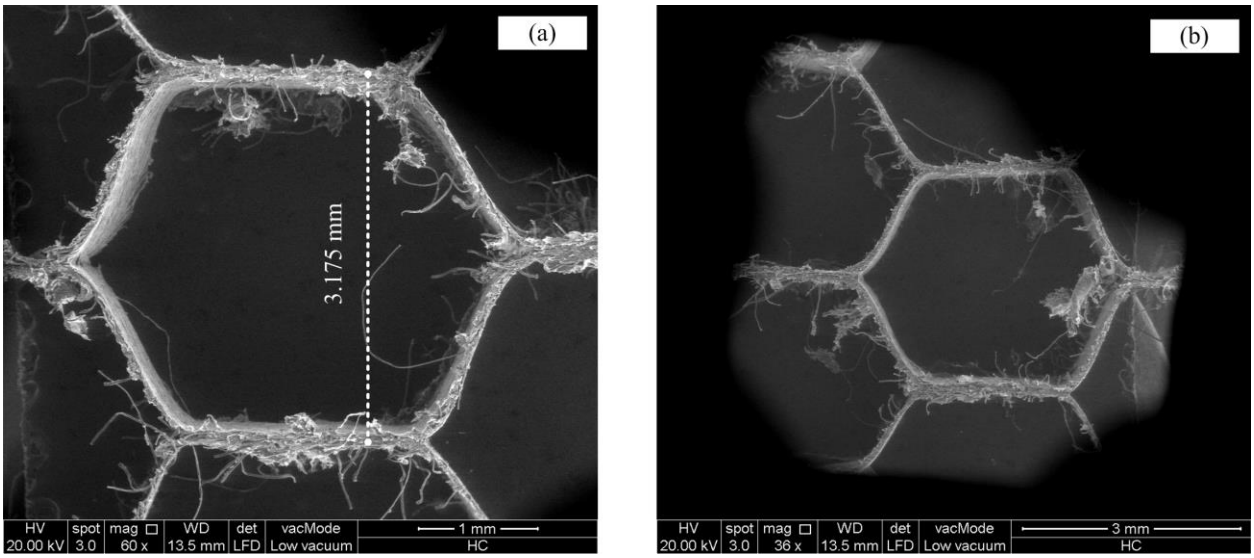


Figure 6-22 SEM images of Nomex honeycomb core. Transverse section of Nomex honeycomb cell at (a) 60 × and (b) 36 ×.

Figure 6-23 illustrates the SEM images of Nomex honeycomb panel with bottom EG filled composite skin from two different cells. The top composite skin was removed after flexural test to scan the vertical section of panel. The ellipses drawn between the cells and bottom skin are the positions required to provide proper bonding between the composite skin and honeycomb core through epoxy adhesive. The epoxy resin only applied between the composite skin and the wall of the honeycomb cell. The reason is that it is desired to apply as low as plausible adhesive materials to keep the weight of structure very light.

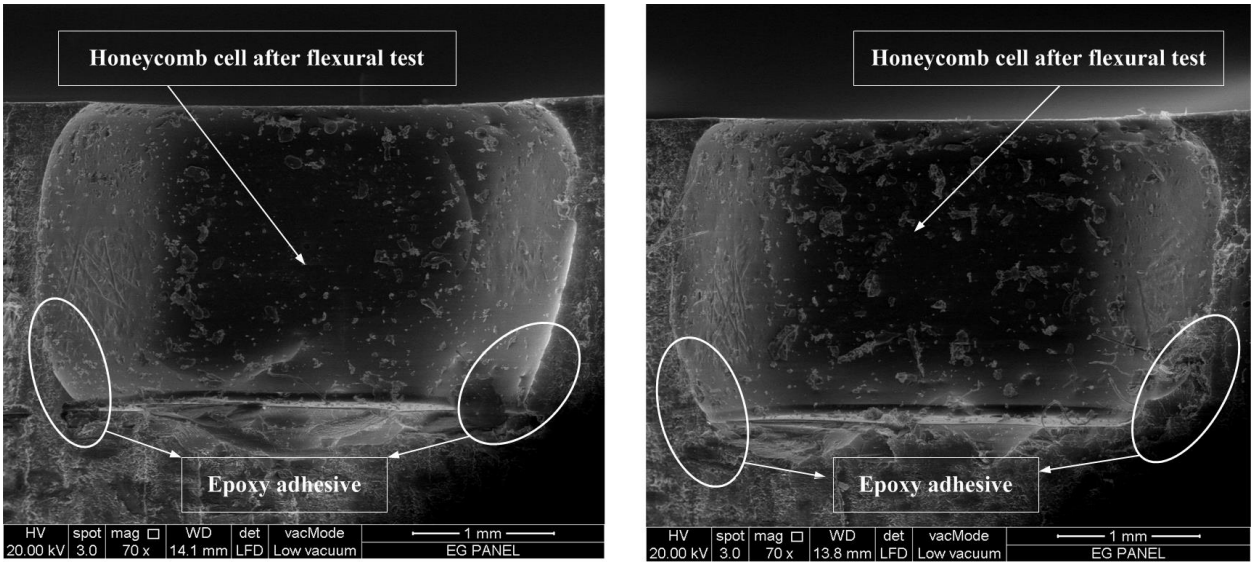


Figure 6-23 SEM micrographs of panel with EG filled skin from two different cells. Vertical section of panel after removal of top skin after flexural test.

6.4 Summary

To the best of author's knowledge, for the first time, Nomex honeycomb core panels were successfully fabricated with the natural fiber composite skins, and their compressive, flexural and shear properties were determined. It was found that Nomex honeycomb core is capable of enhancing the mechanical properties of the structure. For example, the bending stiffness was increased by about 3.25 times for the panels with the presence of honeycomb core. The 12 s vertical Bunsen burner tests were conducted to evaluate the requirements of aircraft interior components. The results showed that the panels met the FAR standard of vertical Bunsen burner test. In order for the composites and panels to be capable of being used for some interior aircraft parts such as partitions, ceilings and sidewalls, 60 s vertical Bunsen burner test was conducted for three composites (EG7, ATH5APP10 and APP10ZB5), and the FAR requirements were met. However,

it is essential to conduct Ohio State University calorimeter and National Bureau of Standards smoke chamber tests in order to conclude that the composite skins and panels are fully capable of being used in aircraft interior parts such as sidewalls, ceilings, partitions, galleys and etc. Each aircraft manufacturer may have its own thermal and mechanical standards as well. In the end, the SEM morphology of Nomex honeycomb core and panels were observed and the bonding between the core and skin was displayed.

The Nomex honeycomb used in this study was an aerospace grade core which encourages the enhancement of the mechanical performances of component to a standard level for use in interior parts, and depending on each aircraft manufacturer's design and its requirements for a particular interior component, various types of cores that possess different thicknesses along with required composite skins can be chosen. Thus, it highlights the importance of collaboration with an aircraft manufacturer in order to formulate, optimize and design the composite skins and the usage of appropriate Nomex honeycomb core in accordance with the requirements of that particular manufacturer.

Chapter 7

7. Conclusions and future work

7.1 Principle findings

- In the first part of the work, various compositions containing epoxy/hardener with flame retardants (FRs) as additives were used to produce natural fiber composite through the resin infusion technique. The effects of natural fiber (NF), ammonium polyphosphate (APP), alumina trihydrate (ATH), zinc borate (ZB), hybrids of ATH/APP, APP/ZB and ZB/ATH on flammability, thermal, and morphological properties of the composites were investigated.

  Addition of APP and ZB particles enhanced the flame resistant properties of the composite with a much reduced total flame time and zero drip flame time. In general, formulations containing only ATH could not provide the effective flame resistivity as compared to that of the APP and ZB-filled composites.

  Formulations with 5% ATH and 10% APP hybrid as well as ZB and APP at 5 to 10 wt% ratio showed the most promising flame retardancy with a self-extinguishing property, where 0 flame time, 0 drip time and less than 1 cm burn length were recorded. The vertical Bunsen burner testing requirements of aircraft interior (FAR 25.853 (b)) could be met with these formulations.

  From the bomb calorimetry analysis, it was observed that composite systems loaded with either APP and ATH or APP and ZB hybrid are capable of providing the lowest gross heat of combustion, with measured values less than 28 MJ/kg. Incorporation of NF into neat

epoxy matrix reduced the gross heat of combustion with improved thermal degradation properties. As obtained from TGA results, mass residue and thermal degradation temperature of 15 wt% ZB loaded composite increased by 124.7% and 4.88%, respectively, compared to the control, which indicates the greatest values compared to other FR filled composites. ZB particles were more effective in enhancement of increased char residue and T_d than other FRs.

- The second part of study aimed to investigate the effect of chemical treatment on the morphological, thermal and structural properties of EFB fibers. Surface modification of fibers was carried out by conducting alkali treatment for the soaking period of 24 hours, and subsequently fibers were neutralized by rinsing with distilled water to the pH level of 7. The fibers were then dried at 70 °C for 24 hours in an oven. To examine the physical and thermal properties of the fibers, Scanning Electron Microscope (SEM), Energy-Dispersive X-ray (EDX) spectroscopy, Fourier Transformed Infrared (FTIR) spectroscopy and Thermogravimetric Analysis (TGA) tests were conducted. SEM micrograph showed that rougher and cleaner surface of treated EFB fibers were apparent relative to those of untreated EFB. FTIR showed the elimination of a large amount of lignin and hemicellulose owing to the alkaline treatment, by significantly reducing the absorbance peaks. TGA tests were performed and the results showed greater thermal degradation temperature compared to those of untreated fibers for the entire temperature increment from 30 °C to 600 °C. The values of onset temperature and mass residue of alkali treated fibers were higher than those of untreated EFB by ca. 39 °C and more than 1 wt%, respectively.

- In the third part of work, the mechanical properties of the best formulations amongst FR filled composites were investigated and compared with the control. The effects of flame

retardants and chemical fibre treatment on tensile and flexural properties were examined. The addition of flame retardants to the EFB fiber reinforced composite reduced the tensile strength and made the composite more brittle, but enhanced the Young's modulus. For flexural properties, composites containing flame retardants showed lower values of strength and slightly higher values of modulus than to those without FRs. The alkali treatment of fibers enhanced the adhesion of fibers with polymer matrix. The epoxy composite containing alkali treated EFB fiber without FRs possessed the best mechanical properties of all the formulations studied. The cross-linked network formed between the matrix and treated EFB fiber helped fabricate intumescent composite with greater tensile and flexural properties than untreated EFB fiber FR filled composite. It was observed that the minimum lab scale mechanical requirements as extracted from various companies were met with the FR filled formulations. However, each aircraft manufacturer has its own lab scale and advanced mechanical requirements which is required to be taken into consideration when dealing with a particular manufacturer.

- In the fourth part of the research study, the effects of expandable graphite (EG) were studied as a flame retardant (FR) in oil palm empty fruit bunch (EFB) fiber reinforced composites. Increasing EG fillers in the composites significantly improved the fire resistivity and thermal properties, this, however, was found to reduce the mechanical properties. When EG particles were used as intumescent coating, at least 5 wt% content of EG was necessary to provide sufficient self-extinguishing properties. Chemical treatment of the EFB fibers could considerably enhance the tensile and flexural performances of EG filled composite. In summary, the flammability and lab scale mechanical properties of aircraft interior parts were passed with EG filled composites, but still heat release from

OSU calorimeter and smoke density from NBS smoke chamber tests are required to be measured and passed in order to claim the FAR requirements were fully met. As highlighted previously, other advanced mechanical and thermal tests may be required by each particular aerospace company as well.

- Lastly, two types of Nomex honeycomb panels with the composite skins were successfully fabricated and a series of mechanical and flammability tests was conducted. It was observed that a Nomex honeycomb is capable of providing enhanced compressive and flexural properties, and a suitable choice of "aerospace grade" core with sufficient bonding to the skins can significantly improve the mechanical properties up to a required level suited for a particular component. Importantly, it was concluded that the panels are capable of meeting the vertical Bunsen burner test requirements of aircraft interiors (FAR 25.853 (b)). For several aircraft interiors such as ceilings, partitions and sidewalls, 60 s vertical Bunsen burner specifications must be met. In this regard, three of the optimum formulations were selected and tested. All the composites were capable of meeting the FAR 25.853 (a) requirement.

7.2 Limitations

With regards to the FAR requirements focused on flammability and smoke properties of airplane interior components, all three tests (vertical Bunsen burner, OSU calorimeter and NBS smoke chamber) are required to be conducted in order to claim the composite materials or panels meet the criteria of FAR. However, to measure heat release from OSU calorimeter test and smoke density from NBS smoke chamber, we require to outsource and measure the required parameters, unfortunately, no company was found to have these two instruments and collaborations with

aircraft manufactures were not easy, and these companies were not interested to consider the outsourcing matter. In the future, collaboration with an aircraft manufacturer is crucial in order to bring a greater possibility to evaluate whether the composites fabricated in this study are capable of fully meeting the requirements by conducting these two tests as well as investigating probably other mechanical, thermal, long term reliability e.g. fatigue, chemical resistant and toxicity requirements suited to that particular aerospace manufacturer. In this case, it will be plausible to provide modification and optimization of composites through the inclusion of different weight fraction of FRs and EG particles, fiber mat systems, fiber treatment procedure, fabrication techniques, etc. in order to possibly pass the test requirements of that particular aircraft manufacturer.

7.3 Recommendation for future work

- The focus of aerospace manufacturers and agencies has directed to composite materials with easy disposal and recyclability. The principle drivers have been shifted to green composites. The future research and market for aircraft interiors will not only be honeycomb panels with natural fiber reinforced composite skins, but also polymeric matrix is required to be bio derived product. This type of green composites leads to promising benefits to the end customers, natural environment and manufacturer companies due to being derived from natural resources and dwindling petroleum resources.

  The chance of epoxy bio resins is much greater due to its manufacturing flexibility and compatibility to be utilized and incorporated with flame retardants and other fillers as well as acting as adhesive in honeycomb panels and also coating materials. Epoxy resins have been utilizing in aerospace industry owing to their potential to produce composites by

various fabrication techniques such as lamination, resin infusion, compression molding, casting, embedments, coatings, etc. Generally, NF reinforced epoxy resins provide higher mechanical properties over thermoplastic reinforced with NFs because of the cross-linked 3-D structure of thermosetting resins and better compatibility (NFs and thermosets are highly active in spite of thermoplastics and NFs).

- Besides, various forms of NFs long/short fiber, fibre mats, micro/nano-sized NFs can be developed to be introduced into bio derived epoxy resins. However, cost and time required for fabrication of nano/micro sized NF as well as its expected benefits are necessary to be taken into consideration. Natural fiber composite skins and NF reinforced composites induce cheaper and remarkable weight savings than current composite skins and composites used in sandwich panels and parts of aircraft interiors, respectively.

References

[1] Red C. Aviation Outlook: Fuel pricing ignites demand for composites in commercial transports. High Performance Composites. 2008;16(4):76.
[2] Hossain MK, Karim MR, Chowdhury MR, Imam MA, Hosur M, Jeelani S, et al. Comparative mechanical and thermal study of chemically treated and untreated single sugarcane fiber bundle. Industrial Crops and Products. 2014;58:78-90.
[3] Dweib M, Hu B, O'donnell A, Shenton H, Wool R. All natural composite sandwich beams for structural applications. Composite structures. 2004;63(2):147-57.
[4] Dorez G, Taguet A, Ferry L, Lopez-Cuesta JM. Thermal and fire behavior of natural fibers/PBS biocomposites. Polymer Degradation and Stability. 2013;98(1):87-95.
[5] Yao F, Wu Q, Lei Y, Guo W, Xu Y. Thermal decomposition kinetics of natural fibers: activation energy with dynamic thermogravimetric analysis. Polymer Degradation and Stability. 2008;93(1):90-8.
[6] Hesser F. Environmental advantage by choice: Ex-ante LCA for a new Kraft pulp fibre reinforced polypropylene composite in comparison to reference materials. Composites Part B: Engineering. 2015;79:197-203.
[7] Scarponi C, Messano M. Comparative evaluation between E-Glass and hemp fiber composites application in rotorcraft interiors. Composites Part B: Engineering. 2015;69:542-9.
[8] Rwawiire S, Tomkova B, Militky J, Jabbar A, Kale BM. Development of a biocomposite based on green epoxy polymer and natural cellulose fabric (bark cloth) for automotive instrument panel applications. Composites Part B: Engineering. 2015;81:149-57.
[9] Boccarusso L, Carrino L, Durante M, Formisano A, Langella A, Capece Minutolo FM. Hemp fabric/epoxy composites manufactured by infusion process: improvement of fire properties promoted by Ammonium Polyphosphate. Composites Part B: Engineering.
[10] Chai MW, Bickerton S, Bhattacharyya D, Das R. Influence of natural fibre reinforcements on the flammability of bio-derived composite materials. Composites Part B: Engineering. 2012;43(7):2867-74.
[11] Szolnoki B, Bocz K, Sóti PL, Bodzay B, Zimonyi E, Toldy A, et al. Development of natural fibre reinforced flame retarded epoxy resin composites. Polymer Degradation and Stability. 2015;119:68-76.
[12] Bourbigot S, Fontaine G. Flame retardancy of polylactide: an overview. Polymer Chemistry. 2010;1(9):1413-22.
[13] Chapple S, Anandjiwala R. Flammability of natural fiber-reinforced composites and strategies for fire retardancy: a review. Journal of Thermoplastic Composite Materials. 2010;23(6):871-93.
[14] John MJ, Thomas S. Biofibres and biocomposites. Carbohydrate polymers. 2008;71(3):343-64.
[15] Mngomezulu ME, John MJ, Jacobs V, Luyt AS. Review on flammability of biofibres and biocomposites. Carbohydrate Polymers. 2014.
[16] Laoutid F, Bonnaud L, Alexandre M, Lopez-Cuesta J-M, Dubois P. New prospects in flame retardant polymer materials: from fundamentals to nanocomposites. Materials Science and Engineering: R: Reports. 2009;63(3):100-25.
[17] Morgan AB, Gilman JW. An overview of flame retardancy of polymeric materials: application, technology, and future directions. Fire and Materials. 2013;37(4):259-79.
[18] Wichman IS. Material flammability, combustion, toxicity and fire hazard in transportation. Progress in Energy and Combustion Science. 2003;29(3):247-99.
[19] Dittenber DB, GangaRao HV. Critical review of recent publications on use of natural composites in infrastructure. Composites Part A: Applied Science and Manufacturing. 2012;43(8):1419-29.
[20] Manfredi LB, Rodríguez ES, Wladyka-Przybylak M, Vázquez A. Thermal degradation and fire resistance of unsaturated polyester, modified acrylic resins and their composites with natural fibres. Polymer Degradation and Stability. 2006;91(2):255-61.

[21] Suardana NPG, Ku MS, Lim JK. Effects of diammonium phosphate on the flammability and mechanical properties of bio-composites. Materials & Design. 2011;32(4):1990-9.
[22] Thakur VK, Thakur MK. Processing and characterization of natural cellulose fibers/thermoset polymer composites. Carbohydrate Polymers. 2014;109(0):102-17.
[23] Anbukarasi K, Kalaiselvam S. Study of effect of fibre volume and dimension on mechanical, thermal, and water absorption behaviour of luffa reinforced epoxy composites. Materials & Design. 2015;66, Part A:321-30.
[24] Reussmann T, Mieck P, Grutzner R, Bayer R. The recycling of polypropylene reinforced with natural fibres. Kunststoffe-Plast Europe. 1999;89(2):80-3.
[25] Faruk O, Bledzki AK, Fink H-P, Sain M. Biocomposites reinforced with natural fibers: 2000–2010. Progress in Polymer Science. 2012;37(11):1552-96.
[26] Quilter A. Composites in aerospace applications. IHS White Paper. 2001;444:1-3.
[27] Arib RMN, Sapuan SM, Ahmad MMHM, Paridah MT, Zaman HMDK. Mechanical properties of pineapple leaf fibre reinforced polypropylene composites. Materials & Design. 2006;27(5):391-6.
[28] Sapuan SM, Leenie A, Harimi M, Beng YK. Mechanical properties of woven banana fibre reinforced epoxy composites. Materials & Design. 2006;27(8):689-93.
[29] Murali Mohan Rao K, Mohana Rao K, Ratna Prasad AV. Fabrication and testing of natural fibre composites: Vakka, sisal, bamboo and banana. Materials & Design. 2010;31(1):508-13.
[30] Composites H. HexWeb™, Honeycomb Attributes and Properties. A comprehensive guide to standard Hexcel honeycomb materials, configurations, and mechanical properties. 2010.
[31] Hariharan ABA, Khalil HA. Lignocellulose-based hybrid bilayer laminate composite: part i-studies on tensile and impact behavior of oil palm fiber-glass fiber-reinforced epoxy resin. Journal of composite materials. 2005;39(8):663-84.
[32] Fire- and Smoke-Resistant Interior Materials for Commercial Transport Aircraft: The National Academies Press; 1995.
[33] Pearce EM. Fire-and smoke-resistant interior materials for commercial transport aircraft: Natl Academy Pr; 1995.
[34] Horner A. Aircraft Materials Fire Test Handbook. DTIC Document; 2000.
[35] Smith EE. Heat release rate calorimetry. Fire Technology. 1996;32(4):333-47.
[36] Hirschler MM. Use of Heat Release Measurements and/or Fire Hazard Assessment in Codes and Standards in the USA. Fire Risk & Hazard Assessment Symposium, National Fire Protection Research Foundation2000.
[37] 3D Systems Corporation. DuraForm® FR 100 Plastic. 2009.
[38] BASF Aerospace Materials. Divinycell® F- Core materials made from Ultrason®. 2012.
[39] BASF Aerospace Materials. Elastollan® Thermoplastic Polyurethane. 2013.
[40] BASF Aerospace Materials. Lightweight Composite Load Panel. 2013.
[41] Evonik Industries AG. EUROPLEX® PPSU sheets for aircraft applications. 2011.
[42] Gurit GmbH. PB1000 Modified Benzoxazine Resin.
[43] GmbH G. EH 250 / EP 112 ESTABLISHED AEROSPACE EPOXY PREPREG.
[44] KYDEX L. For production of high-performance aircraft interior components. 2009.
[45] KYDEX L. Selection Guide: Thermoplastic sheet in specialised grades for demanding applications. 2009.
[46] KYDEX L. Thermoplastic sheet products in specialized grades for demanding applications.
[47] MODERNplastics. KYDEX ® T High impact fire-rated sheet. 2001.
[48] MODERNplastics. KYDEX ® 6565 Low heat release aviation sheet. 2001.
[49] MODERNplastics. KYDEX ®100 High impact fire-rated sheet. 2001.
[50] SABIC. Innovative plastics: Lightweight + compliant. 2013.
[51] ENSINGER GmbH. High-performance Plastics for Aviation and Aerospace.

[52] BERG H-D. Processing and manufacturing of interior components. Deutsche Airbus G m b H, Improved Fire- and Smoke-Resistant Materials for Commercial Aircraft Interiors: A proceedings p 213-220(SEE N 96-24322 08-03). 1995.
[53] Chen H YY, Zhang J. Biotechnological potential of cereal straw and bran residues. In: Nigam PS, Pandey A, editors. Biotechnology for Agro-Industrial Residues Utilisation. Germany: Springer Science+Business Media; 2009. p.327–40.
[54] Bismarck A MS, Lampke T. Plant fibre as Reinforcement for green composites. In: Mohanty AK, Misra M, Drzal LT, editors. Natural Fibres, Biopolymers and Biocomposites. New York: Taylor and Francis; 2005. p. 37–108.
[55] Gnansounou E, Dauriat A. Techno-economic analysis of lignocellulosic ethanol: A review. Bioresource technology. 2010;101(13):4980-91.
[56] Hamzah F, Idris A, Shuan TK. Preliminary study on enzymatic hydrolysis of treated oil palm (< i> Elaeis</i>) empty fruit bunches fibre (EFB) by using combination of cellulase and β 1-4 glucosidase. biomass and bioenergy. 2011;35(3):1055-9.
[57] Piarpuzán D, Quintero JA, Cardona CA. Empty fruit bunches from oil palm as a potential raw material for fuel ethanol production. biomass and bioenergy. 2011;35(3):1130-7.
[58] Ramli R, Yunus R, Beg M. Effects of fiber loading, fiber type, its mesh sizes, and coupling agent on the properties of oil palm biomass/polypropylene composites. Journal of Composite Materials. 2011;45(21):2165-71.
[59] Hill C, Abdul Khalil H. Effect of fiber treatments on mechanical properties of coir or oil palm fiber reinforced polyester composites. Journal of Applied Polymer Science. 2000;78(9):1685-97.
[60] Hill CA, Khalil H, Hale MD. A study of the potential of acetylation to improve the properties of plant fibres. Industrial Crops and Products. 1998;8(1):53-63.
[61] Sreekala M, Kumaran M, Geethakumariamma M, Thomas S. Environmental effects in oil palm fiber reinforced phenol formaldehyde composites: Studies on thermal, biological, moisture and high energy radiation effects. Advanced Composite Materials. 2004;13(3-4):171-97.
[62] Yousif B, El-Tayeb N. High-stress three-body abrasive wear of treated and untreated oil palm fibre-reinforced polyester composites. Proceedings of the Institution of Mechanical Engineers, Part J: Journal of Engineering Tribology. 2008;222(5):637-46.
[63] Rozman H, Saad M, Mohd Ishak Z. Flexural and impact properties of oil palm empty fruit bunch (EFB)–polypropylene composites—the effect of maleic anhydride chemical modification of EFB. Polymer testing. 2003;22(3):335-41.
[64] Raju G, Ratnam CT, Ibrahim NA, Rahman MZA, Yunus WMZW. Enhancement of PVC/ENR blend properties by poly (methyl acrylate) grafted oil palm empty fruit bunch fiber. Journal of Applied Polymer Science. 2008;110(1):368-75.
[65] Jawaid M, Abdul Khalil H. Cellulosic/synthetic fibre reinforced polymer hybrid composites: A review. Carbohydrate Polymers. 2011;86(1):1-18.
[66] Sobczak L, Lang RW, Haider A. Polypropylene composites with natural fibers and wood–General mechanical property profiles. Composites Science and Technology. 2012;72(5):550-7.
[67] Ude A, Eshkoor R, Zulkifili R, Ariffin A, Dzuraidah A, Azhari C. Bombyx mori silk fibre and its composite: a review of contemporary developments. Materials & Design. 2014;57:298-307.
[68] AL-Oqla FM, Sapuan S. Natural fiber reinforced polymer composites in industrial applications: feasibility of date palm fibers for sustainable automotive industry. Journal of Cleaner Production. 2013.
[69] Indran S, Raj RE. Characterization of new natural cellulosic fiber from Cissus quadrangularis stem. Carbohydrate Polymers. 2015;117(0):392-9.
[70] Khalil HA, Yusra AI, Bhat A, Jawaid M. Cell wall ultrastructure, anatomy, lignin distribution, and chemical composition of Malaysian cultivated kenaf fiber. Industrial Crops and Products. 2010;31(1):113-21.

[71] Bhagawan S, Tripathy D, De S. Stress relaxation in short jute fiber-reinforced nitrile rubber composites. Journal of applied polymer science. 1987;33(5):1623-39.
[72] Franck RR. Bast and other plant fibres: Crc Press; 2005.
[73] Thomas S, Idicula M, Joseph K. Mechanical performance of short banana/sisal hybrid fibre reinforced polyester composites. Journal of Reinforced Plastics and Composites. 2010;29(1):12-29.
[74] Abdul Khalil H, Siti Alwani M, Ridzuan R, Kamarudin H, Khairul A. Chemical composition, morphological characteristics, and cell wall structure of Malaysian oil palm fibers. Polymer-Plastics Technology and Engineering. 2008;47(3):273-80.
[75] Mariatti M, Jannah M, Bakar AA, Khalil HA. Properties of banana and pandanus woven fabric reinforced unsaturated polyester composites. Journal of composite materials. 2008;42(9):931-41.
[76] Beg MDH, Pickering KL. Reprocessing of wood fibre reinforced polypropylene composites. Part II: Hygrothermal ageing and its effects. Composites Part A: Applied science and manufacturing. 2008;39(9):1565-71.
[77] Shinoj S, Visvanathan R, Panigrahi S, Kochubabu M. Oil palm fiber (OPF) and its composites: A review. Industrial Crops and Products. 2011;33(1):7-22.
[78] RA. Y, Wood and wood products. In: Kent JA, editor. Handbook of industrial chemistry and biotechnology, vol. 2. New York: Springer; 2007. p. 1234–93.
[79] Hon DN-S, Shiraishi N. Wood and Cellulosic Chemistry, Revised, and Expanded: CRC Press; 2000.
[80] Sreekala M, Kumaran M, Joseph S, Jacob M, Thomas S. Oil palm fibre reinforced phenol formaldehyde composites: influence of fibre surface modifications on the mechanical performance. Applied Composite Materials. 2000;7(5-6):295-329.
[81] Sreekala M, Kumaran M, Thomas S. Oil palm fibers: Morphology, chemical composition, surface modification, and mechanical properties. Journal of Applied Polymer Science. 1997;66(5):821-35.
[82] Srinivasa C, Arifulla A, Goutham N, Santhosh T, Jaeethendra H, Ravikumar R, et al. Static bending and impact behaviour of areca fibers composites. Materials & Design. 2011;32(4):2469-75.
[83] Van de Weyenberg I, Chi Truong T, Vangrimde B, Verpoest I. Improving the properties of UD flax fibre reinforced composites by applying an alkaline fibre treatment. Composites Part A: Applied Science and Manufacturing. 2006;37(9):1368-76.
[84] Azwa Z, Yousif B. Characteristics of kenaf fibre/epoxy composites subjected to thermal degradation. Polymer Degradation and Stability. 2013;98(12):2752-9.
[85] Mamun AA, Heim H-P, Beg DH, Kim TS, Ahmad SH. PLA and PP composites with enzyme modified oil palm fibre: A comparative study. Composites Part A: Applied Science and Manufacturing. 2013;53:160-7.
[86] Moshiul Alam A, Beg M, Reddy Prasad D, Khan M, Mina M. Structures and performances of simultaneous ultrasound and alkali treated oil palm empty fruit bunch fiber reinforced poly (lactic acid) composites. Composites Part A: Applied Science and Manufacturing. 2012.
[87] Rozman H, Ahmadhilmi K, Abubakar A. Polyurethane (PU)—oil palm empty fruit bunch (EFB) composites: the effect of EFBG reinforcement in mat form and isocyanate treatment on the mechanical properties. Polymer testing. 2004;23(5):559-65.
[88] Beg MDH, Pickering KL. Accelerated weathering of unbleached and bleached Kraft wood fibre reinforced polypropylene composites. Polymer Degradation and Stability. 2008;93(10):1939-46.
[89] Joseph S, Joseph K, Thomas S. Green composites from natural rubber and oil palm fiber: physical and mechanical properties. International Journal of Polymeric Materials. 2006;55(11):925-45.
[90] John MJ, Francis B, Varughese K, Thomas S. Effect of chemical modification on properties of hybrid fiber biocomposites. Composites Part A: Applied Science and Manufacturing. 2008;39(2):352-63.
[91] Arrakhiz F, El Achaby M, Malha M, Bensalah M, Fassi-Fehri O, Bouhfid R, et al. Mechanical and thermal properties of natural fibers reinforced polymer composites: Doum/low density polyethylene. Materials & Design. 2013;43:200-5.

[92] Naughton A, Fan M, Bregulla J. Fire resistance characterisation of hemp fibre reinforced polyester composites for use in the construction industry. Composites Part B: Engineering. 2014;60:546-54.
[93] Kalam A, Sahari B, Khalid Y, Wong S. Fatigue behaviour of oil palm fruit bunch fibre/epoxy and carbon fibre/epoxy composites. Composite structures. 2005;71(1):34-44.
[94] Chai L-L, Zakaria S, Chia C-H, Nabihah S, Rasid R. Physico-mechanical properties of PF composite board from EFB fibres using liquefaction technique. Iran Polym J. 2009;18:917-23.
[95] Cerqueira E, Baptista C, Mulinari D. Mechanical behaviour of polypropylene reinforced sugarcane bagasse fibers composites. Procedia Engineering. 2011;10:2046-51.
[96] Baker AAA, Dutton S, Kelly D, Kelly DW. Composite materials for aircraft structures: AIAA; 2004.
[97] Sreekala M, George J, Kumaran M, Thomas S. The mechanical performance of hybrid phenol-formaldehyde-based composites reinforced with glass and oil palm fibres. Composites science and technology. 2002;62(3):339-53.
[98] Marliana M, Hassan A, Yuziah MN, Khalil HA, Inuwa I, Syakir M, et al. Flame retardancy, Thermal and mechanical properties of Kenaf fiber reinforced Unsaturated polyester/Phenolic composite. Fibers and Polymers. 2016;17(6):902-9.
[99] Huang G, Song P, Liu L, Han D, Ge C, Li R, et al. Fabrication of multifunctional graphene decorated with bromine and nano-Sb2O3 towards high-performance polymer nanocomposites. Carbon. 2016;98:689-701.
[100] de Oliveira F, da Silva CG, Ramos LA, Frollini E. Phenolic and lignosulfonate-based matrices reinforced with untreated and lignosulfonate-treated sisal fibers. Industrial Crops and Products. 2017;96:30-41.
[101] Bu Z, Hu J, Li B. Novel silicon-modified phenolic novolac resins: Non-isothermal curing kinetics, and mechanical and thermal properties of their biofiber-reinforced composites. Thermochimica Acta. 2014;575:244-53.
[102] Fisk P, Girling A, Wildey R, Britain G. Prioritisation of flame retardants for environmental risk assessment: Environment Agency; 2003.
[103] Posner S. Survey and technical assessment of alternatives to decabromodiphenyl ether (decaBDE) in textile applications. KemI PM. 2004;5.
[104] Guillaume E, Marquis D, Saragoza L. Calibration of flow rate in cone calorimeter tests. Fire and Materials. 2012.
[105] Grexa O, Lübke H. Flammability parameters of wood tested on a cone calorimeter. Polymer degradation and stability. 2001;74(3):427-32.
[106] Kandola B, Price D. Nanocomposites. Fire retardant materials. 2001.
[107] Kandola B, Horrocks A, Myler P, Blair D. Thermal characterization of thermoset matrix resins. 2001.
[108] Ke C-H, Li J, Fang K-Y, Zhu Q-L, Zhu J, Yan Q, et al. Synergistic effect between a novel hyperbranched charring agent and ammonium polyphosphate on the flame retardant and anti-dripping properties of polylactide. Polymer Degradation and Stability. 2010;95(5):763-70.
[109] Kozlowski R, Wladyka-Przybylank M. Natural polymers, wood and lignocellolosic materials: Woodhead Publishing Limited: Cambridge, UK; 2001.
[110] Horrocks AR, Price D. Fire retardant materials: woodhead Publishing; 2001.
[111] Gibson A. Fire properties of polymer composite materials: Springer; 2007.
[112] Garcia M, Hidalgo J, Garmendia I, García-Jaca J. Wood–plastics composites with better fire retardancy and durability performance. Composites Part A: Applied Science and Manufacturing. 2009;40(11):1772-6.
[113] Sain M, Park S, Suhara F, Law S. Flame retardant and mechanical properties of natural fibre–PP composites containing magnesium hydroxide. Polymer Degradation and Stability. 2004;83(2):363-7.
[114] Schartel B, Braun U, Schwarz U, Reinemann S. Fire retardancy of polypropylene/flax blends. Polymer. 2003;44(20):6241-50.

[115] Hapuarachchi T, Ren G, Fan M, Hogg P, Peijs T. Fire retardancy of natural fibre reinforced sheet moulding compound. Applied Composite Materials. 2007;14(4):251-64.
[116] Reti C, Casetta M, Duquesne S, Bourbigot S, Delobel R. Flammability properties of intumescent PLA including starch and lignin. Polymers for advanced Technologies. 2008;19(6):628-35.
[117] Chen G. In Situ Thermal Condensation of Glucose-Diammonium Phosphate Inwood for Fire and Fungal Decay Protection. Wood and Fiber Science. 2009;41(2):105-16.
[118] Gaan S, Sun G. Effect of phosphorus flame retardants on thermo-oxidative decomposition of cotton. Polymer Degradation and Stability. 2007;92(6):968-74.
[119] Kozłowski R, Władyka-Przybylak M. Flammability and fire resistance of composites reinforced by natural fibers. Polymers for Advanced Technologies. 2008;19(6):446-53.
[120] Kandola BK. Flame Retardant Characteristics of Natural Fibre Composites. Natural Polymers; Volume 1: Composites: The Royal Society of Chemistry United Kingdom; 2012. p. 86-117.
[121] Tang G, Wang X, Xing W, Zhang P, Wang B, Hong N, et al. Thermal degradation and flame retardance of biobased polylactide composites based on aluminum hypophosphite. Industrial & Engineering Chemistry Research. 2012;51(37):12009-16.
[122] ZAVAREZE EDR, DIAS ARG. Relation between Structural Anisotropy in Natural Fibres and Mechanical Properties in Composites. Natural Polymers; Volume 1: Composites: The Royal Society of Chemistry United Kingdom; 2012. p. 63-85.
[123] Chen D, Li J, Ren J. Combustion properties and transference behavior of ultrafine microencapsulated ammonium polyphosphate in ramie fabric-reinforced poly(L-lactic acid) biocomposites. Polymer International. 2011;60(4):599-606.
[124] Bocz K, Szolnoki B, Marosi A, Tábi T, Wladyka-Przybylak M, Marosi G. Flax fibre reinforced PLA/TPS biocomposites flame retarded with multifunctional additive system. Polymer Degradation and Stability. 2014;106(0):63-73.
[125] Hapuarachchi TD, Peijs T. Multiwalled carbon nanotubes and sepiolite nanoclays as flame retardants for polylactide and its natural fibre reinforced composites. Composites Part A: Applied Science and Manufacturing. 2010;41(8):954-63.
[126] Alhuthali A, Low IM, Dong C. Characterisation of the water absorption, mechanical and thermal properties of recycled cellulose fibre reinforced vinyl-ester eco-nanocomposites. Composites Part B: Engineering. 2012;43(7):2772-81.
[127] Becker O, Varley RJ, Simon GP. Thermal stability and water uptake of high performance epoxy layered silicate nanocomposites. European Polymer Journal. 2004;40(1):187-95.
[128] Paul M-A, Alexandre M, Degée P, Henrist C, Rulmont A, Dubois P. New nanocomposite materials based on plasticized poly(l-lactide) and organo-modified montmorillonites: thermal and morphological study. Polymer. 2003;44(2):443-50.
[129] Vyazovkin S, Dranca I, Fan X, Advincula R. Kinetics of the Thermal and Thermo-Oxidative Degradation of a Polystyrene–Clay Nanocomposite. Macromolecular Rapid Communications. 2004;25(3):498-503.
[130] Pavlidou S, Papaspyrides CD. A review on polymer–layered silicate nanocomposites. Progress in Polymer Science. 2008;33(12):1119-98.
[131] Zeng QH, Yu AB, Lu GQ, Paul DR. Clay-Based Polymer Nanocomposites: Research and Commercial Development. Journal of Nanoscience and Nanotechnology. 2005;5(10):1574-92.
[132] Biswal M, Mohanty S, Nayak SK. Thermal stability and flammability of banana-fiber-reinforced polypropylene nanocomposites. Journal of Applied Polymer Science. 2012;125(S2):E432-E43.
[133] Chen RS, Ahmad S, Gan S, Salleh MN, Ab Ghani MH, Tarawneh MaA. Effect of polymer blend matrix compatibility and fibre reinforcement content on thermal stability and flammability of ecocomposites made from waste materials. Thermochimica Acta.
[134] Bharath K, Basavarajappa S. Flammability characteristics of chemical treated woven natural fabric reinforced phenol formaldehyde composites. Procedia Materials Science. 2014;5:1880-6.

[135] Freivalde L, Kukle S, Andžs M, Bukšāns E, Grāvītis J. Flammability of raw insulation materials made of hemp. Composites Part B: Engineering. 2014;67:510-4.
[136] Kim NK, Lin RJT, Bhattacharyya D. Effects of wool fibres, ammonium polyphosphate and polymer viscosity on the flammability and mechanical performance of PP/wool composites. Polymer Degradation and Stability. 2015;119:167-77.
[137] El-Sabbagh A, Steuernagel L, Ziegmann G, Meiners D, Toepfer O. Processing parameters and characterisation of flax fibre reinforced engineering plastic composites with flame retardant fillers. Composites Part B: Engineering. 2014;62:12-8.
[138] Addivant presents new polymer modifiers at Chinaplas. Additives for Polymers. 2014;2014(6):2-3.
[139] Alongi J, Carosio F, Malucelli G. Current emerging techniques to impart flame retardancy to fabrics: An overview. Polymer Degradation and Stability. 2014;106:138-49.
[140] Gallo E, Schartel B, Acierno D, Cimino F, Russo P. Tailoring the flame retardant and mechanical performances of natural fiber-reinforced biopolymer by multi-component laminate. Composites Part B: Engineering. 2013;44(1):112-9.
[141] Shariatinia Z, Javeri N, Shekarriz S. Flame retardant cotton fibers produced using novel synthesized halogen-free phosphoramide nanoparticles. Carbohydrate Polymers. 2015;118:183-98.
[142] Leistner M, Haile M, Rohmer S, Abu-Odeh A, Grunlan JC. Water-soluble polyelectrolyte complex nanocoating for flame retardant nylon-cotton fabric. Polymer Degradation and Stability. 2015;122:1-7.
[143] Bai BC, Kim EA, Jeon Y-P, Lee CW, In SJ, Lee Y-S, et al. Improved flame-retardant properties of lyocell fiber achieved by phosphorus compound. Materials Letters. 2014;135:226-8.
[144] Dorez G, Taguet A, Ferry L, Lopez Cuesta J-M. Phosphorous compounds as flame retardants for polybutylene succinate/flax biocomposite: Additive versus reactive route. Polymer Degradation and Stability. 2014;102:152-9.
[145] Lazko J, Landercy N, Laoutid F, Dangreau L, Huguet MH, Talon O. Flame retardant treatments of insulating agro-materials from flax short fibres. Polymer Degradation and Stability. 2013;98(5):1043-51.
[146] Papadopoulou E, Bikiaris D, Chrysafis K, Wladyka-Przybylak M, Wesolek D, Mankowski J, et al. Value-added industrial products from bast fiber crops. Industrial Crops and Products. 2015;68:116-25.
[147] Parvinzadeh Gashti M, Almasian A. UV radiation induced flame retardant cellulose fiber by using polyvinylphosphonic acid/carbon nanotube composite coating. Composites Part B: Engineering. 2013;45(1):282-9.
[148] Richard Horrocks A. Textile flammability research since 1980 – Personal challenges and partial solutions. Polymer Degradation and Stability. 2013;98(12):2813-24.
[149] Subasinghe A, Bhattacharyya D. Performance of different intumescent ammonium polyphosphate flame retardants in PP/kenaf fibre composites. Composites Part A: Applied Science and Manufacturing. 2014;65:91-9.
[150] Vasiljević J, Hadžić S, Jerman I, Černe L, Tomšič B, Medved J, et al. Study of flame-retardant finishing of cellulose fibres: Organic–inorganic hybrid versus conventional organophosphonate. Polymer Degradation and Stability. 2013;98(12):2602-8.
[151] Wang Q, Yu Y, Ma J, Zhang N, Zhang J, Liu Z, et al. Electrospun melamine resin-based multifunctional nonwoven membrane for lithium ion batteries at the elevated temperatures. Journal of Power Sources. 2016;327:196-203.
[152] Wang X, Zhang Y, Lv L, Cui Y, Wei C, Pang G. Preparation of Mg(OH)2 hybrid pigment by direct precipitation and graft onto cellulose fiber via surface-initiated atom transfer radical polymerization. Applied Surface Science. 2016;363:189-96.
[153] Wu X, Qian X, An X. Flame retardancy of polyaniline-deposited paper composites prepared via in situ polymerization. Carbohydrate Polymers. 2013;92(1):435-40.
[154] Zhang K, Zong L, Tan Y, Ji Q, Yun W, Shi R, et al. Improve the flame retardancy of cellulose fibers by grafting zinc ion. Carbohydrate Polymers. 2016;136:121-7.

[155] Zou J, Guo C, Jiang Y, Wei C, Li F. Structure, morphology and mechanism research on synthesizing xonotlite fiber from acid-extracting residues of coal fly ash and carbide slag. Materials Chemistry and Physics. 2016;172:121-8.
[156] Jaafar M, Razak KA, Ariff ZM, Zabidi H, Netnapa E, Mariatti M, et al. 5th International Conference on Recent Advances in Materials, Minerals and Environment (RAMM) & 2nd International Postgraduate Conference on Materials, Mineral and Polymer (MAMIP)Dielectric Breakdown Strength and Flammability Properties of Flame Retardant Filler/PLLA-PLA Microsphere/Kenaf Fiber Composites. Procedia Chemistry. 2016;19:290-6.
[157] Wang Y-Y, Shih Y-F. Flame-retardant recycled bamboo chopstick fiber-reinforced poly(lactic acid) green composites via multifunctional additive system. Journal of the Taiwan Institute of Chemical Engineers. 2016;65:452-8.
[158] Fei P, Chen X, Xiong H, Zia ud D, Chen L, Cai J. Synthesis of H2Ti2O3·H2O nanotubes and their effects on the flame retardancy of bamboo fiber/high-density polyethylene composites. Composites Part A: Applied Science and Manufacturing. 2016;90:225-33.
[159] Deng Y, Paraskevas D, Tian Y, Van Acker K, Dewulf W, Duflou JR. Life cycle assessment of flax-fibre reinforced epoxidized linseed oil composite with a flame retardant for electronic applications. Journal of Cleaner Production. 2016;133:427-38.
[160] Balakrishnan P, John MJ, Pothen L, Sreekala MS, Thomas S. 12 - Natural fibre and polymer matrix composites and their applications in aerospace engineering. Advanced Composite Materials for Aerospace Engineering: Woodhead Publishing; 2016. p. 365-83.
[161] Idumah CI, Hassan A. Emerging trends in flame retardancy of biofibers, biopolymers, biocomposites, and bionanocomposites. Reviews in Chemical Engineering. 2016;32(1):115-48.
[162] HASSAN A, HAU LY, HASAN M. Effect of Ammonium Polyphosphate on Flame Retardancy, Thermal Stability, and Mechanical Properties of Unsaturated Polyester/Phenolic/Montmorillonite Nanocomposites. Advances in Polymer Technology. 2015.
[163] Baker AAB, Kelly DW. Composite materials for aircraft structures: AIAA; 2004.
[164] Döring M, Bykov Y, Held I. Innovative and Sustainable Flame Retardants in Transportation. Pinfa: Brussels, Belgium. 2010.
[165] Kurańska M, Cabulis U, Auguścik M, Prociak A, Ryszkowska J, Kirpluks M. Bio-based polyurethane-polyisocyanurate composites with an intumescent flame retardant. Polymer Degradation and Stability. 2016;127:11-9.
[166] Schirp A, Su S. Effectiveness of pre-treated wood particles and halogen-free flame retardants used in wood-plastic composites. Polymer Degradation and Stability. 2016;126:81-92.
[167] Thirumal M, Khastgir D, Singha NK, Manjunath B, Naik Y. Effect of expandable graphite on the properties of intumescent flame-retardant polyurethane foam. Journal of applied polymer science. 2008;110(5):2586-94.
[168] Beyer G. Nanocomposites: a new class of flame retardants for polymers. Plastics, Additives and Compounding. 2002;4(10):22-8.
[169] Yang S, Wang J, Huo S, Wang M, Wang J, Zhang B. Synergistic flame-retardant effect of expandable graphite and phosphorus-containing compounds for epoxy resin: Strong bonding of different carbon residues. Polymer Degradation and Stability. 2016;128:89-98.
[170] Liu J, Zhang Y, Peng S, Pan B, Lu C, Liu H, et al. Fire property and charring behavior of high impact polystyrene containing expandable graphite and microencapsulated red phosphorus. Polymer Degradation and Stability. 2015;121:261-70.
[171] Laachachi A, Burger N, Apaydin K, Sonnier R, Ferriol M. Is expanded graphite acting as flame retardant in epoxy resin? Polymer Degradation and Stability. 2015;117:22-9.

[172] Bai G, Guo C, Li L. Synergistic effect of intumescent flame retardant and expandable graphite on mechanical and flame-retardant properties of wood flour-polypropylene composites. Construction and Building Materials. 2014;50:148-53.
[173] Li Z, Qu B. Flammability characterization and synergistic effects of expandable graphite with magnesium hydroxide in halogen-free flame-retardant EVA blends. Polymer Degradation and Stability. 2003;81(3):401-8.
[174] Liu L, Wang H, Guan Z. Experimental and numerical study on the mechanical response of Nomex honeycomb core under transverse loading. Composite Structures. 2015;121:304-14.
[175] Liu L, Meng P, Wang H, Guan Z. The flatwise compressive properties of Nomex honeycomb core with debonding imperfections in the double cell wall. Composites Part B: Engineering. 2015;76:122-32.
[176] Roy R, Nguyen K, Park Y, Kweon J, Choi J. Testing and modeling of Nomex™ honeycomb sandwich Panels with bolt insert. Composites Part B: Engineering. 2014;56:762-9.
[177] Roy R, Park S-J, Kweon J-H, Choi J-H. Characterization of Nomex honeycomb core constituent material mechanical properties. Composite Structures. 2014;117:255-66.
[178] Asprone D, Auricchio F, Menna C, Morganti S, Prota A, Reali A. Statistical finite element analysis of the buckling behavior of honeycomb structures. Composite Structures. 2013;105:240-55.
[179] Menna C, Zinno A, Asprone D, Prota A. Numerical assessment of the impact behavior of honeycomb sandwich structures. Composite Structures. 2013;106:326-39.
[180] Zinno A, Prota A, Di Maio E, Bakis C. Experimental characterization of phenolic-impregnated honeycomb sandwich structures for transportation vehicles. Composite Structures. 2011;93(11):2910-24.
[181] Park Y-B, Kweon J-H, Choi J-H. Failure characteristics of carbon/BMI-Nomex sandwich joints in various hygrothermal conditions. Composites Part B: Engineering. 2014;60:213-21.
[182] Li X, Tabil LG, Panigrahi S. Chemical treatments of natural fiber for use in natural fiber-reinforced composites: a review. Journal of Polymers and the Environment. 2007;15(1):25-33.
[183] Wambua P, Ivens J, Verpoest I. Natural fibres: can they replace glass in fibre reinforced plastics? composites science and technology. 2003;63(9):1259-64.
[184] Shah DU, Schubel PJ, Licence P, Clifford MJ. Hydroxyethylcellulose surface treatment of natural fibres: the new 'twist'in yarn preparation and optimization for composites applicability. Journal of Materials Science. 2012;47(6):2700-11.
[185] Scarponi C. Industrial applications for natural-fibre-reinforced composites. Jec magazine. 2009;46:46-8.
[186] Bledzki AK, Faruk O, Sperber VE. Cars from bio-fibres. Macromolecular Materials and Engineering. 2006;291(5):449-57.
[187] Mougin G, Magnani M, Eikelenberg N. Natural-fibres composites for the automotive industry: challenges, solutions and applications. International Journal of Materials and Product Technology. 2009;36(1-4):176-88.
[188] Xu Y, Hoa SV. Mechanical properties of carbon fiber reinforced epoxy/clay nanocomposites. Composites Science and Technology. 2008;68(3):854-61.
[189] Williams G, Trask R, Bond I. A self-healing carbon fibre reinforced polymer for aerospace applications. Composites Part A: Applied Science and Manufacturing. 2007;38(6):1525-32.
[190] Toldy A, Szolnoki B, Marosi G. Flame retardancy of fibre-reinforced epoxy resin composites for aerospace applications. Polymer Degradation and Stability. 2011;96(3):371-6.
[191] Braun U, Balabanovich AI, Schartel B, Knoll U, Artner J, Ciesielski M, et al. Influence of the oxidation state of phosphorus on the decomposition and fire behaviour of flame-retarded epoxy resin composites. Polymer. 2006;47(26):8495-508.
[192] Formicola C, De Fenzo A, Zarrelli M, Frache A, Giordano M, Camino G. Synergistic effects of zinc borate and aluminiumtrihydroxide on flammability behaviour of aerospaceepoxy system. Express Polymer Letters. 2009;3(6):376-84.

[193] Liu W, Varley RJ, Simon GP. Understanding the decomposition and fire performance processes in phosphorus and nanomodified high performance epoxy resins and composites. Polymer. 2007;48(8):2345-54.
[194] Schartel B, Braun U, Balabanovich A, Artner J, Ciesielski M, Döring M, et al. Pyrolysis and fire behaviour of epoxy systems containing a novel 9, 10-dihydro-9-oxa-10-phosphaphenanthrene-10-oxide-(DOPO)-based diamino hardener. European Polymer Journal. 2008;44(3):704-15.
[195] Karayannidou EG, Achilias DS, Sideridou ID. Cure kinetics of epoxy–amine resins used in the restoration of works of art from glass or ceramic. European Polymer Journal. 2006;42(12):3311-23.
[196] Lee K-Y, Ho KKC, Schlufter K, Bismarck A. Hierarchical composites reinforced with robust short sisal fibre preforms utilising bacterial cellulose as binder. Composites Science and Technology. 2012;72(13):1479-86.
[197] Expandable Flake Graphite. Asbury Carbons; 2016.
[198] Royals WT, Chou TC, Steinberg TA. Flammability and Sensitivity of Materials in Oxygen-Enriched Atmospheres: Eighth Volume. ASTM; 1997.
[199] ASTM D3039 / D3039M Standard Test Method for Tensile Properties of Polymer Matrix Composite Materials.
[200] 790 DD. Standard Test Methods for Flexural Properties of Unreinforced and Reinforced Plastics and Electrical Insulating Materials.
[201] C393/C393M D. Standard Test Method for Core Shear Properties of Sandwich Constructions by Beam Flexure.
[202] C365/C365M D. Standard Test Method for Flatwise Compressive Properties of Sandwich Cores.
[203] ASTM International. Standard Test Method for Shear Properties of Sandwich Core Materials(C273-00). West Conshohocken P, USA; 2000.
[204] Zhang L, Li J, Ding X. Research of the properties of flame-retardant flexible PVC. American Journal of Materials American Journal of Materials Research. 2014;1(1):20-5.
[205] Walker K, Isarov A, Chen T. Fire Performance Synergies of Metal Hydroxides and Metal Molybdates in Antimony-Free Flexible PVC.
[206] Zhang Q, Zhang W, Huang J, Lai Y, Xing T, Chen G, et al. Flame retardance and thermal stability of wool fabric treated by boron containing silica sols. Materials & Design. 2015;85:796-9.
[207] Alongi J, Han Z, Bourbigot S. Intumescence: Tradition versus novelty. A comprehensive review. Progress in Polymer Science. 2015;51:28-73.
[208] Realinho V, Antunes M, Velasco JI. Enhanced fire behavior of Casico-based foams. Polymer Degradation and Stability. 2016;128:260-8.
[209] Ren Y, Wang Y, Wang L, Liu T. Evaluation of intumescent fire retardants and synergistic agents for use in wood flour/recycled polypropylene composites. Construction and Building Materials. 2015;76:273-8.
[210] Chai H, Tang X, Ni M, Chen F, Zhang Y, Chen D, et al. Preparation and properties of flexible flame-retardant neutron shielding material based on methyl vinyl silicone rubber. Journal of Nuclear Materials. 2015;464:210-5.
[211] Sut A, Greiser S, Jäger C, Schartel B. Interactions in multicomponent flame-retardant polymers: Solid-state NMR identifying the chemistry behind it. Polymer Degradation and Stability. 2015;121:116-25.
[212] Shen KK, Kochesfahani S, Jouffret F. Zinc borates as multifunctional polymer additives. Polymers for Advanced Technologies. 2008;19(6):469-74.
[213] Pawlowski KH, Schartel B, Fichera MA, Jäger C. Flame retardancy mechanisms of bisphenol A bis (diphenyl phosphate) in combination with zinc borate in bisphenol A polycarbonate/acrylonitrile–butadiene–styrene blends. Thermochimica Acta. 2010;498(1):92-9.
[214] Weil ED, Levchik S, Moy P. Flame and smoke retardants in vinyl chloride polymers–commercial usage and current developments. Journal of fire sciences. 2006;24(3):211-36.

[215] Lau K-t, Hoi-yan Cheung K, Hui D. Natural fiber composites. Composites Part B: Engineering. 2009;40(7):591-3.
[216] Jeencham R, Suppakarn N, Jarukumjorn K. Effect of flame retardants on flame retardant, mechanical, and thermal properties of sisal fiber/polypropylene composites. Composites Part B: Engineering. 2014;56:249-53.
[217] Shahzad A. Effects of alkalization on tensile, impact, and fatigue properties of hemp fiber composites. Polymer Composites. 2012;33(7):1129-40.
[218] Liu H, You L, Jin H, Yu W. Influence of alkali treatment on the structure and properties of hemp fibers. Fibers and polymers. 2013;14(3):389-95.
[219] Castrovinci A, Camino G, Drevelle C, Duquesne S, Magniez C, Vouters M. Ammonium polyphosphate–aluminum trihydroxide antagonism in fire retarded butadiene–styrene block copolymer. European Polymer Journal. 2005;41(9):2023-33.
[220] Samyn F, Bourbigot S, Duquesne S, Delobel R. Effect of zinc borate on the thermal degradation of ammonium polyphosphate. Thermochimica acta. 2007;456(2):134-44.
[221] Hasan MF. Physical and combustion characteristics of densified palm biomass. 2009.
[222] Nasser RA, Salem MZ, Hiziroglu S, Al-Mefarrej HA, Mohareb AS, Alam M, et al. Chemical Analysis of Different Parts of Date Palm (Phoenix dactylifera L.) Using Ultimate, Proximate and Thermo-Gravimetric Techniques for Energy Production. Energies. 2016;9(5):374.
[223] Duruaku JI, Ajiwe VI, Okoye NH, Arinze RU. An Evaluation of the Calorific Values of the Branches and Stems of 11 Tropical Trees. Journal of Sustainable Bioenergy Systems. 2016;6(02):44.
[224] Suppakarn N, Jarukumjorn K. Mechanical properties and flammability of sisal/PP composites: Effect of flame retardant type and content. Composites Part B: Engineering. 2009;40(7):613-8.
[225] Genovese A, Shanks RA. Fire performance of poly(dimethyl siloxane) composites evaluated by cone calorimetry. Composites Part A: Applied Science and Manufacturing. 2008;39(2):398-405.
[226] Hapuarachchi T, Peijs T. Aluminium trihydroxide in combination with ammonium polyphosphate as flame retardants for unsaturated polyester resin. eXPRESS Polymer Letters. 2009;3(11):743-51.
[227] Le Bras M, Duquesne S, Fois M, Grisel M, Poutch F. Intumescent polypropylene/flax blends: a preliminary study. Polymer Degradation and Stability. 2005;88(1):80-4.
[228] Gao M, Wu W, Yan Y. Thermal degradation and flame retardancy of epoxy resins containing intumescent flame retardant. Journal of Thermal Analysis and Calorimetry. 2009;95(2):605-8.
[229] Wu CS, Liu YL, Chiu YC, Chiu YS. Thermal stability of epoxy resins containing flame retardant components: an evaluation with thermogravimetric analysis. Polymer Degradation and Stability. 2002;78(1):41-8.
[230] Zhang W, He X, Song T, Jiao Q, Yang R. The influence of the phosphorus-based flame retardant on the flame retardancy of the epoxy resins. Polymer Degradation and Stability. 2014;109:209-17.
[231] Deng C-L, Du S-L, Zhao J, Shen Z-Q, Deng C, Wang Y-Z. An intumescent flame retardant polypropylene system with simultaneously improved flame retardancy and water resistance. Polymer Degradation and Stability. 2014;108:97-107.
[232] Wen P, Wang X, Wang B, Yuan B, Zhou K, Song L, et al. One-pot synthesis of a novel s-triazine-based hyperbranched charring foaming agent and its enhancement on flame retardancy and water resistance of polypropylene. Polymer Degradation and Stability. 2014;110(0):165-74.
[233] Shumao L, Jie R, Hua Y, Tao Y, Weizhong Y. Influence of ammonium polyphosphate on the flame retardancy and mechanical properties of ramie fiber-reinforced poly(lactic acid) biocomposites. Polymer International. 2010;59(2):242-8.
[234] Zhang ZX, Zhang J, Lu B-X, Xin ZX, Kang CK, Kim JK. Effect of flame retardants on mechanical properties, flammability and foamability of PP/wood–fiber composites. Composites Part B: Engineering. 2012;43(2):150-8.

[235] De Chirico A, Armanini M, Chini P, Cioccolo G, Provasoli F, Audisio G. Flame retardants for polypropylene based on lignin. Polymer Degradation and Stability. 2003;79(1):139-45.
[236] Patrick Lim WK, Mariatti M, Chow WS, Mar KT. Effect of intumescent ammonium polyphosphate (APP) and melamine cyanurate (MC) on the properties of epoxy/glass fiber composites. Composites Part B: Engineering. 2012;43(2):124-8.
[237] Kandola BK, Horrocks AR. Complex char formation in flame-retarded fibre-intumescent combinations—II. Thermal analytical studies. Polymer Degradation and Stability. 1996;54(2):289-303.
[238] Ning Y, Guo S. Flame-retardant and smoke-suppressant properties of zinc borate and aluminum trihydrate-filled rigid PVC. Journal of Applied Polymer Science. 2000;77(14):3119-27.
[239] Benisek L. Flame retardance of protein fibers. Flame-Retardant Polymeric Materials: Springer; 1975. p. 137-91.
[240] Levchik G, Selevich A, Levchik S, Lesnikovich A. Thermal behaviour of ammonium polyphosphate—inorganic compound mixtures. Part 1. Talc. Thermochimica acta. 1994;239:41-9.
[241] Lu M, Zhang S, Yu D. Study on poly(propylene)/ammonium polyphosphate composites modified by ethylene-1-octene copolymer grafted with glycidyl methacrylate. Journal of Applied Polymer Science. 2004;93(1):412-9.
[242] Gañán P, Zuluaga R, Restrepo A, Labidi J, Mondragon I. Plantain fibre bundles isolated from Colombian agro-industrial residues. Bioresource technology. 2008;99(3):486-91.
[243] Singha AS, Rana RK. Natural fiber reinforced polystyrene composites: Effect of fiber loading, fiber dimensions and surface modification on mechanical properties. Materials & Design. 2012;41:289-97.
[244] Haque MM, Hasan M, Islam MS, Ali ME. Physico-mechanical properties of chemically treated palm and coir fiber reinforced polypropylene composites. Bioresource Technology. 2009;100(20):4903-6.
[245] Olsson A-M, Salmén L. The association of water to cellulose and hemicellulose in paper examined by FTIR spectroscopy. Carbohydrate research. 2004;339(4):813-8.
[246] Liu W, Mohanty A, Drzal L, Askel P, Misra M. Effects of alkali treatment on the structure, morphology and thermal properties of native grass fibers as reinforcements for polymer matrix composites. Journal of Materials Science. 2004;39(3):1051-4.
[247] Yang H, Yan R, Chen H, Lee DH, Zheng C. Characteristics of hemicellulose, cellulose and lignin pyrolysis. Fuel. 2007;86(12):1781-8.
[248] Liu C-F, Sun R-C, Qin M-H, Zhang A-P, Ren J-L, Xu F, et al. Chemical modification of ultrasound-pretreated sugarcane bagasse with maleic anhydride. Industrial Crops and Products. 2007;26(2):212-9.
[249] Amoriello S, Bianco A, Eusebio L, Gronchi P. Evolution of two acid steps sol–gel phases by FTIR. Journal of sol-gel science and technology. 2011;58(1):209-17.
[250] Mwaikambo LY, Ansell MP. Chemical modification of hemp, sisal, jute, and kapok fibers by alkalization. Journal of Applied Polymer Science. 2002;84(12):2222-34.
[251] Hossain MK, Dewan MW, Hosur M, Jeelani S. Effect of surface treatment and nanoclay on thermal and mechanical performances of jute fabric/biopol 'green'composites. Journal of Reinforced Plastics and Composites. 2011;30(22):1841-56.
[252] Brebu M, Vasile C. Thermal degradation of lignin—a review. Cellulose Chemistry & Technology. 2010;44(9):353.
[253] Kurt R, MENGELOĞLU F. Utilization of boron compounds as synergists with ammonium polyphosphate for flame retardant wood-polymer composites. Turkish Journal of Agriculture and Forestry. 2011;35(2):155-63.
[254] Chiu S-H, Wang W-K. Dynamic flame retardancy of polypropylene filled with ammonium polyphosphate, pentaerythritol and melamine additives. Polymer. 1998;39(10):1951-5.
[255] Jiao Y-H, Wang X-L, Wang Y-Z, Wang D-Y, Zhai Y-L, Lin J-S. Thermal degradation and combustion behaviors of flame-retardant polypropylene/thermoplastic polyurethane blends. Journal of Macromolecular Science, Part B. 2009;48(5):889-909.

[256] Song YP, Wang DY, Wang XL, Lin L, Wang YZ. A method for simultaneously improving the flame retardancy and toughness of PLA. Polymers for Advanced Technologies. 2011;22(12):2295-301.
[257] Reti C, Casetta M, Duquesne S, Delobel R, Soulestin J, Bourbigot S. Intumescent biobased-polylactide films to flame retard nonwovens. J Eng Fibers Fabr. 2009;4(2):33e9.
[258] Shah AuR, Lee D-w, Wang Y-q, Wasy A, Ham KC, Jayaraman K, et al. Effect of concentration of ATH on mechanical properties of polypropylene/aluminium trihydrate (PP/ATH) composite. Transactions of Nonferrous Metals Society of China. 2014;24:s81-s9.
[259] Yousif B, Shalwan A, Chin C, Ming K. Flexural properties of treated and untreated kenaf/epoxy composites. Materials & Design. 2012;40:378-85.
[260] Laoutid F, Bonnaud L, Alexandre M, Lopez-Cuesta JM, Dubois P. New prospects in flame retardant polymer materials: From fundamentals to nanocomposites. Materials Science and Engineering: R: Reports. 2009;63(3):100-25.
[261] Wang C, Li Y-c, Hu G-s, Cao D-h. Synergistic flame retardant effects of composites containing organic montmorillonite, Nylon6 and 2-cyclic pentaerythritoloctahydrogen tetraphosphate-4,6-benzene sulfonic acid sodium ammion-triazine. Carbon. 2015;93:1084.
[262] Pinto UA, Visconte LLY, Gallo J, Nunes RCR. Flame retardancy in thermoplastic polyurethane elastomers (TPU) with mica and aluminum trihydrate (ATH). Polymer degradation and stability. 2000;69(3):257-60.
[263] Xie F, Wang YZ, Yang B, Liu Y. A Novel Intumescent Flame-Retardant Polyethylene System. Macromolecular Materials and Engineering. 2006;291(3):247-53.
[264] Bian X-C, Tang J-H, Li Z-M, Lu Z-Y, Lu A. Dependence of flame-retardant properties on density of expandable graphite filled rigid polyurethane foam. Journal of Applied Polymer Science. 2007;104(5):3347-55.
[265] Camino G, Duquesne S, Delobel R, Eling B, Lindsay C, Roels T. Fires and polym: materials and solutions for hazard prevention (symposium series no. 797). Washington DC, ACS Pub. 2001;90.
[266] Modesti M, Lorenzetti A, Simioni F, Camino G. Expandable graphite as an intumescent flame retardant in polyisocyanurate–polyurethane foams. Polymer Degradation and Stability. 2002;77(2):195-202.
[267] Expandable graphite. In: Kropfmühl G, editor.2013.
[268] Wang CQ, Ge FY, Sun J, Cai ZS. Effects of expandable graphite and dimethyl methylphosphonate on mechanical, thermal, and flame-retardant properties of flexible polyurethane foams. Journal of Applied Polymer Science. 2013;130(2):916-26.
[269] Meng XY, Ye L, Zhang XG, Tang PM, Tang JH, Ji X, et al. Effects of expandable graphite and ammonium polyphosphate on the flame-retardant and mechanical properties of rigid polyurethane foams. Journal of applied polymer science. 2009;114(2):853-63.
[270] Han J, Liang G, Gu A, Ye J, Zhang Z, Yuan L. A novel inorganic–organic hybridized intumescent flame retardant and its super flame retarding cyanate ester resins. Journal of Materials Chemistry A. 2013;1(6):2169-82.
[271] Jana S, Zhong W-H. Graphite particles with a “puffed” structure and enhancement in mechanical performance of their epoxy composites. Materials Science and Engineering: A. 2009;525(1):138-46.
[272] Khalili P, Tshai KY, Kong I. Natural fibre reinforced expandable graphite filled composites: Evaluation of the flame retardancy, thermal and mechanical performances. Composites Part A: Applied Science and Manufacturing.
[273] Albano C, Gonzalez J, Ichazo M, Kaiser D. Thermal stability of blends of polyolefins and sisal fiber. Polymer Degradation and Stability. 1999;66(2):179-90.
[274] Arbelaiz A, Fernandez B, Ramos J, Mondragon I. Thermal and crystallization studies of short flax fibre reinforced polypropylene matrix composites: Effect of treatments. Thermochimica Acta. 2006;440(2):111-21.

[275] De Rosa IM, Santulli C, Sarasini F. Mechanical and thermal characterization of epoxy composites reinforced with random and quasi-unidirectional untreated Phormium tenax leaf fibers. Materials & Design. 2010;31(5):2397-405.
[276] Alvarez V, Vázquez A. Thermal degradation of cellulose derivatives/starch blends and sisal fibre biocomposites. Polymer Degradation and Stability. 2004;84(1):13-21.
[277] Fung K, Xing X, Li R, Tjong S, Mai Y-W. An investigation on the processing of sisal fibre reinforced polypropylene composites. Composites Science and Technology. 2003;63(9):1255-8.
[278] Shih Y-F. Mechanical and thermal properties of waste water bamboo husk fiber reinforced epoxy composites. Materials Science and Engineering: A. 2007;445:289-95.
[279] Wielage B, Lampke T, Marx G, Nestler K, Starke D. Thermogravimetric and differential scanning calorimetric analysis of natural fibres and polypropylene. Thermochimica Acta. 1999;337(1):169-77.
[280] Joseph P, Joseph K, Thomas S, Pillai C, Prasad V, Groeninckx G, et al. The thermal and crystallisation studies of short sisal fibre reinforced polypropylene composites. Composites Part A: Applied Science and Manufacturing. 2003;34(3):253-66.
[281] Pearce EM, Liepins R. Public health implications of components of plastics manufacture. Flame retardants. Environmental health perspectives. 1975;11:59.
[282] Shang J, Chen Y, Zhou Y, Liu L, Wang G, Li X, et al. Effect of folded and crumpled morphologies of graphene oxide platelets on the mechanical performances of polymer nanocomposites. Polymer. 2015;68:131-9.
[283] Shojaee SA, Zandiatashbar A, Koratkar N, Lucca DA. Raman spectroscopic imaging of graphene dispersion in polymer composites. Carbon. 2013;62:510-3.
[284] Enríquez E, Fernández J, De la Rubia M. Highly conductive coatings of carbon black/silica composites obtained by a sol–gel process. Carbon. 2012;50(12):4409-17.
[285] Filiou C, Galiotis C. In situ monitoring of the fibre strain distribution in carbon-fibre thermoplastic composites1. Application of a tensile stress field. Composites science and technology. 1999;59(14):2149-61.
[286] Seefeldt H, Braun U, Wagner MH. Residue stabilization in the fire retardancy of wood–plastic composites: Combination of ammonium polyphosphate, expandable graphite, and red phosphorus. Macromolecular chemistry and physics. 2012;213(22):2370-7.
[287] Essabir H, Boujmal R, Bensalah MO, Rodrigue D, Bouhfid R, Qaiss Aek. Mechanical and thermal properties of hybrid composites: Oil-palm fiber/clay reinforced high density polyethylene. Mechanics of Materials. 2016;98:36-43.
[288] Elfehri Borchani K, Carrot C, Jaziri M. Biocomposites of Alfa fibers dispersed in the Mater-Bi® type bioplastic: Morphology, mechanical and thermal properties. Composites Part A: Applied Science and Manufacturing. 2015;78:371-9.
[289] Shalwan A, Yousif B. Influence of date palm fibre and graphite filler on mechanical and wear characteristics of epoxy composites. Materials & Design. 2014;59:264-73.
[290] Xie R, Qu B. Synergistic effects of expandable graphite with some halogen-free flame retardants in polyolefin blends. Polymer degradation and stability. 2001;71(3):375-80.
[291] Giglio M, Manes A, Gilioli A. Investigations on sandwich core properties through an experimental–numerical approach. Composites Part B: Engineering. 2012;43(2):361-74.
[292] Heimbs S, Middendorf P, Hampf C, Hähnel F, Wolf K. Aircraft sandwich structures with folded core under impact load. Proc of the 8th International Conference on Sandwich Structures, ICSS8, Porto, Portugal2008.
[293] Zenkert D, Industrifond N. The handbook of sandwich construction: Engineering Materials Advisory Services Limited (EMAS); 1997.
[294] Composite H. HexWeb tm honeycomb sandwich design technology. http. 2004.

[295] ASTM D7250M. Determining sandwich beam flexural and shear stiffness. West Conshohocken (PA): American Soc for Testing and Materials.
[296] Seemann R, Krause D. Numerical Modeling of Nomex Honeycomb Sandwich Cores at Meso-Scale Level. Composite Structures. 2016.